Investigating an interaction between LRRK2 and HDAC6 in Parkinson's Disease

Richard Lucas BSc (Hons), MSc

Thesis submitted for the degree of Doctor of Philosophy,

The University of Sheffield

The University Of Sheffield.

August 2018

Abstract

Mutations in leucine-rich repeat kinase 2 (LRRK2) are the most common known genetic cause of Parkinson's disease (PD). LRRK2 is a multi-domain protein which has GTPase and kinase activity. Dominant pathogenic mutations have been identified in the LRRK2 Roc-COR GTPase domain which decrease GTPase function (R1441C/G/H and Y1699C) and kinase domain which increase kinase activity (G2019S/I2020T). Evidence suggests that LRRK2 may have a physiological role in protein degradation pathways and these functions may be disrupted by pathogenic LRRK2 mutations, potentially resulting in protein aggregation which is a pathological hallmark of PD. In addition, evidence points to a role for LRRK2 in the maintenance of axonal integrity via an interaction with microtubules and regulation of microtubule acetylation, and defective axonal transport of intracellular cargoes along microtubule tracks has been proposed as a mechanism for PD.

Histone deacetylase 6 (HDAC6) is a cytoplasmic deacetylase which functions at the crossroads between protein degradation pathways and microtubule dynamics. HDAC6 co-ordinates the formation of aggresomes in response to misfolded protein, and aggresomes share many characteristics with Lewy bodies in PD. This thesis therefore aimed to investigate if LRRK2 interacts with HDAC6 to regulate aggresome formation and tubulin acetylation. LRRK2 was found to interact with HDAC6 via its Roc-COR domain and pathogenic LRRK2 mutations altered this interaction. Using mass spectrometry analysis, LRRK2 was found to phosphorylate HDAC6 at serine-22 and serine-689. Cellular studies of the function of these HDAC6 phospho-sites showed that serine-22 phosphorylation was required for HDAC6-mediated aggresome formation and serine-689 phosphorylation correlated with increased HDAC6 tubulin deacetylase activity. Knockdown of LRRK2 by targeted siRNA resulted in defective HDAC6-dependent aggresome formation and rescue of aggresome formation was LRRK2 kinase-dependent. Furthermore, LRRK2 was shown to decrease tubulin acetylation via HDAC6 in a kinase-dependent manner. Together, these results suggested that LRRK2 regulates the function of HDAC6 in aggresome formation and tubulin deacetylation via phosphorylation. Importantly, the role of LRRK2 in HDAC6-dependent aggresome formation was found to be disrupted by the pathogenic G2019S mutation, suggesting that this mechanism may contribute to disease pathogenesis in PD.

Acknowledgments

I owe my thanks and appreciation to a number of people who have supported me during this project and without whom this would not have been possible.

First and foremost, I would like to give a huge thank you to Dr Kurt De Vos for his continual guidance and supervision over the past four years, both in the lab and during the preparation of this thesis, and for being instrumental in aiding my scientific development. Furthermore, I would like to thank the Department of Neuroscience and the Medical School for funding this project. I would also like to thank Dr Heather Mortiboys for her help and support, and to Dr Phil Elks for his guidance and numerous chats over coffee along the way.

I would like to send a special thank you to Dr Kavitha Chinnaiya for her work which makes up part of this thesis, and together with Dr Claudia Bauer for their continuing work on this project. In addition, I would like to thank Dr Mark Collins for his assistance and use of the proteomics lab, as well as all members of the De Vos/Grierson lab group for ongoing support and advice. Thanks to everyone in B10 and friends in SITraN, past and present, for creating such a nice community in which to work and for their love of Friday night games nights.

Lastly, I am grateful to my friends and family for their constant support and enthusiasm for my research. And to Heledd, who I have been fortunate enough to share this journey with.

Contents

List of Figures

List of Tables

Abbreviations

Ambic	*Ammonium bicarbonate*
ANK	*Ankyrin repeats*
APP	*Amyloid precursor protein*
ArfGAP1	*ADP ribosylation factor GTPase activating protein 1*
ARHGEF7	*Rho guanine nucleotide exchange factor 7*
ARID1A	*AT-rich interactive domain-containing protein 1A*
Arp1	*Actin-related protein 1*
ATP	*Adenosine triphosphate*
BAG3	*Bcl-2-associated athanogene 3*
BDNF	*Brain-derived neurotrophic factor*
BSA	*Bovine serum albumin*
cAMP	*Cyclic adenosine monophosphate*
CDK9	*Cyclin-dependent kinase 9*
CFTR	*Cystic fibrosis transmembrane conductance regulator*
CK1α	*Casein kinase 1α*
CK2	*Casein kinase 2*
CMA	*Chaperone-mediated autophagy*
COR	*C-terminal of Roc*
CPS1	*Carbamoyl phosphate synthetase I*
C-terminus	*Carboxy-terminus*
CtIP	*CTBP-interacting protein*
Da	*Dalton*
DA	*Dopamine*
DLB	*Dementia with Lewy bodies*
DMEM	*Dulbecco's modified Eagle's medium*
DMSO	*Dimethyl sulfoxide*
DNA	*Deoxyribonucleic acid*
DNAJB8	*DnaJ Heat Shock Protein Family (Hsp40) Member B8*

EB1	*End-binding 1*
EDTA	*Ethylenediaminetetraacetic acid*
EGFP	*Enhanced green fluorescent protein*
eIF4E	*Eukaryotic translation initiation factor 4E*
ER	*Endoplasmic reticulum*
ERAC	*Endoplasmic reticulum-associated complex*
ERK	*Extracellular signal-regulated kinase*
ERM	*Ezrin, radixin, and moesin protein family*
FBS	*Fetal bovine serum*
FOXO1	*Forkhead box protein O1*
FTD	*Frontotemporal dementia*
FUS	*Fused in sarcoma*
G3BP	*Ras-GAP SH3 domain-binding protein*
GABPß1	*GA binding protein ß1*
GBA	*Glucocerebrosidase*
GDH	*Glutamate dehydrogenase*
GFP	*Green fluorescent protein*
GR	*Glucocorticoid receptor*
GSH	*Glutathione*
GTP	*Guanosine triphosphate*
GWAS	*Genome-wide association studies*
HDAC	*Histone deacetylase*
HDAC6	*Histone deacetylase 6*
HEK293	*Human embryonic kidney 293*
HIF1α	*Hypoxia-inducible factor 1-alpha*
HPOB	*N-hydroxy-4-(2-[(2-hydroxyethyl)(phenyl)amino]-2-oxoethyl)benzamide*
Hsc70	*Heat shock cognate 70 kDa*
HSF1	*Heat shock factor 1*
Hsp70	*Heat shock protein 70 kDa*

Hsp90	*Heat shock protein 90 kDa*
iPSC	*Induced pluripotent stem cell*
JIP1	*JNK-interacting protein 1*
kb	*Kilobase*
LAMP-2A	*Lysosomal-associated membrane protein 2A*
LC3	*Microtubule-associated protein light chain 3*
LC-MS/MS	*Liquid chromatography-tandem mass spectrometry*
LRR	*Leucine-rich repeats*
LRRK2	*Leucine-rich repeat kinase 2*
M	*Molar*
MAP	*Microtubule-associated protein*
MAPT	*Microtubule-associated protein tau*
MARK	*Microtubule affinity-regulating kinase*
MCCC	*Methylcrotonyl-CoA carboxylase*
MCD	*Malonyl CoA decarboxylase*
MEF	*Mouse embryonic fibroblast*
MEF2	*Myocyte enhancer factor 2*
MLP	*Muscle LIM protein*
MPTP	*1-methyl-4-phenyl-1,2,3,6-tetrahydropyridine*
MT	*Microtubule*
mtDNA	*Mitochondrial DNA*
MTOC	*Microtubule-organising centre*
mTOR	*Mammalian target of rapamycin*
NAD	*Nicotinamide adenine dinucleotide*
NBR1	*Neighbour of BRCA1 gene 1*
NF-Kb	*Nuclear factor kappa-light-chain-enhancer of activated B cells*
NGF	*Nerve growth factor*
NLS	*Nuclear localisation signal*
NPD52	*Nuclear dot protein 52 kDa*
N-terminus	*Amino-terminus*

PAF53	*RNA Polymerase I-associated factor 53*
PBS	*Phosphate-buffered saline*
PCAF	*P300/CBP-associated factor*
PCR	*Polymerase chain reaction*
PD	*Parkinson's disease*
PDH	*Pyruvate dehydrogenase*
PINK1	*PTEN-induced putative kinase 1*
PKA	*cAMP-dependent protein kinase*
PRX	*Peroxiredoxin*
PTM	*Post-translational modification*
RILP	*Rab-interacting lysosomal protein*
RNA	*Ribonucleic acid*
Roc	*Ras of complex protein*
ROS	*Reactive oxygen species*
rpm	*Revolutions per minute*
Runx2	*Runt-related transcription factor 2*
SD	*Standard deviation*
SDS-PAGE	*Sodium dodecyl sulphate polyacrylamide gel electrophoresis*
SEM	*Standard error of mean*
siRNA	*Small interfering RNA*
SIRT2	*Sirtuin 2*
SMC3	*Structural maintenance of chromosomes protein 3*
SNARE	*Soluble N-ethylmaleimide-sensitive factor attachment protein receptor*
SNpc	*Substantia nigra pars compacta*
SRY	*Sex-determining region Y*
STAT3	*Signal transducer and activator of transcription 3*
Tat	*Trans-activator of transcription*
TBS	*Tris-buffered saline*
TDP-43	*43-kDa TAR DNA-binding domain protein*

TRAK	*Trafficking kinesin protein*
TSA	*Trichostatin A*
TTL	*Tubulin tyrosine ligase*
TubA	*Tubastatin A*
Ub	*Ubiquitin*
ULK1	*Unc-51-like autophagy activating kinase*
UPS	*Ubiquitin-proteasome system*
VASH1	*Vasohibin-1*
VMAT2	*Vesicular monoamine transporter 2*
WT	*Wild-type*
Y2H	*Yeast 2-hybrid*
YFP	*Yellow fluorescent protein*
αTAT1	*Alpha tubulin acetyl-transferase 1*

1 Introduction

1.1 Parkinson's Disease

Parkinson's disease (PD) is the second most common neurodegenerative disease with over 140,000 people living with PD in the UK alone (Parkinson's UK, 2018). PD is largely an age-related disorder and affects approximately 1% of the population over sixty years of age and around 4% of the population over eighty, however in rare cases symptoms can present before the age of 50. The worldwide prevalence of PD is estimated at around 0.3% with some variation between populations (de Lau and Breteler, 2006).

1.1.1 Clinical and pathological features of PD

Primarily classified as a motor disorder, the clinical features of PD typically include bradykinesia, tremor at rest, muscular rigidity, and postural imbalances which contribute to difficulties in initiating and controlling movement. In addition, various non-motor symptoms have been associated with PD which include olfactory disturbance, constipation, sleep disorders and depression, and these symptoms often occur early in the disease (Chaudhuri et al., 2006). A lack of available diagnostic biomarker tests means that diagnosis of PD is currently based on presentation of clinical symptoms alone and is confirmed by pathological examination at autopsy (Jankovic, 2008).

1.1.1.1 Dopaminergic neuron loss

The primary motor symptoms of PD can be attributed to progressive loss of dopaminergic (DA) neurons in the substantia nigra pars compacta (SNpc) (Damier et al., 1999). The SNpc forms part of the midbrain basal ganglia which control voluntary movement by projecting DA neurons along the nigrostriatal pathway to the striatum where they release dopamine to modulate activity. It is hypothesised that loss of dopaminergic modulation in the basal ganglia disturbs initiation of movement and leads to the classical Parkinsonian motor symptoms (Obeso et al., 2008). However, it is estimated that many motor symptoms do not appear until 50-70% of nigral DA neurons have been lost, meaning that many patients likely remain undiagnosed until the later stages of the disease (Lesage and Brice, 2012).

The reason(s) for the selective loss of DA neurons in the SNpc remains an important question in attempts to understand the cause of PD. DA neurons projecting from the SNpc commonly have long, unmyelinated axons which have a high energy expenditure for signal transmission as well as forming high numbers of synapses compared with other neuronal types (Braak et al., 2004). Additionally, the regular, autonomous firing patterns of DA neurons in the SNpc necessary for maintaining striatal dopamine levels requires sustained entry of intracellular calcium through ion channels, which again has a high energetic requirement (Surmeier et al., 2010). These morphological and functional characteristics place a significant energetic demand on the mitochondria within the DA neurons and lead to increased susceptibility to disruption by mitochondrial dysfunction and oxidative stress, which may eventually result in an energy deficit which disrupts further cell processes and contributes to cell death (Pissadaki and Bolam, 2013).

Currently, the primary symptomatic treatment for PD is the pharmaceutical restoration of dopamine levels in the brain via L-DOPA supplementation, however this does not halt the progression of the disease or prevent further cell loss. Reduced efficacy and adverse side effects such as dyskinesia are commonly seen with long-term use (Marsden, 1994).

1.1.1.2 Lewy body pathology

As well as dopaminergic neuron loss, the second hallmark pathological feature of PD is the presence of intracellular inclusions known as Lewy bodies in multiple brain regions. Lewy bodies are dense insoluble protein spheres found in the cytoplasm of affected neurons in the SNpc as well as other brain regions such as the locus coeruleus and raphe nuclei in the brainstem, hypothalamus and the cerebral cortex (Forno, 1996). Lewy bodies are found in most sporadic and familial cases of PD and their presence increases with disease progression and correlates with resulting neurodegeneration (Braak et al., 2004).

The principle components of Lewy bodies are filamentous aggregates of phosphorylated α-synuclein and they strongly immunostain with ubiquitin, as well as containing over 90 other proteins (major proteins are listed in Table 1.1) (Fujiwara et al., 2002; Tofaris et al., 2003; Wakabayashi et al., 2013). Present as a soluble cytoplasmic monomer of 140 amino acids which is ubiquitously expressed in neurons, α-synuclein is thought to function at the synapse to aid neurotransmitter release (Jakes et al., 1994; Fauvet et al., 2012; Burré et al., 2010). It is also localised to the

inner mitochondrial membrane (Chinta et al., 2010). In disease, α-synuclein monomers aggregate to form oligomers and protofibrils and it is these which are thought to confer cellular toxicity by disrupting various cellular mechanisms such as ion homeostasis, mitochondrial function, protein degradation and causing ER stress (Winner et al., 2011a). The organisation and sequestration of toxic α-synuclein oligomers into filaments to form Lewy bodies has been hypothesised to be a cytoprotective response to facilitate their degradation, therefore Lewy bodies themselves may not drive the pathogenesis of PD (Olanow et al., 2004; Wakabayashi et al., 2007).

Table 1.1. Protein components of Lewy bodies in PD (adapted from Wakabayashi et al., 2013). Highlighted proteins are PD-linked gene products.

Group/Function	Protein	References
Fibril-forming	α-synuclein	Spillantini et al., 1997; Fujiwara et al., 2002
α-synuclein-binding	synphilin-1	Wakabayashi et al., 2000; Bandopadhyay et al., 2005
	agrin	Liu et al., 2005
	14-3-3	Kawamoto et al., 2002; Ubl et al., 2002
Ubiquitin-proteasome system	NUB1	Tanji et al., 2006
	parkin	Schlossmacher et al., 2002; Murakami et al., 2004
	ubiquitin	Kuzuhara et al., 1988; Tofaris et al., 2003
	ubiquitin activating enzyme (E1)	McNaught et al., 2002
	ubiquitin-conjugating enzyme (E2)	Schlossmacher et al., 2002
	proteasome	Ii et al., 1997; Lindersson et al., 2004
	26S ATPase	Fergusson et al., 1996
Autophagy	p62/sequestosome 1	Kuusisto et al., 2003
	LC3	Crews et al., 2010; Higashi et al., 2011; Tanji et al., 2011
	GABARAP	Tanji et al., 2011
	glucocerebrosidase	Goker-Alpan et al., 2010
	NBR1	Odagiri et al., 2012

Group/Function	Protein	References
Aggresome	γ-tubulin	McNaught et al., 2002
	HDAC6	Kawaguchi et al., 2003; Miki et al., 2011
	pericentrin	McNaught et al., 2002
Heat shock proteins	DnaJB6	Durrenberger et al., 2009
	Hsp60	McLean et al., 2002
	Hsp70	McLean et al., 2002
	Hsp90	McLean et al., 2002
Oxidative stress	DJ-1	Bandopadhyay et al., 2004; Jin et al., 2005
	TDP-43	Kokoulina and Rohn, 2010
	FOXO3a	Su et al., 2009
	SOD1/2	Nishiyama et al., 1995
Protein phosphorylation	CAMKII	Iwatsubo et al., 1991
	GSK3β	Nagao and Hayashi, 2009
	CDK5	Brion and Couck, 1995
	LRRK2	Greggio et al., 2006; Miklossy et al., 2006; Giasson et al., 2006; Zhu et al., 2006
	CKII	Ryu et al., 2008
Cytoskeletal	tubulin	Alim et al., 2002
	MAP1	Fukuda et al., 1993
	MAP1B	Jensen et al., 2000
	MAP2	D'Andrea et al., 2001
	tau	Ishizawa et al., 2003
	neurofilament	Forno et al., 1986; Schmidt et al., 1991
Mitochondrial	PINK1	Gandhi et al., 2006
	cytochrome C	Hashimoto et al., 1999

1.1.2 Genetics of PD

PD has been traditionally viewed as an idiopathic disease with the majority of patients presenting with no previous family history. However, single gene mutations have been uncovered through familial linkage analysis in genes coding for α-synuclein (*SNCA*), LRRK2, PINK1, and parkin in 5-10% of PD cases, displaying both autosomal dominant and autosomal recessive patterns of inheritance with varying clinical presentations and age of onset (Lesage and Brice, 2009). These highly penetrant monogenic forms of PD, whilst only a representing a minority of overall cases, have allowed some of the molecular mechanisms underpinning disease pathogenesis to be investigated. Importantly, mutations in *SNCA* and *LRRK2* have highly similar clinical presentations to sporadic disease, offering hope that similar mechanisms may be involved. Table 1.2 shows the designated PARK loci with their associated genes which have so far been linked to familial PD or Parkinsonian disease.

1.1.2.1 Autosomal dominant PD

1.1.2.1.1 SNCA

Rare but highly penetrant mutations in the *SNCA* gene which codes for α-synuclein protein were the first to be linked to PD, with the initial identification of an A53T mutation in Italian and Greek families which showed an autosomal dominant pattern of inheritance (Polymeropoulos et al., 1997). Since then, further mutations have been identified which include A30P, E46K, and more recently G51D and H50Q (Krüger et al., 1998; Zarranz et al., 2004; Lesage et al., 2013; Appel-Cresswell et al., 2013). These mutations all reside in the N-terminal region of the 140-amino acid α-synuclein protein and are thought to promote its aggregation into oligomers, likely by destabilising the conformation of the native protein (Burré et al., 2015). As well as point mutations, chromosomal duplication and triplications of the *SNCA* locus can cause PD (Singleton et al., 2003; Chartier-Harlin et al., 2004). Given that α-synuclein is the major component of Lewy bodies in both familial and sporadic PD, these findings highlight the possible role of protein aggregation as a key driver of disease.

Table 1.2. Genes and loci identified in monogenic PD (adapted and updated from Lesage and Brice, 2012 and Bonifati, 2014). AD = autosomal dominant, AR = autosomal recessive. Highlighted loci have been confirmed in familial PD.

Name	Locus	Gene	Inheritance	Type of PD	References
PARK1/4	4q21	*SNCA*	AD; rare sporadic	Early-onset	Polymeropoulos et al., 1997; Singleton et al., 2003
PARK2	6q25-27	*PRKN*	AR; sporadic	Early-onset; juvenile	Kitada et al., 1998
PARK3	2p13	*SPR?*	AD	Late-onset	Gasser et al., 1998; Sharma et al., 2006
PARK5	4p14	*UCHL1*	AD	Late-onset	Leroy et al., 1998
PARK6	1p35-36	*PINK1*	AR	Early-onset	Valente et al., 2004
PARK7	1p36	*DJ-1*	AR	Early-onset	Bonifati et al., 2003
PARK8	12q12	*LRRK2*	AD; sporadic	Late-onset	Paisán-Ruíz et al., 2004
PARK9	1p36	*ATP13A2*	AR	Kufor-Rakeb syndrome	Ramirez et al., 2006
PARK10	1p32	*Unknown*	*Unknown*	Late-onset	Hicks et al., 2002; Beecham et al., 2015
PARK11	2q36-37	*GIGYF2*	AD	Late-onset	Pankratz et al., 2003b
PARK12	Xq21-25	*Unknown*	*Unknown*	Late-onset	Pankratz et al., 2003a
PARK13	2p12	*HTRA2*	Sporadic	*Unknown*	Strauss et al., 2005*;* Krüger et al., 2011
PARK14	22q12-13	*PLA2G6*	AR	Juvenile	Paisan-Ruiz et al., 2009
PARK15	22q12-13	*FBXO7*	AR	Early-onset	Di Fonzo et al., 2009
PARK16	1q32	*RAB7L1?*	*Unknown*	Late-onset	Satake et al., 2009; Pihlstrøm et al., 2015
PARK17	16q11	*VPS35*	AD; sporadic	Late-onset	Zimprich et al., 2011
PARK18	3q27	*EIF4G1*	AD	Late-onset	Chartier-Harlin et al., 2011
PARK19	1p31	*DNAJC6*	AR	Juvenile	Edvardson et al., 2012
PARK20	21q22	*SYNJ1*	AR	Juvenile	Krebs et al., 2013; Quadri et al., 2013
PARK21	3q22/ 20p12	*DNAJC13/ TMEM230*	AD	Late-onset	Vilariño-Güell et al., 2014; Deng et al., 2016
PARK22	7p11	*CHCHD2*	AD	Late-onset	Funayama et al., 2015
PARK23	15q22	*VPS13C*	AR	Early-onset	Lesage et al., 2016

1.1.2.1.2 LRRK2

Mutations in *leucine-rich repeat kinase 2* (*LRRK2)* are found in up to 10% of autosomal dominant inherited PD and approximately 1% of sporadic cases (L.N. Clark et al., 2006; Bonifati, 2014). Within specific ethnic groups the frequency of *LRRK2* mutations rises significantly, reaching up to 30% of familial PD cases in Ashkenazi Jewish populations (Thaler et al., 2009). This makes mutations in *LRRK2* the most common genetic cause of PD identified to date (Li et al., 2014; Cornejo-Olivas et al., 2017). As LRRK2 is a major focus of this thesis the genetics of *LRRK2* are described in detail in Section 1.2.

1.1.2.2 Autosomal recessive PD

1.1.2.2.1 Parkin

Shortly after the first identification of mutations in *SNCA* that were linked to genetically-inherited PD*,* mutations in the *PRKN* gene were found in Japanese patients who presented with a rare early-onset, juvenile form of PD which showed an autosomal recessive pattern of inheritance (Kitada et al., 1998). Although rare in PD cases overall, *PRKN* mutations account for around 50% of cases of juvenile PD in patients under 25 years of age, and around 9% of total early-onset PD cases (<50 years of age) (Lücking et al., 2000; Lill, 2016). These highly-penetrant *PRKN* mutations result in loss-of-function of the protein Parkin, an E3 ubiquitin ligase which targets damaged mitochondria for degradation by autophagy - a process known as mitophagy (Narendra et al., 2012). Homozygous *PRKN* mutation carriers show comparable clinical presentations to typical late-onset PD and are responsive to treatment with L-DOPA, and whilst symptoms appear much earlier they progress more slowly. Despite severe DA neuron loss in the SNpc, *PRKN* PD patients rarely show Lewy body formation (Schulte and Gasser, 2011).

1.1.2.2.2 PINK1

Autosomal recessive mutations in *PTEN-induced putative kinase 1 (PINK1)* are found in around 4% of cases of early-onset PD (Bonifati et al., 2005). Like mutations in Parkin, *PINK1* mutations are highly penetrant and result in loss-of-function of the PINK1 protein by disrupting its kinase activity (Silvestri et al., 2005). PINK1 functions upstream of Parkin in the mitophagy pathway to detect mitochondrial damage and recruit Parkin to damaged mitochondria (Narendra et al., 2012). Accordingly,

homozygous *PINK1* mutations result in a clinical phenotype similar to that of mutations in *PRKN* with classic motor dysfunction that presents with an early onset but slow progression and good response to L-DOPA (Li et al., 2005). Unlike *PRKN* mutations, patients with *PINK1* mutations have Lewy body pathology and often display psychiatric symptoms and dementia which more closely resembles sporadic PD (Samaranch et al., 2010). Indeed, evidence suggests that heterozygous mutations in *PINK1* may contribute to sporadic PD (Kumazawa et al., 2008).

1.1.2.3 Sporadic PD

Whilst much progress has been made in identifying monogenic forms of familial PD, 90% of PD cases are defined as sporadic and are likely caused by a complex interaction between environmental influences and genetic susceptibility factors which cumulatively lead to disease.

1.1.2.3.1 Genetic risk factors

Genome-wide association studies (GWAS) have identified various genetic polymorphisms and mutations which associate with incidence of PD, though few have been functionally validated in cellular models (Table 1.3). Further mutations in genes responsible for monogenic PD including *SNCA* and *LRRK2* have been identified as PD risk factors, highlighting the role of these genes in sporadic disease as well as dominant familial PD (Satake et al., 2009). Of the risk factors identified to date, heterozygous mutations in the *glucocerebrosidase (GBA*) gene display the greatest increase in PD risk with a >5-fold and up to 20-fold increased risk compared to non-carriers (Lesage et al., 2011; Anheim et al., 2012). Homozygous *GBA* mutations primarily cause Gaucher's disease, a recessive lysosomal storage disease, where Parkinsonian symptoms and Lewy body pathology are occasionally observed (Sidransky and Lopez, 2012). One estimation predicts that 5-25% of all PD cases have *GBA* mutations which contributes to development of disease, making mutations in GBA the highest genetic risk factor for PD identified to date (Beavan and Schapira, 2013; Schapira, 2015). A common feature of several neurodegenerative diseases such as Alzheimer's disease, frontotemporal dementia (FTD) and PD is the aggregation of hyper-phosphorylated microtubule-associated protein tau (MAPT) within neurons (Morris et al., 1999). Genetic variants in the *MAPT* gene have been linked to PD in Caucasian but not Asian populations (Golbe Lawrence I. et al., 2001; Satake et al., 2009). Further GWAS analyses continue to identify novel risk loci for PD in both new and previously identified genes, and although the individual effect of

each locus on disease risk is small, cumulative risk may be significant and highlights the importance of genetic variation in complex diseases such as PD (Nalls et al., 2014; Chang et al., 2017). The use of next-generation sequencing methods such as exome sequencing can be used to identify disease-related genes in PD which may be too rare to be detected by GWAS studies and with too low a penetrance for detection by familial linkage analysis (Bonifati, 2014).

1.1.2.3.1 Environmental factors

Various environmental risk factors have been associated with an increased risk of developing PD, such as head trauma, anxiety or depression, use of beta-blockers and pesticide exposure (Bellou et al., 2016). Conversely, protective effects have been described for physical activity, smoking and coffee consumption (Bellou et al., 2016). Genetic risk factors likely interact with environmental risk factors to influence PD risk. Whilst gene-interaction studies are often challenging to validate due to variations in population samples and difficulties in obtaining robust data on environmental and lifestyle exposures, some genome-wide interaction studies have found associations between gene variants and smoking and coffee consumption in PD (Hamza et al., 2011; Hill-Burns et al., 2013). Further studies are needed to better understand the link between these environmental factors and the risk of PD.

Table 1.3. Risk factors with estimated odds ratio (OR) ≥ 1.1 for developing PD (adapted and updated from Lesage and Brice, 2012 and Nalls et al., 2014). Highlighted loci have been well-validated as PD risk factors.

PARK locus	Map locus	Gene	Risk Variants	OR	References
PARK1/4	4q21	*SNCA*	Promoter Rep1; SNPs	1.2-2.9	Pals et al., 2004; Ritz et al., 2012; Campêlo et al., 2017
PARK8	12q12	*LRRK2*	R1628P, S1647T, G2385R	1.2-3	Tan, 2006; Zheng et al., 2011; Zhang et al., 2016
PARK16	1q32	*RAB7L1?*	Multiple SNPs	1.3-1.4	Yan et al., 2011; Zhou et al., 2014; Wang et al., 2016
PARK17	4p16	*GAK*	Multiple SNPs	1.1-1.5	Zhou et al., 2014
PARK18	6p21	*HLA-DRA*	Multiple SNPs	1.3	Zhou et al., 2014
N/A	1q21	*GBA*	>300 SNPs inc. N370S, L444P	>5-20	Mao et al., 2013 O'Regan et al., 2017
N/A	17q21	*MAPT*	Multiple SNPs	1.4	Charlesworth et al., 2012; Davis et al., 2016
N/A	1q22	*SYT11*	Multiple SNPs	1.2	Int. PD Genomics Consortium, 2011
N/A	4p15	*BST1*	Multiple SNPs	0.9-1.2	Nalls et al., 2014
N/A	2q21	*ACMSD*	Multiple SNPs	1.1	Int. PD Genomics Consortium, 2011
N/A	2q24	*STK39*	Multiple SNPs	1.1	Int. PD Genomics Consortium, 2011
N/A	12q24	*CCDC62*	Multiple SNPs	1.1	Nalls et al., 2014
N/A	10q26	*INPP5F*	rs117896735	1.6	Nalls et al., 2014
N/A	16p11	*STX1B*	Multiple SNPs	1.1	Nalls et al., 2014
N/A	3p24	*SATB1*	rs4073221	1.1	Chang et al., 2017
N/A	4q26	*CAMK2D*	rs78738012	1.1	Chang et al., 2017
N/A	5q12	*ELOVL7*	rs2694528	1.2	Chang et al., 2017
N/A	6p22	*ZNF184*	rs9468199	1.1	Chang et al., 2017

1.1.3 Mechanisms of Disease in PD

1.1.3.1 Oxidative stress

Reactive oxygen species (ROS) are produced in cells as a by-product of ATP generation in mitochondria. During the process of oxidative phosphorylation via the electron transport chain on the inner mitochondrial membrane, electron leakage at Complexes I and III can reduce molecular oxygen to form the ROS superoxide (O_2^-) which can be further dismutated to hydrogen peroxide (H_2O_2) (Cadenas et al., 1977).

Whilst playing an important role in various cell signalling pathways, excess ROS can be quenched into less damaging molecules or scavenged by antioxidant compounds (Shukla et al., 2011). Oxidative stress occurs when the level of ROS production outweighs antioxidant activity in the cell, leading to disruption of a wide-range of cellular processes including exocytosis, protein production and degradation pathways, damage to DNA and ER stress (Brieger et al., 2012). Oxidative stress can damage mitochondrial DNA (mtDNA), leading to disruption of the mitochondrial electron transport chain and changes in ATP production as well as leakage of further ROS into the cytoplasm. High levels of oxidative stress lead to ATP depletion and cell death (Beal, 2005).

Neurons are particularly vulnerable to oxidative stress due to their high metabolic rates and oxygen consumption combined with a lower abundance of antioxidant compounds (Nunomura et al., 2006). DA metabolism within neurons in the SNpc may itself contribute to oxidative stress as oxidation of cytosolic DA produces dopamine-quinones which have been shown to cause mitochondrial dysfunction and interact with PD-related proteins such as parkin, DJ-1 and α-synuclein (Lee et al., 2003; LaVoie et al., 2005; Girotto et al., 2012; da Silva et al., 2013). Furthermore, mice with reduced expression of the dopamine transporter vesicular monoamine transporter 2 (VMAT2) show increased oxidised DA which results in DA-mediated toxicity and DA neuronal death (Caudle et al., 2007).

1.1.3.2 Mitochondrial dysfunction

As the primary source of ROS in neurons, mitochondria are closely associated with the oxidative stress which contributes towards the pathogenesis of PD. Deficiencies in Complex I of the mitochondrial respiratory chain result in increased production of ROS and such deficiencies have been shown in sporadic PD patients (Schapira et al., 1990; Hattingen et al., 2009). Complex I inhibitors such as 1-methyl-4-phenyl-

1,2,3,6-tetrahydropyridine (MPTP) and the pesticide rotenone cause DA neuron death and PD-like symptoms (Langston et al., 1983; Betarbet et al., 2000). MPTP is taken up by astrocytes and oxidised to MPP+ before uptake into DA neurons where it accumulates in the mitochondria and inhibits Complex I (Mizuno et al., 1987). As well as Complex I inhibition, rotenone also causes oxidative protein damage and leads to intracellular inclusions which are morphologically similar to Lewy bodies (Sherer et al., 2003).

The familial PD disease-linked mitochondrial proteins PINK1 and Parkin are important for normal mitochondrial function as well as their role in mitophagy of damaged mitochondria (Scarffe et al., 2014). PD patients with Parkin mutations show a decrease in Complex I activity, and mutations in PINK1 lead to respiratory dysfunction and ROS accumulation (Müftüoglu et al., 2004; Piccoli et al., 2008). Consistent with a loss-of-function model for these mutations, PINK1 and Parkin knockout mice show mitochondrial dysfunction and increased sensitivity to oxidative stress (Palacino et al., 2004; Gautier et al., 2008). Additionally, defects in mitochondrial morphology caused by loss of the PINK1 homolog in *Drosophila* can be rescued by parkin overexpression and suggests that PINK1 acts upstream of Parkin in a common pathway to regulate mitochondrial function (I.E. Clark et al., 2006). The autosomal recessive PD gene *DJ-1* has been linked to the maintenance of mitochondrial function during oxidative stress, with DJ-1 knockout *Drosophila* and mice show reduced mitochondrial membrane potential and increased fragmentation (McCoy and Cookson, 2011). Furthermore, DJ-1 can rescue PINK1 loss of function in *Drosophila* which suggests that DJ-1 may act downstream of PINK1 in the maintenance of mitochondrial integrity (Hao et al., 2010). Hence, mitochondrial dysfunction is intrinsically linked to both sporadic and familial PD and likely plays a central role in disease pathogenesis (Winklhofer and Haass, 2010).

1.1.3.3 Axonal transport defects

Due to their polar morphology and long process length, neurons are particularly reliant on the cellular transport of macromolecules and organelles such as mitochondria along the length of the axon between the cell body and distal synapse. This occurs via loading of the cargo onto the motor proteins dynein and kinesin which move along microtubule tracks away from the cell body (anterograde transport) or towards it (retrograde transport) (Hirokawa and Takemura, 2005). Disruptions in axonal transport are an early pathogenic feature of a range of neurodegenerative diseases including PD, Alzheimer's disease, amyotrophic lateral sclerosis, and hereditary

spastic paraplegia (reviewed by Millecamps and Julien, 2013). Indeed, reduced kinesin levels are seen in the SN of early-stage sporadic PD which precede dopaminergic loss and other morphological changes, and reductions in dynein are observed at later disease stages (Chu et al., 2012).

α-synuclein protein is synthesised in the cell body and transported to the synapse via axonal transport (Kahle et al., 2000). Aggregates and fibrils of α-synuclein also undergo bi-directional axonal transport in neurons (Volpicelli-Daley et al., 2011; Freundt et al., 2012). Studies show that the familial A30P and A53T mutations in α-synuclein reduce its transport in neurons compared to wild-type protein, and α-synuclein oligomers disrupt the kinesin-microtubule interaction and decrease microtubule stability (Saha et al., 2004; Prots et al., 2013). This could provide a mechanism for the accumulation of aggregated α-synuclein in the cell body seen in PD.

In addition, axonal transport is an energy-intensive process. Reduced cellular ATP levels due to mitochondrial dysfunction in turn leads to impaired localisation of mitochondria at the synapse and an imbalance of retrograde mitochondrial transport towards the cell body (De Vos et al., 2007; Morfini et al., 2007; Arnold et al., 2011). This results in ATP depletion at the synapse and likely contributes to axon degeneration, consistent with the 'dying back' pathology seen in DA neurons in PD (Burke and O'Malley, 2013). Indeed, mutations in the familial PD genes *PINK1* and *Parkin* that disrupt mitochondrial function are also associated with defects in axonal transport of mitochondria via the mitochondrial transport regulator Miro1 (Wang et al., 2011; Liu et al., 2012; Moller et al., 2017). As well as mutations in *PINK1* and *Parkin*, the familial R1441C and Y1699C Roc-COR mutations in *LRRK2* have been shown to disrupt anterograde and retrograde axonal transport of mitochondria both in rat cortical neurons *in vitro* and in an *in vivo Drosophila* genetic model (Godena et al., 2014).

Therefore, it is clear that axonal transport is defective in both familial and sporadic PD prior to neuronal death and this may occur as a result of mitochondrial dysfunction or α-synuclein aggregation, whilst perpetuating the severity of both mechanisms to contribute to disease pathogenesis (De Vos et al., 2008; Lamberts et al., 2015).

1.1.3.4 Protein aggregation

Cells must regulate the balance between protein synthesis and the rate of clearance in order to maintain protein homeostasis (proteostasis). Protein aggregation occurs

because of the failure of protein degradation pathways to maintain cellular proteostasis. The two major protein degradation pathways in cells are the proteasome, a cytoplasmic protease complex which recognises select ubiquitinated substrates, and the lysosome, which degrades larger aggregates and organelles via the process of autophagy. Autophagy can be further sub-divided into microautophagy, macroautophagy and chaperone-mediated autophagy (CMA), and can be aided by formation of perinuclear inclusion bodies known as aggresomes (discussed further in section 1.3.3.4).

A hallmark pathological feature of PD, the Lewy body, represents an intracellular accumulation of aggregated α-synuclein in affected neurons. The aggregation of α-synuclein is promoted by familial PD mutations which further suggests a direct link between protein aggregation and PD pathogenesis (Burré et al., 2015). The presence of Lewy bodies raises the question of their cytotoxicity and relevance for driving of disease. In support of their toxicity, Lewy bodies correlate closely with PD progression and are found in highest abundance in regions with greatest neuronal loss (Braak et al., 2004). In addition, the density of Lewy bodies correlates with cognitive impairment both in PD and dementia with Lewy bodies (DLB) (Kövari et al., 2003). However, these correlations do not show that Lewy bodies themselves drive neuronal loss, and indeed Lewy body pathology is not found in certain genetic forms of PD such as those with Parkin mutations (Schulte and Gasser, 2011).

Alternatively, Lewy bodies may represent a protective cellular response to sequester misfolded proteins. Increased number of α-synuclein inclusion bodies correlated with reduced neuronal α-synuclein toxicity in a *Drosophila* PD model, and inhibition of the proteasome stimulated α-synuclein inclusion formation but reduced neuronal loss in a chemically-induced rat PD model (Sawada et al., 2004; Chen and Feany, 2005). Indeed, evidence suggests that α-synuclein fibril formation mitigates the toxicity of α-synuclein oligomers (Olanow et al., 2004; Wakabayashi et al., 2007). As well as α-synuclein, Lewy bodies are positive for many components of protein degradation pathways such as ubiquitin, p62 and proteasomal subunits; autophagy-associated LC3, GABARAP and NBR1; and γ-tubulin and histone deacetylase 6 (HDAC6) involved in aggresome formation (Table 1.1; Wakabayashi et al., 2013). The similarity between Lewy bodies and aggresomes, the molecular mechanisms of which are discussed further in section 1.3.3.4, has led to widespread suggestions that Lewy bodies are the result of an aggresome-related mechanism which sequesters toxic α-synuclein in a cytoprotective role (McNaught et al., 2002; Olanow et al., 2004; Tanaka et al., 2004).

1.2 LRRK2

LRRK2 is a large, 144 kilobase (kb) gene spanning 51 exons that encodes a complex 286 kDa, 2527 amino acid cytoplasmic protein with seven functional domains (Figure 1.1). At the N-terminus of LRRK2, structural armadillo and ankyrin domains are followed by the eponymous leucine rich repeat domain which adopts a parallel ß-strand conformation to aid protein-protein interactions (Mills et al., 2014). LRRK2 is a member of the ROCO protein superfamily of Ras-like GTPases, hence activity is mediated by its catalytic core which consist of a Ras of complex (Roc) GTPase domain and a carboxyl terminal of Roc (COR) domain followed by a MAP kinase kinase kinase (MAPKKK) domain (Bosgraaf and Van Haastert, 2003). At the C-terminus of LRRK2 is a WD40 repeat domain which is predicted to adopt a beta-propeller tertiary structure conformation (Stirnimann et al., 2010; Mills et al., 2012).

As described in Section 1.1.2.1.2, mutations in *LRRK2* are the most common genetic cause of PD found to date. Over 40 different missense variants have currently been identified in *LRRK2*, however only a minority segregate strongly in familial PD lineages with high penetrance and confirmed pathogenicity. These pathogenic mutations all cluster in the catalytic core of LRRK2 and affect its enzymatic activity, with R1441C/G/H and Y1699C in the Roc-COR tandem GTPase domain and G2019S and I2020T in the adjacent kinase domain (Mata et al., 2005; Khan et al., 2005). A further familial *LRRK2* mutation, N1437H, has been found to segregate with PD in several Scandinavian families but has yet to be identified elsewhere (Aasly et al., 2010; Puschmann et al., 2012). The most common dominant mutation in *LRRK2* is G2019S, which is found in an estimated 4% of familial PD patients (Healy et al., 2008). The frequency of the G2019S mutation is population-specific, with high frequencies in the Ashkenazi Jewish and North African Berber populations but much rarer in Asian populations (Tan et al., 2005). LRRK2 G2019S has also been found in sporadic disease at rates of up to 2% in one analysis of European sporadic PD patients (Lesage et al., 2007). Whilst lifetime penetrance can reach up to 45% in North African populations, the frequency of healthy G2019S *LRRK2* mutation carriers has been reported at up to 3% in the Moroccan Berber population (Benamer and de Silva, 2010). In addition to familial pathogenic mutations in *LRRK2*, single-nucleotide polymorphism variants such as G2385R in the WD40 domain and R1628P in the COR domain cause up to a two-fold increased risk of developing PD (Tan et al., 2010). To date, these variants have been found only in PD patients of Asian descent such as those from Chinese and Malaysian populations and have not been seen in European

PD cases (Gopalai et al., 2014; Zhang et al., 2016). Conversely, a protective *LRRK2* R1398H variant which reduces the risk of developing PD has been reported in both Caucasian and Asian populations (Chen et al., 2011; Ross et al., 2011; Heckman et al., 2014).

LRRK2 has been widely studied in attempts to gain further understanding of the pathogenic mechanisms underlying PD. Clinically, the phenotype of LRRK2-related PD shows a strong resemblance to that of sporadic PD with a late disease onset, slow progression and classical parkinsonian symptoms as well as a good response to L-DOPA treatment (Li et al., 2014). In addition, neuropathological analysis shows universal SNpc neuronal loss as well as Lewy body pathology in the majority of LRRK2 patients, with some variation between individuals with different LRRK2 point mutations (Khan et al., 2005). This suggests that pathogenic mechanisms resulting from LRRK2 mutations are likely shared with sporadic forms of PD, hopefully providing insight into common molecular defects.

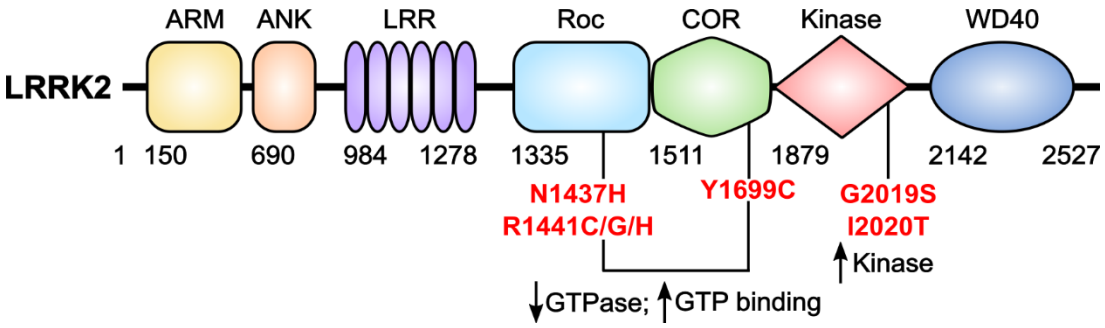

Figure 1.1. Domain structure and mutations of LRRK2. LRRK2 is a multidomain, 2527 amino acid protein with GTPase and kinase activity mediated by its catalytic core. From N-terminus to C-terminus, the domains of LRRK2 comprise the armadillo (ARM) and ankyrin (ANK) repeat domains, leucine-rich repeat domain (LRR), Ras of complex (Roc) domain, C-terminal of Roc (COR) domain, kinase domain, and WD40 domain. The confirmed pathogenic mutations in LRRK2 cluster within its catalytic core and include N1437H in the Roc GTPase domain which increases GTP binding to LRRK2 , R1441C/G/H in the Roc domain and Y1699C in the COR tandem domain which also decrease LRRK2 GTPase activity, and the G2019S and I2020T mutations in the kinase domain which increase kinase activity.

1.2.1 Expression of LRRK2

LRRK2 is expressed at high levels in the brain as well as the liver and heart, with highest expression seen in the kidneys and lungs (Paisán-Ruíz et al., 2004). Analysis of post-mortem human tissue shows that LRRK2 is constitutively expressed in neuronal cells as well as glial cells such as astrocytes and microglia (Miklossy et al., 2006). The relative expression of LRRK2 within nigral neurons is high, and murine studies have indicated that it is also expressed in striatal neurons and cortical regions (Simón-Sánchez et al., 2006; Higashi et al., 2007b; Giesert et al., 2013; West et al., 2014). High levels of LRRK2 are seen within Lewy bodies in the brains of patients with PD as well as those with dementia with Lewy bodies (DLB), as well as to a lower extent in patients with sporadic PD, suggesting that LRRK2 is a major component of Lewy body pathology (Zhu et al., 2006; Higashi et al., 2007a; Guerreiro et al., 2013).

1.2.2 LRRK2 activity

As a member of the ROCO subfamily of Ras-GTPase proteins, LRRK2 has GTPase activity mediated by its Roc-COR tandem domain as well as kinase activity from its adjacent kinase domain (Lewis, 2009). All known pathogenic, familial LRRK2 mutations cluster within these Roc, COR and kinase domains to affect their catalytic function which suggests that the enzymatic activity of LRRK2 is a key part of its role within disease (Figure 1.1).

1.2.2.1 GTPase activity

The Roc domain of LRRK2 provides its GTPase activity, with the C-terminal COR domain thought to aid dimerization (Sen et al., 2009). Small Ras GTPases typically act as molecular switches in signalling pathways, inactive when bound by GDP and becoming active upon GTP binding to activate downstream effectors. This activation cycle is facilitated by the binding of specific regulatory proteins such as guanine nucleotide exchange factors (GEFs) which aid GTP binding, and GTPase activating proteins (GAPs) which promote hydrolysis of GTP to return the GTPase to its inactive state (Takai et al., 2001). Putative LRRK2 GEFs and GAPs include ARHGEF7 which increases the GTPase activity of LRRK2 *in vitro,* and ArfGAP1 which binds and increases the GTP hydrolysis of LRRK2 (Haebig et al., 2010; Xiong et al., 2012). Interestingly, both ARHGEF7 and ArfGAP1 are phosphorylated by LRRK2, thus indicating a reciprocal level of regulation between these proteins.

A different hypothesis suggests that rather than conventional regulation by GEFs and GAPs, LRRK2 is part of a family of GTPases which is instead regulated by homodimerization in a nucleotide-dependent manner (Gasper et al., 2009). Guanosine binding is proposed to stimulate the interaction between the Roc domains of each monomer and create the active site to provide GTPase activity, which subsequently hydrolyses GTP to return the Roc domains to their inactive conformation. This is supported by evidence that GTP-binding regulates LRRK2 dimerisation and the fact that LRRK2 is primarily found as a GTP-bound dimer (Sen et al., 2009; Berger et al., 2010; Biosa et al., 2013).

Familial PD mutations in the LRRK2 Roc-COR tandem GTPase domain such as R1441C/G/H and Y1699C consistently show reduced GTPase activity compared to the wild-type protein (Ito et al., 2007; Li et al., 2007; Daniëls et al., 2011). These mutations as well as the N1437H mutation increase GTP binding to LRRK2 (West et al., 2007; Aasly et al., 2010). Importantly, all pathogenic LRRK2 Roc-COR mutations localise to the interface between the Roc and COR domains, indicating that the interaction between these domains is critical for GTPase function (Gotthardt et al., 2008). The R1441C/G/H mutations disrupt the interaction and dimerisation between the two domains, and Y1699C increases the interaction between domains to reduce the conformational flexibility (Gotthardt et al., 2008; Daniëls et al., 2011).

The downstream effectors of LRRK2 GTPase activity are not currently well-described, therefore the mechanisms of GTPase disruption which lead to LRRK2-induced pathogenicity remain uncertain. Disruption of GTPase activity confers cellular toxicity in a yeast model and this is linked to alterations in vesicle trafficking and autophagosome accumulation, suggesting a role for GTPase activity in endosomal trafficking (Xiong et al., 2010). Models have implicated familial LRRK2 GTPase mutations in a range of phenotypes including disrupted axonal transport and microtubule-association, neurotransmission and autophagy, as will be discussed in Section 1.2.3, and the exact role of GTPase activity in these mechanisms requires further investigation (Li et al., 2009; Tong et al., 2009; Godena et al., 2014; Tsika et al., 2014; Nguyen and Moore, 2017).

1.2.2.2 Kinase activity

The kinase domain of LRRK2 mediates serine/threonine kinase activity for phosphorylation of protein substrates. It comprises a two-lobed structure with an ATP-binding site in the cleft between the lobes, which together with an activation loop

forms the active site of the kinase domain (Gilsbach and Kortholt, 2014). Autophosphorylation of the activation loop promotes a conformational change to allow ATP and substrate binding, thus producing the 'active' state of kinase activity. LRRK2 has multiple known autophosphorylation sites in its kinase activation loop including S2032 and T2035 which are important for regulation of kinase activity (Greggio et al., 2008; Li et al., 2010).

Familial PD mutations in the LRRK2 kinase domain, G2019S and I2020T, both alter the kinase activity of LRRK2. The most common LRRK2 mutation is G2019S and has been consistently shown to increase the kinase activity of LRRK2, whereas I2020T has been shown to both increase it or slightly decrease it in different assays (West et al., 2005; Jaleel et al., 2007; Luzón-Toro et al., 2007; Ray et al., 2014). Both G2019S and I2020T mutations are situated in the inter-lobe cleft region of the kinase domain near to the active site. G2019S is predicted to increase the stability of the active conformation via addition of a hydrogen bond, therefore increasing kinase activity, and evidence suggests that I2020T acts in a similar manner (Gilsbach et al., 2012; Ray et al., 2014).

Like LRRK2 GTPase effectors, investigations into the downstream targets of LRRK2 kinase activity have proved challenging and until recently, the only robust *in vivo* phosphorylation target of LRRK2 was shown to be LRRK2 itself via autophosphorylation (Greggio et al., 2009; Sheng et al., 2012). Additional *in vitro* evidence shows that LRRK2 phosphorylates moesin at a site which regulates moesin-actin binding for interaction between the cytoskeleton and plasma membrane (Jaleel et al., 2007). Moesin is part of the ezrin, radixin, and moesin (ERM) family of proteins which localise to the filopodia of growing neurites to regulate their dynamics, suggesting that LRRK2 has a role in regulation of neurite outgrowth (Parisiadou et al., 2009). More recently, LRRK2 has been shown to phosphorylate multiple Rab GTPases including Rab8a and Rab10 *in vivo*, providing evidence for a role of LRRK2 in membrane trafficking and vesicle dynamics (discussed further in section 1.2.3) (Ito et al., 2016; Steger et al., 2016; Steger et al., 2017).

The pathogenic effects of LRRK2 mutations which alter its kinase activity can be reduced using LRRK2 kinase inhibitors, therefore LRRK2 kinase activity is an attractive therapeutic target (Taymans and Greggio, 2016). Accordingly, LRRK2 kinase inhibitors are currently in various stages of preclinical and phase 1 clinical evaluation for treatment of PD (Alessi and Sammler, 2018).

1.2.2.3 Regulation of LRRK2

LRRK2 commonly exists as a homodimer complex *in vivo* which is a feature of many self-regulatory and membrane-associated signalling kinases (Klemm et al., 1998). As discussed in the previous section, autophosphorylation of the LRRK2 kinase domain promotes the active kinase conformation and acts as a self-regulatory mechanism (Greggio et al., 2008). Dimers of wild-type LRRK2 exhibit higher levels of kinase activity compared to LRRK2 monomers and show increased localisation at the cell membrane (Berger et al., 2010). Dimerisation of LRRK2 may therefore provide a mechanism of self-regulation through autophosphorylation and altered subcellular localisation. Pathogenic LRRK2 mutations have been shown to alter the dimerisation of LRRK2 and suggest a role for disrupted dimerisation in the pathogenesis of PD. The R1441C Roc domain mutation destabilises LRRK2 dimer formation, whereas the G2019S and I2020T kinase domain mutations show increased dimer formation (Deng et al., 2008; Sen et al., 2009). The importance of kinase activity in dimer formation is evident due to disrupted dimer formation as a result of artificial kinase-dead LRRK2 mutations (Sen et al., 2009).

As a dual-enzyme, further mechanisms of LRRK2 self-regulation may occur through interactions between its GTPase and kinase activities. *In vitro* studies show that whilst GTP binding has no effect on LRRK2 kinase activity, the kinase function of LRRK2 requires an intact Roc-COR GTPase domain (Liu et al., 2010; Taymans et al., 2011). However, GTP binding-deficient mutations in the Roc domain cause decreased kinase activity *in vivo* and disrupt the dimerisation and stability of LRRK2 (Biosa et al., 2013). Therefore, the GTP binding capacity likely affects kinase activity through changing the dimerisation state of LRRK2 to regulate kinase function (summarised in Figure 1.2) (Gilsbach and Kortholt, 2014). Conversely, the kinase activity may regulate GTPase function through multiple autophosphorylation sites located at the GTP-binding pocket of the Roc domain including threonine-1348 and threonine-1368 to increase GTPase function (Greggio et al., 2009; Gloeckner et al., 2010; Liu et al., 2015). However, other studies show that kinase-dead LRRK2 shows increased GTPase activity compared to wild-type LRRK2 and the G2019S mutant does not affect GTPase activity (Pungaliya et al., 2010; Ho et al., 2016). Taken together, these results indicate that a complex relationship of self-regulation exists between the GTPase and kinase activities of LRRK2 with regulation in both directions likely contributing to overall LRRK2 function.

As well as auto-regulation, there is evidence of upstream regulation of LRRK2. Phosphorylation of LRRK2 by casein kinase 1α (CK1α) modulates its recruitment to Golgi-derived vesicles which suggests that kinase regulation of LRRK2 is important for Golgi maintenance (Chia et al., 2014). Additionally, cAMP-dependent protein kinase (PKA) phosphorylates LRRK2 to modulate its interaction with the signal transduction protein 14-3-3, in turn regulating the kinase activity of LRRK2 (Muda et al., 2014). More recently, Rab29 has been identified as an upstream regulator of LRRK2 kinase function and Golgi localisation (Purlyte et al., 2018).

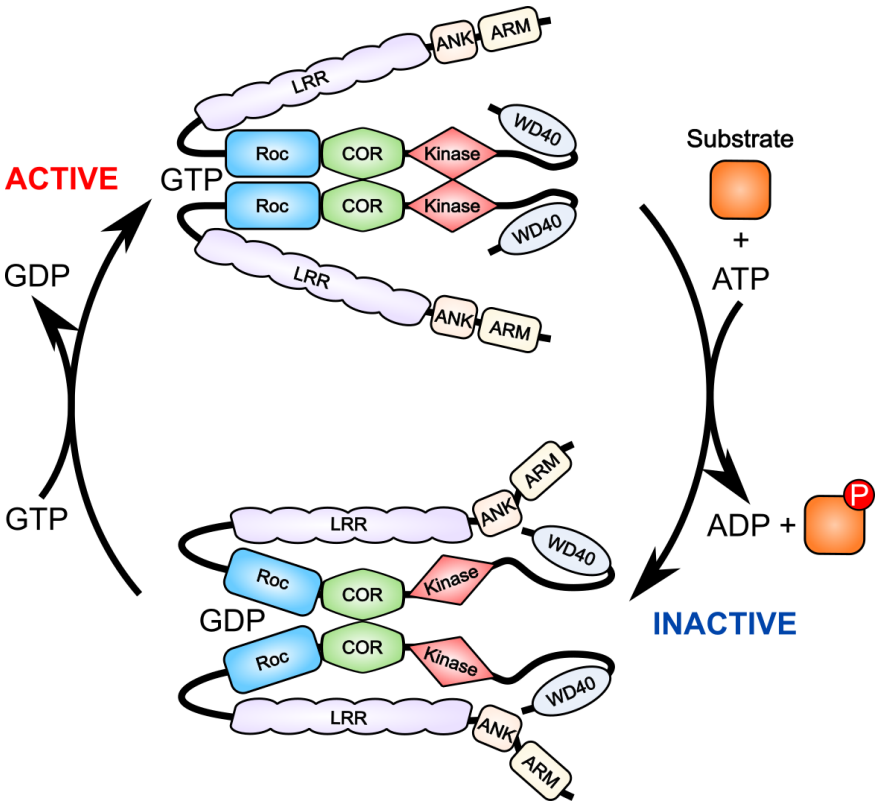

Figure 1.2. Model of LRRK2 dimer activation. The COR domain in each LRRK2 monomer mediates dimer form formation. In the GDP-bound inactive state, the Roc domains are flexible and upon GTP binding they undergo a conformational change to increase their proximity, allowing autophosphorylation of the kinase domain activation loops and activating the LRRK2 dimer. Active LRRK2 phosphorylates protein substrates via the hydrolysis of ATP to ADP. Adapted from Gilsbach and Kortholt (2014) under permission from the Creative Commons Attribution License.

1.2.3 Cellular roles of LRRK2

The large, multi-domain structure of LRRK2 with multiple repeat domains is indicative of a structural role in protein binding, and its dual catalytic core of GTPase and kinase activity suggests multiple roles in cellular signalling pathways. LRRK2 associates with multiple compartments within the cell including the microtubule cytoskeleton, the ER, Golgi, outer mitochondrial membrane, and endosomal vesicles (Biskup et al., 2006; Hatano et al., 2007). Many of these are membranous structures and evidence implicates LRRK2 in a range of cellular roles such as regulation of cytoskeleton dynamics, neurite outgrowth, endosomal function, autophagy and Wnt signalling (MacLeod et al., 2006; Shin et al., 2008; Alegre-Abarrategui et al., 2009; Berwick and Harvey, 2012).

1.2.3.1 Endosomes

The strong localisation of LRRK2 with membrane-associated compartments within the mammalian brain includes a range of vesicular structures such as endosomes, lysosomes, microtubule-associated vesicles and mitochondria, suggesting that LRRK2 is involved in vesicle biogenesis and dynamics (Biskup et al., 2006; Hatano et al., 2007). LRRK2 localises to vacuoles which are positive for endosomal and lysosomal markers in brains of PD and DLB patients and these vacuoles are increased in disease compared to controls which suggests a link to pathogenesis (Higashi et al., 2009). Functionally, the dimerisation and recruitment of LRRK2 to endosomal-autophagic structures such as autophagosomes precedes a role in the regulation of autophagy (Schapansky et al., 2014). LRRK2 also localises to late endosomes and lysosomes and regulates lysosomal transport in *Drosophila* (Dodson et al., 2012).

Multiple studies have shown that LRRK2 interacts with the Rab family of membrane-associated small GTPases, thus providing a mechanism for LRRK2 membrane localisation (Cookson, 2016). Rabs are lipidated proteins which incorporate into a variety of cellular membranes and recruit effector proteins in a GTP-dependent manner to regulate membrane trafficking within the cell (Zhen and Stenmark, 2015). LRRK2 was first shown to interact with Rab5b at synaptic vesicles to regulate their endocytosis at the synapse (Shin et al., 2008). The *Drosophila* LRRK2 homolog interacts with the endosomal transport-associated Rab7 to negatively regulate perinuclear lysosome clustering (Dodson et al., 2012). In addition, LRRK2 interacts with Rab7L1, a candidate risk gene in sporadic PD which is linked to the clearance of

Golgi-derived vesicles via autophagy (MacLeod et al., 2013; Beilina et al., 2014). Rab7L1, Rab8a and Rab10 are kinase substrates of LRRK2 both *in vitro* and in cells, with LRRK2-mediated phosphorylation of the effector-binding switch-II motifs of these proteins controlling their membrane localisation (Steger et al., 2016; Liu et al., 2018). Importantly, PD-associated pathogenic LRRK2 mutations increase phosphorylation of Rabs and induce their membrane localisation which can lead to an excessive accumulation of inactive membrane-bound Rabs (Steger et al., 2017; Yu et al., 2018). Increased phosphorylation of Rab7L1 by LRRK2 G2019S can stimulate LRRK2 autophosphorylation and recruitment to the trans-Golgi network, multiple components of which are linked to PD (Liu et al., 2018). LRRK2 Y1699C phosphorylates Rab8a to increase its activity in promoting lipid storage which may result in enlarged lipid droplets, a phenotype associated with PD pathogenesis (Yu et al., 2018). Additionally, Rab8a phosphorylation by LRRK2 R1441C, Y1699C and G2019S mutants causes centrosome polarity and cohesion deficits as a result of abnormal Rab8a localisation at the centrosome (Madero-Pérez et al., 2018). Elevated phosphorylation of Rab10 by LRRK2 R1441C and G2019S is also stimulated by a PD-associated familial mutation in the membrane-trafficking component VPS35, providing evidence that LRRK2 and VPS35 function in a common pathway to regulate endosomal sorting which is disrupted in PD (Mir et al., 2018). Together, the interaction and phosphorylation of various Rabs by LRRK2 points to an important role for LRRK2 in membrane biology in multiple compartments of the cell, and implicates mutant LRRK2-mediated Rab mislocalisation and defective vesicle trafficking as key pathogenic mechanisms in PD.

1.2.3.2 Autophagy

Multiple studies have implicated LRRK2 in the regulation of autophagy, however often with conflicting reports of its precise role (Manzoni, 2017). LRRK2 co-localises with cytoplasmic multi-vesicular bodies (MVBs) and autophagic vacuoles both in post-mortem human brain and human cell cultures (Alegre-Abarrategui et al., 2009). Knockdown of LRRK2 in cells increases autophagic activity as evidenced by an increased turnover of the autophagy marker LC3-II, indicating that LRRK2 acts as a negative regulator of autophagy (Alegre-Abarrategui et al., 2009). However, studies in LRRK2-knockout mice show age-dependent accumulation of ubiquitinated protein as well as the autophagic markers LC3-II and p62 in the kidney which indicates a defect in autophagy caused by lack of LRRK2 (Tong et al., 2010; Tong et al., 2012). Studies using LRRK2 kinase inhibitors have produced further contradictory results. In

one study, inhibition of LRRK2 kinase activity results in an increase of the autophagy markers LC3-II and p62 due to stimulated autophagic induction, suggesting that LRRK2 kinase activity normally functions to negatively regulate the induction of autophagy (Manzoni et al., 2013). In contrast, subsequent studies have shown reduced autophagic flux and defective cargo clearance after LRRK2 kinase inhibition which suggests that LRRK2 kinase activity promotes autophagic clearance (Schapansky et al., 2014; Esteves et al., 2015).

Although the function of LRRK2 as an up- or down-regulator of autophagy remains unclear, pathogenic mutations in LRRK2 have consistently been shown to disrupt the autophagic process. Pathogenic R1441C LRRK2 impairs autophagy as evident through an accumulation of MVBs and increased p62 levels (Alegre-Abarrategui et al., 2009). Induced pluripotent stem cell (iPSC)-derived dopaminergic neurons from sporadic and LRRK2 G2019S-associated PD patients show accumulation of autophagic vacuoles as a result of failed autophagic clearance, and this is thought to occur through disruption of microtubule-dependent autophagosome trafficking (Sánchez-Danés et al., 2012; Arduíno et al., 2012). Furthermore, R1441C and G2019S transgenic mice show an accumulation of autophagic vacuoles in cortical and striatal neurons which is accompanied by dopaminergic cell death and reduced neurite complexity (Ramonet et al., 2011). Consistent with these results, R1441C and G2019S LRRK2 mutants inhibit autophagy and potentiate age-related autophagic dysfunction in a *C. elegans* model of PD whilst wild-type LRRK2 increases autophagic flux (Saha et al., 2015). A recent study shows that LRRK2 interacts with and phosphorylates p62, with pathogenic mutant LRRK2 increasing this phosphorylation, and this may provide a mechanism by which LRRK2 regulates ubiquitinated cargo recruitment for autophagy (Kalogeropulou et al., 2018).

Together, these results indicate that LRRK2 has a role in regulating autophagy which is disrupted by pathogenic LRRK2 mutations. Disparities between studies that indicate LRRK2 acts as both a positive and negative regulator of autophagy and acts at both the initiation and clearance stage may reflect differences between models, cell types and experimental conditions, as well as the ability for LRRK2 to control autophagy in various ways as part of different protein complexes (Manzoni, 2017).

As well as the autophagic process itself, LRRK2 forms and co-localises with aggresomes after inhibition of the proteasome as part of the cellular response to promote misfolded protein degradation by autophagy (Waxman et al., 2009). Some evidence suggests that both wild-type and G2019S LRRK2 overexpression disrupts

aggresome formation after proteasomal inhibition and causes accumulation of LC3-II/p62-positive protein aggregates which is indicative an autophagic defect (Bang et al., 2016). These studies suggest a role for LRRK2 in the regulation of aggresome formation to aid autophagic protein degradation under proteasomal inhibition (described in section 1.3.3.4.2.3).

1.2.3.3 Microtubule dynamics

LRRK2 co-localises with microtubules and this is enhanced by pathogenic LRRK2 mutations, suggesting that the cytoskeleton is implicated in LRRK2-mediated disease (Kett et al., 2012; Caesar et al., 2013; Godena et al., 2014). LRRK2 directly interacts with β-tubulin via its Roc domain and phosphorylates it *in vitro* to increase microtubule stability (Gillardon, 2009; Law et al., 2014). LRRK2 G2019S increases this phosphorylation and an I2020T transgenic mouse exhibits increased microtubule polymerisation and impaired locomotive ability, suggesting that increased phosphorylation of β-tubulin by mutant LRRK2 may contribute to pathogenesis by dysregulating microtubule polymerisation (Gillardon, 2009; Maekawa et al., 2012). Evidence also implicates LRRK2 in the regulation of α-tubulin acetylation. LRRK2-knockout mice show increased levels of acetylated α-tubulin which can be rescued by overexpression of wild-type human LRRK2, indicating that LRRK2 reduces α-tubulin acetylation (Law et al., 2014). Conversely, sporadic and G2019S PD patients show decreased levels of tubulin acetylation in non-neuronal cells compared to controls which suggests that excessive LRRK2-mediated deacetylation is a feature of disease (Esteves et al., 2015). Therefore, evidence shows that LRRK2 has a role at the microtubule to regulate tubulin dynamics via phosphorylation and acetylation.

Acetylation of tubulin at lysine-40 promotes the structural stability of microtubules and binding of motor proteins required for axonal transport (discussed in detail in section 1.3.3.3). Pathogenic LRRK2 GTPase mutants show an abnormal association with deacetylated microtubules and disruption of axonal transport of mitochondria, also causing motor defects in a transgenic *Drosophila* model (Godena et al., 2014). These phenotypes can be reversed by increasing microtubule acetylation via knockdown or inhibition of HDAC6, suggesting that LRRK2 regulates axonal transport via changes in microtubule acetylation and this mechanism is disrupted in LRRK2-associated PD. In addition, pathogenic LRRK2 mutants disrupt neurite outgrowth which is a further microtubule-dependent process. Overexpression of LRRK2 R1441C, G2019S and I2020T mutants causes significantly decreased neurite length and reduced branching

in cortical neurons compared to wild-type LRRK2, whereas knockdown of LRRK2 increases branching (MacLeod et al., 2006; Parisiadou et al., 2009).

LRRK2 also regulates microtubule dynamics though an interaction with the microtubule-associated protein tau. Tau stimulates neurite outgrowth by binding to microtubules and enhancing their assembly (Avila et al., 2004). LRRK2 phosphorylates tau at the microtubule surface both directly and in a complex with GSK3ß to reduce its tubulin binding, thereby reducing microtubule stability and promoting their disassembly (Kawakami et al., 2012, Kawakami et al., 2013). Furthermore, pathogenic LRRK2 G2019S and I2020T mutants show hyperphosphorylation of tau which may lead to further microtubule destabilisation.

Finally, LRRK2 may influence axonal development and maintenance of neuronal structure indirectly through regulation of Wnt signalling pathways which are known modulators of microtubule morphology (Wallingford and Habas, 2005; Ahmad-Annuar et al., 2006; Ciani and Salinas, 2007). LRRK2 interacts with the dishevelled phosphoprotein DVL1, a key regulator of the neuronal Wnt pathway, and acts as a membrane-associated scaffold for Wnt signalling (Sancho et al., 2009; Berwick and Harvey, 2012). This interaction requires the LRRK2 Roc-COR domain and is altered by pathogenic Roc-COR mutations. DVL1 is a known regulator of small GTPases and LRRK2 Roc-COR mutations may disrupt the activity of LRRK2 partly through disturbed interactions with proteins such as DVL1 (Habas et al., 2001; Sancho et al., 2009).

Altogether, multiple reports suggest that LRRK2 is a regulator of microtubule dynamics through its interactions with tubulin, tau, Wnt signalling pathways and regulation of microtubule acetylation, and therefore influences microtubule-dependent processes such as axonal transport and neurite outgrowth. Furthermore, disruption of these mechanisms by LRRK2 mutations may contribute to pathogenesis in LRRK2-mediated PD.

1.3 HDAC6

In mammals, the histone deacetylase (HDAC) protein family consists of 18 different HDACs which are divided into four classes based on sequence similarities (Table 1.4). Class I, II and IV HDACs are referred to as classical histone deacetylases which require Zn^{2+} as a cofactor for deacetylase activity and are inhibited by the pan-HDAC inhibitors such as trichostatin A (TSA) (Rao et al., 2012). Class I HDACs include HDAC1, HDAC2, HDAC3 and HDAC8 and have a predominantly nuclear localisation, whereas Class II HDACs can shuttle between the nucleus and cytoplasm depending on nuclear localisation and export signals (de Ruijter et al., 2003). Class II HDACs are sub-divided into Class IIa comprising HDAC4, HDAC5, HDAC7 and HDAC9, and Class IIb comprising HDAC6 and HDAC10. Class IIb HDACs are unique in having a second catalytic domain compared to the single deacetylase domain of all other proteins in the HDAC family (Seto and Yoshida, 2014). In contrast to other HDACs, Class III HDACs are a separate group of nicotinamide adenine dinucleotide (NAD^+)-dependent deacetylases known as sirtuins (SIRT1 to SIRT7) with a conserved core domain which is not inhibited by TSA (Seto and Yoshida, 2014). Finally, the Class IV group consists only of HDAC11 which shares sequence homology with both Class I and II HDACs (Gao et al., 2002).

HDACs were first described as nuclear histone deacetylases that regulate chromatin structure and gene expression, although a far more diverse range of non-histone substrates in multiple cellular compartments has since been described (Table 1.4). HDAC6 is a Class IIb deacetylase found primarily in the cytoplasm and is unique in its microtubule association and deacetylation substrates compared to other HDAC family members, including α-tubulin, HSP90, cortactin and β-catenin (Valenzuela-Fernández et al., 2008). These substrates place HDAC6 as a regulator of multiple cellular pathways including microtubule dynamics and cell motility, protein chaperone function and protein degradation (Li et al., 2013). HDAC6 has been linked to a range of neurodegenerative diseases and is a component of Lewy bodies in PD (Kawaguchi et al., 2003; Simões-Pires et al., 2013). Therefore, it is of great interest for understanding the pathogenic mechanisms underlying disease.

Table 1.4. HDAC protein family. Adapted from Seto and Yoshida, 2014.

Class	Subclass	Protein	Localisation	Non-histone substrates
I		HDAC1	*Nucleus*	*p53, STAT3*
		HDAC2	*Nucleus*	*GR, eIF4E, STAT3*
		HDAC3	*Mainly nuclear*	*MEF2, SRY, PCAF, NF-Kb, STAT1/3*
		HDAC8	*Nucleus/cytoplasm*	*SMC3, ARID1A*
II	**a**	HDAC4	*Nucleus/cytoplasm*	*p53, Runx2, MLP, HIF1α, DNAJB8*
		HDAC5	*Nucleus/cytoplasm*	*Unknown*
		HDAC7	*Nucleus/cytoplasm/ mitochondria*	*HIF1α*
		HDAC9	*Nucleus/cytoplasm*	*MEF2*
	b	HDAC6	*Mainly cytoplasmic*	*α-tubulin, HSP90, cortactin, β-catenin, Prx, Tat*
		HDAC10	*Mainly cytoplasmic*	*HSP70*
III		SIRT1	*Nucleus/cytoplasm*	*p53*
		SIRT2	*Nucleus/cytoplasm*	*α-tubulin, p53, FOXO1/3a*
		SIRT3	*Nucleus/mitochondria*	*Acetyl-CoA Synthetase 2, GDH*
		SIRT4	*Mitochondria*	*MCD, PDH, MCCC*
		SIRT5	*Mitochondria*	*CPS1, cytochrome c*
		SIRT6	*Nucleus*	*CtIP*
		SIRT7	*Nucleus/nucleolus/ cytoplasm*	*PAF53, CDK9, GABPß1*
IV		HDAC11	*Nucleus/cytoplasm*	*Unknown*

1.3.1 Structure and expression of HDAC6

HDAC6 is a 131 kDa, 1215 amino acid protein with three main functional domains (Figure 1.3). This includes two catalytic deacetylase domains (HD1 and HD2) which mediate substrate deacetylation and a C-terminal zinc finger (ZnF-UBP) domain which binds ubiquitin with high affinity (Seigneurin-Berny et al., 2001). Additionally, HDAC6 has a cytoplasmic dynein motor-binding linker between its deacetylase domains (Li et al., 2012). The cellular localisation of HDAC6 is regulated by nuclear localisation and leucine-rich nuclear export signals at its N-terminus which control shuttling between the nucleus and cytoplasm (Verdel et al., 2000; Bertos et al., 2004). Furthermore, human HDAC6 possesses an additional cytoplasmic retention signal consisting of eight consecutive Ser-Glu-containing tetradecapeptide repeats (SE14) between its HD2 and ZnF-UBP domains which is not present in the murine protein (Bertos et al., 2004). HDAC6 is expressed ubiquitously in most cell types, with particularly high levels seen in the testis, kidney, liver and brain (Zhang et al., 2008). Within the brain, HDAC6 expression is highest in cerebral cortex, cerebellum and hippocampus (Uhlén et al., 2015).

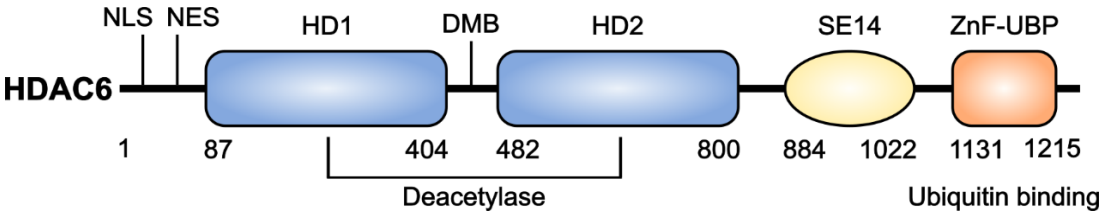

Figure 1.3. Domain structure of HDAC6. HDAC6 is a 1215 amino acid protein with two catalytic deacetylase domains (HD1 and HD2) separated by a dynein binding (DMB) domain, with a C-terminal zinc finger ubiquitin-binding (ZnF-UBP) domain. Nuclear localisation (NLS) and nuclear export (NES) sequences are found at the N-terminus, as well as an SE14 cytoplasmic retention signal between the HD2 and ZnF-UBP domains.

1.3.2 HDAC6 activity

The two deacetylase domains of HDAC6 provide its deacetylase activity for the removal of acetyl groups from substrate lysine residues. The cytoplasmic substrates of HDAC6 deacetylase activity include tubulin, cortactin and heat shock protein 90 (Hsp90) (Hubbert et al., 2002; Kovacs et al., 2005; Zhang et al., 2007). Whilst both deacetylase domains are required for full HDAC6 activity, the HD1 domain is only marginally catalytically active alone *in vitro* and the HD2 domain provides the majority of the deacetylase activity (Zhang et al., 2006; Zou et al., 2006; Miyake et al., 2016). Instead, the N-terminal HD1 domain is thought to primarily interact with substrates and provide specificity of deacetylation. Indeed, most HDAC6 inhibitors target the second deacetylase domain (HD2) to abolish deacetylase activity (Haggarty et al., 2003). These inhibitors chelate Zn^{2+} ions in the catalytic pocket via their zinc binding group (Wang et al., 2018).

HDAC6 is a phosphoprotein with multiple phosphorylation sites identified *in vitro* (Brush et al., 2004; Beausoleil et al., 2004; Linding et al., 2007; Kettenbach et al., 2011). Phosphorylation may therefore regulate the cellular activity and function of HDAC6. In cells, phosphorylation of HDAC6 serine-22 in the N-terminus correlates with increased HDAC6 tubulin deacetylase activity although a direct link has not been shown (Chen et al., 2010). Phosphorylation of HDAC6 serine-458 in the dynein motor-binding domain and serine-1035 in the C-terminus both increase HDAC6 deacetylase activity, whereas phosphorylation of tyrosine-570 in the C-terminal deacetylase domain decreases deacetylase activity (Deribe et al., 2009; Watabe and Nakaki, 2011; Williams et al., 2013). At present, the mechanisms by which phosphorylation of HDAC6 at these sites alters its deacetylase activity are not well understood. In addition to phosphorylation, acetylation of HDAC6 at sites within the N-terminal nuclear localisation signal reduces HDAC6 tubulin deacetylase activity as well as blocking its import into nucleus, suggesting that acetylation is important for regulating the balance between the cytoplasmic and nuclear functions of HDAC6 (Liu et al., 2012). HDAC6 deacetylase activity is also reduced by S-nitrosylation, a further post-translational modification whereby nitric oxide is covalently attached to a cysteine residue (Okuda et al., 2015). Finally, evidence shows that HDAC6 deacetylase activity is inhibited by an interaction with the focal adhesion scaffold protein paxillin, indicating that protein-protein interactions can regulate HDAC6 activity (Deakin and Turner, 2014).

1.3.3 Cellular roles of HDAC6

HDAC6 has multiple cellular roles and this is reflected in its diverse range of substrate proteins and interactors. This includes proteins involved in cell motility and transport, protein degradation, transcription and the immune response, placing HDAC6 as a key regulator of cell growth, proteostasis and survival.

1.3.3.1 Tubulin acetylation

The first deacetylase substrate of HDAC6 to be described was α-tubulin (Hubbert et al., 2002). Together with ß-tubulin, α-tubulin monomers are the building blocks of the microtubule cytoskeleton on which a wide range of cellular processes rely. Microtubules are comprised of heterodimers of α-tubulin and ß-tubulin which associate to form linear protofilaments, with lateral bridges between thirteen protofilaments forming the classical 25 nm microtubule structure (Desai and Mitchison, 1997). In cells, most microtubules consist of thirteen tubulin protofilaments although numbers can vary for individual microtubule populations and microtubules synthesised *in vitro* (Chrétien et al., 1992; Díaz et al., 1998).

Microtubules are highly dynamic and constantly undergo structural remodelling through cycles of polymerisation and depolymerisation, so-called dynamic instability, which allows their role in a wide range of cellular functions (Desai and Mitchison, 1997). Microtubules undergo a range of post-translational modifications (PTMs) which can regulate their dynamic stability, interactions with microtubule-associated proteins (MAPs) and binding of motor proteins (Janke and Bulinski, 2011). The most common, acetylation of lysine-40 on α-tubulin, occurs through the action of α-tubulin N-acetyltransferase 1 (αTAT1), whereas deacetylation is mediated by HDAC6 and SIRT2 (Hubbert et al., 2002; North et al., 2003; Akella et al., 2010; Shida et al., 2010) (Figure 1.4). Unlike HDAC6, SIRT2 deacetylase activity is dependent on the coenzyme nicotinamide adenine dinucleotide (NAD^+) and appears to be preferentially active during mitosis in actively dividing cells (Vaquero et al., 2006).

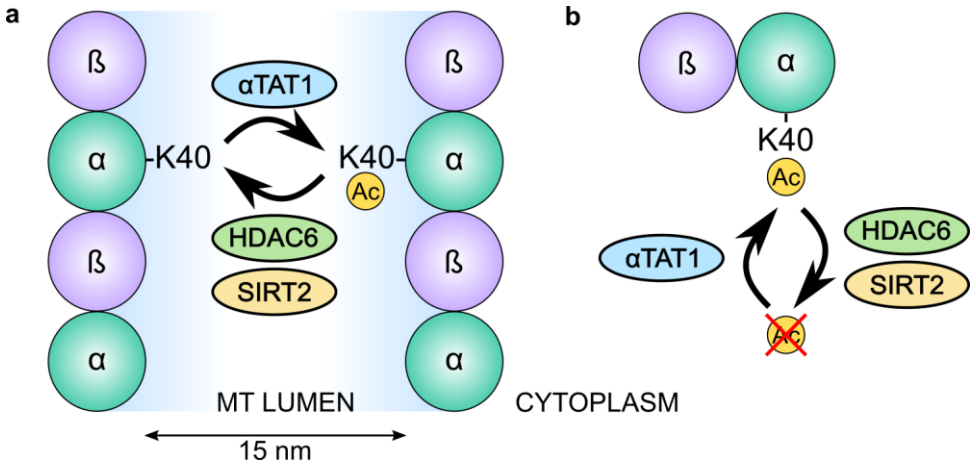

Figure 1.4. Mechanisms of microtubule acetylation. Lysine-40 of α-tubulin is acetylated by αTAT1 acetyltransferase or deacetylated by HDAC6 or SIRT2 deacetylases, proposed to occur either inside the microtubule lumen (a) or on free tubulin dimers in the cytoplasm prior to microtubule polymerisation (b).

Unlike most other external PTM sites, lysine-40 of α-tubulin is located at the luminal-facing inside surface of microtubules (Dráberová et al., 2000). The intraluminal location of lysine-40 raises the question of how it is accessed by αTAT1, HDAC6 or SIRT2 to regulate its acetylation (shown in Figure 1.4). The simplest explanation is that these enzymes enter the microtubule at its open ends and diffuse along the microtubule length to access lysine-40 of α-tubulin. This is supported by evidence that αTAT1 shows a higher affinity for microtubule extremities and acetylates lysine-40 in a longitudinal manner (Coombes et al., 2016; Ly et al., 2016). HDAC6 interacts with the microtubule plus-end tracking protein EB1 which suggests that it also enters the microtubule lumen via the open ends (Zilberman et al., 2009). An alternative explanation is that transient cracks or irregularities in the microtubule structure act as entry points for access to the lumen (Janke and Montagnac, 2017). In support of this, αTAT1 binds to the external microtubule wall which would allow its entry at sites along the entire microtubule length (Howes et al., 2014). In addition, when HDAC6 does deacetylate polymerised microtubules *in vitro* it shows a stochastic pattern of deacetylation along their length which points to it having local points of access (Miyake et al., 2016). Together, these results suggest that a range of mechanisms likely contribute to the localisation of αTAT1 and HDAC6 into the microtubule lumen, with both end-mediated and local assess providing entry. In fact, some *in vitro* studies have shown a preference for HDAC6 to deacetylate free tubulin dimers rather than polymerised microtubules and this could avoid HDAC6 having to regularly enter the microtubule lumen, though the *in vivo* relevance of this requires further investigation (Figure 1.4b; Zhao et al., 2010; Miyake et al., 2016).

Acetylation of α-tubulin at lysine-40 has traditionally been associated with microtubule stability. This is largely due to observations that decreased acetylation due to HDAC6 overexpression leads to increased susceptibility of microtubules to depolymerisation, whereas increased acetylation from HDAC6 inhibition leads to a reduction in dynamic microtubules (Matsuyama et al., 2002; Tran et al., 2007). However, presence of HDAC6 protein itself can inhibit microtubule dynamics irrespective of its catalytic activity and effect on acetylation (Zilberman et al., 2009). In addition, lysine-40 acetylation does not protect microtubules against depolymerisation and takes place after stabilisation has occurred (Palazzo et al., 2003; Janke and Bulinski, 2011). Instead, it is suggested that acetylation protects microtubules against mechanical aging by weakening lateral protofilament interactions to increase flexibility and resilience to stress (Portran et al., 2017). This is reinforced by the observation that

curved sections of microtubules show high levels of acetylation, thus allowing them to flex without breaking (Xu et al., 2017).

1.3.3.2 Cell motility

HDAC6-mediated microtubule deacetylation regulates cell motility by increasing focal adhesion dynamics required for rapid cell migration (Tran et al., 2007). This is suggested to occur due to tubulin deacetylation increasing the pool of dynamic microtubules as well as directing the localised recruitment of adhesion-forming complexes to promote migration. In support of this, overexpression of HDAC6 promotes chemotactic cell movement in fibroblasts whereas inhibition of HDAC6 prevents motility (Hubbert et al., 2002; Tran et al., 2007). In addition, HDAC6-mediated deacetylation of the F-actin binding protein cortactin promotes cortactin localisation at the cell periphery, therefore increasing cortactin binding to F-actin to promote actin polymerisation and aid actin-dependent motility (Zhang et al., 2007). Therefore, deacetylation of tubulin and cortactin by HDAC6 regulates the actin and microtubule cytoskeleton to control cell motility.

1.3.3.3 Axonal transport

An important role of microtubules is to act as tracks for the intracellular transport of cargoes such as proteins and organelles which occurs via the molecular motor proteins kinesin and cytoplasmic dynein. This process of intracellular transport is essential for neuronal cells which require distal axons to be provided with newly-synthesised proteins and organelles such as mitochondria for synaptic function, as well as the removal of damaged components back towards the cell body for recycling. This is known as axonal transport (Figure 1.5).

Acetylation of lysine-40 was initially associated with increased binding of the motor protein kinesin-1 to microtubules *in vitro* and increased transport along them (Reed et al., 2006). However, more recent *in vitro* experiments show no effect of acetylation on kinesin-1 binding and motility (Walter et al., 2012; Kaul et al., 2014). *In vivo* evidence suggests that acetylation stimulates kinesin-1-mediated transport but it is not sufficient to drive kinesin-1 translocation to axons (Hammond et al., 2010). Lysine-40 acetylation has been shown to increase the recruitment of cytoplasmic dynein to microtubules (Dompierre et al., 2007). In addition, axonemal dynein shows increased motility in the presence of acetylated microtubules (Alper et al., 2014). Therefore, microtubule acetylation may promote axonal transport both by maintaining structural

integrity of microtubules to provide stable tracks and influencing the motility of motor proteins along them. This suggests that HDAC6-mediated deacetylation of microtubules acts to increase their dynamics and reduce the preference for axonal transport along deacetylated regions.

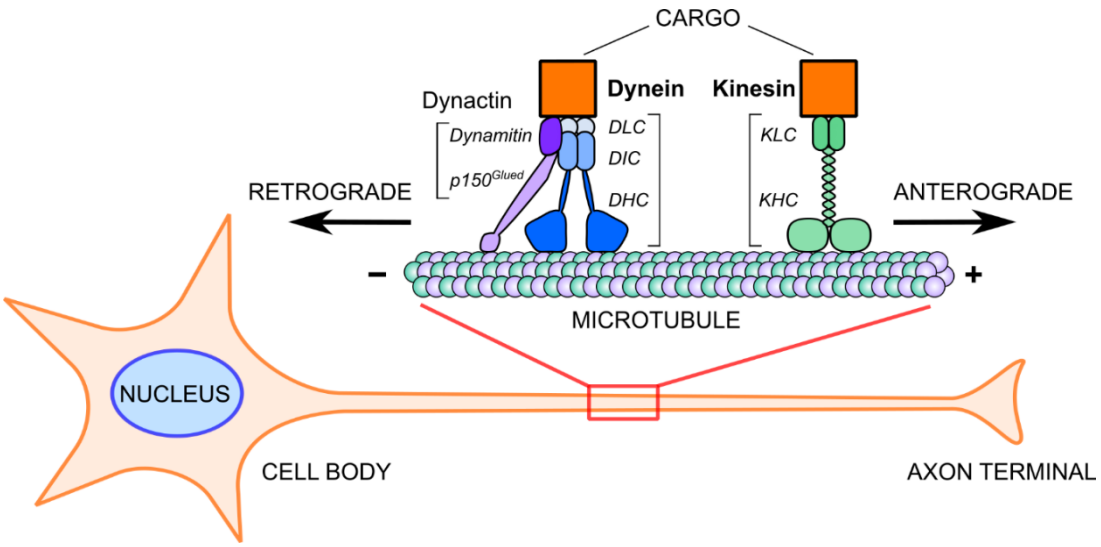

Figure 1.5. Axonal transport in neurons. The motor proteins cytoplasmic dynein and kinesin transport cargoes along microtubule tracks within the neuronal axon. Retrograde transport towards the cell body occurs towards the minus (-) microtubule end and is mediated by cytoplasmic dynein in co-operation with the activator dynactin. Cytoplasmic dynein consists of two heavy chains (DHC) which bind the microtubule and hydrolyse ATP to provide movement, together with intermediate (DIC) and light chains (DLC) which aid cargo binding. The dynactin adaptor binds to both the DIC and microtubules and consists of the subunits dynamitin and $p150^{Glued}$. Anterograde transport towards the axon terminal occurs towards the plus (+) microtubule end and is mediated by kinesin. Kinesin consists of two heavy chains (KHC) for microtubule binding and ATP hydrolysis as well as light chains (KLC) for cargo binding.

1.3.3.4 Protein degradation

As well as its role as a tubulin deacetylase, HDAC6 is an important regulator of cellular protein degradation pathways through its association with ubiquitin. HDAC6 binds to ubiquitin chains on proteins targeted for degradation via its C-terminal ubiquitin-binding domain (ZnF-UBP) and aids their progression down one of several pathways of degradation (outlined in Figure 1.7) (Hook et al., 2002). Proteins undergo two main routes of degradation in eukaryotic cells; the ubiquitin-proteasome system (UPS) and the autophagy pathway. These pathways ensure that the balance between protein synthesis and turnover is maintained to preserve proteostasis and promote cell survival.

1.3.3.4.1 Ubiquitin-Proteasome System

Small, high-turnover cytoplasmic and nuclear proteins are primarily degraded by the proteasome, as well as misfolded proteins in the endoplasmic reticulum (ER) (Ciechanover, 2006). The proteasome is a multimeric, barrel-shaped protease complex found in the cytoplasm which passes target protein substrates through its central core where they are reduced to peptides to be further degraded by cytoplasmic peptidases. The mammalian proteasome complex, the 26S proteasome, consists of a core 20S protease capped with two 19S regulatory subunits (Zwickl et al., 1999).

Proteasome substrates are targeted for degradation by tagging with ubiquitin, a small 8.5 kDa protein which is covalently bonded to lysine residues at the C-terminus of the target protein (Ciehanover et al., 1978). This targeted substrate ubiquitination requires the activity of three enzymes – firstly, E1 ubiquitin-activating enzyme hydrolyses ATP to activate ubiquitin before forming a thioester-linked conjugate with the ubiquitin molecule; E2 ubiquitin-conjugating enzyme subsequently receives the ubiquitin from E1; and finally E3 ubiquitin-ligase transfers the ubiquitin from E2 to the target substrate (Rubinsztein, 2006). Human cells utilise over 600 different E3 ubiquitin-ligases which target a wide range of proteins and provide substrate specificity (Li et al., 2008). The ubiquitin tag on the substrate can itself undergo further cycles of ubiquitination at one of seven of its internal lysine residues, leading to formation of a polyubiquitin chain which specifies the fate of the target protein. Polyubiquitin chains linked via lysine-48 (K48) of ubiquitin typically form a recognition signal for substrate degradation by the proteasome (Richly et al., 2005). The proteasome requires substrate proteins to undergo unfolding to pass through its

central pore, and therefore is unsuitable for degradation of larger protein complexes or aggregates as well as organelles, and these substrates are instead degraded by the lysosome in the process of autophagy.

HDAC6 appears to have a key role in promoting the autophagy of ubiquitinated substrates over their degradation by the proteasome. HDAC6 shows a high binding affinity for ubiquitin which stabilises the substrate-associated polyubiquitin chains and disrupts their recognition by the proteasome (Hook et al., 2002; Boyault et al., 2006). In addition, HDAC6 interacts with the chaperone p97/VCP, a promoter of proteasomal degradation and ubiquitin turnover, to regulate the progression of polyubiquitinated proteins down the pathway of autophagy (Figure 1.7) (Boyault et al., 2006).

1.3.3.4.2 Autophagy

Large protein complexes and organelles which are inaccessible to the proteasome are degraded by the process of autophagy. There are three types of autophagy, all of which converge on substrate degradation at the lysosome; these are microautophagy, macroautophagy and chaperone-mediated autophagy (CMA) (Figure 1.6). These sub-types of autophagy differ in their complexity of the mechanism of substrate delivery to the lysosome. The simplest type of autophagy is microautophagy, whereby cytoplasmic substrates are directly engulfed by invagination of the lysosomal membrane without the need for any adaptor or intermediate proteins, therefore HDAC6 is not involved in this process (Marzella et al., 1981).

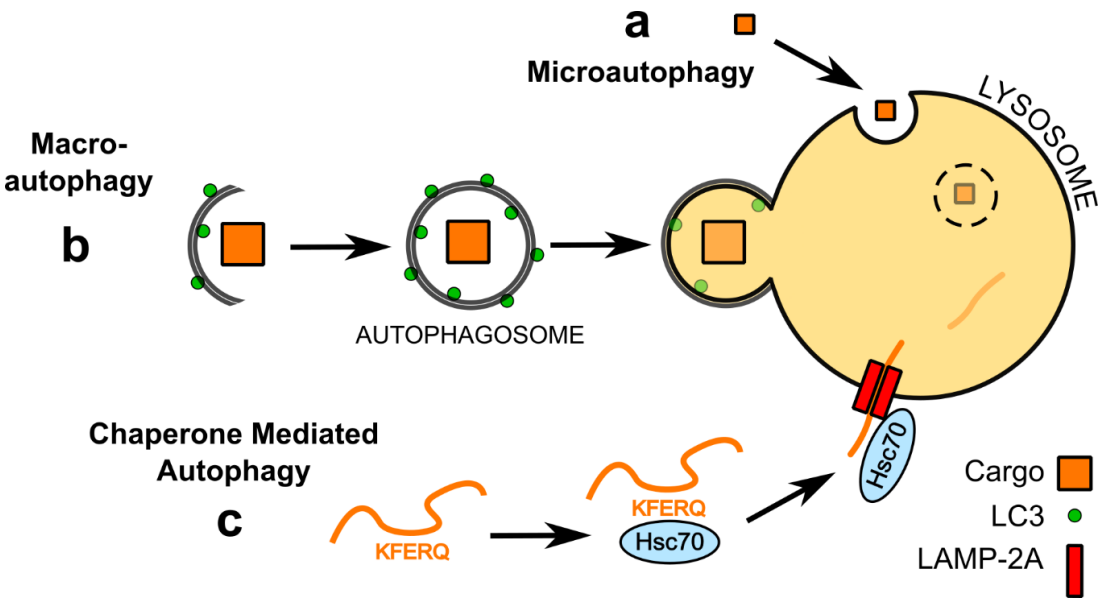

Figure 1.6. Micro, Macro and Chaperone Mediated Autophagy pathways. a) In microautophagy, cytoplasmic cargoes are directly engulfed by invagination of the lysosomal membrane and degraded by lysosomal hydrolases. b) In macroautophagy, a double isolation membrane forms and elongates around the cargo to form an autophagosome which is marked by the membrane-associated protein LC3. The mature autophagosome is transported to the MTOC where it fuses with the lysosome and the cargo is degraded by lysosomal hydrolases. c) In chaperone mediated autophagy, target proteins containing the KFERQ motif are recognised by Hsc70 and transported to the lysosome where they bind LAMP-2A and are unfolded for translocation into the lysosome for degradation.

1.3.3.4.2.1 Chaperone-mediated autophagy

CMA targets single proteins which contain a Lys-Phe-Glu-Arg-Gln (KFERQ) motif for lysosomal degradation via the chaperone activity of heat shock response proteins (Dice, 1990). HDAC6 forms a cytoplasmic complex with the heat shock protein Hsp90 and heat shock factor 1 (HSF1) in which Hsp90 prevents activation of HSF1 (Boyault et al., 2007). HDAC6 detects ubiquitinated proteins and subsequently deacetylates Hsp90, which causes the complex to dissociate and allows the activation of the heat shock response (Figure 1.7) (Kovacs et al., 2005). Protein chaperones such as heat shock cognate 70 (Hsc70) then transport the ubiquitinated proteins to the lysosome (Dice, 1990). At the lysosomal membrane, the complex then binds lysosomal-associated membrane protein 2A (LAMP-2A) and unfolds before being translocated into the lysosomal lumen for substrate degradation (Kaushik and Cuervo, 2012).

In addition to the activation of CMA, HDAC6-mediated deacetylation of Hsp90 promotes its chaperone activity to maintain protein folding and stability in the cytoplasm and preventing aggregation (Zhao and Houry, 2005). Interestingly, activated Hsp90 forms a complex with LRRK2 and stabilises it to prevent LRRK2 proteasomal degradation (Wang et al., 2008). Therefore, HDAC6 activity has a role in maintaining protein stability via Hsp90 as well as degradation of unwanted or misfolded proteins.

1.3.3.4.2.2 Macroautophagy

Macroautophagy, hereafter simply referred to as autophagy, is the bulk degradation of large cytoplasmic protein complexes and organelles such as mitochondria and requires many adaptor and intermediate proteins. In autophagy, a double-membrane vacuole known as the autophagosome forms around the substrates and fuses with the lysosome to form autophagolysosomes, thereby internally degrading the substrates using lysosomal hydrolases (Yorimitsu and Klionsky, 2005). Whilst autophagy is present at basal levels in many cells in order to maintain the turnover of proteins and organelles, it can be further induced by cellular stresses such as starvation to promote cell survival under nutrient deprivation under regulation of kinases such as mammalian target of rapamycin (mTOR) (Glick et al., 2010). In addition, selective autophagy can recognise specific substrates such as aggregated proteins, damaged organelles or intracellular pathogens through selective autophagy receptors such as the ubiquitin-binding proteins p62/SQSTM1, neighbour of BRCA1 gene 1 (NBR1), optineurin or nuclear dot protein 52 kDa (NPD52) which link the

ubiquitinated substrate to the autophagic machinery for removal (Zaffagnini and Martens, 2016).

To initiate the process of autophagy, a double membrane structure termed the isolation membrane is formed through the recruitment of various autophagy regulator proteins such as Unc-51-like autophagy activating kinase (ULK1). The origin of this membrane is thought to be mainly from the ER and other pre-existing cellular membrane formations such as the Golgi, endosomes and plasma membrane (Axe et al., 2008; English et al., 2009; Hayashi-Nishino et al., 2009; Ylä-Anttila et al., 2009). More recently, the isolation membrane has been shown to form using lipids from the mitochondria-associated ER membrane at ER-mitochondria contact sites (Hailey et al., 2010; Hamasaki et al., 2013). Once the isolation membrane is established, activated ULK1 phosphorylates Beclin-1 to recruit further proteins which make up the Class III PI3 kinase complex required for autophagosome elongation (Glick et al., 2010). The microtubule-associated protein light chain 3 (LC3) is processed to form LC3-II which localises to the autophagosome membrane and acts as an autophagosome marker (Barth et al., 2010). At this stage the target ubiquitinated substrates are recruited to the developing autophagosome by autophagy receptors such as p62/SQSTM1, NBR1, optineurin or NDP52 which bind both ubiquitin on the substrate and LC3 on the autophagosome membrane (Kirkin et al., 2009; Zaffagnini and Martens, 2016). As p62/SQSTM1 itself is targeted to autophagosomes as well as the substrate, accumulation of p62/LC3-positive inclusions within cells indicates a failure of completion of autophagy, and are found in a range of neurodegenerative diseases which show intracellular protein aggregation (Wooten et al., 2006). Polyubiquitin chains formed through linkage of ubiquitin at lysine-63 (K63) have been shown to target substrates for degradation by autophagy (Olzmann and Chin, 2008; Tan et al., 2008).

Autophagosomes can be formed at many locations in the cytoplasm, and whilst lysosomes can also be widely-distributed they are often concentrated at perinuclear regions such as the microtubule-organising centre (MTOC) (Jongsma et al., 2016). Therefore, after autophagosomes have formed around and isolated their target substrates in a certain cytoplasmic region they are transported towards the MTOC to allow fusion with lysosomes and subsequent substrate degradation (Kimura et al., 2008). This is especially important in polarised cells such as neurons where distal autophagosomes must often travel large distances along the axon towards the cell body where mature lysosomes are enriched (Lee et al., 2011; Maday et al., 2012). Such retrograde transport of autophagosomes occurs along microtubules and is

mediated by the motor protein cytoplasmic dynein and its activator dynactin (Katsumata et al., 2010; Ikenaka et al., 2013; Cheng et al., 2015). This occurs through recruitment of the small GTPase Rab7 to autophagosomes which interacts with Rab-interacting lysosomal protein (RILP) and acts as a bridge between the autophagosome and the dynein/dynactin complex (Nakamura and Yoshimori, 2017).

Once autophagosomes have been transported towards the lysosome-rich regions at the cell body or MTOC, they are fused with lysosomes to initiate degradation of their substrate cargoes with the resulting structures termed autolysosomes (Jahreiss et al., 2008). For autophagy of targeted substrates such as ubiquitinated protein aggregates, HDAC6 recruits the cortactin-dependent actin remodelling machinery to assemble the actin network which stimulates autophagosome-lysosome fusion (Lee et al., 2010) (Figure 1.7). This process also requires the actin motor protein myosin VI and its cargo adaptor Tom1 (Tumbarello et al., 2012). Fusion occurs through recruitment of tethering complexes by various Rab proteins such as Rab7 which promote membrane fusion through the action of soluble N-ethylmaleimide-sensitive factor attachment protein receptors (SNAREs) (Itakura et al., 2012). Autophagic substrates are degraded within the autolysosome by lysosomal acid hydrolases and resulting metabolites such as amino acids are recycled back into the cytoplasm for reuse (Pu et al., 2016). Evidence suggests that p62/SQSTM1 interacts with HDAC6 at the point of autophagosome-lysosome fusion to regulate its deacetylase activity for cortactin deacetylation (Yan et al., 2013). Absence of p62 results in excessive cortactin deacetylation and leads to over-assembly of F-actin in the cytoplasm and aggregate accumulation. Therefore, regulation of HDAC6 deacetylase activity by p62 is important for protein degradation by autophagy.

1.3.3.4.2.3 Aggresome formation

In cases where a misfolded protein is not targeted for degradation or exceeds the capacity of available cytoplasmic degradation pathways, it may be actively transported to a single juxtanuclear site within the cell called the aggresome (Johnston et al., 1998). Aggresomes reduce the cytotoxicity of misfolded proteins by sequestering them from their sites of action in the cytoplasm as well as aiding their degradation by autophagy and therefore can be considered a cytoprotective response (Kopito, 2000). Indeed, pharmacological inhibition of aggresome formation by disrupting the transport of aggregated protein results in increased cytotoxicity of aggregated proteins whilst stimulating aggresome formation reduces it (Taylor et al., 2003; Bodner et al., 2006).

Ubiquitinated, misfolded proteins are recruited to the dynein motor complex via HDAC6 (Figure 1.7). Acting as a cargo adaptor, HDAC6 binds polyubiquitinated proteins through its C-terminal Zn-UBF ubiquitin-binding domain and cytoplasmic dynein through its dynein motor binding domain (Kawaguchi et al., 2003). Knockdown of HDAC6 expression abolishes aggresome formation of polyubiquitinated misfolded proteins, thus identifying HDAC6 as a crucial component of aggresome formation (Kawaguchi et al., 2003). The dynein complex consists of the cytoplasmic dynein motor core which has two heavy chains for microtubule binding as well as intermediate and light chains for cargo binding, together with the associated dynactin complex containing the $p150^{Glued}$ subunit which provides a further microtubule contact site (Vaughan and Vallee, 1995; King, 2000). Retrograde movement is generated through ATP hydrolysis in the AAA motifs of the core motor domain (Vale, 2003). HDAC6-mediated regulation of tubulin acetylation may also influence the rate of retrograde aggregate transport towards the aggresome as described in section 1.3.3.3. In support of this, HDAC6 catalytic activity is required for the rescue of aggresome formation after HDAC6-knockdown as well as the stimulation of autophagy to rescue degeneration caused by UPS dysfunction *in vivo* (Kawaguchi et al., 2003; Pandey et al., 2007).

Once transported to the MTOC, misfolded proteins are accumulated into a dense sphere which is encapsulated by an intermediate filament cage. In mitotic cells this cage is formed of the intermediate filament vimentin, whereas in neurons it consists of neurofilaments (Johnston et al., 1998; Taylor et al., 2003). The intermediate filament cage is thought to ensure aggresome stability and provide a sequestration barrier to prevent non-specific interactions between the aggregated protein and outside cytoplasmic components (Olzmann et al., 2008). In evidence for misfolded protein clearance as well as sequestration, aggresomes show co-localisation with components of the proteasome system including ubiquitin, the 26S proteasome, and the proteasomal activator complexes PA28 and PA700 (Wigley et al., 1999; Fabunmi et al., 2000). Despite this, aggregated proteins are not efficient substrates of the UPS due to the requirement for protein unfolding and movement through the central pore of the 20S proteasome, and can act to inhibit UPS function entirely (Bence et al., 2001; Bennett et al., 2005). It is therefore unclear if proteasomal machinery retains a functional role at the aggresome. Aggresomes also show co-localisation with many components of the autophagy pathway including LC3, lysosomes and HDAC6, suggesting that autophagy is involved in the clearance of aggresomes (Fortun et al., 2003; Iwata et al., 2005a; Iwata et al., 2005b). Indeed, aggresome clearance is

increased by autophagy induction and prevented by autophagy inhibition (Ravikumar et al., 2002; Yamamoto et al., 2006). Aggresomes may therefore represent an intermediate step in the cellular response to aggregated protein by aiding eventual degradation by autophagy (Olzmann et al., 2008).

Whilst ubiquitination of misfolded proteins is widely used to selectively target them to cellular degradation pathways, non-ubiquitinated proteins can also form aggresomes (García-Mata et al., 1999). This suggests that there is an alternative mechanism for selection and recruitment of non-ubiquitinated cargo to cytoplasmic dynein which is independent of the ubiquitin-dynein adaptor function of HDAC6. Indeed, a chaperone-based mechanism for cargo-loading mechanism onto dynein has been described which is controlled by the co-chaperone Bcl-2-associated athanogene 3 (BAG3) (Gamerdinger et al., 2011). The chaperone 70 kDa heat shock protein (Hsp70) interacts with hydrophobic peptide sequences of target proteins in an ATP-dependent manner, with substrate selectivity provided by a range of co-chaperones including the BAG family of proteins (Mayer and Bukau, 2005). BAG1 and BAG3 proteins direct substrates to proteasomal and autophagic degradation pathways, respectively, and a switch to BAG3-mediated regulation promotes autophagic degradation (Gamerdinger et al., 2009). Under conditions of cellular stress, BAG3 binds Hsp70 via its Bag domain and is thought to recruit Hsp70-associated substrates to the dynein motor complex via 14-3-3 proteins (Takayama and Reed, 2001; Xu et al., 2013). Expression of BAG3 has been shown to be up-regulated by proteasome inhibition and this likely increases aggresomal transport of aggregated proteins (Du et al., 2009).

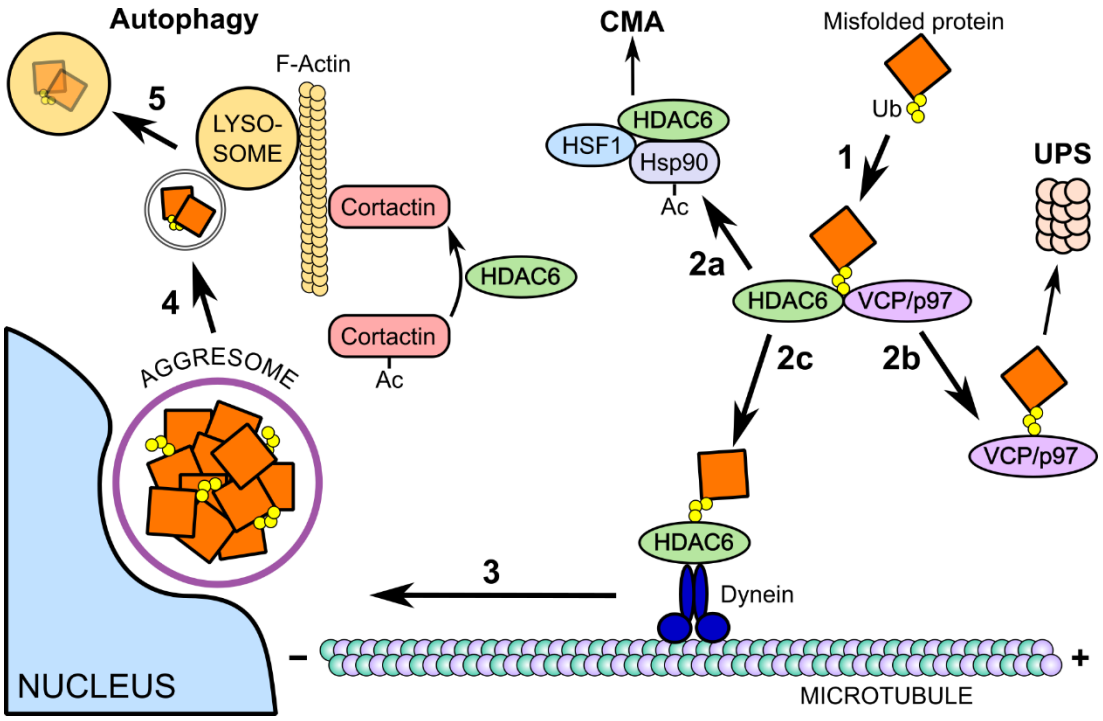

Figure 1.7. The roles of HDAC6 in protein degradation pathways 1) Misfolded proteins in the cytoplasm are ubiquitinated and are recognised by the ZnF-UBP domain of HDAC6. 2a) HDAC6 bound in a complex with Hsp90 and HSF1 deacetylates Hsp90 and causes dissociation of the complex and activation of chaperone mediated autophagy (CMA). 2b) For degradation via the ubiquitin-proteasome system (UPS), VCP/p97 directs the misfolded protein to the proteasome. 2c) Under cellular stress, an excess of misfolded protein is detected by HDAC6 and recruited to the cytoplasmic dynein motor complex. 3) Dynein-mediated retrograde transport of the misfolded proteins along microtubules towards the MTOC forms a perinuclear aggresome which is surrounded by a vimentin cage (shown in purple). 4) For degradation by autophagy, an autophagosome containing misfolded protein is formed. HDAC6 deacetylates cortactin to initiate polymerisation of F-actin which in turn stimulates fusion of the autophagosome and lysosome. 5) Misfolded protein is degraded by lysosomal hydrolases in the fused autolysosome.

1.3.3.4.3 Stress granule formation

A further cellular response to the aggregation of misfolded protein is through the formation of stress granules. Stress granules are cytoplasmic accumulations of mRNA and RNA-binding proteins which act to suppress protein translation after proteasomal impairment, therefore preventing additional protein production whilst degradation pathways are overwhelmed (Mazroui et al., 2007). HDAC6 is a component of stress granules and co-localises with the stress granule marker G3BP, and formation of stress granules requires both the deacetylase activity and ubiquitin-binding domain of HDAC6 (Kwon et al., 2007). Stress granule formation is microtubule-dependent and is inhibited by disruption of cytoplasmic dynein motor proteins, indicating that stress granule components are transported along microtubules via cytoplasmic dynein and possibly under regulation by HDAC6 (Kwon et al., 2007). Additionally, the stress granule-associated RNA-binding proteins TDP-43 and FUS bind to HDAC6 mRNA and promote its expression to upregulate HDAC6 protein production, therefore aiding the cellular response to protein aggregation (Kim et al., 2010; Fiesel et al., 2010).

1.3.4 HDAC6 in neurodegeneration

Due to its important roles in protein degradation and microtubule-based transport, HDAC6 has emerged as a key player in neurodegenerative diseases which share common defects in these mechanisms. These diseases include PD, Alzheimer's disease, amyotrophic lateral sclerosis, and Huntington's disease, all of which show abnormal ubiquitinated protein aggregation and defects in axonal transport (Ross and Poirier, 2004; De Vos et al., 2008). The function of HDAC6 as both a binding partner of damaged proteins and as a regulator of their transport for degradation has led to suggestions that HDAC6 is crucial for the balance between neuroprotection and neurodegeneration (d' Ydewalle et al., 2012). Following impairment of the UPS by accumulation of ubiquitinated proteins, HDAC6 recruitment drives their transport and degradation by autophagy to prevent cytotoxicity. At the same time, HDAC6-mediated deacetylation of microtubules and cortactin may cause cytoskeletal alternations which suppress the effective clearance of aggregates. Therefore, a disturbance in the balance between these functions of HDAC6 may lead to neurodegeneration.

Evidence suggests that HDAC6 is implicated in PD. HDAC6 strongly co-localises with filamentous protein structures within Lewy bodies in PD and DLB, indicating that it has a role in Lewy body formation (Kawaguchi et al., 2003; Miki et al., 2011). HDAC6

co-localises with α-synuclein at perinuclear aggresome-like structures in MPP(+)-treated cell models of PD and deficiency of HDAC6 results in increased α-synuclein aggregation and decreased autophagic clearance (Su et al., 2011). In addition, depletion of HDAC6 increases α-synuclein toxicity, inhibits inclusion formation and increases neuronal loss in a *Drosophila* model of PD whereas HDAC6 overexpression has the opposite effect, highlighting the protective role of HDAC6-mediated inclusion formation (Du et al., 2010). Importantly, HDAC6 is regulated by the PD-associated proteins Parkin and DJ-1 to promote aggresome formation of ubiquitinated proteins (Olzmann and Chin, 2008). Mutations in Parkin cause autosomal recessive PD with the absence of Lewy bodies, a feature which may be explained by a disruption of HDAC6 aggresome formation due to Parkin loss-of-function. Furthermore, Parkin recruits HDAC6 and p62 to damaged mitochondria to promote their removal by mitophagy and this is disrupted by PD-associated Parkin mutations (Lee et al., 2010b). These studies therefore suggest a neuroprotective effect for HDAC6 in PD through the formation of aggresome-like inclusions and regulation of autophagy.

Due to the apparent balance between HDAC6-mediated deacetylation supressing microtubule-based transport and HDAC6-ubiquitin binding promoting protein degradation and sequestration, inhibitors of HDAC6 deacetylase activity which leave its ubiquitin-binding functions unaffected are attractive therapeutic targets (Simões-Pires et al., 2013; Sharma and Taliyan, 2015; Benoy et al., 2017). HDAC6 inhibitors reverse axonal loss in peripheral nervous system disorders such as Charcot-Marie-Tooth disease (CMT) and hereditary motor neuropathy (HMN) which show reduced α-tubulin acetylation levels and defects in axonal transport (d'Ydewalle et al., 2011; Benoy et al., 2017). Evidence from some PD models suggests a therapeutic benefit from HDAC6 inhibitors. For example, inhibition of HDAC6 deacetylase activity increases microtubule acetylation and rescues axonal transport and motor defects caused by mutant LRRK2 in a transgenic *Drosophila* model of PD (Godena et al., 2014). Additionally, HDAC6 inhibition rescues cellular metabolism, reduced TH immunofluorescence and partially rescues some behavioural readouts of locomotion in an MPP(+) zebrafish PD model (Pinho et al., 2016). However, in a proteasomal inhibitor-treated mouse model of PD inhibition of HDAC6 increases α-synuclein oligomers, DA neuron loss and behavioural deficits in an Hsp90-dependent manner, indicating that loss of HDAC6-mediated deacetylation of Hsp90 is pathogenic through loss of chaperone activity (Du et al., 2014). Therefore, differences between models of PD, with the caveat that none fully recapitulate human disease, indicate that whilst

the multiple functions of HDAC6 complicate its inhibition as a therapeutic target in PD, further research into this area is warranted.

1.4 Hypothesis and aims

As the most common familial genetic defect in PD found to date, and with many phenotypical and pathological similarities to sporadic PD, better understanding the cellular roles of LRRK2 is crucial for insight into the pathogenic mechanisms of PD.

Multiple reports place LRRK2 as a key regulator of microtubule dynamics, and evidence suggests that LRRK2 regulates acetylation of α-tubulin at lysine-40. LRRK2 regulation of tubulin acetylation may regulate microtubule-dependent processes such as axonal transport and neurite outgrowth, with pathogenic mutations in LRRK2 disrupting these processes to contribute to cytotoxicity. In addition, emerging evidence suggests a role for LRRK2 in endosomal trafficking, autophagy and the misfolded protein response.

At the intersection of microtubule dynamics and protein degradation pathways is HDAC6, which acts as a cytoplasmic tubulin deacetylase to regulate microtubule dynamics and transport, a cargo adaptor for transport of ubiquitinated proteins, and a regulator of autophagic maturation. HDAC6 is a known phosphoprotein, and we hypothesised that LRRK2 may interact with and phosphorylate HDAC6 to regulate its role in the misfolded protein response and tubulin deacetylation. The aim of this thesis is therefore to investigate an interaction between LRRK2 and HDAC6 using both *in vitro* and cell models and characterise the functional role of LRRK2 in HDAC6-mediated aggresome formation and tubulin deacetylation.

2 Materials and Methods

2.1 Materials & reagents

2.1.1 Stock solutions

Note: all chemicals purchased from Sigma unless stated otherwise.

Acrylamide-bis-acrylamide (30%) (National Diagnostics)

Ammonium persulfate (APS) (10%)

Ampicillin (100 mg/ml)

Bovine serum albumin (BSA)

Bradford reagent (5x) (Bio-Rad)

Dimethyl sulfoxide (DMSO) (100%)

Ethanol (100%) (Fisher Scientific)

Ethidium bromide (10 mg/ml)

Ethylenediaminetetraacetic acid (EDTA) (0.5 M)

Fetal bovine serum (FBS) (Labtech)

Formaldehyde (37%)

Glacial acetic acid (100%)

Glycerol (100%) (Fisher Scientific)

GSK2578215A (5 mM in DMSO) (Tocris Bioscience)

HEPES (pH 7.5; 1 M)

Kanamycin (50 mg/ml)

LRRK2 inhibitor III (HG-10-102-01) (5 mM in DMSO) (Calbiochem)

LRRK2in1 (10 mM in DMSO) (Calbiochem)

Magnesium chloride ($MgCl_2$) (1 M)

Methanol (100%) (Fisher Scientific)

MG132 (N-benzyloxycarbonyl-L-leucyl-L-leucyl-L-leucinal) (10 mM in DMSO)

NP40 (IGEPAL CA-630)

Potassium acetate (KOAc) (1 M)

Potassium hydroxide-buffered piperazine-N,N′-bis(2-ethanesulfonic acid) (K-PIPES) (pH 6.8; 400 mM)

Sodium chloride (NaCl) (5 M)

Sodium dodecyl sulphate (SDS) (10%)

Sodium pyruvate (100 mM)

Tetramethylethylenediamine (TEMED)

Tris-HCl (pH 6.8; 0.5 M)

Tris-HCl (pH 8.8; 1.5 M)

Triton X-100

Trypsin-EDTA

Tubastatin A (20 mM in DMSO)

Tween 20

β-mercaptoethanol

2.1.2 Expression plasmids

Table 2.1. DNA expression plasmids for transient transfection of eukaryotic cells

Name	Protein	Backbone	Source
pCI-neo	--	pCI-neo	Promega
2XMyc-LRRK2-WT	Human LRRK2 WT	pCMV-Tag 3B	Mark Cookson (NIH) (Addgene #25361)
2XMyc-LRRK2-RCKW	Human LRRK2 (aa 1328-2527)	pCMV-Tag 3B	Mark Cookson (NIH) (Addgene #25064)
2XMyc-LRRK2-RCK	Human LRRK2 (aa 1329-2219)	pCMV-Tag 3B	Mark Cookson (NIH) (Addgene #25065)
2XMyc-LRRK2-Roc-COR	Human LRRK2 (aa 1329-1881)	pCMV-Tag 3B	In house mutagenesis of Addgene #25065
2XMyc-LRRK2-Roc	Human LRRK2 (aa 1329-1515)	pCMV-Tag 3B	In house mutagenesis of Addgene #25065
2XMyc-LRRK2-COR	Human LRRK2 (aa 1408-1850)	pCMV-Tag 3B	Mark Cookson (NIH) (Addgene #25069)
2XMyc-LRRK2-Kinase	Human LRRK2 (aa 1863-2218)	pCMV-Tag 3B	Mark Cookson (NIH) (Addgene ##25071)
2XMyc-LRRK2-R1441C	Human LRRK2 (R1441C)	pCMV-Tag 3B	Mark Cookson (NIH) (Addgene #25363)
2XMyc-LRRK2-Y1699C	Human LRRK2 (Y1699C)	pCMV-Tag 3B	Mark Cookson (NIH) (Addgene #25364)
2XMyc-LRRK2-G2019S	Human LRRK2 (G2019S)	pCMV-Tag 3B	Mark Cookson (NIH) (Addgene #25362)
2XMyc-LRRK2-D1994A	Human LRRK2 (D1994A)	pCMV-Tag 3B	In house mutagenesis of Addgene #25361
2XMyc-LRRK2-T1343G	Human LRRK2 (T1343G)	pCMV-Tag 3B	In house mutagenesis of Addgene #25361
2XMyc-LRRK2-K1347A	Human LRRK2 (K1347A)	pCMV-Tag 3B	In house mutagenesis of Addgene #25361
HDAC6	Human HDAC6	pCMV6-XL4	Origene (#SC111132)
FLAG-HDAC6	Human HDAC6	pCI-neo-FLAG	In house cloning

Name	Protein	Backbone	Source
FLAG-HDAC6-HD1	Human HDAC6 (aa 1-404)	pCI-neo-FLAG	In house mutagenesis
FLAG-HDAC6-HD2	Human HDAC6 (aa 407-800)	pCI-neo-FLAG	In house cloning
FLAG-HDAC6-HD1+2	Human HDAC6 (aa 1-800)	pCI-neo-FLAG	In house mutagenesis
FLAG-HDAC6-dUB	Human HDAC6 (aa 1-1149)	pCI-neo-FLAG	In house mutagenesis
FLAG-HDAC6-S22A	Human HDAC6 (S22A)	pCI-neo-FLAG	In house mutagenesis
FLAG-HDAC6-S22E	Human HDAC6 (S22E)	pCI-neo-FLAG	In house mutagenesis
FLAG-HDAC6-S689A	Human HDAC6 (S689A)	pCI-neo-FLAG	In house mutagenesis
FLAG-HDAC6-S689E	Human HDAC6 (S289E)	pCI-neo-FLAG	In house mutagenesis
FLAG-HDAC6-S22A-S689A	HDAC6 (S22A-S689A)	pCI-neo-FLAG	In house mutagenesis
GFP-CFTR-ΔF508	Human CFTR (ΔF508)	pEGFP-C1	Ron Kopito (Stanford)
GFP-250	Human p115 (aa 1-252)	pEGFP-C2	Elizabeth Sztul (University of Alabama)

2.1.3 siRNAs

Table 2.2. siRNA targeting sequences for knockdown of endogenous protein expression

Name	Target	Sequence	Reference
HDAC6	Human HDAC6	CTGCAAGGGATGGATCTGAAC	Hubbert et al., 2002
LRRK2 #1	Human LRRK2	CTCGTCGACTTATACGTGTAA	Häbig et al., 2007
LRRK2 #2	Human LRRK2	*Proprietary; Thermo Fisher ID 263837*	Alegre-Abarrategui et al., 2009
Non-targeting (NTC)	--	*MISSION® siRNA Universal Negative Control #1 (Sigma SIC001)*	Jiwani et al., 2012

2.1.4 DNA primers

Table 2.3. Primer sequences for plasmid PCR and sequencing

Plasmid/*gene*	Primer	Primer Sequences (5'-3')
HDAC6	**H1**	TTGATCTGATGGAAACAACCC
	H2	CTACATTGCTGCTTTCCTGC
	H3	GACCAAAATATGATGAATCACTGC
	H4	CCACCACGGTAATGGAACTC
	H5	TCACTGAGACCATCCAAGTCC
	H6	TGTAGGAGGAGCTACACTGGC
	***(SalI)*-F**	*(GTCGAC)*-CCCATGCTGGAGTCACCT
	***(NotI)*-R**	*(GCGGCCGC)*-TTAGTGTGGGTGGGGCATA
LRRK2	**L1**	GCTGATATTGGATGAAGAAAGTGA
	L2	GGCCCTCCTCACTGAGACTA
	L3	TGGTCCCCAAAATACTAACAG
	L4	AGCAATCCTCAAATTGTCAGC
	L5	GAAGATGTGCTGTCTAAATTTGATG
	L6	ACTGAAGCGAAAAAGAAAAAT
	L7	GAAATAAAATATCAGGGATATGCTCC
	L8	TGGAACTAAGATCCTTTCCCAA
	L9	TGATTCTCGTTGGCACACAT
	L10	GAAGGTTGTCCAAAACACCC
	L11	TGGACCACATTGATTCTCTCA
	L12	GTTAGCCTCCAAGGGTTCCT
	L13	GAAAGAAAATCCTCAAGAAAGGC
	L14	TTGCAATTCCTTTTCCAAGC
	L15	GGAGGATGTGGCACAAAGAT
	L16	AAGAGATACAATCTTGCTTGACCG
pCR-Blunt II-TOPO	**M13-F**	GTAAAACGACGGCCAGT
	M13-R	CAGGAAACAGCTATGAC
pCI-neo-3xFLAG	**T7-EEV**	AAGGCTAGAGTACTTAATACGA
	T3	ATTAACCCTCACTAAAGGGA

Table 2.4. Primer sequences for plasmid site-directed mutagenesis

Plasmid	Mutation	Primer Sequences (5'-3')
FLAG-HDAC6	**S22A**	CCTGAGGGGGCGCCTGGGGGTTCTG CAGAACCCCCAGGCGCCCCCTCAGG
	S22E	GTCCTGAGGGGGCTCCTGGGGGTTCTGC GCAGAACCCCCAGGAGCCCCCTCAGGAC
	S689A	CCGGCCGATCTGGGCGCTGGCACCCTCA TGAGGGTGCCAGCGCCCAGATCGGCCGG
	S689E	AGCCCGGCCGATCTGCTCGCTGGCACCCTCATC GATGAGGGTGCCAGCGAGCAGATCGGCCGGGCT
FLAG-HDAC6-HD1	**D405***	ATGGGGCAAGGCTATCCCAGAAGGGTGTGGAGC GCTCCACACCCTTCTGGGATAGCCTTGCCCCAT
FLAG-HDAC6-HD1+2	**D801***	GGGGTGGTGGCTATCCAAGGAGGGAGCGAGT ACTCGCTCCCTCCTTGGATAGCCACCACCCC
FLAG-HDAC6-dUB	**Q1150***	CACAGTAGACCTAATAGCAAGAGAGACACACCCAAT ATTGGGTGTGTCTCTCTTGCTATTAGGTCTACTGTG
Myc-LRRK2-RocCOR	**E1882***	GTTGGAATTTGAACAAGCTCCATAGTTTCTCCTAGGTGATG CATCACCTAGGAGAAACTATGGAGCTTGTTCAAATTCCAAC
Myc-LRRK2-Roc	**Q1516***	GCTGTCCAACAACAAGCTAATCTCGGATCTTGAAATTAAGG CCTTAATTTCAAGATCCGAGATTAGCTTGTTGTTGGACAGC
Myc-LRRK2	**T1343G**	GTTTTACCACTCCCACCATTTCCCACAATCATAAGTTTCATTCGGT ACCGAATGAAACTTATGATTGTGGGAAATGGTGGGAGTGGTAAAAC
	K1347A	TTGCTGCAATAAGGTGGTTGCACCACTCCCAGTATTTCCC GGGAAATACTGGGAGTGGTGCAACCACCTTATTGCAGCAA
	D1994A	ACATTGTGGGGTTTCAGGGCTCGGTATATAATCATGG CCATGATTATATACCGAGCCCTGAAACCCCACAATGT

2.1.5 Antibodies

Table 2.5. Antibodies for western blotting (WB), immunofluorescence (IF) and immunoprecipitation (IP). M = monoclonal, P = polyclonal

Antibody	Immunogen	Host	Clonality	Dilution	Company
Primary antibodies					
Anti-HDAC6 (D2E5)	Human HDAC6 C-terminus	Rabbit	M	1:1000 (WB) 1:200 (IF)	Cell Signaling
Anti-HDAC6-pS22 (ab61058)	Human HDAC6 pS22	Rabbit	P	1:500 (WB)	Abcam
Anti-FLAG (M2)	DYKDDDDK peptide	Mouse	M	1:2000 (WB, IF, IP)	Sigma
Anti-Myc (9B11)	EQKLISEED L peptide	Mouse	M	1:2000 (WB, IF, IP)	Cell Signaling
Anti-LRRK2 (MJFF2)	Human LRRK2 aa 950-2527	Rabbit	M	1:1000 (WB) 1:50 (IF)	Abcam
Anti-LRRK2 (UDD3)	Human LRRK2 aa 100-500	Rabbit	M	1:1000 (WB, IP) 1:100 (IF)	Abcam
Anti-LRRK2-pS935 (UDD2)	Human LRRK2 p935	Rabbit	M	1:1000 (WB) 1:200 (IF)	Abcam
Anti-tubulin (DM1A)	*G. gallus* microtubules	Mouse	M	1:10,000 (WB)	Sigma
Anti-tubulin (ab4074)	Human alpha-tubulin aa 1-100	Rabbit	P	1:5000 (WB)	Abcam
Anti-acetylated tubulin (6-11B-1)	*S. purpuratus* acetylated tubulin	Mouse	M	1:5000 (WB) 1:2000 (IF)	Sigma
Anti-GFP (JL-8)	GFP/EGFP	Mouse	M	1:5000 (WB)	Clontech
Anti-vimentin (AB5733)	Recombinant vimentin	Chicken	P	1:4000 (IF)	Merck

Antibody	Immunogen	Host	Clonality	Dilution	Company
Secondary antibodies					
Anti-mouse HRP	Mouse IgG	Goat	P	1:5000 (WB)	Dako
Anti-rabbit HRP	Rabbit IgG	Goat	P	1:5000 (WB)	Dako
Alexa568 anti-mouse	Mouse IgG	Donkey	P	1:500 (IF)	Invitrogen
Alexa488 anti-rabbit	Rabbit IgG	Goat	P	1:500 (IF)	Invitrogen
Alexa488 anti-mouse	Mouse IgG	Donkey	P	1:500 (IF)	Invitrogen
BV421 anti-rabbit	Rabbit IgG	Goat	P	1:500 (IF)	BD Bio-sciences
Cy5 anti-chicken	Chicken IgG	Donkey	P	1:500 (IF)	Jackson Immuno-Research

2.1.6 Buffers and solutions

Table 2.6. Prepared buffers and solutions. (Note: All made up to volume w/ deionised H_2O unless stated otherwise)

Name	Composition
Plasmid propagation	
Lysogeny broth (LB)	*10 g/L tryptone, 10 g/L NaCl, 5 g/L yeast extract*
LB agar	*10 g/L agar, 10 g/L tryptone, 5 g/L NaCl, 5 g/L yeast extract*
Terrific broth (TB)	*24 g/L yeast extract, 12 g/L casein peptone, potassium phosphate (monobasic) 2.2 g/L, potassium phosphate (dibasic) 9.4 g/L, 0.4% glycerol*
Glycerol stock solution	*Glycerol (50%)*
DNA electrophoresis	
TAE buffer	*40 mM TRIS, 1 mM EDTA, 0.11% glacial acetic acid, pH 8.0 with NaOH*
TAE agarose gel	*TAE buffer, 0.8-1% agarose*
Cell culture	
DMEM culture medium	*DMEM (4.5 g/L glucose), 10% FBS, 1 mM sodium pyruvate*
Trypsin	*1x Trypsin-EDTA in PBS*
Freezing medium	*10% DMSO in FBS*
PEI	*1 mg/ml polyethylenimine (Polysciences Inc, 23966)*
Protein binding	
RB100 buffer	*25 mM HEPES (pH 7.5), 100 mM KOAc, 10 mM $MgCl_2$, 1 mM DTT, 0.05% Triton X-100, 10% glycerol*
GSH elution buffer	*50 mM Tris-HCl (pH 7.5), 100 mM NaCl, 40 mM reduced glutathione*
BRB80 buffer	*80 mM K-PIPES (pH 6.8), 1 mM EDTA, 1 mM $MgCl_2$, 1% NP40, 150 mM NaCl, 10 mM NaF, 1 mM Na_2VO_4, 10 mM β-Glycerophosphate, 5 mM $Na_4P_2O_7$*
Lysis buffer	*BRB80 w/ 1x Halt Protease Inhibitor Cocktail (Thermo Scientific)*

SDS-PAGE and Western Blot	
5x Laemmli buffer	*250 mM Tris HCl (pH 6.8), 50% glycerol, 10% SDS, 25% ß-mercaptoethanol, 0.5% bromophenol blue*
Resolving gel buffer	*1.5 M Tris HCl (pH 8.8)*
Resolving gel (7.5%)	375 mM *Tris HCl (pH 8.8), 7.5% acrylamide, 0.1% SDS, 0.1% APS, 0.1% TEMED*
Stacking gel buffer	*0.5 M Tris HCl (pH 6.8)*
Stacking gel (4%)	117 mM *Tris HCl (pH 6.8), 4% acrylamide, 0.1% SDS, 0.05% APS, 0.3% TEMED*
10x Running buffer	*250 mM Tris, 1.92 M glycine*
Running buffer	*10% 10x Running buffer, 0.1% SDS*
Transfer buffer	*10% 10x Running buffer, 20% methanol*
Ponceau stain	*0.1% Ponceau S, 5% glacial acetic acid*
20x Tris-buffered saline (TBS)	*400 mM Tris, 2.742 M NaCl, pH 7.6 with HCl*
TBS-T	*5% 20x TBS, 0.02% Tween 20*
Blocking buffer	*5% non-fat dry milk / 5% BSA in TBS-T*
Kinase assay	
10x kinase buffer	*500 mM Tris HCl, 100 mM $MgCl_2$, 15 mM 2-mercaptoethanol, 1.5 M NaCl*
Coomassie staining solution	*0.1% Coomassie Brilliant Blue R-250, 50% methanol, 10% glacial acetic acid*
Destain solution	*30% methanol, 10% glacial acetic acid*
Mass spectrometry	
Ammonium bicarbonate	*50 mM NH_4HCO_3 (pH 8.5)*
Trypsin (stock)	*1 µg/µl trypsin (MS grade; Thermo Scientific), 0.1% CF_3CO_2H*
Trypsin (working)	*1 ng/µl trypsin (stock), 50 mM NH_4HCO_3 (pH 8.5)*
Immunofluorescence	
Phosphate-buffered saline (PBS)	*137 mM NaCl, 2.7 mM KCl, 10 mM Na_2HPO_4, 1.8 mM KH_2PO_4*
PBS-T	*PBS + 0.02% Tween 20*
PBS/BLOCK	*PBS + 0.2% fish gelatin*

2.2 Methods

2.2.1 Plasmids

2.2.1.1 Transformation into competent cells

Plasmids were sourced as listed in Table 2.1. Competent DH5α (Invitrogen) and XL10-Gold (Agilent Technologies) *E. coli* were stored at -80°C until required. For transformation of plasmid DNA, 25 µl of competent cells per reaction were thawed on ice. 1 µl ß-mercaptoethanol solution (Agilent Technologies) was added to each reaction to increase transformation efficiency and incubated for 2 min on ice (XL10-Gold competent cells only). 0.5-2 µl plasmid DNA was added to the cells and incubated on ice for 30 min. Cells were heat-shocked for 30 s at 42°C and immediately placed on ice for 2 min. 500 µl of pre-heated (42°C) LB broth was added to the cells before incubated for 1 h at 37°C with shaking at 220 rpm. Cells were briefly centrifuged for 2 min at 500 rpm and resuspended in ~50 µl LB broth before being spread onto LB-antibiotic plates (100 µg/ml ampicillin or 50 µg/ml kanamycin) and incubated for 16 h at 37°C.

2.2.1.2 Glycerol stocks

After transformation into competent cells, single bacterial colonies containing the plasmid of interest were grown up into 1 ml starter cultures of LB broth (Sigma) containing the appropriate antibiotic (100 µg/ml ampicillin or 50 µg/ml kanamycin) for 6 h at 37°C with shaking at 220 rpm. All *E. coli* containing Myc-LRRK2 plasmids were cultured in nutrient-rich Terrific Broth (TB) containing 0.4% glycerol (Fisher Scientific) for increased growth and higher plasmid yield. 50 µl of the starter culture was expanded into 5 ml LB or TB broth with antibiotic for 16 h at 37°C with shaking. Glycerol stocks were prepared by addition of 500 µl bacterial culture to 500 µl 50% glycerol in a cryogenic vial (Thermo Scientific) with mixing to produce a 25% glycerol stock and stored at -80°C.

2.2.1.3 Preparation of plasmid DNA

For plasmid propagation and purification, a stab culture from the glycerol stock containing the plasmid of interest was streaked out onto LB agar plates containing the appropriate antibiotic (100 µg/ml ampicillin or 50 µg/ml kanamycin) and cultured for 16 h at 37°C. Single bacterial colonies were grown up into 1 ml starter cultures of LB or TB broth with antibiotic for 6 h at 37°C with shaking at 220 rpm, before 50 µl of

the starter culture was expanded into 5 ml LB broth with antibiotic for 16 h at 37°C with shaking. All plasmid DNA was purified using a Nucleospin Plasmid purification kit (Macherey-Nagel) following the manufacturer's protocol. Briefly, cells were harvested by centrifugation for 10 min at 4000 x g and bacterial pellets were resuspended in 250 µl Buffer A1. Cells were lysed by addition of 250 µl Buffer A2 and mixed by inversion, before addition of 300 µl Buffer A3 to precipitate protein and chromosomal DNA. The lysates were clarified by centrifugation for 10 min at 17,000 x g and the supernatant was loaded into a binding column and centrifuged for 1 min at 17,000 x g to bind the plasmid DNA. The binding column membrane was washed with 500 µl Buffer AW and centrifuged for 1 min at 17,000 x g, followed by a further wash with 600 µl Buffer A4 and centrifugation for 1 min at 17,000 x g. The membrane was dried by centrifugation for 2 min at 17,000 x g and plasmid DNA was eluted into a new collection tube by incubation in 50 µl Buffer AE for 1 min at room temperature followed by centrifugation for 1 min at 17,000 x g. Plasmids were stored at 4°C.

2.2.1.4 Quantification of plasmid DNA

The concentration of 1 µl purified plasmid was determined using a NanoDrop 1000 spectrophotometer (Thermo Scientific). 1 µl Buffer AE was used as a blank measurement. The ratio of absorbance at 260 nm and 280 nm was used to indicate sample purity, with a ratio of >1.8 indicating pure DNA.

2.2.1.5 Cloning

2.2.1.5.1 PCR amplification

For cloning of the FLAG-tagged HDAC6 constructs, cDNA was generated from the pCMV6-HDAC6 plasmid (Origene) by PCR using Phusion High Fidelity DNA polymerase (NEB) with HDAC6-specific forward (F) and reverse (R) primers containing SalI and NotI restriction sites (Table 2.3) according to manufacturer's protocol (Table 2.7).

Table 2.7. Phusion PCR mix and cycling conditions

Plasmid DNA	1 µl
5x buffer	4 µl
10 µM dNTPS	1 µl
50 µM $MgCl_2$	0.5 µl
10 µM Primer F	1 µl
10 µM Primer R	1 µl
Phusion enzyme	0.25 µl
dH_2O	11.25 µl
TOTAL	**20 µl**

Step	Temp	Time	
Initiation	98°C	2 min	
Melting	98°C	20 s	x35 cycles
Annealing	64°C	20 s	
Extension	72°C	30 s/kb	
Final extension	72°C	7.5 min	
Cooling	4°C	Hold	

2.2.1.5.2 Gel extraction

The PCR product was separated using gel electrophoresis on a 0.8% agarose in TAE gel (containing 1 µl ethidium bromide per 100 ml) at 100 V for 40 min, and the band corresponding to the correct PCR product was excised under a UV transilluminator and DNA extracted using a GenElute gel extraction kit (Sigma) following the manufacturer's protocol. Excised bands were incubated with three gel volumes of Gel Solubilisation Buffer for 10 min at 55°C with intermittent vortexing to solubilise the gel slice. A binding column was prepared by adding 500 µl Column Preparation Solution and centrifuged for 1 min at 17,000 x g into a collection tube to maximise DNA binding to the column membrane. 1 gel volume of 100% isopropanol was added to the solubilised gel and mixed until homogenous, before adding the mixture to the binding column with empty collection tube and centrifuging for 1 min at 17,000 x g. The DNA bound to the column was washed with 700 µl Wash Solution and centrifuged for 1 min at 17,000 x g before the flow-through was discarded and the column centrifuged again for 1 min at 17,000 x g to remove excess ethanol. Finally, bound DNA was eluted from the column by addition of 50 µl pre-heated (65 °C) Elution Solution and incubation for 1 min at room temperature, before centrifugation for 1 min at 17,000 x g into a fresh collection tube. Recovered DNA concentration was determined using a NanoDrop 1000 spectrophotometer (Thermo Scientific) as previously described.

2.2.1.5.3 Subcloning into pCR-Blunt II-TOPO

The extracted PCR product was ligated into a pCR-Blunt II-TOPO cloning vector using a Zero Blunt TOPO cloning kit (Invitrogen) according to manufacturer's protocol (Table 2.8). The reaction was subsequently incubated for 10 min at room temperature.

Table 2.8. Zero Blunt TOPO ligation mix

Extracted PCR product	4 µl
Salt solution	1 µl
TOPO vector	0.5 µl
TOTAL	**5.5 µl**

2.2.1.5.4 Transformation and screening

TOPO plasmids were transformed into XL10 Gold *E. coli* (Agilent Technologies) following the manufacturer's protocol as previously described, plated onto LB-kanamycin agar plates and incubated for 16 h at 37°C. The resulting colonies were picked using sterile inoculation loops and screened for the correct insert using colony PCR with 5x FIREPol Master Mix (Solis Biodyne) and M13 primers (Table 2.9). PCR products were run on a 1% agarose gel to identify positive clones.

Table 2.9. Colony PCR mix and cycling conditions

5x Firepol	4 µl
10 µM M13 F	1 µl
10 µM M13 R	1 µl
dH_2O	14 µl
TOTAL	**20 µl**

Step	Temp	Time	
Initiation	95°C	5 min	
Melting	95°C	40 s	x30 cycles
Annealing	55°C	45 s	
Extension	72°C	60 s/kb	
Final extension	72°C	10 min	
Cooling	4°C	Hold	

2.2.1.5.5 Restriction digestion of insert and vector linearisation

Positive clones were grown up in 5 ml LB + kanamycin overnight at 37°C and plasmid DNA was purified using a Nucleospin Plasmid purification kit (Macherey-Nagel) following the manufacturer's protocol as previously described. The HDAC6 insert was cut from the TOPO vector using FastDigest SalI and NotI restriction enzymes (Thermo Scientific) for 30 min at 37°C (Table 2.10). To ensure insert-compatibility, the pCI-neo-3xFLAG destination vector was linearised using FastDigest XhoI and NotI restriction enzymes (Thermo Scientific) for 30 min at 37°C (Table 2.11). Both the TOPO and vector digestion reactions were run on a 0.8% agarose gel at 100V for 40

min and the insert and linearised vector were extracted from the gel as previously described.

Table 2.10. TOPO insert restriction digest mix

2 µg TOPO with insert	4 µl
10x FD buffer	2 µl
FD SalI	0.5 µl
FD NotI	0.5 µl
dH_2O	13 µl
TOTAL	**20 µl**

Table 2.11. Vector linearisation mix

3 µg vector	6 µl
10x FD buffer	2 µl
FD XhoI	0.5 µl
FD NotI	0.5 µl
dH_2O	11 µl
TOTAL	**20 µl**

2.2.1.5.6 Dephosphorylation of linearised vector

To prevent re-ligation of the linearised vector, Antarctic Phosphatase (NEB) was used for vector dephosphorylation following the manufacturer's protocol and incubated for 20 min at 37°C before a further incubation of 10 min at 75°C to deactivate the enzyme (Table 2.12).

Table 2.12. Vector dephosphorylation mix

Linearised vector	27 µl
10x AP buffer	2.8 µl
Antarctic phosphatase	0.2 µl
TOTAL	**30 µl**

2.2.1.5.7 Ligation of insert into vector

The HDAC6 insert was ligated into the linearised pCI-neo-3xFLAG vector using a Quick T4 DNA Ligation kit (NEB) following the manufacturer's instructions with a 1:3 molar ratio of vector to insert for efficient ligation (Table 2.13). Ligation reactions were incubated for 10 min at room temperature then placed on ice.

Table 2.13. Insert-vector ligation mix

Vector	1 µl
Insert	3 µl
2x QL buffer	10 µl
Quick T4 ligase	1 µl
dH_2O	5 µl
TOTAL	**20 µl**

Final pCI-neo-3xFLAG-HDAC6 plasmids were transformed into XL10 Gold *E. coli* and grown for 16 h at 37°C on LB agar plates with the appropriate resistance antibiotic, followed by PCR to screen for positive clones using 5x FIREPol Master Mix (Solis Biodyne) with T7-EEV and T3 primers (Table 2.9). Positive clones were grown up in 5 ml LB + ampicillin overnight at 37°C and plasmid DNA was purified using a Nucleospin Plasmid purification kit (Macherey-Nagel) following the manufacturer's protocol as previously described. All constructs were verified by sequencing using T7-EEV and T3 primers to check correct orientation of the insert, and glycerol stocks prepared by addition of 500 µl LB culture with 500 µl 50% glycerol followed by storage at -80°C.

2.2.1.6 Mutagenesis

Point mutations in FLAG-HDAC6 and Myc-LRRK2 constructs were generated using site-directed mutagenesis of the respective plasmids using a QuikChange Lightning Site-Directed Mutagenesis Kit (Agilent Technologies) using PCR according to the manufacturer's instructions (Table 2.14). Mutagenesis primer sequences are listed in Table 2.4.

Table 2.14. Mutagenesis PCR mix and cycling conditions

25 ng/µl Plasmid DNA	1 µl
10x reaction buffer	5 µl
dNTP mix	1 µl
QuikSolution	1.5 µl
100 ng/µl Primer F	1.25 µl
100 ng/µl Primer R	1.25 µl
QuikChange enzyme	1 µl
dH_2O	38 µl
TOTAL	**50 µl**

Step	Temp	Time	
Initiation	95°C	2 min	
Melting	95°C	20 s	x18 cycles
Annealing	60°C	10 s	
Extension	68°C	30 s/kb	
Final extension	68°C	5 min	
Cooling	4°C	Hold	

Following PCR amplification, 2 µl of Dpn I restriction enzyme was added to each amplification reaction and incubated for 5 min at 37°C to digest the template (non-mutated) DNA. 2 µl of the mutagenesis PCR reaction were subsequently transformed into XL10 Gold *E. coli* (Agilent Technologies), plated onto LB-antibiotic agar plates and incubated for 16 h at 37°C. Two colonies per mutated construct were picked and grown up into 1 ml starter cultures of LB broth containing antibiotic for 6 h at 37°C with shaking, before expansion of 50 µl starter culture into 5 ml LB broth with antibiotic for 16 h at 37°C with shaking. Plasmids were purified using a Nucleospin Plasmid purification kit (Macherey-Nagel) following the manufacturer's protocol as previously described. All constructs were verified by sequencing using the appropriate internal primers (Table 2.3) and glycerol stocks prepared by addition of 500 µl LB culture with 500 µl 50% glycerol followed by storage at -80°C.

2.2.2 Cell culture

HEK293 cells (ATCC) and LRRK2-knockout mouse embryonic fibroblasts (gifted from Prof. K. Harvey, UCL) were cultured in Dulbecco's Modified Eagle Medium (Thermo Scientific) with 4.5 g/l glucose supplemented with 10% fetal bovine serum (FBS; Sigma) and 1% sodium pyruvate (Sigma) at 37°C with 5% CO_2. Adherent cells were passaged twice per week and/or plated for experiments at 90%-100% confluency. Cells were washed once with sterile PBS and detached by incubation with trypsin-EDTA solution (Sigma) for 2 min at 37°C to create a cell suspension followed by quenching with culture medium to prevent further trypsin digestion. The cell suspension was pipetted up and down to triturate cells and remove cell clumps before being added to fresh culture medium at the desired dilution for passaging or plating. Diluted cell suspension in culture medium was added to sterile culture flasks or plates (Greiner Bio-One) and incubated at 37°C with 5% CO_2 for cell growth.

2.2.2.1 Storage of cell lines

For medium-term storage of cell lines, adherent cells at 100% confluency were detached using trypsin-EDTA solution as previously described and quenched with culture medium, before being centrifuged for 4 min at 400 x g to gently pellet the cells. Excess culture medium was removed and the cell pellet was resuspended in freezing medium (10% DMSO in FBS). The cell suspension was transferred to a cryogenic vial (Thermo Scientific) and cooled down to -80°C in a Mr Frosty freezing container (Thermo Scientific) at a rate of 1°C/minute. Cells were stored at -80°C until required.

2.2.2.2 Transient plasmid DNA transfection

Cells were transiently transfected with DNA plasmids at 70-80% confluency in 24-well, 12-well, 6-well plates or 10 cm dishes (Corning) using polyethylenimine (PEI) transfection reagent (Table 2.15). PEI and plasmid DNA (at a ratio of 3 µl PEI: 1 µg DNA) were diluted in separate microcentrifuge tubes containing 5% well volume of Opti-MEM reduced serum media (Invitrogen) each, before mixing and incubating for 20 min at room temperature and adding drop-wise onto cells. Media was replaced after 6 hours and all cells were used in experiments 24 hours post-transfection.

Table 2.15. DNA transfection with PEI

Plate	DNA (µg /well)	PEI (µl /well)	Final OptiMEM volume (µl)
24-well	0.5	1.5	50
12-well	1	3	100
6-well	2	6	200
10 cm	10	30	1000

2.2.2.3 siRNA knockdown of endogenous protein

HEK293 cells were cultured as described previously such that they would reach 70-80% confluency at 3 days post-knockdown. Cells were transfected with siRNA using Lipofectamine RNAiMAX (Invitrogen) according to the manufacturer's instructions (Table 2.16). 100 µM stocks of siRNA were diluted to 10 µM in dH_2O, and equal volumes of Lipofectamine RNAiMAX and 10 µM siRNA were further diluted in separate microcentrifuge tubes containing 5% well volume of Opti-MEM reduced serum media (Invitrogen) each at a ratio of 2.4 µl per 100 ml Opti-MEM. For pooled siRNA, half volumes of each individual siRNA were added. Both solutions were mixed and incubated for 20 min at room temperature before drop-wise addition onto cells to give a final siRNA concentration of 6 pM per well. Media was replaced after 6 hours and cells were used in experiments 96 hours post-knockdown. For transient DNA transfection in siRNA-treated cells, DNA was transfected as previously described at 72 hours post-knockdown.

Table 2.16. siRNA transfection with RNAiMAX

Plate	10 µM siRNA (µl /well)	RNAiMAX (µl /well)	Final OptiMEM volume (µl)
24-well	0.6	0.6	50
10 cm	12	12	1000

2.2.2.4 Drug treatments

For HDAC6 deacetylase inhibition, cells were incubated with 10 µM Tubastatin A (Sigma) for 18 h. For LRRK2 kinase inhibition, cells were incubated with either 1 µM LRRK2in1 (Calbiochem), 3 µM LRRK2 Inhibitor III (HG-10-102-01; Calbiochem) or 1 µM GSK2578215A (Tocris) for 4 h. For proteasome inhibition, cells were incubated with 5 µM MG132 (Sigma) for 4 h. Where cells were treated with both MG132 and LRRK2 kinase inhibitors for 4 h, drugs were added simultaneously.

2.2.3 Immunoblotting

2.2.3.1 Cell lysis and protein quantification

Cells were washed once in phosphate-buffered saline (PBS), scraped into ice-cold lysis buffer and lysed on ice for 30 min. Lysates were cleared via centrifugation for 20 min at 17,000 x g at 4°C. Protein concentration of cell lysates was measured via colorimetry using a Bradford protein assay following the manufacturer's protocol (Bio-Rad). The absorbance values of the samples at 595 nm were measured using a PheraSTAR FS plate reader (BMG Labtech) and protein concentrations calculated from a standard curve of bovine serum albumin (BSA) standards of known concentration.

2.2.3.2 SDS-PAGE and immunoblotting

Samples were denatured in Laemmli buffer at 95°C for 5 minutes and separated by SDS-PAGE on a 7.5% polyacrylamide gel at 100 V for 2 h in running buffer using a Mini-PROTEAN Tetra Cell gel electrophoresis system (Bio-Rad). A Precision Plus Protein prestained protein standard ladder (Bio-Rad) was used as a molecular weight marker on all gels. After separation, protein was transferred onto a 0.45 µm nitrocellulose (GE Healthcare) or 0.45 µm PVDF (Merck) membrane by electroblotting

overnight at 30 V in transfer buffer. Protein transfer was checked using reversible Ponceau S stain. Membranes were rinsed for 1 min in ultrapure H_2O followed by blocking for 1 hour at room temperature in 5% non-fat dry milk or 5% BSA in Tris-buffered saline with 0.2% Tween 20 (TBST). Membranes were incubated with primary antibody (Table 2.5) diluted in blocking buffer for 1 hour at room temperature or 4°C overnight. The membrane was washed 3 times for 10 min in TBS-T before being incubated with HRP-conjugated secondary antibody diluted in blocking buffer for 1 hour at room temperature and further washed 3 times for 10 min in TBS-T. Antibody binding was detected using SuperSignal West Pico chemiluminescent substrate (Thermo Scientific) and imaged using a GBox chemiluminescence imager (Syngene). Alternatively, the membrane was exposed onto Amersham ECL hyperfilm (GE Healthcare) in an autoradiography cassette and developed using Ilford MULTIGRADE developer and RAPID fixer (HARMAN) for 2 minutes each in a darkroom. If required, membrane was subsequently re-probed with a second primary antibody as previously described.

2.2.3.3 Co-immunoprecipitation

HEK293 cells were cultured in a 10 cm plate and co-transfected with 5 µg of each plasmid DNA as previously described, before being washed once with PBS and scraped into ice cold lysis buffer and gently inverted for 1 hour at 4°C. Lysates were cleared via centrifugation at 17,000 x g for 20 min at 4°C. Protein concentrations were quantified using Bradford assay as previously described, and 2 mg of protein was incubated with 2-4 µg of primary antibody (Table 2.5) for 16 h at 4°C. The primary antibody was captured using 30 µl of 50% Protein G Sepharose beads (Sigma) in BRB80 buffer for 2 h at 4°C. The beads were gently spun down for 30 s at 3000 x g to avoid crushing the beads and washed 5 times in ice cold BRB80 buffer to remove unbound protein. Following the final wash, excess BRB80 buffer was removed using a gel loading tip and bound protein was eluted in 2x Laemmli buffer by boiling for 5 minutes at 95°C. Samples were run on SDS-PAGE and immunoblotted as previously described.

2.2.3.4 Densitometry analysis

Chemiluminescent signal from immunoblots was quantified using FIJI software (Schindelin et al., 2012). Protein bands were selected using the rectangle selection tool to produce a region of interest and peak profile histograms for bands were produced using the plot lanes tool. Background signal was subtracted using the

straight-line selection tool and vertical lines of separation created between lanes to create closed peaks of interest corresponding to each protein band. The area under each closed peak in the histogram was used to represent protein level. All levels of protein of interest were normalised to a loading control.

2.2.4 *In vitro* binding assay

1 µg recombinant GST-tagged human LRRK2 wild-type, R1441C and G2019S protein (amino acids 970-2527; Invitrogen) was incubated with 1 µg recombinant His-tagged human HDAC6 protein (EMD Millipore) in 250 µl RB100 buffer for 1 hour at 4°C under gentle inversion. GST-tagged proteins were captured by addition of 20 µl of glutathione sepharose (GE Healthcare) beads for 30 minutes at 4°C. The beads were gently centrifuged for 1 min at 2000 x g and washed 3 times with RB100 buffer for removal of unbound protein. After removal of excess RB100 buffer following the final wash, bound protein was eluted in 20 µl GSH elution buffer for 10 minutes at room temperature. 5 µl of 5x Laemmli buffer was added to the eluate and samples were boiled for 5 min at 95°C for protein denaturation. Samples were subsequently run on SDS-PAGE and immunoblotted as previously described.

2.2.5 *In vitro* kinase assay

500 ng recombinant GST-tagged human LRRK2 wild-type, R1441C and G2019S protein (amino acids 970-2527; Invitrogen) and 500 ng recombinant His-tagged human HDAC6 protein (EMD Millipore) were incubated with 57 nm ^{32}P-ATP in 1x kinase buffer for 1 hour at 37°C. Samples were denatured in Laemmli buffer at 95°C for 5 min and run on SDS-PAGE. Proteins were stained in the gel with warm Coomassie for 20 min at room temperature followed by destaining twice for 1 h each at room temperature to remove background gel staining. Stained protein bands were imaged using the G:Box transilluminator (Syngene). The gel was dried onto Whatman paper in a 583 vacuum dryer (Bio-Rad) at 80°C for 1 hour until fully dehydrated. The dried gel was placed in a phosphor-imaging cassette with a phosphor-screen and exposed for 3-4 h before being imaged using a PMI autoradiograph imager (Bio-Rad).

2.2.6 Mass spectrometry

2.2.6.1 Sample preparation

400 ng GST-LRRK2 (aa 970-2527) was incubated with 1 µg His-HDAC6 and 1 mM ATP in 1x kinase buffer for 1 hour at 37°C. The kinase reaction was halted by addition of 20 mM EDTA and the samples were snap frozen in liquid nitrogen. Samples were boiled in NuPAGE LDS sample buffer (Thermo Scientific) for 10 min at 70°C in a Thermomixer (Eppendorf) at 800 rpm. 10 mM iodoacetamide was added and samples were incubated for 30 min at room temperature in the dark for alkylation of cysteine residues. Samples were run on a NuPAGE 4-12% Bis-TRIS precast gel (Thermo Scientific) at 150 V for 20 min with a PageRuler unstained protein ladder (Thermo Scientific). The gel was fixed in 40% methanol and 2% acetic acid for 30 min at room temperature before being stained with Brilliant Blue G Colloidal Coomassie (Sigma) in 20% methanol for 1 h at room temperature to stain protein bands. The gel was destained in 25% methanol for 1 h and the HDAC6 band of interest was cut out for further processing.

2.2.6.2 In gel digestion

The gel slice was incubated with 50% acetonitrile/50mM ammonium bicarbonate for 2 h at room temperature or 4°C overnight with gentle shaking at 600 rpm in a Thermomixer (Eppendorf). Liquid was removed and the process was repeated 4-5 times until the gel slices were colourless. When destaining was complete, the gel slices were incubated in 100% acetonitrile for 15 min at room temperature to shrink the gel pieces before all liquid was removed. For trypsin protein digestion, the dry gel slices were incubated in 1 ng/µl trypsin (Thermo Scientific) in 50 mM ammonium bicarbonate for 1 h at 37°C with shaking at 600 rpm in a Thermomixer followed by incubation for 16 h at room temperature. For peptide extraction, the gel slices were incubated with 100% acetonitrile for 15 min at 37°C with shaking at 600 rpm in a Thermomixer, before transfer of the supernatant to a new 1.5 ml peptide collection tube and incubation of the gel slices in 0.5% formic acid for 15 min at 37°C with shaking at 600 rpm in a Thermomixer. The gel slices were further incubated with 100% acetonitrile for 15 min at 37°C with shaking at 600 rpm in a Thermomixer and the supernatant was removed and added to the previous peptide collection tube. This process was repeated once with 0.5% formic acid followed by two times with 100% acetonitrile, and the final peptide collection tube was dehydrated in a SpeedVac

(Thermo Scientific) for 16 h at room temperature. The resulting peptides were stored at -20°C.

2.2.6.3 Analysis

Samples were analysed using LC-MS/MS on an Ultimate 3000 RSLC Nano LC System (Dionex) coupled to an LTQ Orbitrap Elite hybrid mass spectrometer (Thermo Scientific) equipped with an Easy-Spray (Thermo Scientific) ion source. Peptides were desalted online using an Acclaim PepMap100 capillary trap column (Thermo Scientific) and separated using 120 min RP gradient (4-30% acetonitrile/0.1% formic acid) on an Acclaim PepMap100 RSLC C18 analytical column (Thermo Scientific) with a flow rate of 0.25 µl/min. The mass spectrometer was operated in standard data dependent acquisition mode controlled by Xcalibur software (Thermo Scientific). The instrument was operated with a cycle of one MS (in the Orbitrap) acquired at a resolution of 60,000 at m/z 400, with the top 20 most abundant multiply-charged (2+ and higher) ions in each chromatographic window being subjected to CID fragmentation in the linear ion trap. An FTMS target value of 1e6 and an ion trap MSn target value of 5000 were used. Dynamic exclusion was enabled with a repeat duration of 30 s, an exclusion list of 500 and an exclusion duration of 60 s. Lock mass of 401.922 was enabled for all experiments.

Data was analysed using MaxQuant software (Cox & Mann, 2008). Data was searched against a UniProt human sequence database using the following search parameters: trypsin with a maximum of 2 missed cleavages, 7 ppm for MS mass tolerance, 0.5 Da for MS/MS mass tolerance, with acetyl (Protein N-term), phospho (STY) and oxidation (M) as variable modifications and carbamidomethyl (C) as a fixed modification. A protein FDR of 0.01 and a peptide FDR of 0.01 were used for identification level cut offs and high confidence phosphorylation sites were defined using a PEP cut-off of 0.01. Class I phosphorylation sites were defined with a localization probability of >0.75 and a score difference of >5. The ratio of intensity scores for phosphorylation sites in each experimental condition was calculated to show fold-increase compared to control samples.

2.2.7 HDAC6 activity assay

In vitro HDAC6 deacetylase activity was measured using a FLUOR DE LYS HDAC6 fluorometric drug discovery kit according to the manufacturer's protocol (Enzo Life Sciences) with the addition of 250 ng GST-tagged human LRRK2 wild-type, R1441C

or G2019S protein (amino acids 970-2527; Invitrogen) and 200 µM ATP. Samples were incubated with 5 µM acetylated substrate in Assay Buffer II for 45 min at room temperature in a half-volume white 96-well plate (Enzo Life Sciences), followed by addition of 1 µM TSA in Developer for 45 min at room temperature to halt HDAC6 activity and produce fluorescent signal. A PheraSTAR FS plate reader (BMG Labtech) was used to measure emission at 460 nm. All samples were run in triplicate and averaged before normalisation to HDAC6-only control for each independent experiment.

2.2.8 Immunofluorescence microscopy

2.2.8.1 Staining

Cells were grown on 13mm circular glass coverslips (Scientific Laboratory Supplies) in a 24-well plate (Sigma) and transfected at 60-80% confluence as previously described. At 24 h post-transfection, cells were fixed in 3.7% formaldehyde in PBS for 20 min at room temperature, washed twice with PBS and quenched in 0.05 M NH_4Cl for 15 min at room temperature. Cells were then permeabilised with 0.2% Triton X-100 in PBS for 3 minutes and washed once with PBS, followed by blocking in PBS with 0.2% fish gelatin (PBS/BLOCK) for 20 minutes at room temperature to reduce non-specific antibody binding. The coverslips were incubated with 30 µl of the primary antibody (Table 2.5) diluted in PBS/BLOCK on parafilm in a damp box for 1 h at room temperature, before 3 washes with PBS/BLOCK and incubation with diluted secondary antibody in PBS/BLOCK with 1:5000 of 10 µg/µl Hoechst 33342 (Thermo Scientific) for 1 hour at room temperature. Cells were washed 3 times with PBS/BLOCK and mounted onto glass slides (Fisherbrand) with fluorescence mounting medium (Dako).

2.2.8.2 Microscopy

Images were recorded using a 63x Plan-Apochromate 1.4 NA oil objective on a Zeiss Axioplan 2 microscope fitted with a Retiga R3 CCD camera using MicroManager software (Edelstein et al., 2014), or a 63x HCX PL APO 1.4 NA oil objective on a Leica TCS SP5 confocal microscope using LAS AF software (Leica Microsystems). All illumination, camera and acquisition settings remained constant during experiments to ensure comparability.

2.2.8.3 Quantification of tubulin acetylation

All image analysis was performed using FIJI software (Schindelin et al., 2012). Tubulin acetylation was quantified by calculating the mean gray value of signal intensity in the acetylated tubulin channel for a polygonal selection of cell area, where possible based on fluorescence in the appropriate channel indicating cell transfection. For each independent experiment, the individual raw acetylated tubulin intensity values from transfected cells were normalised to the average acetylated tubulin intensity of empty vector control-transfected cells to allow comparison between experiments.

2.2.8.4 Aggresome scoring

Aggresome counts were performed in FIJI software (Schindelin et al., 2012) by quantifying the number of GFP-CFTR-ΔF508 or GFP-250-expressing cells exhibiting co-localisation of the GFP signal with vimentin at a single, perinuclear aggresome structure. The percentage of aggresome-containing cells was calculated from the total number of GFP-CFTR-ΔF508 or GFP-250-expressing cells for each experimental condition.

2.2.9 Statistical analysis

All calculations were performed using Excel (Microsoft Corporation) and statistical analysis was performed in Prism 7 (GraphPad Software Inc.). Statistical significance between groups was determined by one-way ANOVA or t-test as indicated.

3 HDAC6 is a substrate of LRRK2

3.1 Introduction

Evidence suggests that LRRK2 plays a role in the regulation of microtubule acetylation. Embryonic fibroblasts from LRRK2 knockout mice show increased levels of α-tubulin acetylation at lysine-40 compared to fibroblasts from wild-type littermates (Law et al., 2014). PD-associated LRRK2 GTPase mutants show an abnormal interaction with deacetylated microtubules, reduce the axonal transport of mitochondria and cause locomotor deficits in a transgenic *Drosophila* model (Godena et al., 2014). These abnormal phenotypes are reversed by increasing microtubule acetylation using inhibitors of HDAC6 and SIRT2 deacetylase activity (Godena et al., 2014). In addition, peripheral cells from sporadic and G2019S patients show decreased levels of tubulin acetylation compared to peripheral cells from control subjects (Esteves et al., 2015). Disruption of microtubule acetylation by mutant LRRK2 may therefore be a pathogenic event in PD.

LRRK2 itself does not possess acetyltransferase or deacetylase activity. Acetylation of α-tubulin at lysine-40 is mediated by the acetyltransferase αTAT1 (Shida et al., 2010; Akella et al., 2010), whereas deacetylation occurs via HDAC6 or SIRT2 (Hubbert et al., 2002; North et al., 2003). The role of SIRT2 in regulating tubulin acetylation in the mammalian central nervous system remains controversial and it may preferentially deacetylate a subset of perinuclear-localised microtubules (Bobrowska et al., 2012; Taes et al., 2013; Skoge and Ziegler, 2016). Therefore, HDAC6 is considered to be the primary cytoplasmic tubulin deacetylase in neurons.

HDAC6 is a known phosphoprotein and phosphorylation may regulate its deacetylase activity (Brush et al., 2004; Linding et al., 2007; Chen et al., 2010). Furthermore, LRRK2 serine/threonine kinase activity is dysregulated in disease (West et al., 2005). This chapter therefore aims to establish if LRRK2 regulates HDAC6 activity by firstly testing if LRRK2 interacts with HDAC6 using co-immunoprecipitation experiments and *in vitro* binding assays. Furthermore, LRRK2 phosphorylation of HDAC6 is investigated using an *in vitro* kinase assay, followed by mass spectrometry analysis to identify potential target phospho-sites. Finally, HDAC6 phospho-sites identified *in vitro* are validated in cells using a phospho-specific antibody.

3.2 Results

3.2.1 LRRK2 interacts with HDAC6

To investigate if there is an interaction between LRRK2 and HDAC6, Myc-tagged LRRK2 was co-expressed with HDAC6 in HEK293 cells. Cells were lysed 24 hours post-transfection to allow exogenous protein expression and Myc-LRRK2 was immunoprecipitated using an anti-Myc antibody. Immunoprecipitates were subjected to SDS-PAGE and immunoblot for protein detection. HDAC6 was found to efficiently co-immunoprecipitate with Myc-LRRK2, therefore showing an interaction between LRRK2 and HDAC6 in HEK293 cells (Figure 3.1).

Whilst providing a good measure of whether two proteins interact in a cellular environment, co-immunoprecipitation does not necessarily indicate that an interaction is direct as proteins can co-immunoprecipitate as part of a complex with other interacting proteins. Therefore, to investigate if LRRK2 directly binds to HDAC6, an *in vitro* pull-down assay was performed using recombinant proteins. Recombinant GST-tagged human LRRK2 consisting of amino acids 970 to 2527 (N-terminal truncated as shown in Figure 3.2a) or a GST control was incubated with full-length human His-tagged HDAC6. GST-tagged proteins were pulled down using glutathione (GSH) beads. Bound GST-tagged protein was eluted using excess glutathione and samples were run on SDS-PAGE followed by immunoblot for protein detection. His-tagged HDAC6 was found to pull down with GST-tagged LRRK2 but not with the GST-only control, hence LRRK2 and HDAC6 interact *in vitro* (Figure 3.2a). As both HDAC6 and LRRK2 directly bind to β-tubulin (Zhang et al., 2003; Law et al., 2014), the presence of tubulin dimers in the GST-LRRK2 or His-HDAC6 recombinant protein samples could result in an indirect interaction between these two proteins after GST pull-down. To exclude this possibility, the presence of tubulin dimers in recombinant protein samples was checked using an anti-α-tubulin antibody. HEK293 cell lysate was used as a positive control for presence of tubulin. No tubulin was detected in either GST-LRRK2 or His-HDAC6 samples (Figure 3.2b). Taken together, the results from Figure 3.1 and Figure 3.2 show that there is an interaction between LRRK2 and HDAC6 in cells and that this interaction is direct *in vitro*.

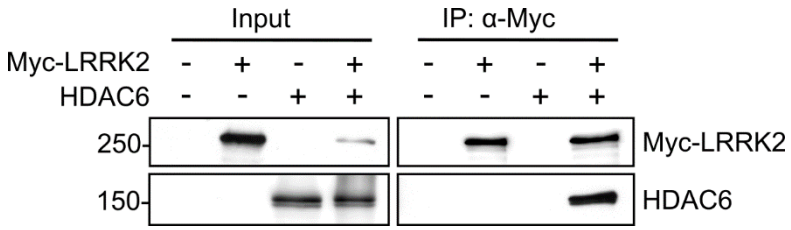

Figure 3.1. HDAC6 interacts with Myc-LRRK2 in HEK293 cells. HEK293 cells were co-transfected with Myc-LRRK2 or HDAC6 either with empty vector or together and lysed 24 h post-transfection. Anti-Myc antibody was used to immunoprecipitate Myc-LRRK2 along with interacting partners before protein separation by SDS-PAGE and immunoblotting with anti-Myc and anti-HDAC6 antibodies.

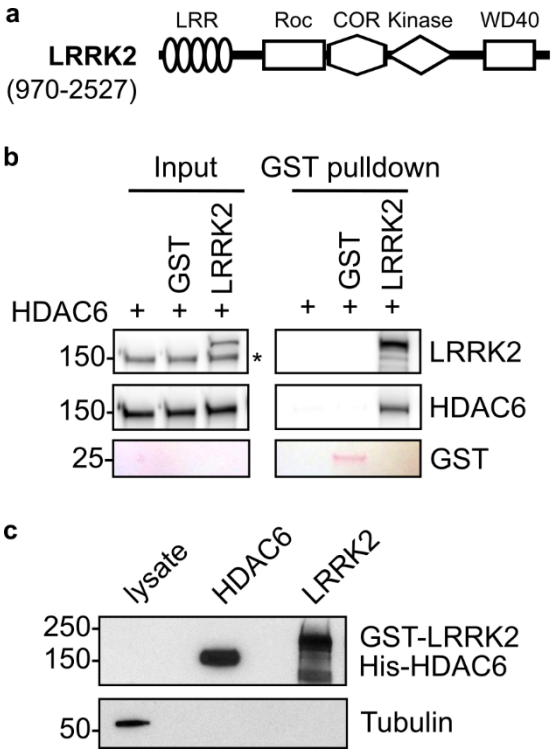

Figure 3.2. His-HDAC6 directly interacts with GST-LRRK2 *in vitro.* a) 1 µg full-length human His-HDAC6 was incubated with 1 µg human GST-tagged LRRK2 (aa 970-2527 as indicated). GST protein was used as a negative binding control. GSH beads were used to isolate GST-LRRK2 along with LRRK2 interacting partners. Middle panel is membrane after probing with anti-HDAC6 antibody. Upper panel is membrane after re-probing with anti-LRRK2 antibody (MJFF2), with HDAC6 signal still visible (*). Lower panel is Ponceau-S stained membrane to show presence of GST control. b) 1 µg His-HDAC6 or GST-LRRK2 variants were tested for presence of tubulin using an anti-tubulin antibody. 10 µg HEK293 cell lysate was used as positive control.

3.2.2 The LRRK2 Roc-COR tandem domain interacts with the HDAC6 deacetylase domains

As described in Chapter 1, LRRK2 is a 286 kDa, multi-domain protein which includes N-terminal armadillo (ARM) and ankyrin (ANK) repeat domains, a leucine-rich repeat (LRR) domain, a Ras of complex (Roc) GTPase domain and C-terminal of Roc (COR) domain, kinase domain, and a C-terminal WD40 domain (Figure 1.1) (Mills et al., 2012). HDAC6 is a 131 kDa protein which consists of two catalytic deacetylase domains, HD1 and HD2, and a C-terminal zinc finger domain (ZnF-UBP) which binds ubiquitinated proteins (Seigneurin-Berny et al., 2001). As shown in Figure 3.2, the interaction between LRRK2 and HDAC6 does not require the N-terminal amino acids 1 to 969 of LRRK2 which contain the ARM and ANK repeat domains as this region is truncated in the recombinant GST-LRRK2 protein. To further characterise the interaction between LRRK2 and HDAC6, tagged constructs containing multiple or individual domains from either protein were expressed in HEK293 cells. Firstly, Myc-tagged LRRK2 constructs comprising the Roc-COR, kinase and WD40 (RCKW) domains, Roc-COR and kinase (RCK) domains, Roc-COR domains, Roc domain, COR domain, or kinase domain (Figure 3.3a) were co-expressed with full-length HDAC6 or empty vector as a control. Cells were lysed 24 hours post-transfection and Myc-LRRK2 was immunoprecipitated using an anti-Myc antibody. The immunoprecipitates were subjected to SDS-PAGE followed by immunoblot to detect the Myc-LRRK2 constructs and any interacting HDAC6. HDAC6 co-immunoprecipitated efficiently with Myc-LRRK2-RCKW and RCK constructs, indicating that the interaction with HDAC6 does not require the N-terminal LRR or the C-terminal WD40 domain (Figure 3.3b). HDAC6 co-immunoprecipitated to a far weaker extent with the LRRK2 COR domain alone compared to with the LRRK2 RCK construct and did not co-immunoprecipitate at all with the LRRK2 kinase domain (Figure 3.3b). Expression of further Myc-LRRK2 domains showed that HDAC6 co-immunoprecipitated efficiently with the LRRK2 Roc domain alone, however the Roc-COR domain showed a weak interaction with HDAC6 (Figure 3.3c). These results indicate that the interaction between LRRK2 and HDAC6 is primarily mediated by the Roc domain of LRRK2, with a weak interaction occurring between the LRRK2 COR domain and HDAC6.

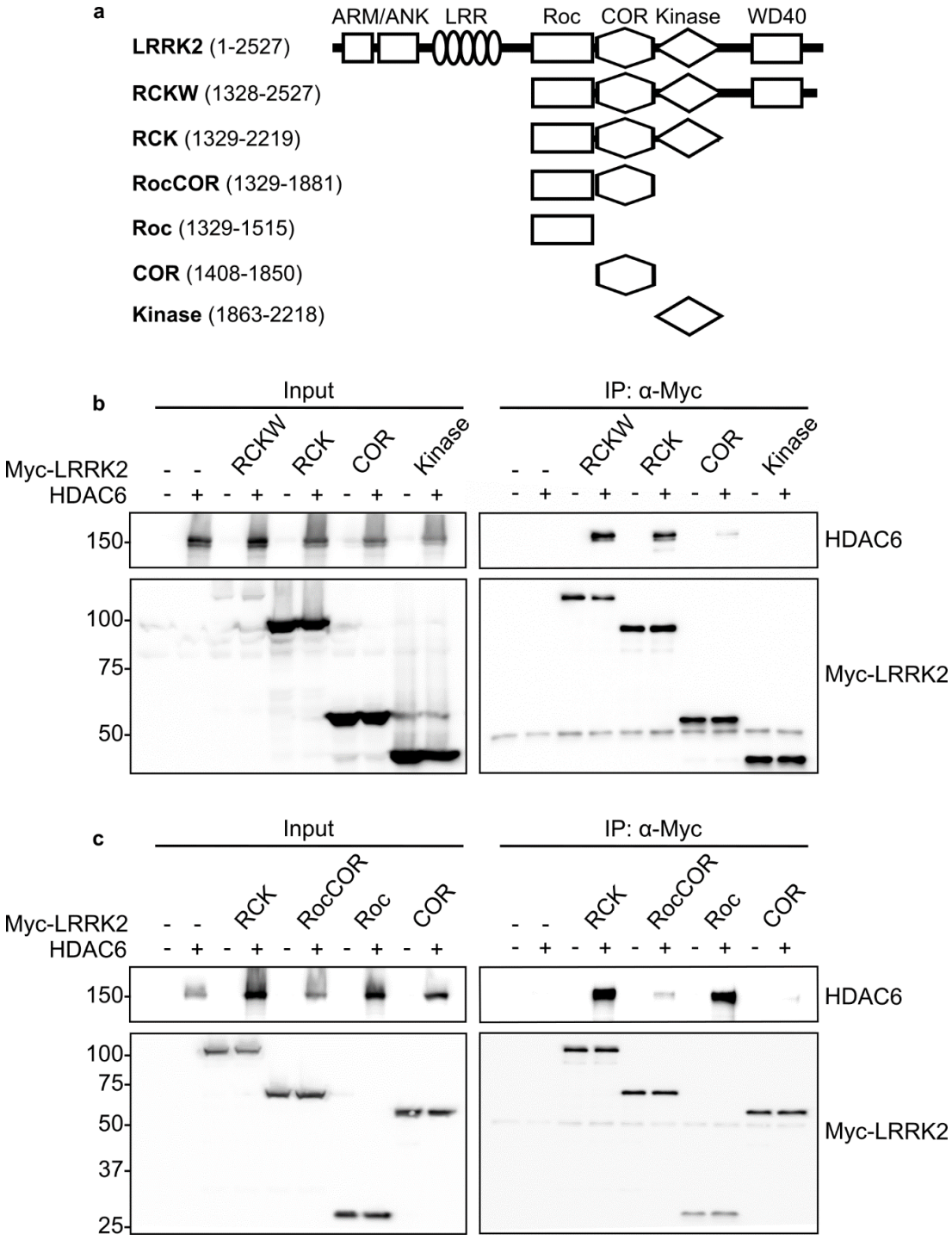

Figure 3.3. LRRK2 Roc-COR domain interacts with HDAC6. a) Myc-LRRK2-RCKW, RCK, Roc-COR, Roc, COR and kinase domain constructs were generated as indicated. b) HEK293 cells were co-transfected with Myc-LRRK2-RCKW, RCK, COR or kinase domain constructs (b) or Myc-LRRK2-RCK, Roc-COR, Roc or COR domain constructs (c) with either empty vector or HDAC6. Cells were lysed 24 h post-transfection and Myc-LRRK2 was immunoprecipitated using anti-Myc antibody. Following SDS-PAGE separation, proteins were immunoblotted using anti-HDAC6 and anti-Myc antibodies.

To identify the HDAC6 domains which mediate the interaction with LRRK2, the reverse experiment was performed with FLAG-tagged HDAC6 constructs comprising full-length HDAC6, the HD1 and HD2 deacetylase domains, HD1 domain, or the HD2 domain (Figure 3.4a). These FLAG-HDAC6 constructs were co-expressed with empty vector or Myc-LRRK2-RCK as the LRRK2 RCK region was shown to interact strongly with HDAC6 in Figure 3.3. Cells were lysed 24 hours post-transfection and FLAG-HDAC6 constructs were immunoprecipitated using an anti-FLAG antibody, before separation using SDS-PAGE and protein detected on immunoblot. Myc-LRRK2-RCK co-immunoprecipitated efficiently with full-length FLAG-HDAC6 as expected (Figure 3.4b). Myc-LRRK2-RCK also co-immunoprecipitated with the HDAC6 HD1+2 construct which contained both deacetylase domains of HDAC6 but not the C-terminal ZnF-UBP domain, showing that ubiquitin-binding ZnF-UBF domain is not required for the interaction with LRRK2. Furthermore, Myc-LRRK2-RCK co-immunoprecipitated with both the HD1 and HD2 domains of HDAC6 individually. These results show that both the HD1 and HD2 deacetylase domains of HDAC6 mediate the interaction with LRRK2-RCK and that the C-terminal ZnF-UBP domain is not required. Therefore, the interaction between LRRK2 and HDAC6 interaction is independent of the ubiquitin-binding capacity of HDAC6. Taken together, the results from Figure 3.3 and Figure 3.4 indicate that the LRRK2 Roc-COR domain, and primarily the Roc domain, interacts with both deacetylase domains of HDAC6.

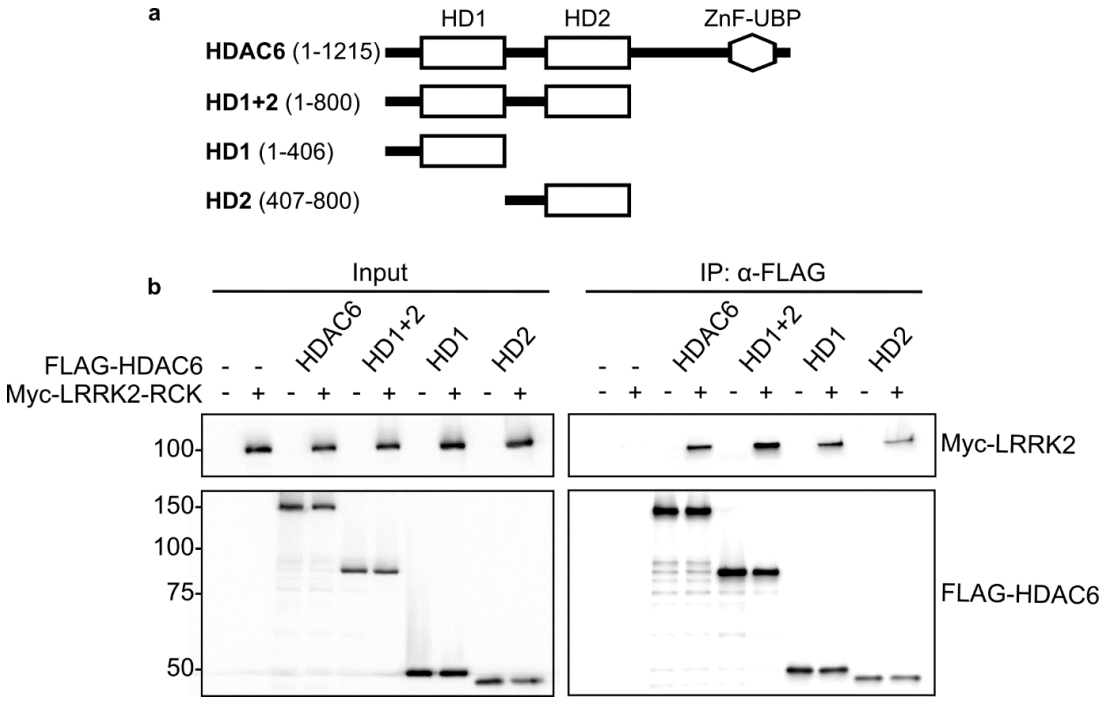

Figure 3.4. HDAC6 deacetylase domains interact with LRRK2-RCK domain. a) FLAG-HDAC6 full-length, HD1+2, HD1 or HD2 domain constructs were generated as indicated. b) HEK293 cells were co-transfected with FLAG-HDAC6 full-length, HD1+2, HD1 or HD2 domain constructs with either empty vector or Myc-LRRK2-RCK. Cells were lysed 24 h post-transfection and FLAG-HDAC6 was immunoprecipitated using anti-FLAG antibody. Following SDS-PAGE separation, proteins were immunoblotted using anti-Myc and anti-FLAG antibodies.

3.2.3 Pathogenic LRRK2 mutations alter LRRK2/HDAC6 complex formation

Pathogenic mutations in LRRK2 cluster within the Roc-COR and kinase domains and alter the catalytic GTPase and kinase activity of LRRK2. The R1441C mutation in the Roc domain and Y1699C mutation in the COR domain decrease the GTPase activity of LRRK2, whereas the G2019S mutation in the kinase domain increases its kinase activity (West et al., 2005; Greggio et al., 2006; Lewis et al., 2007; Daniëls et al., 2011). The R1441C mutation has been shown to increase the interaction between LRRK2 and β-tubulin which is mediated by the Roc domain (Law et al., 2014). Conversely, mutations which mimic autophosphorylation of the LRRK2 Roc domain and act as a proxy for increased LRRK2 kinase activity, T1343D and T1491D, show decreased β-tubulin binding domain (Law et al., 2014). These results suggest that the GTPase and kinase activity of LRRK2 regulates protein binding to the LRRK2 Roc domain.

As the interaction between LRRK2 and HDAC6 is mediated by the Roc-COR GTPase domain (Figure 3.3), the requirement for LRRK2 GTPase and kinase activity for the interaction with HDAC6 was tested by co-immunoprecipitation using GTP binding-deficient K1347A (Lewis et al., 2007) or kinase-dead D1994A (West et al., 2007) mutants. In addition, the effects of pathogenic mutations in the LRRK2 Roc-COR domain (R1441C and Y1699C) and kinase domain (G2019S) were investigated to determine if they alter the interaction with HDAC6. Myc-tagged LRRK2 wild-type, K1347A, D1994A or pathogenic R1441C, Y1699C and G2019S mutants were co-expressed with HDAC6 in HEK293 cells. Following cell lysis at 24 hours post-transfection, the Myc-LRRK2 variants were immunoprecipitated from the lysate using an anti-Myc antibody. The resulting immunoprecipitates were separated using SDS-PAGE and Myc-LRRK2 and HDAC6 were detected on immunoblot (Figure 3.5a). HDAC6 showed increased co-immunoprecipitation with LRRK2 K1347A and D1994A compared to wild-type LRRK2, indicating that both LRRK2 GTP binding and kinase activity regulate the interaction with HDAC6 (Figure 3.5b). HDAC6 showed increased co-immunoprecipitation with the pathogenic LRRK2 Y1699C mutant but not the R1441C mutant, highlighting differing effects of these mutations on the interaction with HDAC6 despite both mutations being reported to lower the GTPase activity of LRRK2 (Lewis et al., 2007; Daniëls et al., 2011). In contrast, HDAC6 showed decreased co-immunoprecipitation with LRRK2 G2019S (Figure 3.5b). The opposing effects of kinase-dead D1994A and G2019S mutations on the co-immunoprecipitation

of HDAC6 suggests that elevated LRRK2 kinase activity reduces the interaction between LRRK2 and HDAC6. Together, these results suggest that both the GTPase and kinase activities of LRRK2 mediate its interaction with HDAC6 in cells and the strength of this interaction is altered by both functional and pathogenic mutations in the catalytic domains of LRRK2.

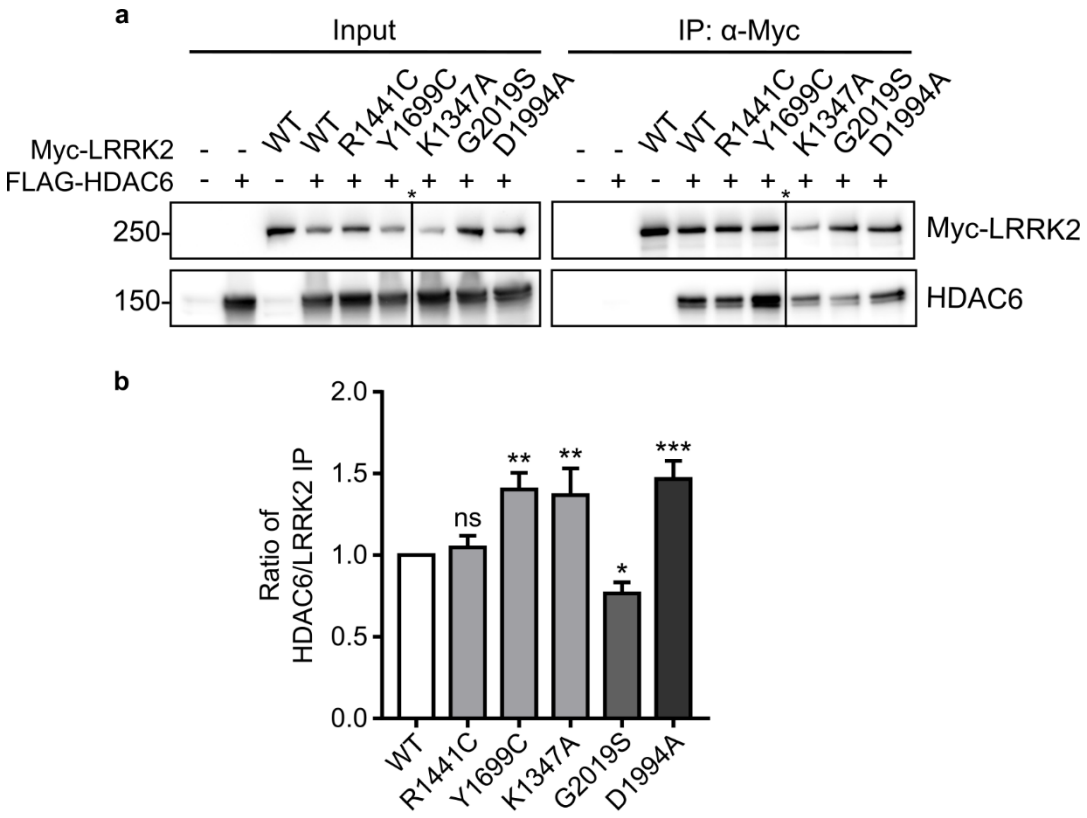

Figure 3.5. LRRK2 mutations affect binding to HDAC6. a) HEK293 cells were co-transfected with empty vector or Myc-LRRK2 wild-type, R1441C, Y1699C, K1347A, G2019S and D1994A variants with HDAC6. Cells were lysed 24 h post-transfection and Myc-LRRK2 was immunoprecipitated using anti-Myc antibody. Following SDS-PAGE separation, proteins were visualised using anti-myc antibody (upper panels) and anti-HDAC6 antibody (lower panels). * indicates location of removed lane due to unrelated sample loading. b) Quantification of relative HDAC6 to Myc-LRRK2 levels in immunoprecipitated samples (data shown as mean ± SEM; one-way ANOVA with Fisher's LSD test, ns = non-significant, * = $P \leq 0.05$, ** = $P \leq 0.01$, *** = $P \leq 0.001$; N=5 experiments (WT, R1441C, G2019S), N=4 (Y1699C, D1994A), N=3 (K1347A)).

3.2.4 LRRK2 phosphorylates HDAC6 *in vitro* at serine-22 and serine-689

HDAC6 is a known phosphoprotein (Brush et al., 2004; Linding et al., 2007) and phosphorylation may regulate its function. Phosphorylation of HDAC6 at serine-22 correlates with increased deacetylase activity in rat hippocampal neurons and is potentially mediated by the kinase GSK3β (Chen et al., 2010). Similarly, phosphorylation of HDAC6 serine-458 is stimulated by casein kinase 2 (CK2) and phosphorylation of serine-1035 by extracellular signal-regulated kinase (ERK), both of which increase deacetylase activity (Watabe and Nakaki, 2011; Williams et al., 2013). Conversely, phosphorylation of HDAC6 tyrosine-570 in the second deacetylase domain HD2 by epidermal growth factor receptor (EGFR) inhibits deacetylase activity (Deribe et al., 2009). Therefore, phosphorylation of HDAC6 by LRRK2 could provide a mechanism to regulate its function.

To determine if HDAC6 could be phosphorylated by LRRK2 *in vitro*, a kinase assay with recombinant protein was performed. GST-LRRK2 (amino acids 970-2527) was incubated with two separate manufacturer lots of His-HDAC6 and radiolabelled ^{32}P-ATP. Phosphorylation events in the presence of ^{32}P-ATP transfer ^{32}P onto substrate proteins and therefore allow detection of phosphorylated proteins. Following SDS-PAGE separation, total protein was detected using a Coomassie protein stain (Figure 3.6a) and ^{32}P incorporation was detected by radiography. As expected, LRRK2 showed a high level of autophosphorylation when incubated with ^{32}P-ATP (Figure 3.6b; Webber et al., 2011). HDAC6 showed increased ^{32}P signal in the presence of LRRK2, indicating HDAC6 was phosphorylated by LRRK2 (Figure 3.6b). Interestingly, LRRK2 autophosphorylation was markedly increased in the presence of HDAC6 which suggests that HDAC6 may stimulate the kinase activity of LRRK2. LRRK2 is not known to undergo acetylation and therefore the mechanism which promotes this increase in autophosphorylation requires further investigation.

To further characterise the phosphorylation of HDAC6 by LRRK2, mass spectrometry analysis was performed to identify specific LRRK2-mediated phosphosites on HDAC6. His-HDAC6 was incubated with GST-LRRK2 and unlabelled ATP, with His-HDAC6-only samples used as a control for baseline levels of HDAC6 phosphorylation. Following separation by SDS-PAGE, proteins were stained with Coomassie and the HDAC6 band of interest was extracted and digested with trypsin to create peptide fragments. Peptides were subsequently analysed using liquid chromatography-tandem mass spectrometry (LC-MS/MS). The intensities of two

high-confidence HDAC6 phosphorylation sites were found to be increased in the presence of LRRK2; serine-22 (10.17 fold-increase versus HDAC6-only control; Figure 3.7a) and serine-689 (3.22 fold-increase versus HDAC6-only control; Figure 3.7b). Taken together, these results indicate that HDAC6 is phosphorylated *in vitro* by LRRK2 at serine-22 in the N-terminus and serine-689 in the C-terminal deacetylase domain HD2.

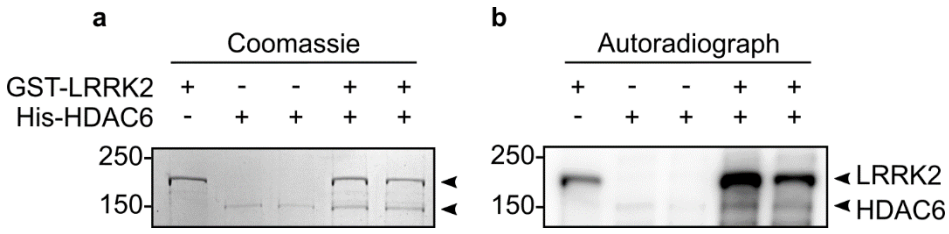

Figure 3.6. LRRK2 phosphorylates HDAC6 *in vitro*. 500 ng GST-LRRK2 (aa 970-2527) was incubated with 500 ng His-HDAC6 and 57 nm ^{32}P-ATP for 1 h at 37°C. Following separation with SDS-PAGE, proteins were visualised using Coomassie staining (left panel) and incorporation of ^{32}P onto HDAC6 and LRRK2 was detected using a phosphor screen (right panel).

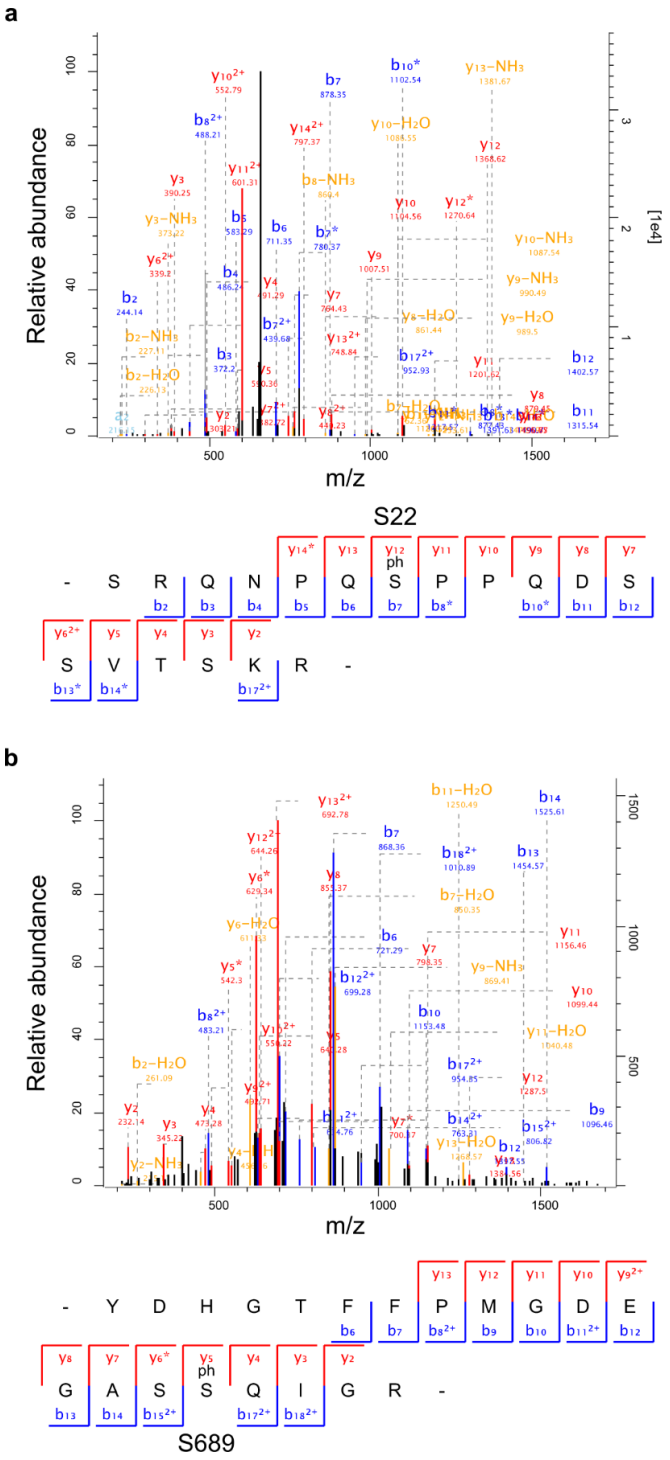

Figure 3.7. LRRK2 phosphorylates HDAC6 at serine-22 and serine-689 *in vitro*. 400 ng GST-LRRK2 (aa 970-2527) was incubated with 1 µg His-HDAC6 and 1 mM ATP. Following separation on SDS-PAGE, proteins were digested using trypsin and peptide fragments analysed using LC-MS/MS. High-confidence HDAC6 phosphorylation sites were identified at serine-22 (a) and serine-689 (b) after incubation with LRRK2. Sample analysis performed in collaboration with Dr M. Collins (University of Sheffield).

3.2.5 LRRK2 increases HDAC6 phosphorylation at serine-22

Phosphorylation of HDAC6 at serine-22 has been studied in rat hippocampal neurons using the commercial antibody ab61058 (Abcam) for immunolocalisation experiments (Chen et al., 2010). The specificity of this antibody for detection of HDAC6 phosphorylated at serine-22 on western blot was tested in view of providing a tool for the detection of LRRK2-mediated phosphorylation of HDAC6 serine-22 in cells. To check specificity of this antibody, HEK293 cells were transfected with human FLAG-HDAC6 wild-type or a mutant with serine-22 mutated to alanine. A serine to alanine mutation prevents phosphorylation at a specific site whilst retaining the same overall charge as the wild-type protein (Egelhoff et al., 1993). Cells were lysed 24 hours post-transfection and FLAG-HDAC6 constructs were immunoprecipitated using an anti-FLAG antibody to enrich the levels of phosphorylated HDAC6 for detection on immunoblot. Phospho-serine-22 was detected after immunoprecipitation for wild-type HDAC6 but not the S22A mutant (Figure 3.8), showing that the phospho-antibody is specific for HDAC6 serine-22.

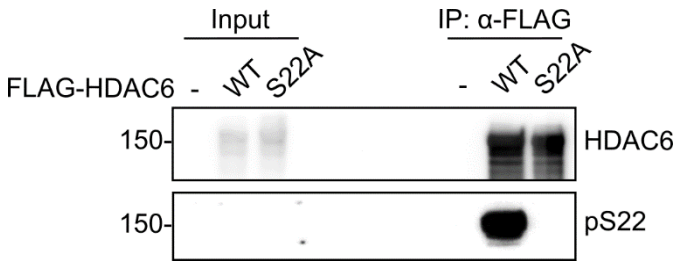

Figure 3.8. HDAC6 phospho-serine 22 antibody is site-specific. HEK293 cells were transfected with empty vector, FLAG-HDAC6 or FLAG-HDAC6-S22A and lysed 24h post-transfection before immunoprecipitation using anti-FLAG antibody. Lysates were run on SDS-PAGE and immunoblot. Anti-HDAC6 antibody was used for total HDAC6 protein detection. HDAC6 phospho-serine-22 was detected using ab61058 (Abcam).

Using the phospho-specific antibody for HDAC6 serine-22 validated in Figure 3.8, the effect of LRRK2 overexpression on levels of FLAG-HDAC6 phosphorylation was investigated in HEK293 cells. FLAG-HDAC6 was co-expressed with empty vector or Myc-LRRK2 and kinase-dead LRRK2 D1994A was used as a negative control. In addition, the pathogenic LRRK2 G2019S mutant was included. LRRK2 G2019S has been well-described to possess elevated kinase activity compared to wild-type LRRK2 and therefore may cause increased HDAC6 phosphorylation (West et al., 2005; Greggio et al., 2006). Cells were lysed 24 hours post-transfection and FLAG-HDAC6 was immunoprecipitated using an anti-FLAG antibody. Following separation using SDS-PAGE, levels of phospho-HDAC6 serine-22, total FLAG-HDAC6 and Myc-LRRK2 were detected on immunoblot. The level of immunoprecipitated FLAG-HDAC6 phosphorylated at serine-22 was increased ~1.4 to 1.5-fold when co-expressed with Myc-LRRK2 wild-type and G2019S compared to the FLAG-HDAC6-only control (Figure 3.9). The kinase-dead LRRK2 D1994A mutant showed no change in HDAC6 serine-22 phosphorylation. These results provide evidence for LRRK2-mediated phosphorylation of HDAC6 at serine-22 in HEK293 cells.

To confirm that serine-22 phosphorylation was not influenced by FLAG-HDAC6 overexpression, endogenous HDAC6 phosphorylation at serine-22 was investigated after Myc-LRRK2 overexpression. Myc-LRRK2 or empty vector were expressed in HEK293 cells and following cell lysis at 24 hours post-transfection, endogenous HDAC6 was immunoprecipitated using an anti-HDAC6 antibody. As before, proteins were separated using SDS-PAGE and detected on immunoblot. Endogenous levels of phosphorylated HDAC6 at serine-22 were detected after immunoprecipitation and showed a ~1.25 fold-increase after expression of Myc-LRRK2 compared to the empty vector control (Figure 3.10). This increase in serine-22 phosphorylation after Myc-LRRK2 expression was likely an underestimation due to the incomplete transfection efficiency of Myc-LRRK2 in all cells. Taken together, the results from Figure 3.9 and Figure 3.10 show that expression of wild-type LRRK2 but not kinase-dead LRRK2 increases levels of HDAC6 serine-22 phosphorylation, therefore indicating that LRRK2 phosphorylates HDAC6 at serine-22 in cells.

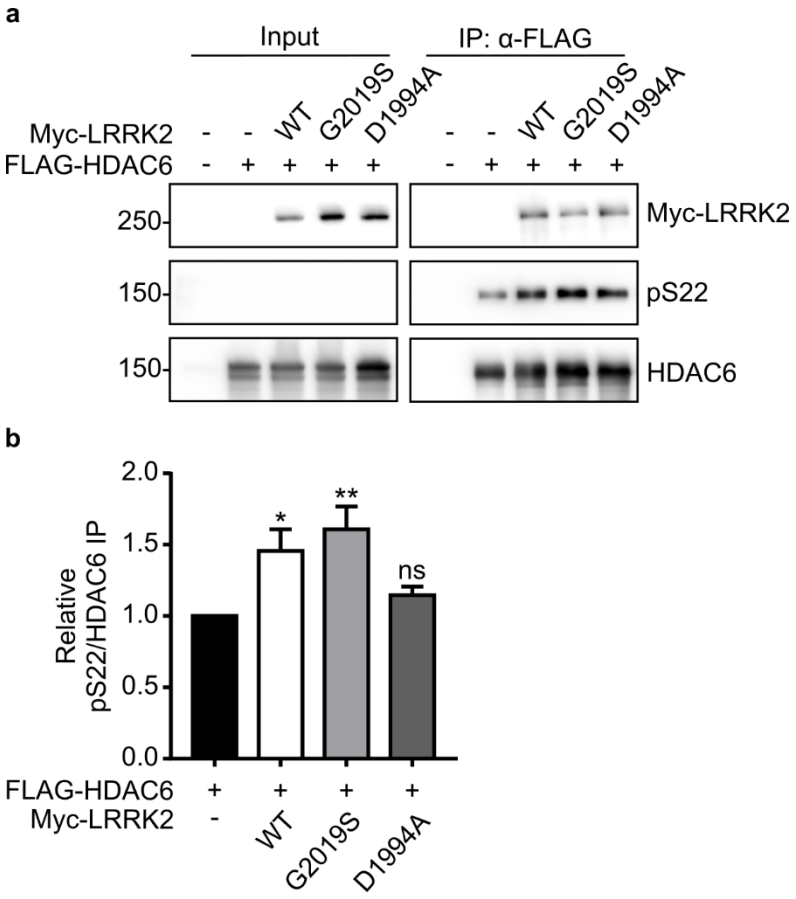

Figure 3.9. LRRK2 increases FLAG-HDAC6-S22 phosphorylation in HEK293 cells. a) HEK293 cells were co-transfected with empty vector, Myc-LRRK2-WT, Myc-LRRK2-G2019S or Myc-LRRK2-D1994A with FLAG-HDAC6. Cells were lysed 24h post-transfection and immunoprecipitated using anti-FLAG antibody. HDAC6 phospho-serine 22 was detected using ab61058 (Abcam). b) Quantification of the ratio of pS22 to total FLAG-HDAC6 in IP samples normalised to FLAG-HDAC6-only control from four independent experiments (data shown as mean ± SEM; one-way ANOVA with Fisher's LSD test, * = $P \leq 0.05$, **= $P \leq 0.01$, N=4).

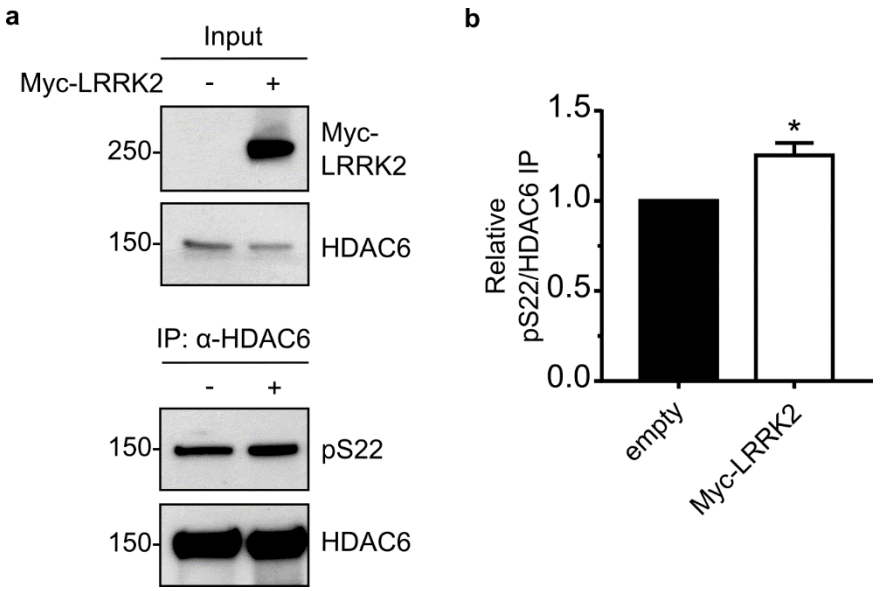

Figure 3.10. LRRK2 increases endogenous HDAC6-S22 phosphorylation in HEK293 cells. a) HEK293 cells were transfected with empty vector or Myc-LRRK2. Cells were lysed 24h post-transfection and immunoprecipitated using anti-HDAC6 antibody. Following SDS-PAGE separation, proteins were immunoblotted using anti-Myc and anti-HDAC6 antibodies. HDAC6 phospho-serine 22 was detected using ab61058 (Abcam). b) Quantification of the ratio of pS22 to total HDAC6 in IP samples normalised to empty vector control from three independent experiments (data shown as mean ± SEM; student's t-test, * = $P \leq 0.05$, N=3).

3.3 Discussion

Increased tubulin acetylation is a key feature of both LRRK2 knockout and HDAC6 knockout mice, suggesting that LRRK2 and HDAC6 may function in a common pathway for the regulation of tubulin acetylation (Zhang et al., 2008; Law et al., 2014). In this chapter, LRRK2 was shown to interact with HDAC6 in HEK293 cells through co-immunoprecipitation (Figure 3.1) and this interaction was confirmed to be direct in an *in vitro* pull-down assay using recombinant LRRK2 and HDAC6 protein (Figure 3.2). Further characterisation showed that HDAC6 interacts with the Roc-COR GTPase domain of LRRK2, suggesting the involvement of LRRK2 GTPase function or GTP binding in the interaction between LRRK2 and HDAC6 (Figure 3.3). In support of this, functional and pathogenic LRRK2 mutations in the GTPase domain which disrupt LRRK2 GTPase activity were found to affect the interaction with HDAC6 (Figure 3.5). The pathogenic Y1699C mutation in the COR domain and the GTP-binding deficient K1347A mutant in the Roc domain both increased HDAC6 binding (Figure 3.5). The Y1699C mutation is thought to strengthen the intra-molecular interaction between the Roc and COR domains of LRRK2 and weaken dimer formation to reduce the GTPase activity of LRRK2, whereas the K1347A mutation prevents GTP binding to the GTP γ-phosphate coordinating motif (Lewis et al., 2007; Daniëls et al., 2011; Taymans et al., 2011). These results suggest that LRRK2 GTPase function negatively regulates the interaction with HDAC6. However, the pathogenic LRRK2 R1441C mutation in the Roc domain had no effect on HDAC6 binding despite disrupting the GTPase activity of LRRK2 (Lewis et al., 2007). The reasons for this disparity are not clear but may reflect differences in the effect of these mutations on LRRK2 dimer structure despite a common disruption of GTPase activity. Both Y1699C and K1347A mutations disrupt the dimerisation of LRRK2, whereas R1441C does not appear to affect dimer formation (Sen et al., 2009; Daniëls et al., 2011; Biosa et al., 2013). LRRK2 dimers show increased membrane localisation whereas LRRK2 monomers are primarily cytosolic (Berger et al., 2010). HDAC6 exists predominantly in the cytoplasm as a microtubule deacetylase (Hubbert et al., 2002; Bertos et al., 2004). Therefore, reduced LRRK2 dimer formation as a result of the Y1699C and K1347A mutations may increase the binding of LRRK2 to HDAC6 in the cytoplasm. The kinase activity of LRRK2 may also regulate its interaction with HDAC6. The G2019S mutation in the LRRK2 kinase domain reduced the interaction between LRRK2 and HDAC6 (Figure 3.5). The G2019S mutation has been consistently shown to increase LRRK2 kinase activity (West et al., 2005; Greggio et al., 2006; Jaleel et al., 2007). Conversely, the kinase-dead D1994A mutation in

LRRK2 increased the interaction with HDAC6. These results suggest that LRRK2 kinase activity acts to negatively regulate the interaction with HDAC6. In the context of the LRRK2 activation model described in Chapter 1, increased LRRK2 kinase activity correlates with increased dimer formation (Gilsbach and Kortholt, 2014). The G2019S mutation increases LRRK2 dimer formation and the D1994A mutation disrupts dimer formation compared to wild-type LRRK2 (Sen et al., 2009). Therefore, increased LRRK2 dimer formation caused by the G2019S mutation may reduce the interaction with HDAC6. Together, these results suggest that the dimer status of LRRK2 may be important for the interaction between LRRK2 and HDAC6 and both pathogenic and functional LRRK2 mutations which alter the propensity of LRRK2 to dimerise subsequently affect this interaction.

Further characterisation of the interaction between LRRK2 and HDAC6 showed that both deacetylase domains of HDAC6 (HD1 and HD2) mediate the interaction with LRRK2 (Figure 3.4). LRRK2 directly interacts with ß-tubulin via its Roc domain and this interaction is decreased by the pathogenic G2019S mutation after co-immunoprecipitation and increased by the pathogenic R1441C mutation in a yeast 2-hybrid (Y2H) assay (Law et al., 2014). HDAC6 also binds to β-tubulin and this interaction is mediated by both its deacetylase domains (Zhang et al., 2003). It is therefore a possibility that LRRK2 and HDAC6 form a complex with ß-tubulin at the microtubule to regulate α-tubulin acetylation. Evidence shows that the two deacetylase domains have distinct roles in the overall activity of HDAC6. *In vitro*, the first deacetylase domain is not catalytically active alone and deacetylase activity is conferred by the C-terminal deacetylase domain (Zou et al., 2006). Furthermore, both deacetylase domains are required for full deacetylase activity both *in vitro* and *in vivo* but selectively interact with different substrates (Zhang et al., 2006). The majority of HDAC6 inhibitors which abolish tubulin deacetylase activity target the second deacetylase domain, suggesting that the C-terminal deacetylase confers tubulin deacetylation activity whilst the N-terminal domain recruits tubulin substrates (Haggarty et al., 2003). Hence, the interaction of LRRK2 with the HDAC6 deacetylase domains raised the possibility that LRRK2 regulates HDAC6 deacetylase activity via phosphorylation of these domains. LRRK2-mediated phosphorylation of HDAC6 was therefore investigated in Figure 3.6 to Figure 3.10.

Using mass spectrometry, wild-type LRRK2 was found to phosphorylate human HDAC6 *in vitro* at serine-22 and serine-689 (Figure 3.7). Use of an HDAC6 serine-22 phospho-specific antibody confirmed that this residue is phosphorylated by LRRK2 in cells for both overexpressed and endogenous HDAC6 (Figure 3.9 and Figure 3.10).

Serine-22 is situated at the N-terminus of HDAC6 in a region containing a nuclear localisation signal (NLS) (Bertos et al., 2004). Phosphorylation of the NLS of other members of the histone deacetylase (HDAC) family of proteins such as HDAC5 regulates their nuclear import (Greco et al., 2011). However, evidence suggests that HDAC6 nuclear import is regulated by acetylation rather than phosphorylation (Liu et al., 2012b). Phosphorylation of HDAC6 at serine-22 correlates with increased HDAC6 deacetylase activity in hippocampal neurons (Chen et al., 2010). Therefore, LRRK2-mediated phosphorylation of HDAC6 serine-22 may stimulate HDAC6 deacetylase activity. Serine-689 is a novel HDAC6 phosphosite situated within the second deacetylase domain of HDAC6. As a novel phosphosite, no phospho-specific antibodies are commercially available for HDAC6 serine-689 and hence a custom antibody is being optimised at the time of writing. This will be used to confirm that LRRK2 phosphorylates HDAC6 at serine-689 in cells and aid further study of its relevance to HDAC6 function. Given that the HD2 domain confers HDAC6 tubulin deacetylase activity, phosphorylation of this domain may regulate deacetylase activity. Indeed, phosphorylation of tyrosine-570 inversely correlates with deacetylase activity (Deribe et al., 2009). Therefore, phosphorylation of HDAC6 serine-689 by LRRK2 may regulate the deacetylase activity of HDAC6, and this will be investigated in Chapter 5.

HDAC6 has an important role in the cellular degradation of ubiquitinated proteins (Boyault et al., 2007). In response to misfolded protein, HDAC6 mediates the formation of aggresome structures and is also involved in autophagic clearance (Kawaguchi et al., 2003; Lee et al., 2010). This is of great significance in neurodegenerative diseases such as PD of which a hallmark pathology is accumulation of aggregated protein. Indeed, HDAC6 is a component of Lewy bodies in PD patients (Kawaguchi et al., 2003). The next chapter will focus on the role of HDAC6 in aggresome formation and how the interaction between LRRK2 and HDAC6 may regulate this pathway, as well as investigating a functional role for the LRRK2 phosphorylation sites within HDAC6.

4 LRRK2 regulates HDAC6-mediated aggresome formation

4.1 Introduction

In Chapter 3, LRRK2 was shown to directly interact with and phosphorylate the Class IIb histone deacetylase HDAC6. HDAC6 coordinates the cellular degradation of ubiquitinated proteins in the cytoplasm by aiding their progression down degradation pathways (Boyault et al., 2007). Under normal cellular conditions, many proteins are ubiquitinated to allow their recognition by the proteasome for degradation (reviewed by Glickman and Ciechanover, 2002). If the proteasome becomes damaged or overwhelmed, HDAC6 binds poly-ubiquitinated proteins via its C-terminal ZnF-UBP ubiquitin-binding domain and recruits them to cytoplasmic dynein motors for transport along the microtubule network to a single, perinuclear structure at the microtubule-organising centre (MTOC) called the aggresome for subsequent removal by autophagy (Johnston et al., 1998; Kawaguchi et al., 2003). These ubiquitin-rich structures are surrounded by a cage consisting of the intermediate filament vimentin (Johnston et al., 1998). In neurons, microtubules are not associated with a central MTOC and multiple inclusion bodies can occur in the neuronal cytoplasm (Yu and Baas, 1994; Kopito, 2000). Furthermore, neuronal aggresomes are encapsulated by a cage consisting of neurofilaments rather than vimentin (Taylor et al., 2003). HDAC6 promotes aggresome formation over proteasomal degradation via its interaction with the proteasomal promoter chaperone VCP/p97, thereby acting at a crossroads for determining the fate of misfolded protein (Boyault et al., 2006).

LRRK2 has been shown to co-localise with aggresomes after proteasomal inhibition and may have a role in aggresome formation (Waxman et al., 2009; Bang et al., 2016). Given that LRRK2 interacts with HDAC6, and HDAC6 has a well-described role in formation of ubiquitin-positive aggresomes, the regulation of HDAC6-mediated aggresome formation by LRRK2 is investigated in this chapter. The relevance of the LRRK2-mediated phosphorylation of HDAC6 at serine-22 and serine-689 described in Chapter 3 is studied to investigate if phosphorylation of HDAC6 regulates its function in ubiquitinated aggresome formation. Furthermore, the effects of pathogenic LRRK2 mutations on HDAC6-mediated aggresome formation are investigated to determine if this is a mechanism which may be disrupted in disease.

4.2 Results

4.2.1 LRRK2 is required for HDAC6-dependent aggresome formation

Aggresome formation was first described using a mutant form of the transmembrane protein cystic fibrosis transmembrane conductance regulator (CFTR) which causes the autosomal recessive disease cystic fibrosis. CFTR is a cAMP-activated chloride ion channel which regulates fluid transport in epithelial cells (Denning et al., 1992). The pathogenic ΔF508 mutation prevents the correct folding and membrane localisation of CFTR and leads to its ubiquitination and proteasomal degradation (Ward and Kopito, 1994; Jensen et al., 1995). Upon proteasomal inhibition, green fluorescent protein (GFP)-tagged CFTR-ΔF508 forms aggresome structures encapsulated by a vimentin cage at the MTOC (Johnston et al., 1998). Formation of GFP-CFTR-ΔF508 aggresomes is HDAC6-dependent and occurs via binding of HDAC6 to poly-ubiquitin chains on GFP-CFTR-ΔF508 (Kawaguchi et al., 2003).

Expression of the cytosolic protein chimera GFP-250 also results in aggresome formation (García-Mata et al., 1999). GFP-250 consists of the first N-terminal 250 amino acids of the cytosolic protein p115 fused at its N-terminus to full length GFP. Unlike GFP-CFTR-ΔF508, aggresomes formed by GFP-250 are not poly-ubiquitinated and can form without proteasomal inhibition in an HDAC6-independent mechanism which requires the chaperone Bcl-2-associated athanogene 3 (BAG3) (Gamerdinger et al., 2011). Therefore, GFP-CFTR-ΔF508 and GFP-250 can be used as aggresome markers to investigate both ubiquitin/HDAC6 dependent and independent aggresome formation. To promote aggresome formation, cells can be treated with small molecule proteasome inhibitors to prevent proteasomal degradation of cytoplasmic proteins and stimulate the aggresome response (Johnston et al., 1998). MG132 is a potent, reversible peptide inhibitor which blocks the proteolytic activity of the 26S proteasome complex and promotes aggresome formation (Lee and Goldberg, 1998; Kawaguchi et al., 2003).

To generate a loss-of-function model for studying the role of LRRK2 in aggresome formation, two siRNAs were obtained which target human LRRK2 and show successful knockdown of endogenous LRRK2 protein (Häbig et al., 2007; Alegre-Abarrategui et al., 2009). These were designated LRRK2 siRNA #1 and #2, respectively (Table 2.2). To test the efficiency of these siRNAs, HEK293 cells were transfected with LRRK2 siRNA #1 and siRNA #2 individually and together (LRRK2 siRNA pool). Non-targeting siRNA was used as a negative control. Cells were

harvested 96 hours post-knockdown and LRRK2 was immunoprecipitated using the anti-LRRK2 (UDD3) antibody to aid the detection of endogenous LRRK2 which is not highly expressed. Following separation on SDS-PAGE, proteins were detected using anti-LRRK2 and anti-tubulin antibodies on immunoblot. Endogenous LRRK2 was detected after immunoprecipitation in the non-transfected and non-targeting control-treated samples (Figure 4.1a). Treatment with both LRRK2 siRNAs #1 and #2 as well as the siRNA pool reduced the amount of immunoprecipitated LRRK2 by around 80% compared to treatment with the non-targeting control. LRRK2 knockdown using pool siRNA was further verified using immunofluorescence in HEK293 cells. Following treatment with non-targeting control or LRRK2 pool siRNA, cells were fixed at 96 hours-post knockdown and stained with the anti-LRRK2 antibody UDD3 or the anti-LRRK2-phospho-S935 antibody UDD2 (Figure 4.1b). For both anti-LRRK2 antibodies used, a marked reduction in staining was seen after LRRK2 siRNA knockdown compared to the non-targeting control (NTC) siRNA. Together, these results indicate that endogenous LRRK2 protein expression in HEK293 cells is significantly reduced after treatment with LRRK2 siRNA.

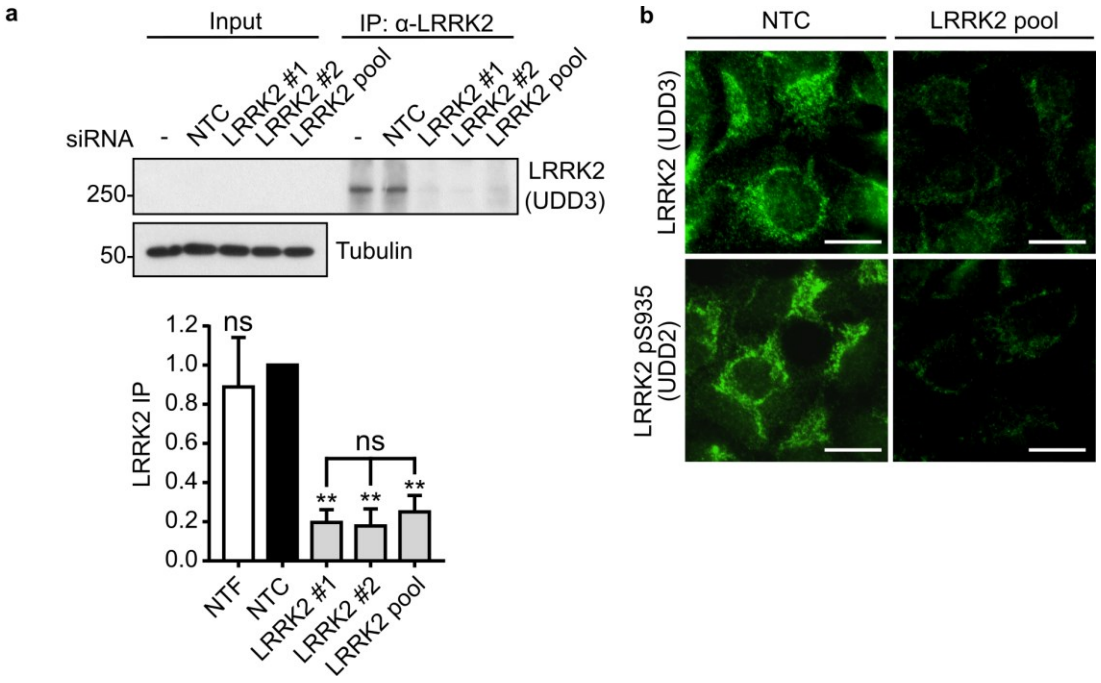

Figure 4.1. LRRK2 siRNA knockdown in HEK293 cells. a) HEK293 cells were transfected with either NTC, LRRK2 #1, LRRK2 #2 or both LRRK2 #1 and #2 (pool) siRNA. Cells were lysed at 72h post-knockdown and LRRK2 was immunoprecipitated using anti-LRRK2 (UDD3) antibody. Following SDS-PAGE separation, proteins were visualised on immunoblot using anti-LRRK2 (UDD3) and anti-tubulin antibodies. Graph shows quantification of immunoprecipitated LRRK2 in siRNA-transfected samples normalised to NTC from three independent experiments (data shown as mean ± SEM; One-way ANOVA with Fisher's LSD test, ns = non-significant, ** = $P \leq 0.01$, N=3). b) HEK293 cells were transfected with either non-targeting control (NTC) or LRRK2 pool siRNA and fixed at 72 hours post-knockdown before immunostaining with anti-LRRK2 UDD3 or UDD2 antibodies. Scale bar, 20 μm.

To investigate the role of LRRK2 in aggresome formation, cells were treated with non-targeting control (NTC) or LRRK2 pool siRNA and transfected with GFP-CFTR-ΔF508 or GFP-250. Cells were treated with MG132 to inhibit the proteasome and fixed at 24 hours post-transfection before being immunostained with anti-LRRK2, anti-HDAC6 and anti-vimentin antibodies. Aggresome-containing cells were scored from the co-localisation of GFP and vimentin at a single, perinuclear structure. Knockdown of endogenous LRRK2 was confirmed through staining of NTC and LRRK2 siRNA-treated cells with anti-LRRK2 (UDD3) and anti-LRRK2-pS935 (UDD2) antibodies. LRRK2 staining was markedly decreased after treatment with LRRK2 siRNA for both antibodies which indicated knockdown of endogenous LRRK2 protein (Figure 4.2e). NTC siRNA-treated cells showed diffuse, cytoplasmic expression of GFP-CFTR-ΔF508 under basal conditions with aggresome formation in less than 5% of cells (Figure 4.2a-b). After treatment with MG132, clear vimentin-positive perinuclear aggresomes formed in ~40% of NTC cells. As expected, HDAC6 co-localised with GFP-CFTR-ΔF508 and vimentin at the aggresome. LRRK2 siRNA cells showed no increase in GFP-CFTR-ΔF508 aggresome formation after MG132 treatment compared to untreated cells (Figure 4.2b). HDAC6 also did not localise to the aggresome in LRRK2 siRNA-treated cells.

GFP-250 showed a diffuse, cytoplasmic expression in NTC-treated cells with vimentin-positive aggresome formation in ~25% of cells without proteasomal inhibition (Figure 4.2c-d). LRRK2 siRNA-treated cells also formed aggresomes in ~25% of cells without proteasomal inhibition. After MG132 treatment, both NTC and LRRK2 siRNA-treated cells formed GFP-250 aggresomes in ~45% of cells, showing that LRRK2 siRNA did not affect GFP-250 aggresome formation (Figure 4.2d). As expected, GFP-250 aggresomes were HDAC6-negative. These results show that LRRK2 is required for the formation of HDAC6-dependent GFP-CFTR-ΔF508 aggresomes in HEK293 cells but not for HDAC6-independent GFP-250 aggresome formation.

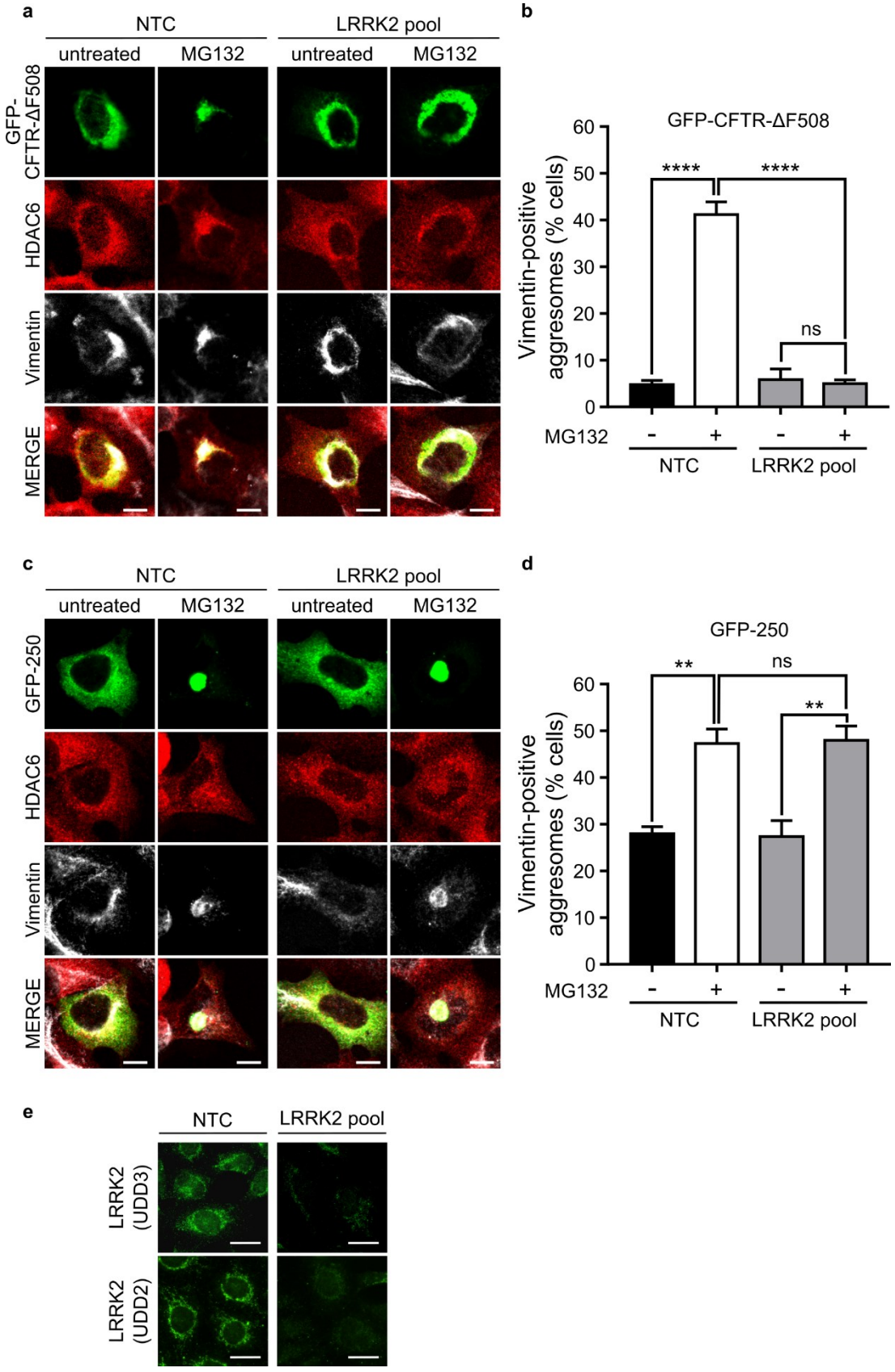
a
NTC
LRRK2 pool
untreated
MG132
untreated
MG132
GFP-CFTR-ΔF508
HDAC6
Vimentin
MERGE
b
GFP-CFTR-ΔF508
Vimentin-positive aggresomes (% cells)
60
50
40
30
20
10
0
****
****
ns
MG132
-
+
-
+
NTC
LRRK2 pool
c
NTC
LRRK2 pool
untreated
MG132
untreated
MG132
GFP-250
HDAC6
Vimentin
MERGE
d
GFP-250
Vimentin-positive aggresomes (% cells)
60
50
40
30
20
10
0
**
ns
**
MG132
-
+
-
+
NTC
LRRK2 pool
e
NTC
LRRK2 pool
LRRK2 (UDD3)
LRRK2 (UDD2)

Figure 4.2. LRRK2 is required for HDAC6-dependent aggresome formation. Non-targeting (NTC) or LRRK2 pool siRNA knockdown HEK293 cells were transfected with either GFP-CFTR-ΔF508 (a) or GFP-250 (c) (green), followed at twenty hours post-transfection by treatment with 5 μM MG132 for 4h. Cells were subsequently fixed and immunostained with anti-HDAC6 (red) and anti-vimentin (white) antibodies. Scale bar, 10 μm. The percentage of NTC and LRRK2 pool siRNA cells containing vimentin-positive GFP-CFTR-ΔF508 (b) and GFP-250 (d) aggresomes was quantified with and without MG132 treatment from three independent experiments (data shown as mean ± SEM; One-way ANOVA with Fisher's LSD test, **= $P \leq 0.01$, **** = $P \leq 0.0001$; N(cells) = CFTR/NTC/untreated: 210; CFTR/NTC/MG132: 218; CFTR/LRRK2/untreated: 181; CFTR/LRRK2/MG132: 220; 250/NTC/untreated: 222; 250/NTC/MG132: 192; 250/LRRK2/untreated: 222; 250/LRRK2/MG132: 194). e) Staining with anti-LRRK2 UDD3 and UDD2 antibodies for confirmation of LRRK2 siRNA knockdown. Scale bar, 20 μm.

To corroborate the finding that LRRK2 is required for the formation of HDAC6-dependent aggresomes (Figure 4.2), GFP-CFTR-ΔF508 aggresome formation was studied in embryonic fibroblasts from LRRK2 knockout mice. LRRK2 knockout fibroblasts were co-transfected with GFP-CFTR-ΔF508 and Myc-LRRK2 or empty vector and treated with MG132 to inhibit proteasome function and promote aggresome formation. Cells were fixed at 24 hours-post transfection and immunostained with an anti-Myc antibody for identification of cells co-expressing Myc-LRRK2 with GFP-CFTR-ΔF508. Empty vector-transfected LRRK2-knockout cells treated with MG132 formed single, perinuclear aggresomes in only ~5% of cells (Figure 4.3), showing a similar phenotype to that observed after LRRK2 knockdown (Figure 4.2). In contrast, LRRK2 knockout cells expressing Myc-LRRK2 formed GFP-CFTR-ΔF508 aggresomes in ~25% of cells. In addition, Myc-LRRK2 co-localised at the GFP-CFTR-ΔF508 aggresome after treatment with MG132.

These results indicate that LRRK2 is required for GFP-CFTR-ΔF508 aggresome formation. As previously described, GFP-CFTR-ΔF508 aggresomes are formed in an HDAC6-dependent manner (Kawaguchi et al., 2003). To further test the requirement for HDAC6 for LRRK2-mediated GFP-CFTR-ΔF508 aggresome formation, cells were treated with the HDAC6 inhibitor Tubastatin A in combination with MG132. As for cells treated with MG132 only, treatment with MG132 and Tubastatin A showed GFP-CFTR-ΔF508 aggresome formation in less than 5% of LRRK2-knockout cells transfected with empty vector (Figure 4.3). Treatment with MG132 and Tubastatin A in cells co-expressing Myc-LRRK2 prevented an increase in the number of cells displaying GFP-CFTR-ΔF508 aggresomes compared to empty vector transfected cells, and Myc-LRRK2 showed a strong localisation with non-aggresome-associated GFP-CFTR-ΔF508. This suggests that HDAC6 is required for the role of LRRK2 in GFP-CFTR-ΔF508 aggresome formation.

Taken together, the results from Figure 4.2 and Figure 4.3 show that LRRK2 is required for the formation of GFP-CFTR-ΔF508 aggresomes in cells in an HDAC6-dependent manner. This suggests that LRRK2 may act in a common pathway with HDAC6 to promote ubiquitinated protein aggresome formation.

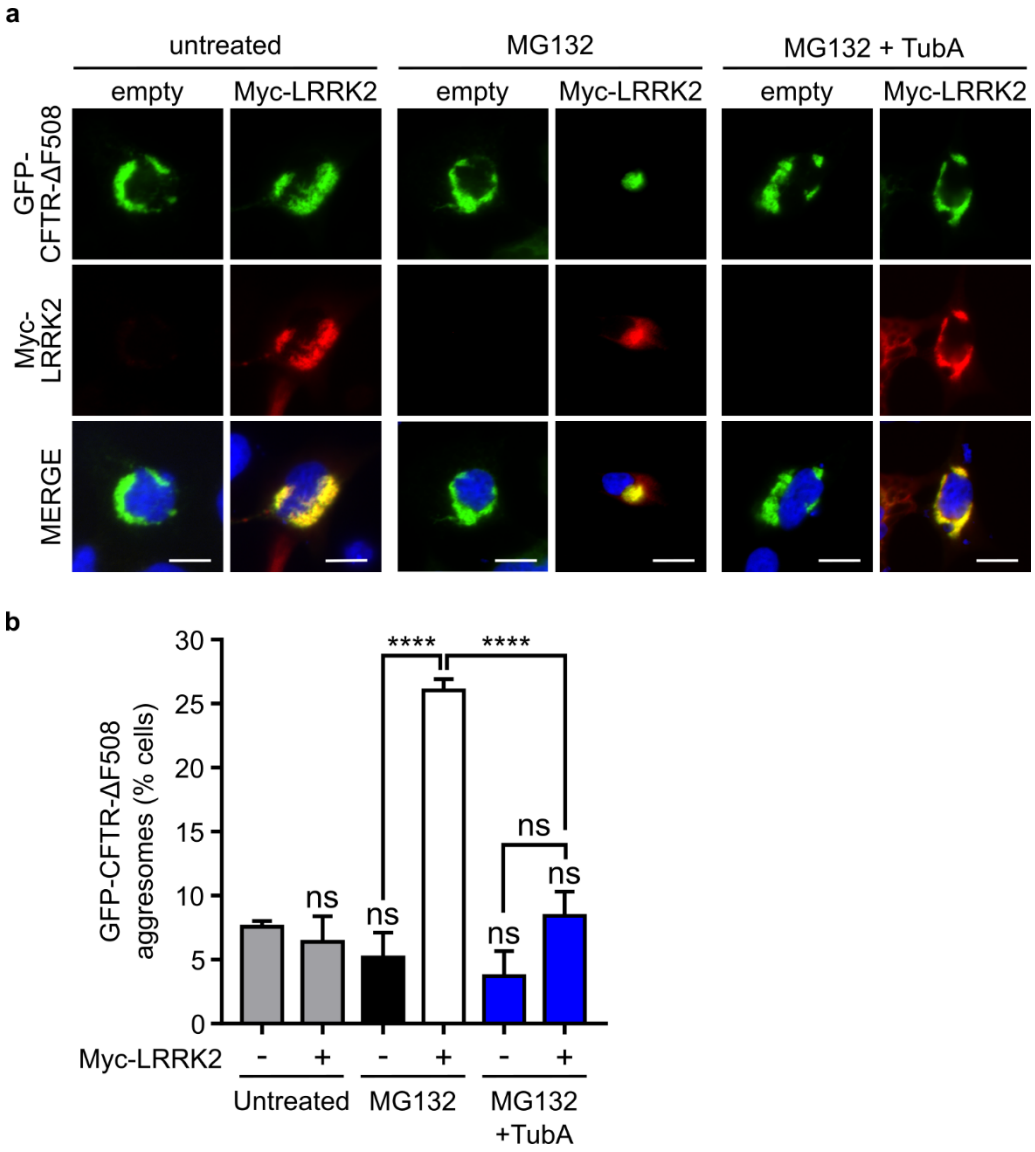

Figure 4.3. LRRK2-dependent GFP-CFTR-ΔF508 aggresome formation requires HDAC6. a) LRRK2-knockout mouse embryonic fibroblasts were co-transfected with GFP-CFTR-ΔF508 (green) and Myc-LRRK2 (red) or empty vector. Cells were treated with 5 μM MG132 for 4 h alone or together with 10 μM Tubastatin A, before fixation and immunostaining with an anti-Myc antibody and Hoechst 33342 (blue). Scale bar, 10 μm. b) Quantification of cells containing GFP-CFTR-ΔF508 aggresomes after MG132 treatment from three independent experiments (data shown as mean ± SEM; One-way ANOVA with Fisher's LSD test, ns = non-significant, **** = P ≤ 0.0001; N (cells) = empty/untreated: 120; LRRK2/untreated: 113; empty/MG132: 135; LRRK2/MG132: 108; empty/MG132+TubA: 135; LRRK2/MG132+TubA = 110).

4.2.2 GFP-CFTR-ΔF508 aggresome formation requires LRRK2 kinase activity

To investigate if the kinase activity of LRRK2 is important for HDAC6-dependent aggresome formation, the ability of wild-type and kinase-dead LRRK2 to rescue the defect in GFP-CFTR-ΔF508 aggresome formation caused by knockdown of LRRK2 (Figure 4.2) was compared. HEK293 cells were treated with NTC or LRRK2 siRNA before co-transfection of GFP-CFTR-ΔF508 with Myc-LRRK2 wild-type or kinase-dead D1994A constructs. Cells were treated with MG132 to inhibit the proteasome and fixed at 24 hours post-transfection before being immunostained with anti-Myc, anti-HDAC6 and anti-vimentin antibodies as markers of aggresome formation (Figure 4.4a). NTC cells treated with MG132 formed vimentin-positive GFP-CFTR-ΔF508 aggresomes in ~30% of cells and aggresome formation was prevented by knockdown of LRRK2 (Figure 4.4b). As expected, expression of wild-type LRRK2 rescued the defect in aggresome formation caused by LRRK2 knockdown back to control levels, and Myc-LRRK2 co-localised with GFP-CFTR-ΔF508 and vimentin at the aggresome. Importantly, expression of the kinase-dead LRRK2 D1994A mutant did not rescue GFP-CFTR-ΔF508 aggresome formation after LRRK2-knockdown (Figure 4.4b). Unlike wild-type LRRK2, LRRK2 D1994A did not form a single aggresome structure, predominantly co-localised with GFP-CFTR-ΔF508 which was aggregated in the cytoplasm and suggesting that aggregate transport was disrupted. In addition, vimentin did not redistribute into an aggresome cage surrounding GFP-CFTR-ΔF508.

Therefore, the results from Figure 4.4 suggest that HDAC6-dependent GFP-CFTR-ΔF508 aggresome formation requires LRRK2 kinase activity. In cells expressing kinase-dead LRRK2, HDAC6 did not localise to the aggresome and colocalised with aggregated GFP-CFTR-ΔF508 in the cytoplasm after proteasomal inhibition (Figure 4.4a). This suggests that LRRK2 kinase activity may be required to stimulate the transport of HDAC6/GFP-CFTR-ΔF508 complexes along microtubules to the aggresome.

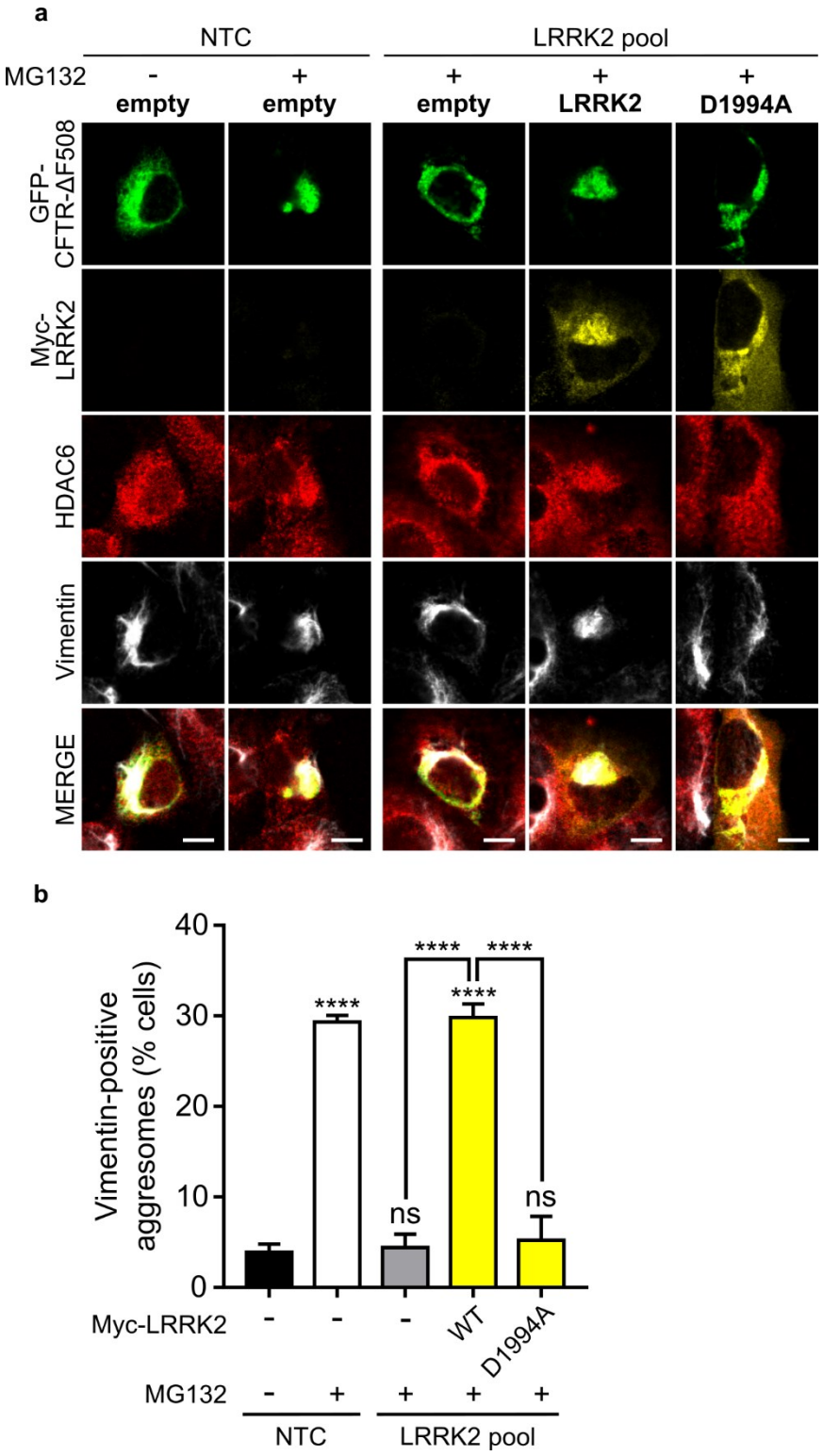

Figure 4.4. LRRK2 kinase activity is required for GFP-CFTR-ΔF508 aggresome formation. Non-targeting (NTC) or LRRK2 pool siRNA knockdown HEK293 cells were co-transfected with GFP-CFTR-ΔF508 (green) and Myc-LRRK2 wild-type or D1994A (yellow), followed by treatment with 5 μM MG132 for 4 h at 20 h post-transfection. Cells were subsequently fixed and immunostained with anti-Myc,

anti-HDAC6 (red) and anti-vimentin (white) antibodies (a). Scale bar, 10 μm. (b) The percentage of NTC and LRRK2 pool siRNA cells containing vimentin-positive GFP-CFTR-ΔF508 aggresomes was quantified with and without MG132 treatment from three independent experiments (data shown as mean ± SEM; One-way ANOVA with Fisher's LSD test, ns = non-significant, **** = P ≤ 0.0001 versus NTC; N(cells) = NTC/empty/untreated: 156; NTC/empty/MG132: 156; LRRK2 pool/empty/MG132: 140; LRRK2 pool/WT/MG132: 100; LRRK2 pool/D1994A/MG132: 117).

4.2.3 Phosphorylation of HDAC6 serine-22 is required for GFP-CFTR-ΔF508 aggresome formation

The results from this chapter so far suggest that HDAC6 acts downstream of LRRK2 in the GFP-CFTR-ΔF508 aggresome formation pathway. To test the ability of HDAC6 to rescue defects in aggresome formation caused by LRRK2 knockdown, FLAG-HDAC6 was co-transfected with GFP-CFTR-ΔF508 in HEK293 cells treated with NTC or LRRK2 siRNA. C-terminal truncated HDAC6 missing the ZnF-UBP ubiquitin-binding domain (dUB) was used as a negative control for the rescue of aggresome formation. Following MG132 treatment to inhibit the proteasome, cells were fixed at 24 hours post-transfection and immunostained using anti-FLAG and anti-vimentin antibodies to identify aggresomes (Figure 4.5a). Quantification of cells with vimentin-positive GFP-CFTR-ΔF508 aggresomes showed aggresome formation in ~30% of NTC cells treated with MG132, and aggresome formation was prevented by LRRK2-knockdown (Figure 4.5b). Importantly, overexpression of wild-type HDAC6 caused a partial rescue of GFP-CFTR-ΔF508 aggresome formation in ~15% of cells after LRRK2-knockdown. As expected, the HDAC6-dUB construct did not rescue aggresome formation as it is unable to bind ubiquitinated GFP-CFTR-ΔF508 for transport to the aggresome. These results indicate that defects in HDAC6-dependent aggresome formation caused by LRRK2 knockdown can be rescued by overexpression of HDAC6, suggesting that HDAC6 acts downstream of LRRK2.

As described in Chapter 3, LRRK2 phosphorylates HDAC6 at serine-22 and serine-689 *in vitro.* To study the effects of phosphorylation at these sites on the function of HDAC6 in aggresome formation, constructs were generated where HDAC6 serine-22 or serine-689 were mutated to prevent or mimic their phosphorylation. Mutating a serine residue to alanine prevents phosphorylation of this site whilst retaining overall protein charge, whereas mutating a serine residue to glutamic acid can mimic phospho-serine (Egelhoff et al., 1993; Maciejewski et al., 1995). FLAG-HDAC6-S22A, S22E, S689A or S689E constructs were expressed cells treated with LRRK2 siRNA and compared to wild-type HDAC6 in their ability to rescue the defect in GFP-CFTR-ΔF508 aggresome formation caused by LRRK2. HDAC6-S22A did not rescue the defect in GFP-CFTR-ΔF508 aggresome formation, in contrast to the partial rescue seen from expression of wild-type HDAC6 (Figure 4.5). This indicates that phosphorylation of HDAC6 at serine-22 is required for the function of HDAC6 in mediating aggresome formation. In support of this, HDAC6-S22E rescued GFP-CFTR-ΔF508 aggresome formation after LRRK2 knockdown to NTC control levels,

with aggresome formation in ~30% of cells (Figure 4.5b). The number of cells with GFP-CFTR-ΔF508 aggresomes increased with expression of HDAC6-S22E compared to expression of wild-type HDAC6, indicating that mimicking serine-22 phosphorylation promotes aggresome formation after LRRK2 knockdown. In contrast, there was no change in the number of cells with GFP-CFTR-ΔF508 aggresomes between cells co-expressing HDAC6 S689A or S689E mutants compared to cells co-expressing wild-type HDAC6, indicating that phosphorylation of HDAC6 serine-689 has no effect on the function of HDAC6 in aggresome formation.

Taken together, these results show that overexpression of HDAC6 can partially rescue the defect in GFP-CFTR-ΔF508 aggresome formation after LRRK2 knockdown in HEK293 cells, providing evidence that HDAC6 acts downstream of LRRK2 to regulate the formation of polyubiquitinated aggresomes. Importantly, phosphorylation of HDAC6 at serine-22 is crucial for its function in aggresome formation and suggests that LRRK2-mediated phosphorylation of HDAC6 at serine-22 may regulate aggresome formation.

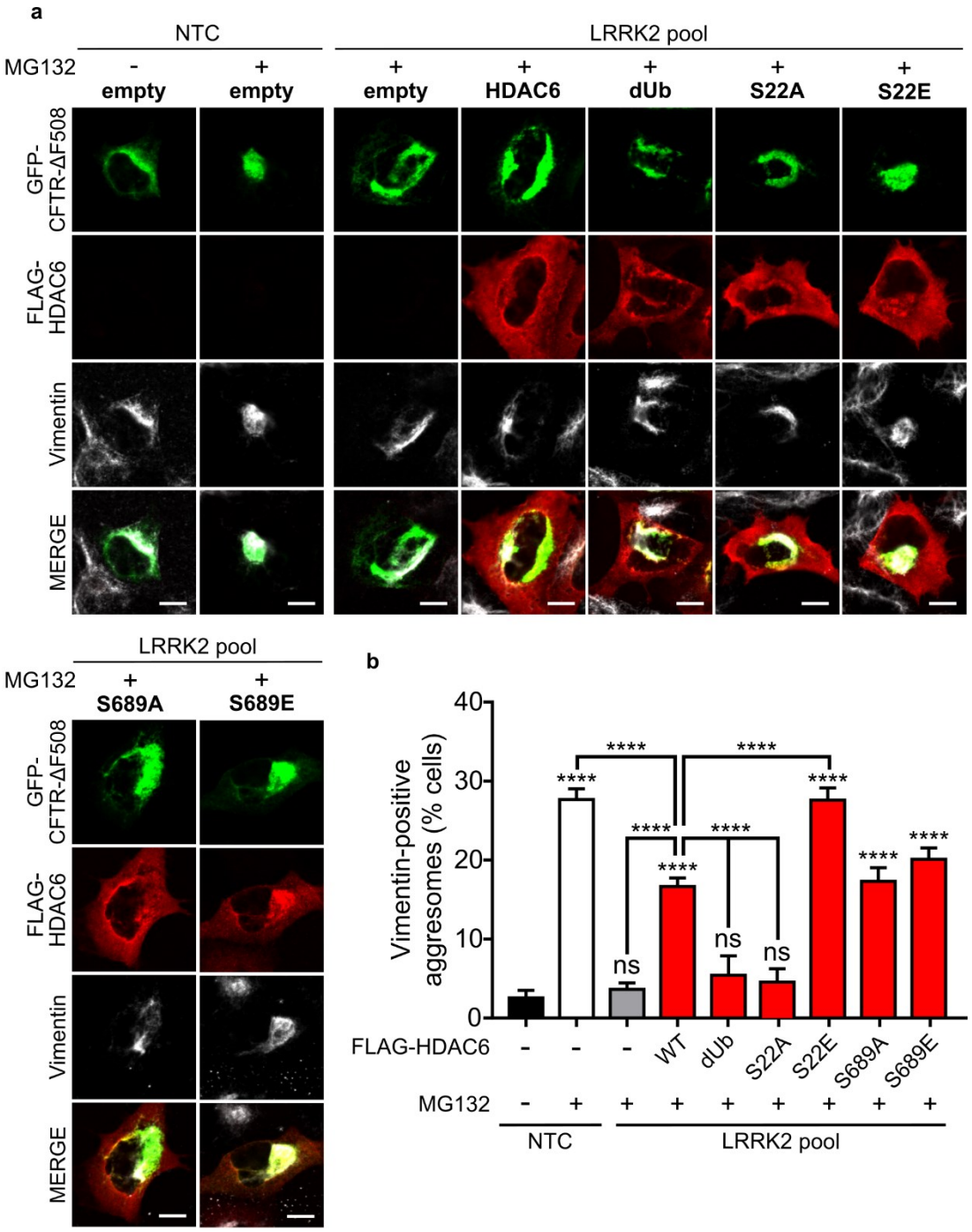

Figure 4.5. Phosphorylation of HDAC6-S22 is required for GFP-CFTR-ΔF508 aggresome formation. Non-targeting (NTC) or LRRK2 pool siRNA knockdown HEK293 cells were co-transfected with GFP-CFTR-ΔF508 (green) and FLAG-HDAC6-WT, dUb, S22A, S22E, S689A or S689E (red), followed by treatment with 5 μM MG132 for 4h at twenty hours post-transfection. Cells were subsequently fixed and immunostained with anti-FLAG, and anti-vimentin (white) antibodies (a). Scale bar, 10 μm. (b) The percentage of NTC and LRRK2 pool siRNA cells containing

vimentin-positive GFP-CFTR-ΔF508 aggresomes with each FLAG-HDAC6 construct was quantified with and without MG132 treatment from three independent experiments (data shown as mean ± SEM; One-way ANOVA with Fishers LSD test, ns = non-significant, **** = P ≤ 0.0001, versus NTC; N(cells) = NTC/empty/untreated: 200; NTC/empty/MG132: 184; LRRK2 pool/empty/MG132: 191; LRRK2 pool/WT/MG132: 198; LRRK2 pool/dUb/MG132: 162; LRRK2 pool/S22A/MG132: 177; LRRK2 pool/S22E/MG132: 157; LRRK2 pool/S689A/MG132: 145; LRRK2 pool/S689E/MG132: 109).

4.2.4 LRRK2 G2019S disrupts aggresome formation

The results in this chapter point to a model whereby LRRK2 phosphorylates HDAC6 at serine-22 to promote the transport of ubiquitinated aggregates to the aggresome. Given the importance of LRRK2 kinase activity in this mechanism (Figure 4.4), mutations in LRRK2 which dysregulate its kinase activity might be predicted to affect HDAC6-dependent aggresome formation. The pathogenic LRRK2 G2019S mutation elevates LRRK2 kinase activity (Greggio et al., 2006; West et al., 2007). The effects of the LRRK2 G2019S mutation on HDAC6-dependent aggresome were therefore investigated.

GFP-CFTR-ΔF508 was co-expressed with Myc-LRRK2 wild-type or G2019S in HEK293 cells following treatment with NTC or LRRK2 siRNA. Cells were treated with MG132 to inhibit the proteasome and fixed at 24 hours post-transfection, before being immunostained using anti-Myc, anti-HDAC6 and anti-vimentin antibodies for identification of aggresomes. As shown in Figure 4.4, expression of Myc-LRRK2 wild-type fully rescued the defect in GFP-CFTR-ΔF508 aggresome formation caused by LRRK2 knockdown, with aggresomes formed in ~30% of cells (Figure 4.6). In contrast, expression of Myc-LRRK2 G2019S partially rescued the defect in aggresome formation in ~15% of cells, suggesting that the G2019S mutant LRRK2 cannot support GFP-CFTR-ΔF508 aggresome formation to the same level as wild-type LRRK2. In Myc-LRRK2 G2019S-expressing cells with no aggresome formation, LRRK2 G2019S strongly co-localised with aggregated GFP-CFTR-ΔF508 and HDAC6 in the cytoplasm after proteasomal inhibition (Figure 4.6a). Interestingly, a perinuclear vimentin cage was detected in many LRRK2 G2019S-expressing cells despite the lack of a single, perinuclear GFP-CFTR-ΔF508 aggresome structure. This may reflect failed or incomplete aggresome formation in cells expressing LRRK2 G2019S. These results suggest that the G2019S mutation in LRRK2 disrupts the ability of LRRK2 to support HDAC6-dependent aggresome formation and may provide a possible pathogenic mechanism of LRRK2 G2019S-mediated toxicity.

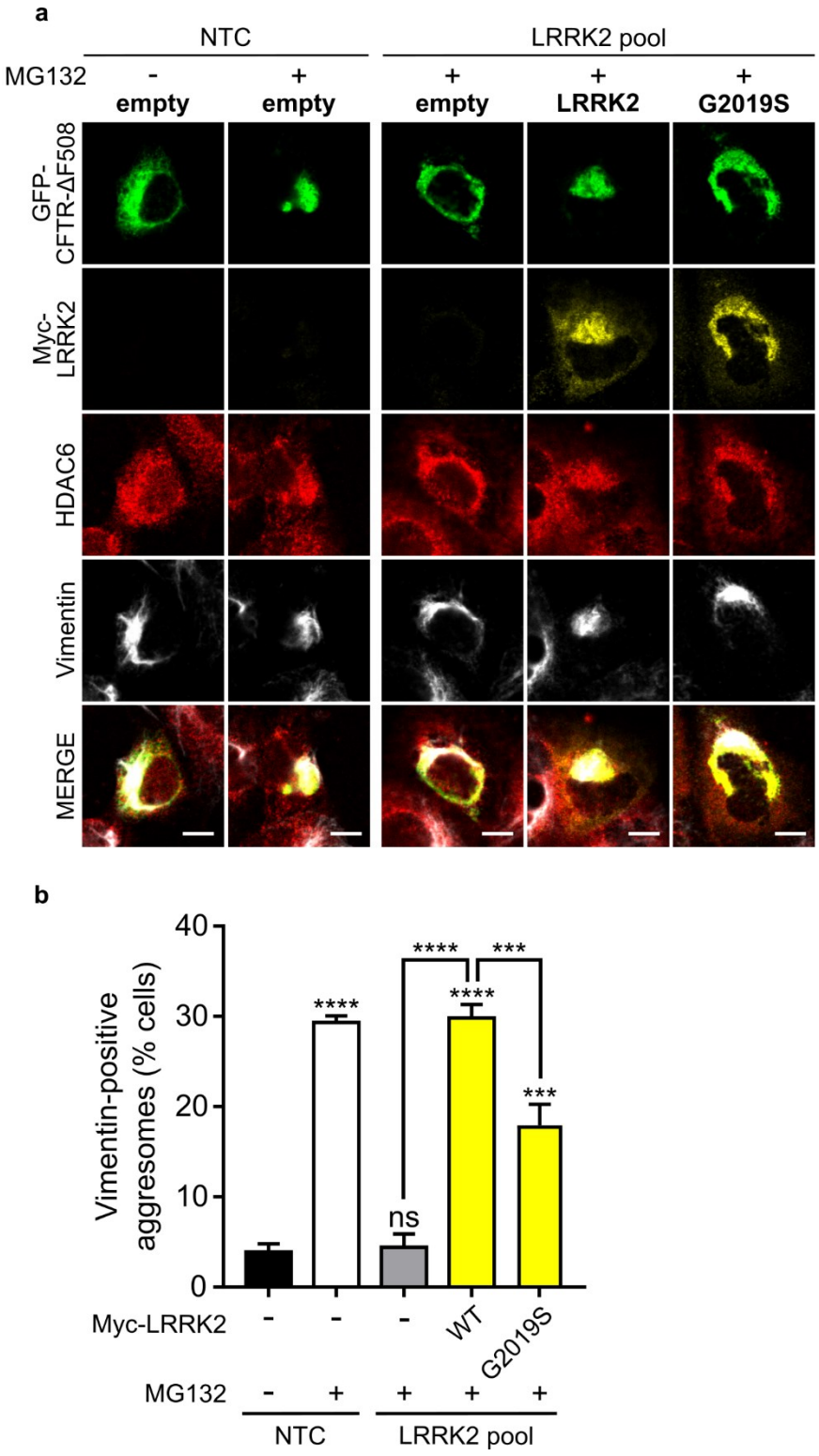

Figure 4.6. LRRK2 G2019S cannot fully support GFP-CFTR-ΔF508 aggresome formation. Non-targeting (NTC) or LRRK2 pool siRNA knockdown HEK293 cells were co-transfected with GFP-CFTR-ΔF508 (green) and Myc-LRRK2 wild-type or G2019S (yellow), followed by treatment with 5 μM MG132 for 4 h at 20 h post-transfection. Cells were subsequently fixed and immunostained with anti-Myc, anti-

HDAC6 (red) and anti-vimentin (white) antibodies (a). Scale bar, 10 μm. (b) The percentage of NTC and LRRK2 pool siRNA cells containing vimentin-positive GFP-CFTR-ΔF508 aggresomes was quantified with and without MG132 treatment from three independent experiments (data shown as mean ± SEM; One-way ANOVA with Fisher's LSD test, ns = non-significant, *** = P ≤ 0.001, **** = P ≤ 0.0001 versus LRRK2 knockdown-only control; N(cells) = NTC/empty/untreated: 156; NTC/empty/MG132: 156; LRRK2 pool/empty/MG132: 140; LRRK2 pool/WT/MG132: 100; LRRK2 pool/G2019S/MG132: 101). NB: Dataset is the same as Figure 4.4 for all conditions except LRRK2 G2019S.

4.2.5 LRRK2 localises to the aggresome independently of HDAC6

As a key regulator of polyubiquitinated aggresome formation, HDAC6 is a component of aggresomes formed by polyubiquitinated proteins such as GFP-CFTR-ΔF508 but not those formed by non-ubiquitinated proteins such as GFP-250 (Kawaguchi et al., 2003). In LRRK2-knockout mouse fibroblasts, overexpressed Myc-LRRK2 co-localised with GFP-CFTR-ΔF508 at the aggresome after treatment with MG132 (Figure 4.3). Localisation of LRRK2 at the aggresome has been previously described in HEK293T and COS-7 cells and this is facilitated by proteasomal inhibition (Waxman et al., 2009).

To characterise LRRK2 localisation at the aggresome and to test if it requires HDAC6, NTC and HDAC6 siRNA-treated HEK293 cells were co-transfected with GFP-CFTR-ΔF508 or GFP-250 and Myc-LRRK2. Cells were treated with MG132 to promote aggresome formation before being fixed at 24 hours post-transfection and immunostained with anti-Myc and anti-HDAC6 antibodies. In NTC-treated cells, MG132 treatment promoted the formation of a single GFP-CFTR-ΔF508 aggresome which co-localised with both Myc-LRRK2 and HDAC6 (Figure 4.7a). HDAC6 knockdown prevented GFP-CFTR-ΔF508 aggresome formation after MG132 treatment, however Myc-LRRK2 still localised to a juxtanuclear structure resembling an aggresome. This indicates that LRRK2 localises to the aggresome independently of HDAC6. Consistent with the HDAC6-independent formation of GFP-250 aggresomes, MG132 treatment promoted the formation of GFP-250 aggresomes in both NTC and HDAC6 knockdown cells (Figure 4.7b). Myc-LRRK2 co-localised with GFP-250 aggresomes in NTC and HDAC6 knockdown cells.

These results indicate that LRRK2 localises to aggresomes independently of HDAC6. Under basal conditions, LRRK2 is degraded by the proteasome (Wang et al., 2008). After proteasomal inhibition LRRK2 is recruited to the aggresome for degradation (Waxman et al., 2009). Therefore, the results from Figure 4.7 suggest that LRRK2 may be a substrate of the GFP-250 aggresome pathway independently of its role in HDAC6-mediated aggresome formation.

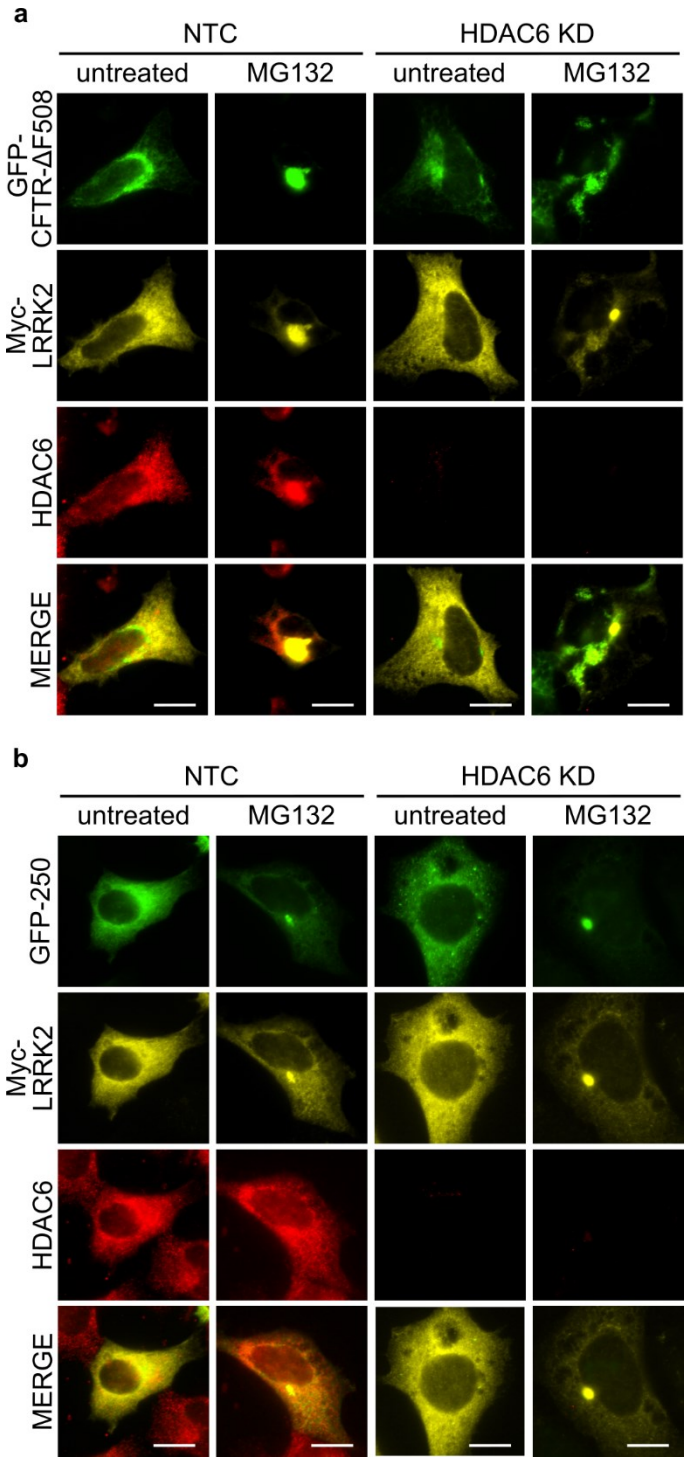

Figure 4.7. LRRK2 localisation at the aggresome is HDAC6-independent. Non-targeting control (NTC) or HDAC6 siRNA-treated HEK293 cells were co-transfected with GFP-CFTR-ΔF508 (a; green) or GFP-250 (b; green) and Myc-LRRK2 and treated with 5 μM MG132 for 4 h at 20 h post-transfection, before fixation and immunostaining with anti-Myc (yellow) and anti-HDAC6 (red) antibodies. Scale bar, 10 μm.

4.3 Discussion

HDAC6 is a key player in aggresome formation by binding ubiquitinated misfolded protein in the cytoplasm and recruiting it to the motor protein cytoplasmic dynein for transport along microtubules to the aggresome (Kawaguchi et al., 2003). In this chapter, a role for LRRK2 in regulating aggresome formation through its interaction with HDAC6 was investigated. Firstly, LRRK2 was shown to be required for the formation of HDAC6-dependent aggresomes of the polyubiquitinated protein GFP-CFTR-ΔF508 but not for HDAC6-independent non-ubiquitinated GFP-250 aggresome formation (Figure 4.2). The ability of LRRK2 to promote GFP-CFTR-ΔF508 aggresome formation was shown to be HDAC6-dependent (Figure 4.3). These results indicated that LRRK2 has a specific role in HDAC6-dependent aggresome formation and suggests that LRRK2 and HDAC6 act in the same aggresome pathway.

Further investigation of the role of LRRK2 in the HDAC6-dependent aggresome pathway revealed that LRRK2 kinase activity is specifically required for GFP-CFTR-ΔF508 aggresome formation (Figure 4.4). This suggests that LRRK2 may phosphorylate HDAC6 to promote GFP-CFTR-ΔF508 aggresome formation. Furthermore, genetic ablation of LRRK2 kinase activity prevented HDAC6 from localising to aggresomes and it remained co-localised with GFP-CFTR-ΔF508 aggregates in the cytoplasm. These observations suggest that LRRK2 kinase activity does not affect the recognition and binding of HDAC6 to ubiquitinated GFP-CFTR-ΔF508 but rather may promote the transport of GFP-CFTR-ΔF508/HDAC6 complexes to the aggresome along the microtubule network. Aggresomes rely on microtubule transport for their formation and this is blocked by microtubule polymerisation inhibitors such as nocodazole which destabilise the microtubule network (Johnston et al., 1998). Results from Chapter 5 will show that inhibition of LRRK2 kinase activity does not grossly disrupt microtubule network structure, therefore LRRK2 kinase inhibition likely disrupts GFP-CFTR-ΔF508 aggresome formation through prevention of transport initiation rather than disruption of the microtubule network.

These results suggest that LRRK2 phosphorylates HDAC6 to regulate its function in the formation of ubiquitinated protein aggresomes. In support of LRRK2 and HDAC6 functioning in a common pathway, GFP-CFTR-ΔF508 aggresome formation disrupted by LRRK2 knockdown was partially rescued by overexpression of wild-type HDAC6 (Figure 4.5). Whilst this partial rescue of aggresome formation likely occurred due to the dominant effect of HDAC6 overexpression, a full rescue to control levels

was not observed and indicates that LRRK2-mediated phosphorylation of HDAC6 may be required. Expression of phospho-mutant HDAC6 showed that phosphorylation of HDAC6 serine-22 is crucial for GFP-CFTR-ΔF508 aggresome formation (Figure 4.5). The phospho-dead HDAC6 S22A mutant retained co-localisation with GFP-CFTR-ΔF508 in the cytoplasm with a phenotype resembling that of kinase-dead LRRK2 (Figure 4.4). This indicates that serine-22 phosphorylation does not affect the binding of HDAC6 to ubiquitinated aggregates. Alternatively, LRRK2-mediated phosphorylation of HDAC6 serine-22 may be required for the binding of HDAC6 to cytoplasmic dynein for transport of GFP-CFTR-ΔF508 aggregates to the aggresome. This could be tested through co-immunoprecipitation experiments using HDAC6 phospho-mutant constructs to determine the effect of serine-22 phosphorylation on cytoplasmic dynein binding.

Intracellular accumulation of aggregated protein in Lewy bodies is a pathological hallmark of PD and Lewy bodies share many characteristics with aggresomes (Forno, 1996; Kopito, 2000; McNaught et al., 2002). Importantly, HDAC6 is a component of Lewy bodies in PD patients and Lewy bodies may be formed through an aggresome-like mechanism (Kawaguchi et al., 2003). Therefore, pathogenic mutations in LRRK2 may disrupt its role in HDAC6-mediated aggresome formation and could contribute to the pathogenesis of PD. The LRRK2 G2019S mutation elevates LRRK2 kinase activity (Greggio et al., 2006; West et al., 2007) and might be predicted to increase phosphorylation of HDAC6 serine-22 to further stimulate HDAC6-dependent aggresome formation. However, LRRK2 G2019S did not rescue GFP-CFTR-ΔF508 aggresome formation to the same level as wild-type LRRK2 in cells following LRRK2 knockdown, indicating that LRRK2 G2019S is not able to fully support HDAC6-dependent aggresome formation (Figure 4.6). This may reflect the decreased binding of LRRK2 G2019S to HDAC6 as shown in Chapter 3. Furthermore, a perinuclear vimentin cage-like structure was evident in many of the G2019S-expressing cells without a defined GFP-CFTR-ΔF508 aggresome. It may be possible that LRRK2 G2019S promotes aggregate transport via HDAC6 but causes excessive GFP-CFTR-ΔF508 accumulation at the aggresome region due to inhibition of subsequent degradation of the aggresome by autophagy. LRRK2 G2019S has been shown to impair autophagic flux (Saha et al., 2015), and expression of LRRK2 G2019S accelerates the accumulation of cytoplasmic ubiquitin- and p62-positive protein aggregates after proteasomal inhibition in SH-SY5Y neuroblastoma cells which is suggestive of a defect in aggresome formation or autophagic degradation (Bang et al., 2016). Furthermore, LRRK2 G2019S transgenic mice show higher protein

accumulation in the brain after proteasomal inhibition compared to wild-type littermates (Bang et al., 2016). Therefore, LRRK2 G2019S may affect multiple steps in the aggresome pathway.

Finally, the localisation of LRRK2 at the aggresome (Figure 4.3-Figure 4.4) was characterised. LRRK2 is degraded by the proteasome and can form aggresomes when overexpressed which is facilitated by but not a direct result of proteasome inhibition (Waxman et al., 2009; Ding et al., 2017). LRRK2 co-localised with HDAC6 at GFP-CFTR-ΔF508 aggresomes, but also with HDAC6-independent GFP-250 aggresomes (Figure 4.7). Furthermore, knockdown of HDAC6 did not prevent the aggresome localisation of LRRK2. These results indicated that LRRK2 recruitment to the aggresome after proteasomal inhibition is independent of HDAC6 and suggests that LRRK2 is a substrate of the same aggresome pathway as GFP-250. As GFP-250 is non-ubiquitinated, it is recruited to the aggresome via BAG3 rather than HDAC6 (Gamerdinger et al., 2011). Whilst LRRK2 is ubiquitinated to regulate its turnover via the UPS (Ding and Goldberg, 2009), the ubiquitination status of aggresome-associated LRRK2 is not known. These results therefore suggest that aggresome-associated LRRK2 may be non-ubiquitinated.

In conclusion, the results in this chapter provide evidence that LRRK2 acts upstream of HDAC6 to initiate polyubiquitinated aggresome formation through its kinase activity. Furthermore, the LRRK2 phosphosite at HDAC6 serine-22 is crucial for HDAC6 function in aggresome formation. These results therefore suggest that LRRK2-mediated phosphorylation of HDAC6 serine-22 may be required for the formation of polyubiquitinated aggresomes. A possible mechanism for how this occurs is through facilitation of the binding of the HDAC6/aggregate complex to cytoplasmic dynein to promote aggregate transport, and this mechanism should be investigated in future experiments. Ultimately, the relevance of this aggresome pathway to LRRK2-mediated PD should be explored.

5 LRRK2 regulates tubulin acetylation via HDAC6

5.1 Introduction

Evidence suggests that LRRK2 regulates tubulin acetylation (Godena et al., 2014; Law et al., 2014; Esteves et al., 2015). In Chapter 3, an interaction between LRRK2 and the α-tubulin deacetylase HDAC6 was characterised both *in vitro* and in HEK293 cells. These results suggest that LRRK2 may regulate tubulin acetylation via HDAC6. This chapter therefore focuses on investigating the role of LRRK2 in regulating tubulin acetylation. Firstly, tubulin acetylation is studied in cells following knockout or knockdown of endogenous LRRK2 to confirm the effects of LRRK2 loss of function on tubulin acetylation. Next, the role of LRRK2 GTPase and kinase activity in the regulation of tubulin acetylation is investigated using overexpression of LRRK2 wild-type, GTP-binding deficient K1347A and kinase-dead D1994A mutants, as well as inhibitors of LRRK2 kinase activity.

In Chapter 3, LRRK2 was shown to phosphorylate HDAC6 at serine-22 and serine-689 *in vitro,* and LRRK2-mediated phosphorylation of HDAC6 serine-22 was confirmed in cells. Phosphorylation of HDAC6 at serine-22 correlates with increased deacetylation of tubulin in hippocampal neurons (Chen et al., 2010). As a novel phosphosite in the C-terminal deacetylase domain of HDAC6, the effects of serine-689 phosphorylation on tubulin acetylation are not known. The C-terminal deacetylase domain of HDAC6 confers the majority of the tubulin deacetylase activity of HDAC6 and phosphorylation of another site in this domain, tyrosine-570, alters the deacetylase activity of HDAC6 (Haggarty et al., 2003; Deribe et al., 2009). Therefore, the effects of phosphorylation of HDAC6 at serine-22 and serine-689 on HDAC6 deacetylase activity are studied in cells using HDAC6 mutants which harbour mutations at these residues to inhibit or mimic phosphorylation.

Lastly, the effects of pathogenic LRRK2 mutations on tubulin acetylation are investigated. LRRK2 R1441C and Y1699C pathogenic GTPase mutants abnormally associate with deacetylated microtubules and this phenotype is reversed by increasing tubulin acetylation levels using an HDAC6 deacetylase inhibitor (Godena et al., 2014). Pathogenic GTPase mutations in LRRK2 may therefore dysregulate LRRK2 regulation of tubulin acetylation. Furthermore, sporadic and LRRK2 G2019S patients show reduced levels of tubulin acetylation compared to healthy controls

(Esteves et al., 2015). Therefore, disruption of tubulin acetylation by pathogenic mutations in LRRK2 may be a feature of disease.

5.2 Results

5.2.1 LRRK2 reduces tubulin acetylation via HDAC6

Embryonic fibroblasts from LRRK2-knockout mice show increased levels of tubulin acetylation compared to wild-type littermates and this phenotype can be rescued by transient overexpression of human wild-type LRRK2 (Law et al., 2014). To reproduce these results in a human cell line, levels of tubulin acetylation were investigated after LRRK2 knockdown using the LRRK2-specific siRNAs described in Chapter 4. HEK293 cells were transfected with non-targeting control (NTC) or LRRK2 pool siRNA and harvested 96 hours post-knockdown. Endogenous LRRK2 was immunoprecipitated using anti-LRRK2 (UDD3), before proteins were separated on SDS-PAGE and detected on immunoblot. Treatment with LRRK2 siRNA pool reduced endogenous LRRK2 expression and caused a ~1.4-fold increase in tubulin acetylation compared to the non-targeting control-treated cells (Figure 5.1a). Importantly, overexpression of Myc-LRRK2 in the LRRK2 siRNA pool-treated cells rescued this increase in tubulin acetylation back to control levels. These results therefore show that knockdown of endogenous LRRK2 increases tubulin acetylation and overexpression of LRRK2 after knockdown restores acetylation to control levels, indicating that LRRK2 decreases tubulin acetylation in HEK293 cells.

In addition, Myc-LRRK2 was expressed in LRRK2-knockout fibroblasts and tubulin acetylation levels were measured by immunofluorescence. Fibroblasts from LRRK2-knockout mice were transfected with Myc-LRRK2 or empty vector. Cells were fixed 24 hours post-transfection and immunostained using anti-Myc and anti-acetylated tubulin antibodies. LRRK2-knockout cells overexpressing Myc-LRRK2 showed a ~25% reduction in tubulin acetylation compared to the empty vector control (Figure 5.1b). Taken together, the results from both LRRK2 knockdown and LRRK2 knockout models indicate that LRRK2 reduces tubulin acetylation.

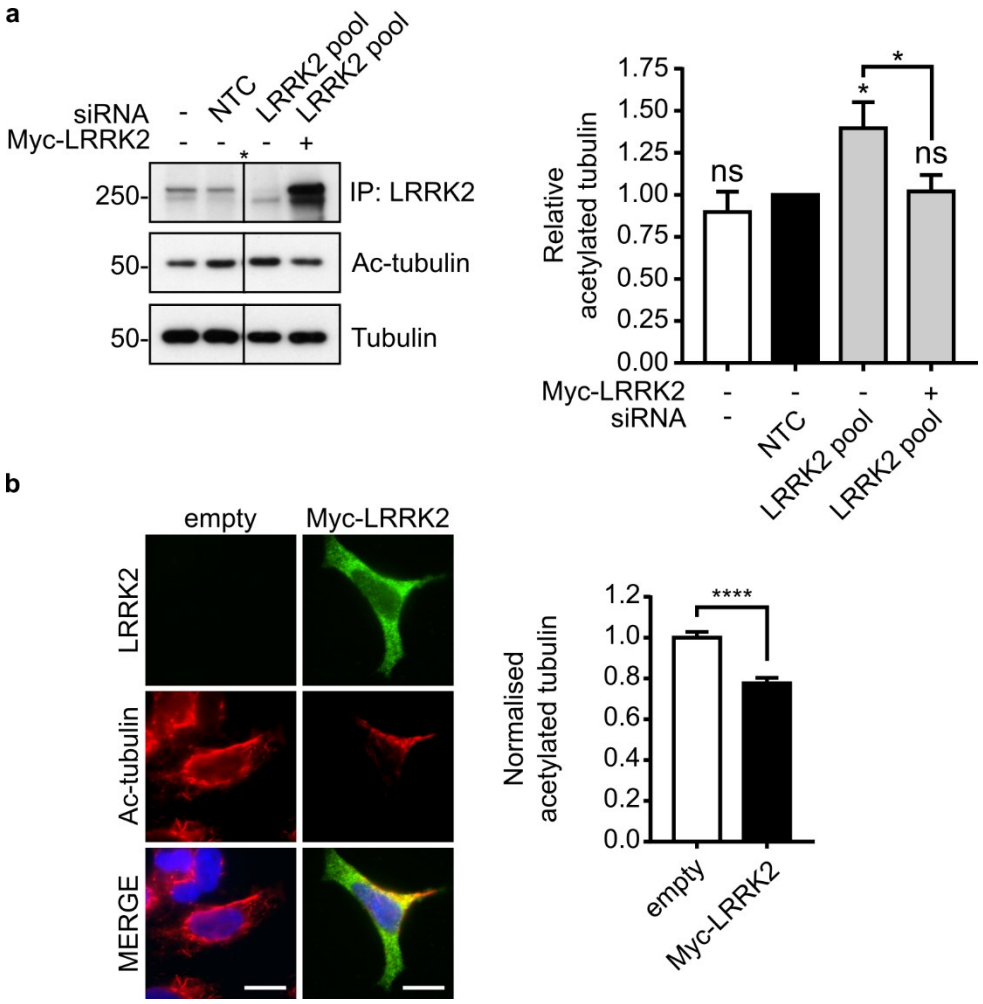

Figure 5.1. LRRK2 reduces tubulin acetylation. a) HEK293 cells were transfected with either NTC or LRRK2 pool siRNA followed by further transfection with Myc-LRRK2 at 48 hours post-knockdown where indicated. Cells were lysed at 72h post-knockdown and LRRK2 was immunoprecipitated using anti-LRRK2 (UDD3) antibody. Following SDS-PAGE separation, proteins were visualised using anti-LRRK2 (UDD3), anti-acetylated tubulin and anti-tubulin antibodies. * indicates location of removed lane due to unrelated sample loading. Graph shows quantification of ratio of acetylated to total tubulin in siRNA-transfected samples normalised to NTC from three independent experiments (data shown as mean ± SEM; One-way ANOVA with Fisher's LSD test, ns = non-significant, * = $P \leq 0.05$, N=3). b) LRRK2-knockout mouse embryonic fibroblasts were transfected with either empty vector or Myc-LRRK2 (green). Cells were fixed at 24h post-transfection and immunostained with anti-LRRK2 and anti-acetylated tubulin (red) antibodies and Hoechst (blue). Scale bar, 10 µm. Graph shows quantification of acetylated tubulin intensity normalised to empty vector control from three independent experiments (data shown as mean ± SEM; Student's t-test, **** = $P \leq 0.0001$, N (cells) = empty: 93; Myc-LRRK2: 85).

The LRRK2-mediated reduction in tubulin acetylation shown in Figure 5.1 could be the result of stimulation of HDAC6 deacetylase activity by LRRK2. To test this, an inhibitor of HDAC6 deacetylase activity was used to investigate if HDAC6 is required for LRRK2 to reduce acetylation. Small molecule HDAC6 inhibitors chelate Zn^{2+} ions in the catalytic pocket of HDAC6 to prevent deacetylase activity and increase microtubule acetylation (Hubbert et al., 2002; Zilberman et al., 2009; Asthana et al., 2013; Wang et al., 2018). Tubastatin A is a highly selective HDAC6 deacetylase inhibitor with low cellular toxicity which targets the C-terminal deacetylase domain (Butler et al., 2010). Fibroblasts from LRRK2-knockout mice were transfected with either empty vector or human Myc-LRRK2 wild-type and treated with Tubastatin A for 18 hours. Following fixation at 24 hours post-transfection, cells were immunostained with anti-LRRK2 and anti-acetylated tubulin antibodies and the levels of tubulin acetylation in empty-vector and Myc-LRRK2-expressing cells with and without Tubastatin A treatment were quantified for comparison (Figure 5.2a). LRRK2 knockout fibroblasts expressing Myc-LRRK2 showed a ~25% reduction in tubulin acetylation compared to the empty vector control (Figure 5.2b). Following treatment with Tubastatin A, empty-vector control cells showed increased tubulin acetylation levels compared to untreated cells due to HDAC6 inhibition (Figure 5.2b). Furthermore, treatment with Tubastatin A prevented Myc-LRRK2 from reducing levels of tubulin acetylation. These results suggest that the decrease in tubulin acetylation from overexpression of LRRK2 is HDAC6-dependent, providing evidence that HDAC6 acts downstream of LRRK2 to promote tubulin deacetylation.

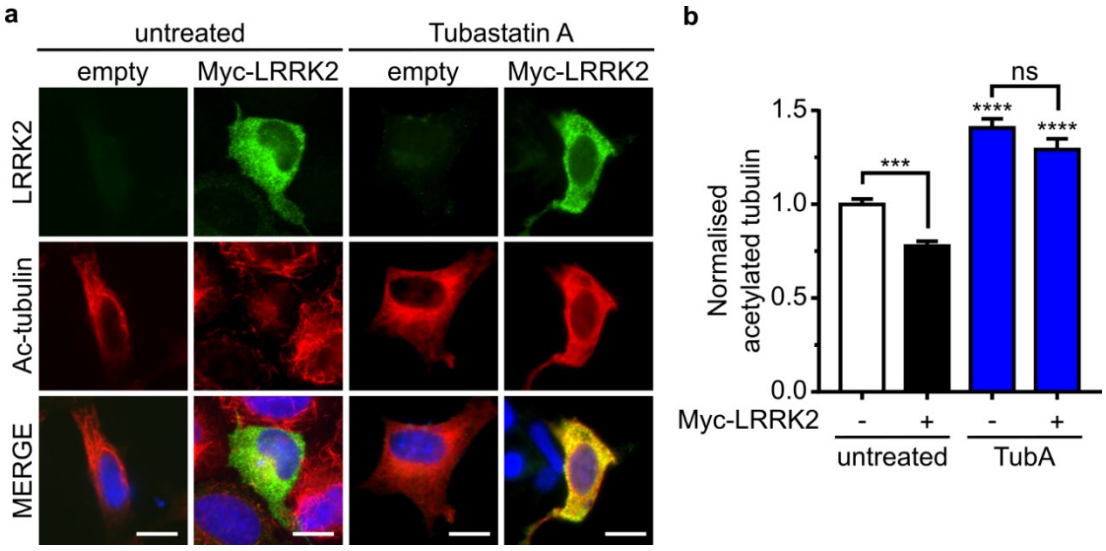

Figure 5.2. LRRK2 decreases tubulin acetylation via HDAC6. a) LRRK2-knockout mouse embryonic fibroblasts were transfected with either empty vector or Myc-LRRK2 and treated with 10 μM Tubastatin A (TubA) for 18 hours. Cells were fixed at 24h post-transfection and immunostained with anti-LRRK2 and anti-acetylated tubulin antibodies and Hoechst. Scale bar, 10 μm. b) Quantification of acetylated tubulin intensity normalised to empty vector control from three independent experiments (data shown as mean ± SEM; One-way ANOVA with Fisher's LSD test, ns = non-significant, *** = $P \leq 0.001$, **** = $P \leq 0.0001$, N (cells) = empty/untreated: 93; Myc-LRRK2/untreated: 85; empty/TubA: 90; Myc-LRRK2/TubA: 93) NB: for purposes of comparison, untreated cells were the same as those quantified in Figure 5.1b.

5.2.2 LRRK2 increases HDAC6 deacetylase activity *in vitro*

The results from Figure 5.2 indicate that LRRK2 decreases tubulin acetylation via an HDAC6-dependent mechanism. This suggests that LRRK2 stimulates the deacetylase activity of HDAC6 to reduce tubulin acetylation. To investigate if LRRK2 regulates HDAC6 activity *in vitro*, a commercially-available HDAC6 fluorometric assay was used to provide a measure of HDAC6-mediated substrate deacetylation. Acetylated substrate was incubated with His-HDAC6 and GST-LRRK2 recombinant protein (amino acids 970-2527). A molar excess of ATP was added to the reaction to allow LRRK2-mediated phosphorylation of HDAC6 to occur. His-HDAC6-only was used to compare normal levels of deacetylase activity and Trichostatin A (TSA) was used to inhibit HDAC6 activity as a negative-control. Substrate deacetylation by HDAC6 produced a fluorescent signal in the presence of the developer compound and this fluorescence was measured as a readout of HDAC6 deacetylase activity (Figure 5.3a). There was over a 1.5-fold increase in HDAC6 deacetylase activity in the presence of GST-LRRK2 compared to the HDAC6-only control (Figure 5.3b). GST-LRRK2 had no effect on substrate acetylation without His-HDAC6, therefore these effects were mediated by HDAC6 only and not a result of an interaction between LRRK2 and the acetylated substrate or developer compound. These results indicate that LRRK2 increases the deacetylase activity of HDAC6 *in vitro*.

Additionally, the effects of pathogenic LRRK2 mutations on HDAC6 deacetylase activity were studied using GST-LRRK2 R1441C and G2019S mutants. LRRK2 R1441C and G2019S showed a comparable increase in HDAC6 deacetylase activity to wild-type LRRK2. These results therefore indicate that the pathogenic LRRK2 R1441C and G2019S mutations do not alter the ability of LRRK2 to stimulate HDAC6 deacetylase activity *in vitro*.

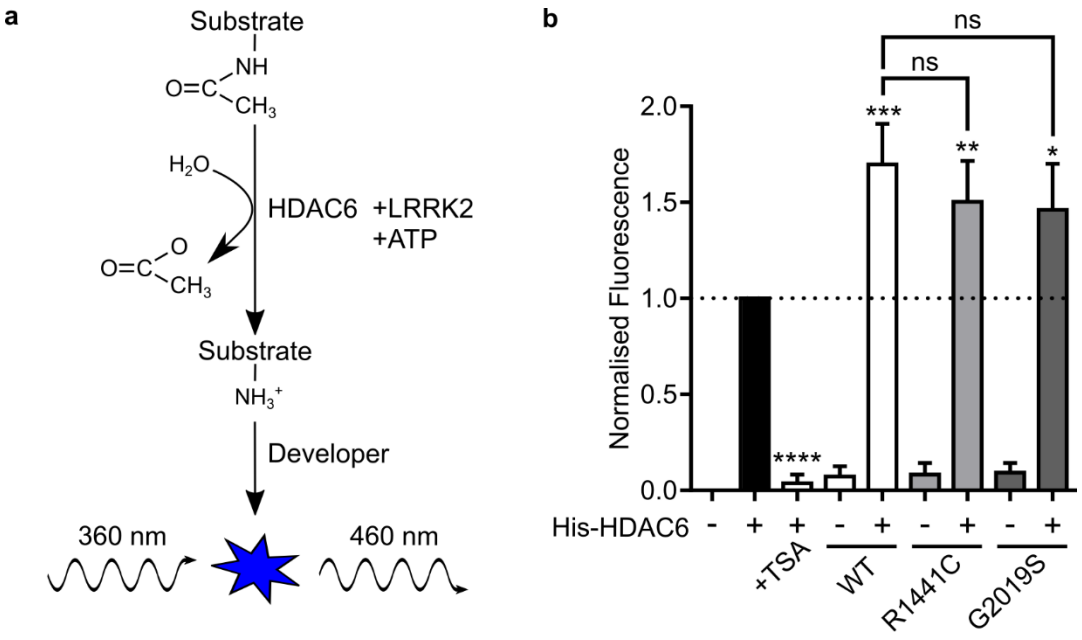

Figure 5.3. LRRK2 increases HDAC6 deacetylase activity *in vitro.* a) Overview of the FLUOR DE LYS® HDAC6 fluorometric drug discovery kit used to measure HDAC6 deacetylase activity (Adapted from product data sheet; Enzo Lifesciences). b) His-HDAC6 deacetylase activity was measured in the presence of 250 ng GST-LRRK2 wild-type, R1441C and G2019S variants and 200 µM ATP. 1 µM Trichostatin A (TSA) was used to inhibit HDAC6 activity as a negative control (data shown as mean ± SEM from five independent experiments with samples run in triplicate; one-way ANOVA with Fisher's LSD test, ns= non-significant, * = P ≤ 0.05, ** = P ≤ 0.01, *** = P ≤ 0.001, **** = P ≤ 0.0001).

5.2.3 LRRK2 kinase activity is required to reduce tubulin acetylation

As described in this chapter, LRRK2 expression reduces tubulin acetylation in cells in an HDAC6-dependent manner which suggests that LRRK2 modulates the deacetylase activity of HDAC6 (Figure 5.1 and Figure 5.2). Indeed, LRRK2 increases HDAC6 deacetylase activity *in vitro* (Figure 5.3). In Chapter 3, LRRK2 was shown to phosphorylate HDAC6 *in vitro* and in cells. Therefore, LRRK2-mediated phosphorylation of HDAC6 may stimulate its deacetylase activity and promote tubulin deacetylation in cells. To test the requirement for LRRK2 kinase activity in promoting tubulin deacetylation, HEK293 cells expressing either empty vector or Myc-LRRK2 were treated with the selective, structurally distinct LRRK2 kinase inhibitors LRRK2in1 (Deng et al., 2011), LRRK2 inhibitor III (also known as HG 10-102-01; Choi et al., 2012) or GSK2578215A (Reith et al., 2012). Cells were treated with LRRK2 inhibitors for four hours before being fixed at twenty-four hours post-transfection and immunostained with anti-LRRK2 and anti-acetylated-tubulin antibodies (Figure 5.4a). Following expression of Myc-LRRK2, cells showed a ~20% reduction in tubulin acetylation (Figure 5.4b). Importantly, treatment with all three LRRK2 inhibitors prevented the decrease in tubulin acetylation from expression of Myc-LRRK2, with LRRK2 inhibitor III and GSK2578215A-treated cells showing levels of tubulin acetylation comparable to the empty vector control (Figure 5.4b). LRRK2in1-treated cells showed a small increase in tubulin acetylation compared to the empty vector control. These results suggest that the reduction in tubulin acetylation seen with LRRK2 overexpression is mediated by the kinase activity of LRRK2, and treatment with LRRK2 inhibitors increases tubulin acetylation.

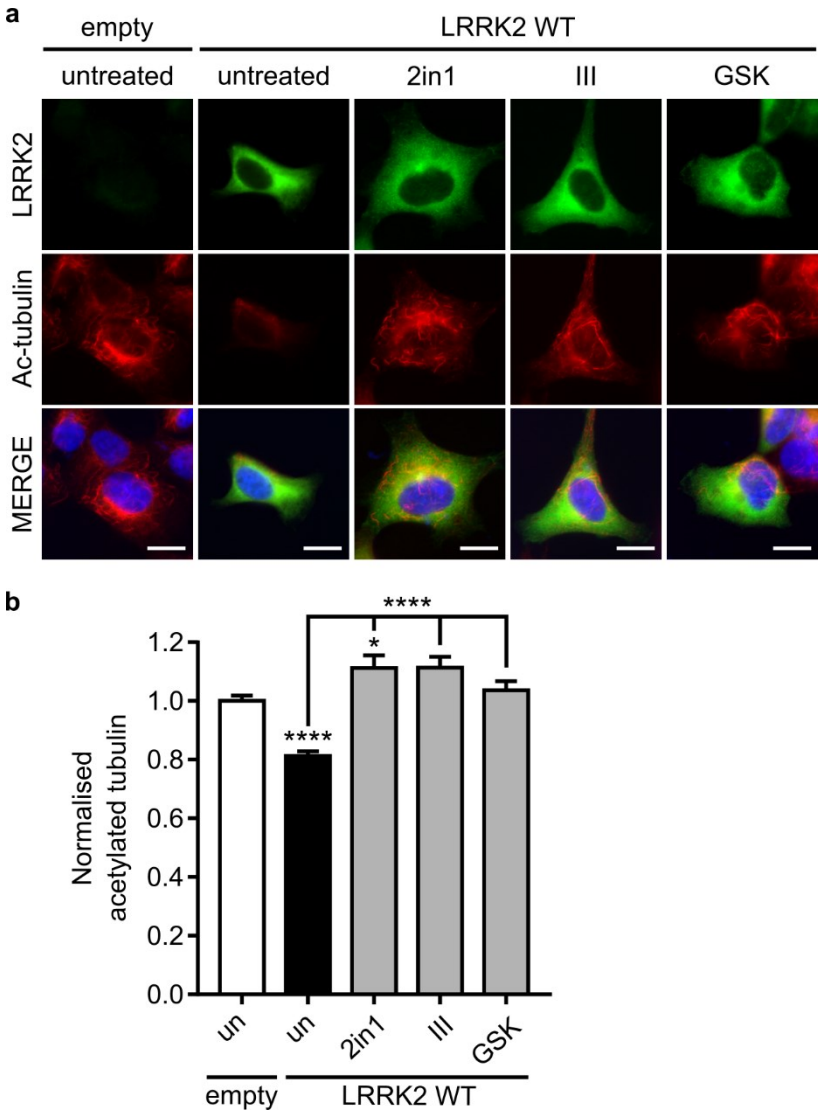

Figure 5.4. LRRK2 kinase inhibitors increase tubulin acetylation. a) HEK293 cells were transfected with either empty vector or Myc-LRRK2 (green) and treated with either 1 μM LRRK2in1, 3 μM LRRK2 Inhibitor III (HG-10-102-01) or 1 μM GSK2578215A for 4h at twenty hours post-transfection, before fixation at 24h post-transfection and immunostaining with anti-LRRK2 and anti-acetylated tubulin (red) antibodies and Hoechst (blue). Scale bar, 10 μm. b) Quantification of acetylated tubulin intensity normalised to empty vector control from three independent experiments (N (cells) = empty/untreated: 120; empty/2in1: 138; empty/III: 117; empty/GSK: 120; LRRK2/untreated: 103; LRRK2/2in1: 107; LRRK2/III: 91; LRRK2/GSK: 97; data shown as mean ± SEM; One-way ANOVA with Fisher's LSD test, * = P ≤ 0.05, ** = P ≤ 0.01, **** = P ≤ 0.0001). Experiment performed in collaboration with Dr K. Chinnaiya (University of Sheffield).

To study the role of LRRK2 kinase activity in mediating tubulin deacetylation using a parallel approach to small molecule LRRK2 inhibitors, the ability of kinase-dead D1994A LRRK2 to reduce acetylation was compared to wild-type LRRK2. HEK293 cells expressing Myc-LRRK2 wild-type or D1994A were fixed at twenty-four hours post-transfection and immunostained with anti-LRRK2 and anti-acetylated tubulin antibodies (Figure 5.5a). Quantification of acetylated tubulin levels in LRRK2-expressing cells showed that Myc-LRRK2 wild-type expression reduced tubulin acetylation by ~20% compared to the empty vector control (Figure 5.5b). Importantly, cells expressing kinase-dead LRRK2 D1994A did not show a decrease in tubulin acetylation compared to the empty vector control (Figure 5.5b). These results indicate that LRRK2 kinase activity is required for the ability of LRRK2 to decrease tubulin acetylation. Taken together, the results from Figure 5.4 and Figure 5.5 show that the kinase activity of LRRK2 is required for the ability of LRRK2 to reduce tubulin acetylation in cells. This is consistent with the hypothesis that LRRK2 phosphorylates HDAC6 to stimulate its deacetylase activity and consequently promote the deacetylation of tubulin.

In addition to the requirement for LRRK2 kinase activity for the reduction of tubulin acetylation, the requirement for GTP binding to LRRK2 was also tested using the GTP binding-deficient LRRK2 K1347A mutant. Cells expressing LRRK2 K1347A showed a comparable decrease in tubulin acetylation to wild-type LRRK2, indicating that LRRK2-induced tubulin deacetylation is independent of GTP binding to LRRK2 (Figure 5.5b).

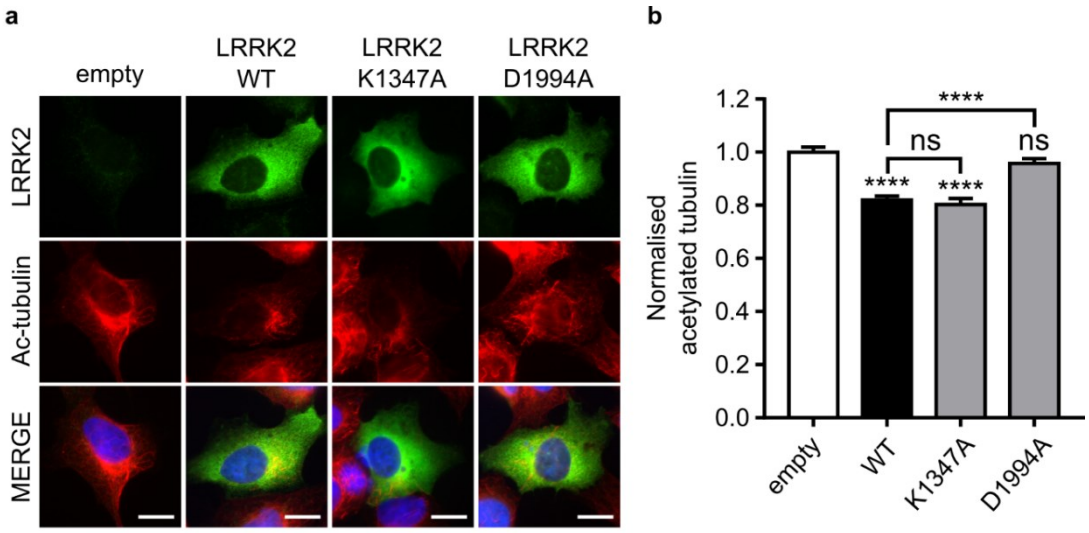

Figure 5.5. LRRK2 kinase activity is required to reduce tubulin acetylation. a) HEK293 cells were transfected with either empty vector or Myc-LRRK2 variants (green) and fixed at 24h post-transfection before immunostaining with anti-LRRK2 and anti-acetylated tubulin antibodies (red) and Hoechst (blue). Scale bar, 10 μm. b) Quantification of acetylated tubulin intensity in Myc-LRRK2 transfected samples normalised to empty vector control from three (empty, WT, D1994A) or two (K1347A) independent experiments (data shown as mean ± SEM; One-way ANOVA with Fisher's LSD test, ns = non-significant, **** = $P \leq 0.0001$; N (cells) = empty: 109; WT: 125; K1347A: 56; D1994A: 116). Experiment performed in collaboration with Dr K. Chinnaiya (University of Sheffield).

5.2.4 Phosphorylation of HDAC6 regulates deacetylase activity

Evidence from this chapter so far suggests that LRRK2 reduces tubulin acetylation via HDAC6 in a kinase-dependent manner (Figure 5.1 to Figure 5.5). In Chapter 3, LRRK2 was shown to phosphorylate HDAC6 at serine-22 and serine-689 *in vitro* and phosphorylation of HDAC6 serine-22 by LRRK2 was validated in cells using a phospho-specific antibody. Therefore, phosphorylation of HDAC6 serine-22 and serine-689 by LRRK2 may stimulate the deacetylase activity of HDAC6 to reduce tubulin acetylation. Phosphorylation of HDAC6 at serine-22 correlates with decreased tubulin acetylation in hippocampal neurons but a direct effect on HDAC6 deacetylase activity has not been shown (Chen et al., 2010). Furthermore, serine-689 is a novel HDAC6 phosphosite in the C-terminal deacetylase domain and its effects on HDAC6 deacetylase activity are not known.

To study the effects of phosphorylation at these sites on HDAC6 deacetylase activity, FLAG-HDAC6 wild-type, S22A or S689A phospho-mutant constructs described in Chapter 4 were expressed in HEK293 cells with transfection of empty vector as a control. The levels of tubulin acetylation were subsequently analysed by both western blot and immunofluorescence. For western blot analysis, cells were lysed 24 hours post-transfection and separated on SDS-PAGE before HDAC6, acetylated tubulin and total tubulin were detected on immunoblot (Figure 5.6a). Expression of wild-type FLAG-HDAC6 caused a marked ~60% reduction in tubulin acetylation compared to the empty vector control (Figure 5.6b). The FLAG-HDAC6-S22A phospho-mutant reduced tubulin acetylation by the same degree as wild-type HDAC6, indicating that preventing serine-22 phosphorylation had no effect on HDAC6 deacetylase activity. Cells expressing the FLAG-HDAC6-S689A phospho-mutant showed levels of tubulin acetylation around 10% higher than those expressing wild-type HDAC6 (Figure 5.6b). This indicates that preventing serine-689 phosphorylation reduces the deacetylase activity of HDAC6.

For immunofluorescence analysis of tubulin acetylation, cells were fixed 24 hours post-transfection and immunostained with anti-FLAG and anti-acetylated tubulin antibodies (Figure 5.6c). Expression of wild-type FLAG-HDAC6 reduced levels of acetylation by ~40% compared to the empty vector control (Figure 5.6d). Cells expressing the FLAG-HDAC6-S22A phospho-mutant showed a ~35% reduction in tubulin acetylation compared to empty vector. Furthermore, cells expressing FLAG-HDAC6-S689A caused a ~30% reduction in acetylation compared to empty vector,

indicating that the FLAG-HDAC6-S689A phospho-mutant is less active than wild-type HDAC6 (Figure 5.6d).

The results from Figure 5.6 show that both the HDAC6 S22A and S689A phospho-mutant proteins retain most of their tubulin deacetylase activity, therefore phosphorylation of these sites is not critical for HDAC6 function. The S22A phospho-mutant showed comparable levels of tubulin acetylation to wild-type HDAC6 on western blot (Figure 5.6b) and a small increase in acetylation when quantified from immunofluorescence (Figure 5.6d), suggesting that phosphorylation of HDAC6 serine-22 may have a minor effect on increasing HDAC6 deacetylase activity. The S689A phospho-mutant consistently showed a small increase in tubulin acetylation compared to wild-type HDAC6 when assessed by both western blot (Figure 5.6b) and immunofluorescence analysis (Figure 5.6d), suggesting that phosphorylation of HDAC6 serine-689 may act to stimulate HDAC6 deacetylase activity.

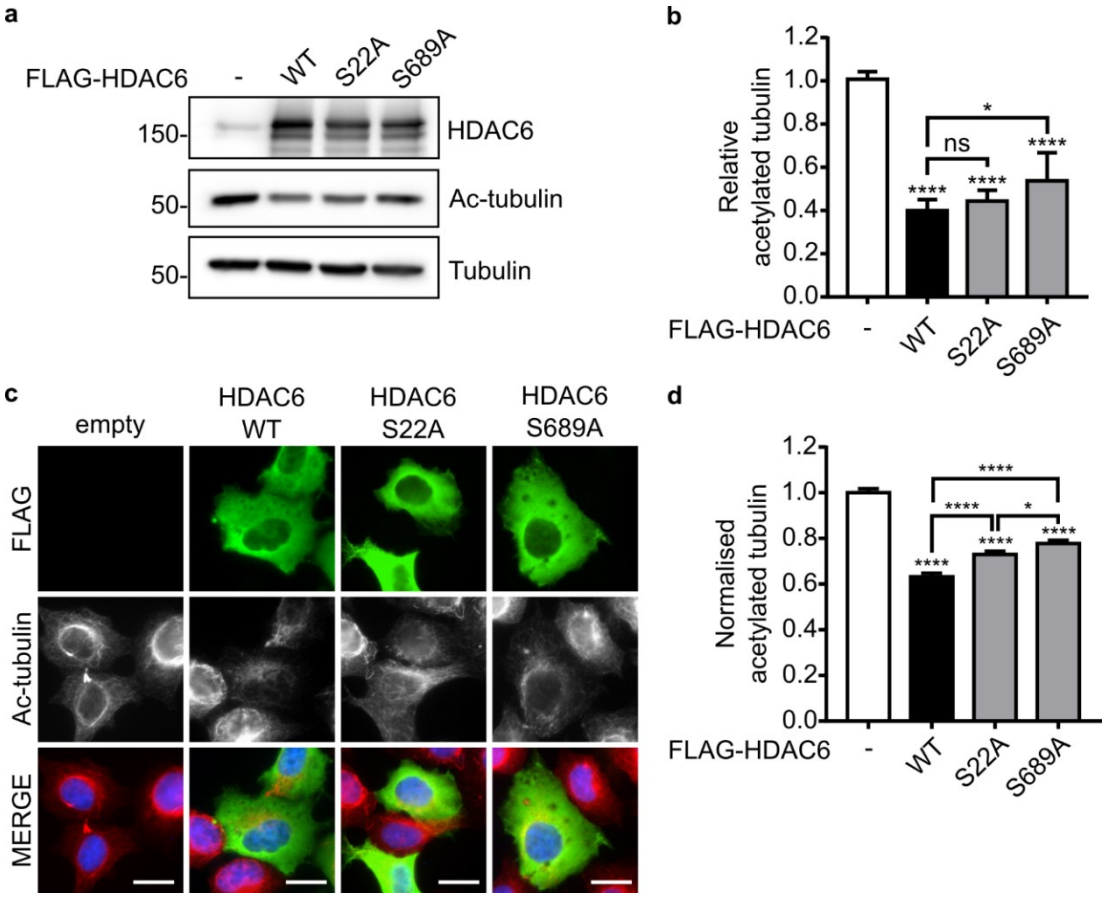

Figure 5.6 HDAC6 phosphorylation regulates deacetylase activity. a) HEK293 cells were transfected with either empty vector, FLAG-HDAC6-WT, S22A or S689A variants. Cells were lysed at 24h post-transfection and separated by SDS-PAGE before protein visualisation using anti-HDAC6, anti-acetylated tubulin and anti-tubulin antibodies. b) Quantification of ratio of acetylated to total tubulin in FLAG-HDAC6 transfected samples normalised to empty vector control (data shown as mean ± SD; One-way ANOVA with Fisher's LSD test, * = P ≤ 0.05, **** = P ≤ 0.0001, N=4). c) HEK293 cells were transfected with either empty vector, FLAG-HDAC6-WT, S22A or S689A variants and fixed at 24h post-transfection before immunostaining using anti-FLAG and anti-acetylated tubulin antibodies and Hoechst. Scale bar, 20 μm. d) Quantification of acetylated tubulin intensity in FLAG-HDAC6 transfected samples normalised to empty vector control from three independent experiments (data shown as mean ± SEM; One-way ANOVA with Fisher's LSD test, * = P ≤ 0.05, **** = P ≤ 0.0001; N (cells) = empty: 121; WT: 130; S22A: 138; S689A: 139). Experiment performed in collaboration with Dr K. Chinnaiya (University of Sheffield).

5.2.5 Phosphorylation of HDAC6 alters binding to tubulin

In cells, tubulin exists in α/ß heterodimers which polymerise into linear protofilaments to form tubular microtubule structures (Desai and Mitchison, 1997). HDAC6 binds to tubulin heterodimers at ß-tubulin via its deacetylase domains and deacetylates lysine-40 of α-tubulin (Zhang et al., 2003). Inhibition of HDAC6 deacetylase activity increases the microtubule association of HDAC6, possibly through a conformational change which increases tubulin binding (Asthana et al., 2013). Phosphorylation of HDAC6 may therefore alter both its deacetylase activity (Figure 5.6) and affect its binding to tubulin. To investigate if HDAC6 phosphorylation at serine-22 or serine-689 changes the propensity of HDAC6 to bind to tubulin, the serine to alanine phospho-mutants described in Section 5.2.4, FLAG-HDAC6-S22A and S689A, were expressed in HEK293 cells. Following lysis at 24 hours post-transfection, cells were lysed and FLAG-HDAC6 was immunoprecipitated using an anti-FLAG antibody. Proteins were separated on SDS-PAGE and FLAG-HDAC6 and co-immunoprecipitated tubulin were detected on immunoblot. Endogenous tubulin co-immunoprecipitated with FLAG-HDAC6 but not empty vector which reflected the interaction between these proteins (Figure 5.7a). Mutating serine-22 to alanine had no effect on tubulin binding compared to wild-type HDAC6, whereas mutating serine-689 to alanine increased tubulin binding (Figure 5.7b).

These results indicate that preventing phosphorylation of serine-689 in the HDAC6 C-terminal deacetylase domain increases the interaction between HDAC6 and tubulin, whereas preventing serine-22 phosphorylation does not affect the interaction between HDAC6 and tubulin. Preventing phosphorylation of serine-689 was shown to increase tubulin acetylation which is indicative of reduced HDAC6 deacetylase activity (Figure 5.6). Therefore, these results are in agreement with increased tubulin binding after HDAC6 inhibition (Asthana et al., 2013). Furthermore, these results suggest that phosphorylation of HDAC6 at serine-689 may both increase HDAC6 deacetylase activity and decrease HDAC6-tubulin binding, potentially increasing the rate at which HDAC6 can move along microtubules to deacetylate tubulin.

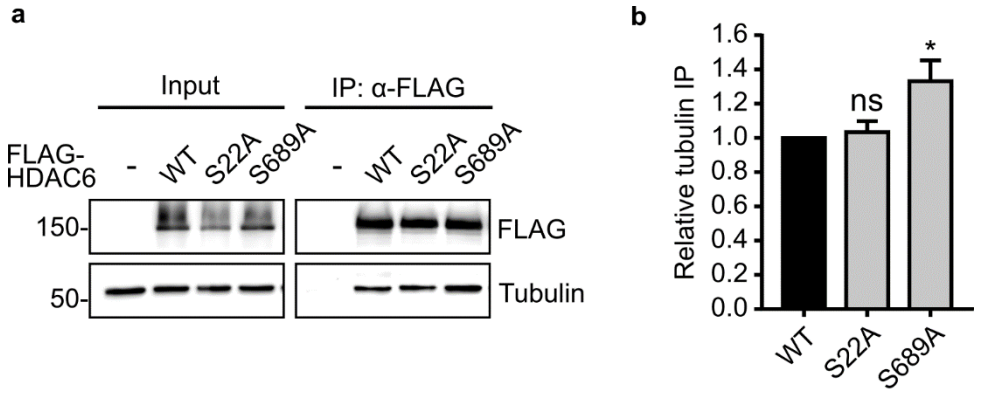

Figure 5.7. Phosphorylation of HDAC6 at serine-689 alters tubulin binding. a) HEK293 cells were transfected with either empty vector, FLAG-HDAC6-WT, S22A, S689A or S22A-S689A variants. Cells were lysed at 24h post-transfection and immunoprecipitated using anti-FLAG antibody before separation by SDS-PAGE. Proteins were immunoblotted using anti-FLAG and anti-tubulin antibodies. b) Quantification of relative tubulin co-immunoprecipitation (ratio of tubulin Co-IP to HDAC6 IP) normalised to FLAG-HDAC6-WT from four independent experiments (data shown as mean ± SEM; One-way ANOVA with Fisher's LSD test, ns = non-significant, * = $P \leq 0.05$; N=4).

5.2.6 Pathogenic LRRK2 mutations do not disrupt tubulin acetylation

Evidence from this chapter suggests that LRRK2 plays a role in the regulation of tubulin acetylation and this may occur via phosphorylation of HDAC6. PD-associated mutations in LRRK2 alter its GTPase and kinase activity and therefore may alter this function of LRRK2. The pathogenic LRRK2 mutations R1441C and Y1699C in the Roc-COR tandem domain abnormally associate with deacetylated microtubules to form filamentous structures (Godena et al., 2014). The microtubule localisation of these filamentous mutant LRRK2 structures has recently been shown to require GTP binding (Blanca Ramírez et al., 2017). Importantly, this abnormal LRRK2 phenotype can be reversed by increasing microtubule acetylation, suggesting that dysregulated microtubule acetylation may be implicated in pathogenesis (Godena et al., 2014). Furthermore, sporadic and LRRK2 G2019S patients show reduced levels of tubulin acetylation compared to healthy controls in peripheral blood mononuclear cells (Esteves et al., 2015). Pathogenic LRRK2 mutations may therefore disrupt the role of LRRK2 in regulation of tubulin acetylation.

To investigate the effects of pathogenic LRRK2 mutations on levels of tubulin acetylation, Myc-LRRK2 wild-type, R1441C, Y1699C or G2019S constructs were expressed in HEK293 cells. Following fixation at 24 hours post-transfection, cells were immunostained with anti-Myc and anti-acetylated tubulin antibodies and levels of tubulin acetylation were quantified (Figure 5.8). Consistent with previous results, expression of wild-type Myc-LRRK2 reduced tubulin acetylation by ~20% compared to the empty vector control (Figure 5.8b). The R1441C, Y1699C and G2019S mutants decreased tubulin acetylation to levels comparable with those for wild-type LRRK2. These results therefore indicate that pathogenic LRRK2 mutations do not alter the role of LRRK2 in decreasing tubulin acetylation in this assay.

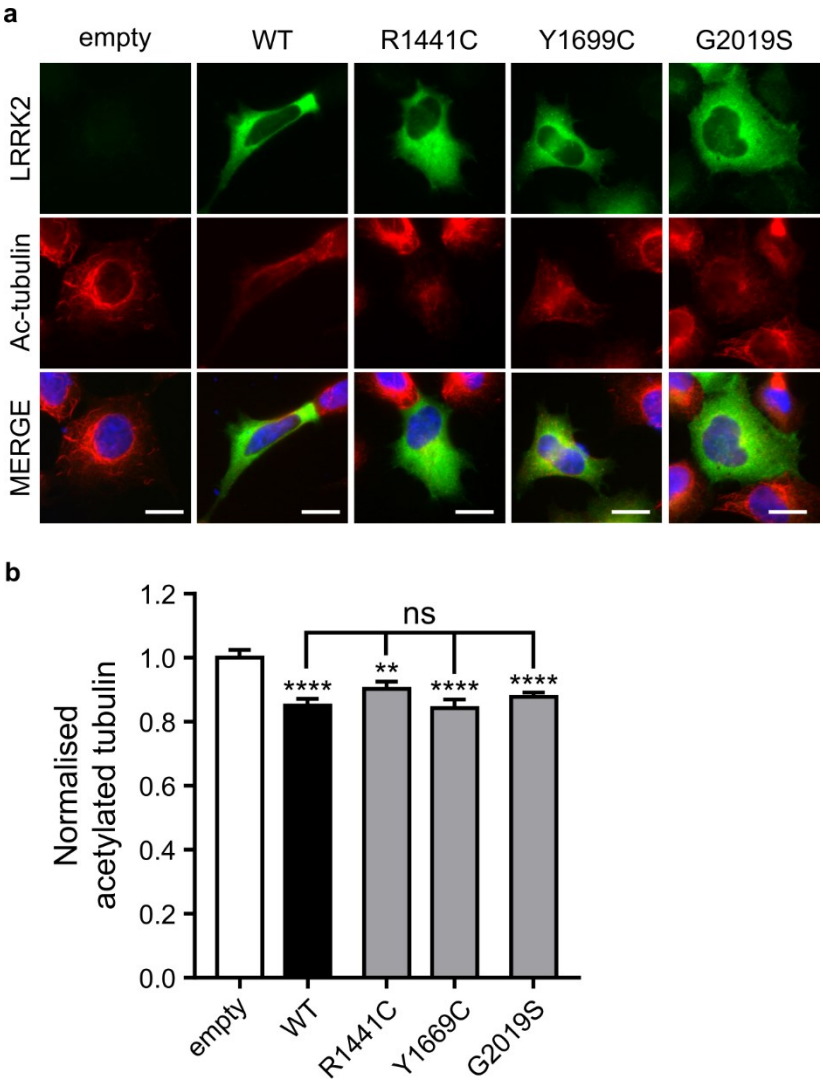

Figure 5.8. Pathogenic LRRK2 mutations do not disrupt tubulin acetylation. a) HEK293 cells were transfected with either empty vector, Myc-LRRK2-WT, R1441C, Y1699C or G2019S constructs. Cells were fixed at 24h post-transfection and immunostained with anti-LRRK2 and anti-acetylated tubulin antibodies and Hoechst. Scale bar, 10 µm. b) Quantification of acetylated tubulin intensity normalised to empty vector control from two (empty, WT, R1441C, Y1699C) or three (G2019S) independent experiments (data shown as mean ± SEM; One-way ANOVA with Fisher's LSD test, ns = non-significant, ** = P ≤ 0.01, **** = P ≤ 0.0001; N (cells) = empty: 72; WT: 50; R1441C: 61; Y1699C: 52; G2019S: 170).

5.3 Discussion

In this chapter the role of LRRK2 in regulating tubulin acetylation was investigated. First, knockdown of LRRK2 in HEK293 cells was shown to increase tubulin acetylation and LRRK2 expression rescued this increase in acetylation (Figure 5.1). This is consistent with evidence from LRRK2-knockout mouse embryonic fibroblasts which show higher levels of tubulin acetylation compared to fibroblasts from wild-type littermates (Law et al., 2014). The ability of LRRK2 to decrease tubulin acetylation was shown to be HDAC6-dependent, providing evidence that LRRK2 acts via HDAC6 to deacetylate tubulin (Figure 5.2). These results suggested that LRRK2 stimulates the deacetylase activity of HDAC6 to reduce tubulin acetylation. In support of this, LRRK2 was found to increase HDAC6 deacetylase activity *in vitro* (Figure 5.3).

Phosphorylation of HDAC6 regulates its deacetylase activity (Deribe et al., 2009; Chen et al., 2010; Williams et al., 2013). The ability of LRRK2 to decrease tubulin acetylation in cells required functional LRRK2 kinase activity and was disrupted by LRRK2 kinase inhibitors and kinase-dead mutations (Figure 5.4 and Figure 5.5). These results therefore suggested that LRRK2 may phosphorylate HDAC6 to stimulate its deacetylase activity. As shown in Chapter 3, LRRK2 phosphorylated HDAC6 both *in vitro* and in cells. Mass spectrometry analysis showed that HDAC6 was phosphorylated by LRRK2 at serine-22 and serine-689 *in vitro.* Phosphorylation of HDAC6 at serine-22 correlates with a reduction in tubulin acetylation in hippocampal neurons, suggesting that serine-22 phosphorylation increases HDAC6 deacetylase activity (Chen et al., 2010). However, expression of HDAC6 with serine-22 mutated to prevent phosphorylation did not show consistent differences in deacetylase activity compared to wild-type HDAC6, indicating that serine-22 phosphorylation does not significantly regulate the activity of overexpressed HDAC6 in HEK293 cells (Figure 5.6). Serine-689 is a novel phosphosite situated in the C-terminal deacetylase domain of HDAC6 which provides the majority of its deacetylase activity (Haggarty et al., 2003). Evidence shows that phosphorylation of another residue in the HD2 domain, tyrosine-570, inhibits HDAC6 deacetylase activity (Deribe et al., 2009). Expression of an HDAC6 serine-689 phospho-mutant showed a small decrease in deacetylase activity compared to wild-type HDAC6, suggesting that whilst not crucial for HDAC6 function, phosphorylation of serine-689 stimulates HDAC6 deacetylase activity (Figure 5.6).

Inhibition of HDAC6 activity increases the microtubule association of HDAC6 through increased binding to tubulin (Asthana et al., 2013). Consistent with this, mutating

HDAC6 serine-689 to prevent phosphorylation increased the interaction between HDAC6 and tubulin (Figure 5.7). Increased binding of HDAC6 to tubulin caused by HDAC6 inhibition reduces microtubule dynamics and increases microtubule stability, possibly by HDAC6 acting as a MAP independent of its deacetylase function (Zilberman et al., 2009; Asthana et al., 2013). Recent studies show that acetylation increases microtubule flexibility and resilience to mechanical stress and acts as a marker of stability (Portran et al., 2017; Xu et al., 2017). The results from Figure 5.6 and Figure 5.7 suggest that phosphorylation of HDAC6 at serine-689 may stimulate HDAC6 deacetylase activity to reduce tubulin acetylation as well as reducing the binding of HDAC6 to tubulin, both of which could promote the dynamic instability of microtubules.

Whilst phosphorylation of HDAC6 serine-689 by LRRK2 requires validation in cell models, the results in this chapter suggest a model whereby wild-type LRRK2 may phosphorylate HDAC6 at serine-689 to reduce tubulin acetylation via stimulation of HDAC6 deacetylase activity. In addition, LRRK2-mediated phosphorylation of serine-689 may reduce the binding of HDAC6 to tubulin. Therefore, LRRK2 may promote increased microtubule dynamics and instability through phosphorylation of HDAC6 serine-689. This is consistent with studies which show that LRRK2 knockdown increases neurite branching, a process which is linked to microtubule stability (MacLeod et al., 2006; Parisiadou et al., 2009, Song et al., 2013).

Lastly, the effects of PD-associated LRRK2 mutations on the regulation of tubulin acetylation by LRRK2 were investigated to identify if this mechanism is disrupted in disease. The R1441C and Y1699C LRRK2 mutants abnormally associate with deacetylated microtubules and lead to defects in mitochondrial transport, possibly through dysregulation of microtubule acetylation (Godena et al., 2014). However, LRRK2 R1441C did not alter HDAC6 deacetylase activity compared to wild-type LRRK2 *in vitro* and cells overexpressing LRRK2 R1441C and Y1699C showed no changes in tubulin acetylation compared to cells overexpressing wild-type LRRK2 (Figure 5.3 and Figure 5.8). Therefore, these results suggest that LRRK2 R1441C and Y1699C mutations do not directly affect the level of microtubule acetylation. In Chapter 3, LRRK2 Y1699C was shown to increase binding to HDAC6 (Figure 3.5). The R1441C mutation increases binding of LRRK2 to tubulin (Law et al., 2014). Therefore, LRRK2 R1441C and Y1699C may disrupt microtubule-dependent processes through increased binding to HDAC6 and tubulin at the microtubule surface rather than by directly affecting HDAC6 deacetylase activity.

LRRK2 G2019S disrupts neurite outgrowth, growth cone dynamics and cortical branching which suggests it alters microtubule stability (MacLeod et al., 2006; Parisiadou et al., 2009; Winner et al., 2011; Law et al., 2014). These effects could be attributed to alterations in microtubule acetylation by LRRK2 G2019S. In the context of the results shown in this chapter, increased LRRK2 kinase activity caused by the G2019S mutation might be predicted to elevate phosphorylation of HDAC6 and further stimulate deacetylase activity, thereby reducing tubulin acetylation to a greater level than wild-type LRRK2. Indeed, peripheral cells from sporadic and G2019S PD patients show reduced tubulin acetylation compared to control individuals (Esteves et al., 2015). However, LRRK2 G2019S did not increase HDAC6 activity compared to wild-type LRRK2 *in vitro* and expression of LRRK2 G2019S causes a decrease in tubulin acetylation comparable to wild-type LRRK2 (Figure 5.3 and Figure 5.8). Therefore, the effects of LRRK2 G2019S on microtubule acetylation require further investigation to determine if this is a mechanism altered in disease.

6 Discussion

6.1 LRRK2 regulates HDAC6 function

Mutations in LRRK2 are the most common familial genetic cause of PD (Li et al., 2014). All confirmed pathogenic mutations cluster within the GTPase and kinase domain catalytic core of LRRK2, either decreasing GTPase activity or increasing kinase activity (Gilsbach and Kortholt, 2014). This indicates that the catalytic functions of LRRK2 are central to its role in disease. LRRK2-associated PD shares many symptomatic and pathological characteristics to sporadic PD, therefore understanding LRRK2 biology is important to gain insight into universal mechanisms of pathogenesis in PD (Li et al., 2014). HDAC6 has been implicated in a range of neurodegenerative diseases including PD through its central role in aggresome formation, autophagy and microtubule acetylation (Simões-Pires et al., 2013). HDAC6 is a component of aggresome-like Lewy bodies found in PD brains where it is proposed to represent a cytoprotective response to α-synuclein aggregation (Kawaguchi et al., 2003; Du et al., 2010; Su et al., 2011). The roles of HDAC6 in aggresome formation utilises its ubiquitin-binding capacity. However, inhibition of HDAC6 deacetylase activity has shown therapeutic benefit in some models of PD, suggesting that its deacetylase activity also plays a role in disease (Godena et al., 2014; Pinho et al., 2016).

The aim of this thesis was to characterise a novel interaction between LRRK2 and HDAC6 and investigate the role of LRRK2 in HDAC6-mediated aggresome formation and tubulin deacetylation. In Chapter 3, HDAC6 was shown to be a direct interactor and phosphorylation substrate of LRRK2, providing an indication that LRRK2 regulates the activity and function of HDAC6. LRRK2 phosphorylated HDAC6 at serine-22, a site previously linked to the regulation of HDAC6 deacetylase activity (Chen et al., 2010), and the novel phosphosite serine-689 in the second HDAC6 deacetylase domain (Figure 3.7). The location of these phosphosites in sites associated with HDAC6 deacetylase activity suggested that LRRK2 may be a regulator of HDAC6 function.

HDAC6 is a crucial co-ordinator of the misfolded protein response through its ubiquitin-binding capacity and HDAC6 is required for aggresome formation of polyubiquitinated proteins (Kawaguchi et al., 2003; Ouyang et al., 2012). Section 4 therefore investigated the role of LRRK2 in HDAC6-mediated aggresome formation.

Knockdown of endogenous LRRK2 using siRNA was shown to disrupt the formation of GFP-CFTR-ΔF508 aggresomes but not GFP-250 aggresomes in HEK293 cells (Figure 4.3). This was consistent with the role of HDAC6 in the formation of poly-ubiquitinated aggresomes but not ubiquitin-independent aggresomes (Kawaguchi et al., 2003) and indicates that LRRK2 may act upstream of HDAC6 in this pathway. The GFP-CFTR-ΔF508 aggresome formation defect after LRRK2 knockdown was rescued by expression of LRRK2 wild-type but not the D1994A kinase-dead mutant, showing that LRRK2 kinase activity was required for its role in promoting GFP-CFTR-ΔF508 aggresome formation (Figure 4.4). Furthermore, phosphorylation of HDAC6 serine-22 was crucial for the ability of HDAC6 to rescue GFP-CFTR-ΔF508 aggresome formation after LRRK2 knockdown (Figure 4.6). Together, these data indicate that LRRK2-mediated phosphorylation of HDAC6 at serine-22 as described in Chapter 3 is a critical step in the formation of polyubiquitinated aggresomes. HDAC6 serine-22 phosphorylation appeared to regulate the microtubule-based transport of ubiquitinated protein to the aggresome but not the recognition of HDAC6 to its ubiquitinated cargo (Figure 4.6). A potential mechanism for this could be via LRRK2 phosphorylation of HDAC6 serine-22 stimulating the interaction between HDAC6 and cytoplasmic dynein to promote the dynein-mediated transport of ubiquitinated protein towards the aggresome. This model is summarised in Figure 6.1A.

A previous study found that LRRK2 overexpression causes cytoplasmic accumulation of a marker of endogenous ubiquitinated aggregates after proteasomal inhibition in SH-SY5Y cells, suggesting that LRRK2 acts to disrupt endogenous protein aggresome formation (Bang et al., 2016). Interestingly, this effect was not seen in HEK293 cells, indicating that there may be differences in the aggresome response between neuronal and non-neuronal cell types (Bang et al., 2016). However, non-transgenic mice exposed to a proteasome inhibitor did not show significant accumulation of aggregated protein in the brain compared to transgenic mice expressing LRRK2 G2019S (Bang et al., 2016). This suggests that wild-type LRRK2 overexpression in SH-SY5Y cells may mimic a kinase gain of function in the same manner as LRRK2 G2019S and contribute to a protein accumulation phenotype, thereby highlighting a potential limitation of such an overexpression model *in vitro* (Bang et al., 2016).

In addition to its role in polyubiquitinated aggresome formation, HDAC6 is a major cytoplasmic α-tubulin deacetylase (Hubbert et al., 2002). The role of LRRK2 in the regulation of tubulin acetylation via HDAC6 was therefore investigated in Chapter 5.

Knockdown of LRRK2 with targeted siRNA increased tubulin acetylation and expression of LRRK2 decreased acetylation in a kinase and HDAC6-dependent manner, suggesting that LRRK2 reduces tubulin acetylation via stimulation of HDAC6 deacetylase activity (Figure 5.1 to Figure 5.5). In support of this, LRRK2 was shown to increase the deacetylase activity of HDAC6 *in vitro* (Figure 5.3). Furthermore, LRRK2 phosphorylated HDAC6 at serine-689 in the second deacetylase domain of HDAC6 *in vitro* (Figure 3.7), and phosphorylation of serine-689 was associated with reduced tubulin acetylation and binding of HDAC6 to tubulin in cells (Figure 5.6 and Figure 5.7). This indicates that serine-689 phosphorylation stimulates the tubulin deacetylase function of HDAC6. Therefore, these results suggest that LRRK2-mediated phosphorylation of HDAC6 serine-689 increases the deacetylase activity of HDAC6 to reduce α-tubulin acetylation (Figure 6.1B).

As well as α-tubulin, HDAC6 deacetylates other substrates to regulate cellular pathways such as protein chaperoning and autophagy (Li Yingxiu et al., 2013). HDAC6-mediated deacetylation of cortactin is required to recruit the F-actin network in autophagosome-lysosome fusion during autophagic maturation, and HDAC6 deficiency leads to failure of autophagic degradation, accumulation of aggregated protein and neurodegeneration (Lee et al., 2010a). HDAC6-mediated deacetylation of Hsp90 is required for activation of its protein chaperone activity (Kovacs et al., 2005). Hsp90 preferentially binds to unstable proteins and is a key regulator of the fate of misfolded proteins such as CFTR-ΔF508 by aiding their refolding or ubiquitination and degradation (Schneider et al., 1996; Fuller and Cuthbert, 2000; Wang et al., 2006; Lindberg et al., 2015). Hsp90 also regulates the stability of a wide range of protein kinases including LRRK2 to regulate cellular signalling pathways (Wang et al., 2008; Schopf et al., 2017). Whilst not a focus of this thesis, it is therefore possible that LRRK2-mediated phosphorylation of HDAC6 may influence the deacetylation of cortactin to regulate autophagosome-lysosome fusion (Figure 6.1C) and Hsp90 to regulate chaperone activity protein stability, perhaps even acting in a feedback loop for regulation of LRRK2 protein levels (Figure 6.1D).

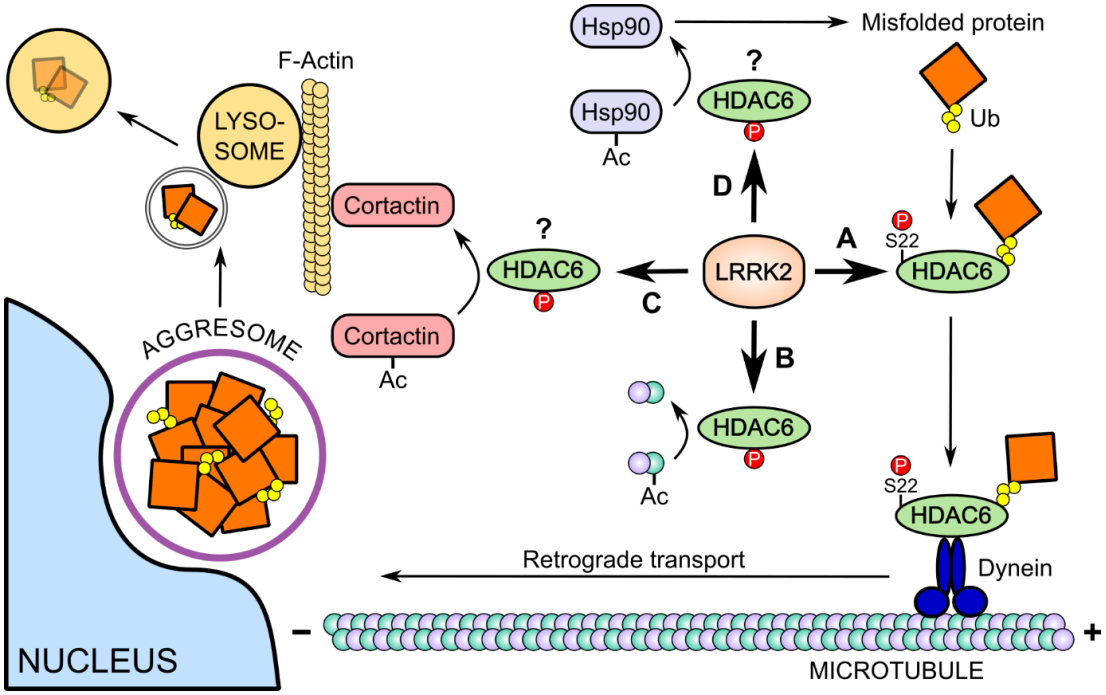

Figure 6.1. Model for the possible pathways regulated by LRRK2 phosphorylation of HDAC6. A) Ubiquitinated misfolded protein which exceeds the degradation capacity of the proteasome is recognised by HDAC6 via its ubiquitin-binding ZnF-UBP domain. LRRK2 phosphorylates HDAC6 at serine-22 which allows HDAC6 to bind to dynein via its dynein-binding (DMB) domain and transport misfolded protein in a retrograde direction towards the MTOC to form an aggresome surrounded by a vimentin cage. **B)** LRRK2 phosphorylation of HDAC6 serine-689 stimulates HDAC6 deacetylase activity to deacetylate α-tubulin either as free tubulin dimers in the cytoplasm or as part of polymerised microtubules, altering microtubule dynamics. **C)** LRRK2 phosphorylation of HDAC6 may stimulate the deacetylation of cortactin to promote F-actin polymerisation and autophagosome-lysosome fusion in autophagy. **D)** LRRK2 phosphorylation of HDAC6 may stimulate the deacetylation of Hsp90 to activate its chaperone activity and regulation of misfolded protein stability and degradation.

6.1.1 Effects of PD-associated LRRK2 mutations on HDAC6 function

The role of LRRK2 in HDAC6-mediated aggresome formation and tubulin deacetylation described in this thesis provides potential mechanisms by which pathogenic PD-associated LRRK2 mutations might manifest cytotoxicity. In Chapter 5, expression of pathogenic LRRK2 mutants reduced levels of tubulin acetylation comparable to wild-type LRRK2 (Figure 5.8). These results therefore indicated that PD-associated mutations in LRRK2 did not disrupt its function as a regulator of tubulin acetylation via HDAC6. However, in Chapter 4 LRRK2-mediated aggresome formation was shown to be disrupted by the PD-associated G2019S LRRK2 mutation. LRRK2 G2019S was not able to support the aggresome formation of ubiquitinated protein to the same level as wild-type LRRK2 (Figure 4.7). As aggresomes are considered a cytoprotective response to aggregated protein, this result indicated that disruption of the normal function of LRRK2 in aggresome formation could be a pathogenic mechanism in disease. LRRK2 G2019S increases cytoplasmic ubiquitinated aggregates in the brains of transgenic mice after proteasomal inhibition compared to non-transgenic controls (Bang et al., 2016). Furthermore, iPSC-derived neurons from LRRK2 G2019S patients show increased cytoskeletal-associated aggregate formation compared to unaffected controls (Schwab and Ebert, 2015). Therefore, LRRK2 G2019S may disrupt normal processing of aggregated protein along the aggresome pathway.

In the context of the model proposed here (Figure 6.1), if elevated LRRK2 kinase activity due to the G2019S mutation increases phosphorylation of HDAC6 at serine-22 this may promote excessive binding between HDAC6 and cytoplasmic dynein. A possible mechanism for how this could disrupt normal aggresome formation is through constitutive activation of aggregate transport along an incomplete microtubule network, leading to protein aggregation in cytoplasmic regions other than the perinuclear aggresome. However, the presence of acetylated microtubules in cells expressing LRRK2 G2019S suggests that the microtubule network remains intact and able to support transport (Figure 5.8). Alternatively, excessive binding between HDAC6 and cytoplasmic dynein could sequester HDAC6 in a dynein-bound complex could prevent the deacetylation of cellular substrates such as α-tubulin, cortactin and Hsp90. Proteasomal inhibition, as with proteasomal dysfunction in PD, causes accumulation of ubiquitinated protein aggregates and recruits HDAC6 to promote the aggresome response (Su et al., 2011). Therefore, in disease proteasomal stress may reduce the availability of HDAC6 for deacetylation of its other

cellular substrates and this may be exacerbated by LRRK2 G2019S-mediated stimulation of HDAC6 binding to cytoplasmic dynein.

Reduced HDAC6 deacetylation of cortactin due to mutant LRRK2-induced sequestration of HDAC6 in a dynein-bound complex could inhibit autophagosome-lysosome fusion during autophagy. Indeed, LRRK2 G2019S has been shown to cause an accumulation of autophagic vacuoles in multiple models as described in Chapter 1 which is indicative of failed autophagic clearance (Ramonet et al., 2011; Arduíno et al., 2012; Sánchez-Danés et al., 2012). Furthermore, LRRK2 G2019S reduces autophagic flux whereas wild-type LRRK2 increases it (Saha et al., 2015). This is consistent with a possible model where wild-type LRRK2 stimulates HDAC6 deacetylation of cortactin for autophagosome-lysosome fusion, whereas excessive HDAC6 phosphorylation by LRRK2 G2019S sequesters HDAC6 in a dynein-bound complex to reduce cortactin deacetylation.

Reduced HDAC6 deacetylation of Hsp90 could inhibit its chaperone function (Scroggins et al., 2007; Mollapour and Neckers, 2012). Hsp90 binds to monomeric α-synuclein and promotes fibril formation in an ATP-dependent manner to prevent the accumulation of toxic α-synuclein oligomers in PD, suggesting that Hsp90 chaperone activity is neuroprotective (Falsone et al., 2009). Conversely, mutant LRRK2 may increase HDAC6 phosphorylation to further stimulate Hsp90 deacetylation. HDAC6 deacetylation of Hsp90 promotes the accumulation of abnormal tau by increasing the binding affinity of the Hsp90 chaperone complex to tau to block its degradation, and suggests that Hsp90 chaperone activity requires tight regulation (Cook et al., 2012). Furthermore, active Hsp90 regulates the stability of LRRK2 and Hsp90 inhibitors have been shown to rescue the LRRK2 G2019S-induced neuronal toxicity by increasing LRRK2 proteasomal degradation (Wang et al., 2008). This raises the possibility that mutant LRRK2 causes Hsp90 hypoacetylation to increase the stability of LRRK2 in a positive feedback loop, possibly through increased HDAC6 phosphorylation and Hsp90 deacetylation. Therefore, dysregulated Hsp90 deacetylation due to either mutant LRRK2-induced HDAC6 sequestration or HDAC6 overactivation may impact the chaperone function of Hsp90 and drive pathogenicity.

6.2 Aggresome formation in PD

The data in this thesis provides evidence that wild-type LRRK2 phosphorylates HDAC6 at serine-22 to promote the formation of ubiquitinated aggresomes after proteasome dysfunction. Aggresome formation can be induced in cell models through proteasomal inhibition, and similarly proteasome dysfunction is a feature of PD (McNaught et al., 2006; Lim, 2007). The PD-associated aggregating protein α-synuclein is a substrate of the proteasome and toxic α-synuclein oligomers inhibit proteasome function (Snyder et al., 2003; Lindersson et al., 2004; Zondler et al., 2017). Lewy bodies contain components of the 20S proteasome bound to filamentous α-synuclein and act to sequester these toxic α-synuclein oligomers (Cook and Petrucelli, 2009). Hence, Lewy bodies may represent an aggresome-like protective response to misfolded protein in affected neurons (Olanow et al., 2004; Olzmann et al., 2008; Wakabayashi et al., 2013). In support of this, post-mortem SNpc neurons containing Lewy bodies often show reduced apoptosis compared to surrounding neurons without Lewy body formation, and the presence of Lewy bodies is not unusual in individuals without any symptoms of PD (Forno, 1996; Tompkins and Hill, 1997).

The morphological and biochemical similarities between aggresomes and Lewy bodies suggests a functional overlap in their biogenesis. Lewy bodies consist of densely-packed α-synuclein and strongly stain for ubiquitin which shows an accumulation of ubiquitinated protein (Tofaris et al., 2003). Additionally, Lewy bodies show high levels of intermediate filament proteins such as neurofilaments, similar to the localisation of the intermediate filament vimentin at non-neuronal aggresomes, as well as the centrosome components γ-tubulin and pericentrin (Trojanowski and Lee, 1998; Johnston et al., 1998; McNaught et al., 2002). Lewy bodies therefore appear to be formed in a mechanism like that of aggresomes.

Unlike aggresomes, not all Lewy bodies are juxtanuclear and are often present in multiple locations within the neuronal cytoplasm (Wakabayashi et al., 2007). However, neurons show differences in microtubule organisation compared to non-neuronal mitotic cells, with increased katanin-induced microtubule severing from the centrosome combined with ninein-mediated microtubule recapture at multiple cytoplasmic anchoring points resulting in a non-centrosome-focused microtubule distribution (Ahmad et al., 1999; Baird et al., 2004). This may result in aggregate transport to locations other than the neuronal centrosome and account for the

differential distribution of Lewy bodies in contrast to juxtanuclear non-neuronal aggresomes.

Importantly, both LRRK2 and HDAC6 are components of Lewy bodies in PD (Kawaguchi et al., 2003; Guerreiro et al., 2013). The data presented in this thesis shows that, like Lewy bodies, LRRK2 and HDAC6 are present in aggresomes and furthermore act in a common pathway for aggresome formation. In view of the similarities between aggresomes and Lewy bodies described here, this raises the possibility that LRRK2 may phosphorylate HDAC6 at serine-22 to promote the transport of toxic α-synuclein aggregates to form Lewy bodies, and disruption of this process by LRRK2 mutations may contribute to pathogenesis in PD.

6.2.1 PD genes associated with the aggresome response

In addition to LRRK2, many other PD-associated genes are implicated in the aggresome response to misfolded protein. α-synuclein is the primary toxic protein species in degenerating DA neurons, and familial PD-associated α-synuclein mutations such as A30P, E46K, H50Q, G51D and A53T promote the formation of oligomers and may hasten the aggresome response to mitigate their cytotoxicity (Burré et al., 2015). Interestingly, whilst these different mutations all show similar propensities to form oligomers, their abilities to aggregate and form inclusions in cells vary, with the A30P mutant showing decreased inclusion formation and the E46K mutant showing increased inclusion formation (Lázaro et al., 2014). This correlates with the recent finding that the E46K mutant shows the highest neuronal toxicity, whereas A30P is less toxic and instead disrupts the membrane association of α-synuclein in a different mechanism of pathogenicity (Íñigo-Marco et al., 2017). Therefore, evidence suggests that the cell responds to α-synuclein toxicity by invoking the formation of inclusions, with PD-associated mutations in α-synuclein altering the load of toxic cargo to be sequestered.

The α-synuclein-associated protein synphilin-1 is also present in Lewy bodies and plays a neuroprotective role by promoting inclusion formation (Engelender et al., 1999; Tanaka et al., 2004). Synphilin-1 enhances aggresome formation and attenuates neurodegeneration in a transgenic α-synuclein mouse model of PD (Smith et al., 2010). An R621C mutation in synphilin-1 which reduce its ability to form inclusions has been identified in PD patients, suggesting that this mutation increases the sensitivity of neurons to toxic insults by reducing the aggresome response (Marx et al., 2003). Recently, synphilin-1 has been shown to bind to LRRK2, reduce its

kinase activity and promote the formation of inclusions containing LRRK2 (Liu et al., 2016). Expression of synphilin-1 attenuates the toxicity of LRRK2 G2019S and reduces DA neuron degeneration and locomotor deficits in transgenic *Drosophila*, with these effects proposed to result from a Synphilin-1-mediated reduction in elevated LRRK2 G2019S kinase activity. Therefore, there is a clear interplay between LRRK2 and synphilin-1 in the formation of aggresome-like inclusions in PD.

Synphilin-1 is ubiquitinated by Parkin, a further familial PD gene, to promote the formation of ubiquitinated inclusions (Chung et al., 2001). Functional parkin is a component of Lewy bodies in both sporadic and familial PD as well as DLB (Schlossmacher et al., 2002). PD-associated mutations in Parkin disrupt synphilin-1 ubiquitination and prevent inclusion formation, suggesting that Parkin is required for Lewy body formation. This is observed in parkin PD patients which show a pathological absence of Lewy bodies (Mori et al., 1998). As described in Chapter 1, HDAC6 is a target of Parkin regulation to promote ubiquitinated aggresome formation (Olzmann and Chin, 2008). This occurs via parkin-mediated ubiquitination of DJ-1 which is subsequently recruited to cytoplasmic dynein by HDAC6 and transported to the aggresome (Olzmann et al., 2007). Mutations in DJ-1 which induce protein misfolding and aggregation cause autosomal recessive familial PD (Olzmann et al., 2004). Closely-linked to Parkin in the mitophagy pathway is PINK1, which phosphorylates parkin to recruit it to damaged mitochondria (reviewed by Narendra et al., 2012). PINK1 is also a component of Lewy bodies in PD brains and localises to aggresomes after proteasomal inhibition in cell models (Muqit et al., 2006). PINK1 acts as a sensor of proteasomal dysfunction and phosphorylates p62/SQSTM1 to increase the transport of ubiquitinated proteins to the aggresome (Gao et al., 2016).

Altogether, the interactions between many different familial PD-associated genes such as α-synuclein, Parkin, DJ-1, PINK1 and LRRK2 in the aggresome formation pathway, either as misfolded substrates or regulators of the cellular response, provides strong evidence that this pathway is a key mechanism in the pathogenesis of PD. Furthermore, the established links of HDAC6 to the regulation of aggresome formation implicates that dysregulation of HDAC6 function by mutant LRRK2 may be a possible therapeutic target for the treatment of PD.

6.2.2 Consequences for the treatment of PD

As described in this thesis, LRRK2-mediated phosphorylation of HDAC6 at serine-22 is proposed to regulate the formation of ubiquitinated aggresomes. An inability to fully support normal aggresome formation by LRRK2 G2019S as shown in Chapter 4 suggested that this mutation might dysregulate the role of HDAC6 in promoting aggregate transport to the aggresome and this may be caused by elevated LRRK2 kinase activity (discussed in Section 4.3). Excessive kinase activity of PD-associated LRRK2 mutations has a pathogenic effect in multiple cellular functions such as autophagy, Rab-associated vesicle trafficking and microtubule dynamics (described in Chapter 1). Targeting elevated LRRK2 kinase activity may therefore show a beneficial effect in restoring ubiquitinated aggresome formation and preventing cytoplasmic protein aggregation.

Small molecule inhibitors of LRRK2 kinase activity are currently in various stages of development and evaluation in animal models of PD (West, 2017). As LRRK2 kinase inhibitors with high specificity and bioavailability have only recently become available, much of the research into the effects of LRRK2 inhibition has so far come from knockout animal models where total LRRK2 protein levels are reduced or ablated entirely. LRRK2 knockout mouse and rat models show some neuroprotection from α-synuclein overexpression with reduced neurodegeneration and neuroinflammation (Lin et al., 2009; Daher et al., 2014), although others show little to no effect (Andres-Mateos et al., 2009; Daher et al., 2012). In addition, evidence of changes to kidney and lung function, the tissues with highest LRRK2 expression, provide additional safety concerns for complete LRRK2 inhibition (Herzig et al., 2011; Boddu et al., 2015). The latest generation of LRRK2 kinase inhibitors including MLi-2 and PFE360 show improved selectivity and brain permeability, reducing off-target effects and improving bioavailability, however have yet to show consistent effects on reducing neurodegeneration (Daher et al., 2015; Fell et al., 2015).

An important observation from the data in this thesis is that total ablation of LRRK2 kinase activity in the kinase-dead mutant prevented all ubiquitinated aggresome formation, therefore in the context of a neuroprotective model for Lewy body formation complete LRRK2 kinase inhibition might be predicted to increase cytotoxicity rather than reduce it. This suggests that targeting the elevated kinase activity of pathogenic LRRK2 mutants to return the balance of LRRK2 kinase activity to wild-type levels may be desirable to normalise LRRK2 function whilst preventing potentially cytotoxic disruption of its function. Targeting this therapeutic window would also hopefully

minimise the unwanted effects of total LRRK2 inhibition in peripheral tissue such as in lung and kidney (West, 2017).

As discussed in Chapter 1, the targeting of HDAC6 with deacetylase inhibitors has shown neuroprotective effects in some PD models as well as other neurodegenerative diseases (Section 1.3.4). Increasing microtubule acetylation by inhibiting HDAC6 reverses the abnormal association of pathogenic LRRK2 GTPase mutants with microtubules and restores the deficits in the axonal transport of mitochondria caused by these mutants (Godena et al., 2014). These mutants may exert their pathogenic effects on axonal transport either by interfering with tubulin acetylation to alter microtubule stability and motor protein binding, or rather by physically blocking the progress of transport due to the enhanced microtubule association. Axonal transport slows down in the vicinity of stationary organelles on the microtubule via a mechanism of steric hindrance, and it is conceivable that microtubule binding of a large, cytoplasmic protein such as LRRK2 could act in a similar manner (Che et al., 2016). Like the axonal transport of mitochondria, aggresome formation requires an intact yet dynamic microtubule network for the cytoplasmic dynein-mediated transport of aggregates (Bauer and Richter-Landsberg, 2006). Whilst the effect of pathogenic GTPase mutations in LRRK2 on aggresome formation requires further investigation, it is interesting to hypothesise that they may disrupt retrograde aggregate transport to the aggresome in a comparable way to mitochondrial transport. Stimulation of aggregate transport by increasing acetylation using HDAC6 inhibitors may therefore promote aggresome formation and provide a neuroprotective effect.

Given that the role of HDAC6 formation in ubiquitinated aggresome formation is dependent on its ubiquitin and dynein-binding properties, preserving these functions whilst inhibiting its deacetylase activity to increase microtubule acetylation may provide therapeutic benefits in PD. Inhibition of HDAC6 deacetylase activity with many currently-available HDAC6 inhibitors has been reported to prevent aggresome formation in conjunction with proteasome inhibitors and has been investigated for induction of tumour cell apoptosis in cancers such as multiple myeloma (Hideshima et al., 2005; Nawrocki et al., 2006; Komatsu et al., 2013; Mishima et al., 2015). HDAC6 inhibitors such as tubacin block the interaction of HDAC6 with cytoplasmic dynein and cause accumulation of ubiquitinated proteins due to failed aggresome formation (Hideshima et al., 2005). This may be due to inhibitor binding to the HDAC6 deacetylase domains in proximity to the dynein-binding domain and physically blocking this region. Other selective HDAC6 inhibitors such as HPOB have been

shown to inhibit catalytic activity without affecting HDAC6 complex formation with ubiquitinated proteins and the aggresome autophagy response (Lee et al., 2013). Importantly, inhibition of HDAC6 deacetylase activity also prevents the deacetylation of Hsp90 and dissociation of the Hsp90/HSF1 complex required for CMA, leading to toxic aggregation of α-synuclein in a PD model (Du et al., 2014).

Therefore, inhibition of HDAC6 as a therapy to promote microtubule-based transport of aggregates in PD would require small molecule inhibitors which preserve its function in aggresome formation, however the roles of HDAC6-mediated deacetylation in further aspects of chaperone function and autophagy may have negative consequences for other cellular mechanisms implicated in PD.

6.3 Future directions

Further to the results described in this thesis for the interaction between LRRK2 and HDAC6 and its role in tubulin acetylation and aggresome formation, some questions remain and should be addressed.

Firstly, whilst a commercially-available phospho-specific antibody was used in Chapter 3 for detection of HDAC6 at phosphorylated serine-22 and confirmation of LRRK2-mediated phosphorylation of this site in cells, none such antibody was available for study of the novel HDAC6 phosphosite at serine-689 at the time of writing this thesis. A custom phospho-specific antibody for serine-689 has recently been produced and is currently undergoing evaluation to determine if LRRK2 phosphorylates HDAC6 at serine-689 in cells.

Next, the mechanism by which HDAC6 phosphorylation at serine-22 promotes ubiquitinated aggresome formation requires further investigation. Preliminary data from co-immunoprecipitation experiments (data not shown) suggests that serine-22 phosphorylation may alter the binding of HDAC6 to cytoplasmic dynein, therefore promoting the transport of the HDAC6/aggregate complex to the aggresome. If confirmed, this would indicate that LRRK2-mediated phosphorylation of HDAC6 at serine-22 regulates aggresome formation through regulation of the interaction between HDAC6 and cytoplasmic dynein. Furthermore, the effects of pathogenic LRRK2 mutations on this interaction should be studied through co-expression of LRRK2 mutants with HDAC6 followed by co-immunoprecipitation of cytoplasmic dynein.

The role of LRRK2 GTPase function in HDAC6-mediated aggresome formation should be investigated through the expression of LRRK2 GTPase mutants such as T1343G/R1398Q (increased GTPase activity) and K1347A (GTP-binding deficient) (Ito et al., 2007; West et al., 2007). Further to the LRRK2 G2019S mutant studied in Chapter 4, the effects of pathogenic LRRK2 GTPase mutants (R1141C/G/H, Y1699C) on HDAC6-mediated aggresome formation require investigation to further determine if this is a mechanism universally disrupted in LRRK2-linked disease.

Ultimately, the relevance of LRRK2 function in aggresome formation should be studied in the context of neuronal cells which better recapitulate the physiology of PD-linked DA neurons and Lewy body formation. Additionally, the study of aggresome formation in cells derived from PD patients should provide further evidence of physiological disruption of this mechanism in disease.

Further to its roles in tubulin acetylation and ubiquitinated aggresome formation, the effects of LRRK2 regulation of HDAC6 in other pathways should be explored (summarised in Figure 6.1). For example, LRRK2 effects on HDAC6-mediated deacetylation of cortactin to promote autophagosome-lysosome fusion in autophagy could be investigated using specific inhibitors of the autophagic process such as Bafilomycin A1 to provide a measure of autophagic flux (Figure 6.1C). In addition, LRRK2 may regulate HDAC6-mediated deacetylation of Hsp90 to regulate its protein chaperone activity and role in degradation pathways (Figure 6.1D). Evidence from immunoblots in Chapter 3 suggests that levels of overexpressed LRRK2 may be reduced in the presence of HDAC6 overexpression. LRRK2 is degraded by the proteasome and its stability relies on the chaperone activity of Hsp90 (Wang et al., 2008). Therefore, the interplay between LRRK2 and HDAC6-mediated deacetylation of Hsp90 should be investigated and may provide a mechanism for altered LRRK2 protein levels after HDAC6 overexpression.

Finally, in the study of *in vitro* HDAC6 phosphorylation by LRRK2 (Figure 3.6), there was a marked increase in LRRK2 autophosphorylation in the presence of HDAC6 as detected by incorporation of ^{32}P onto LRRK2. This suggests that binding of HDAC6 to LRRK2 stimulates its autophosphorylation, a process which is a crucial regulator of LRRK2 catalytic activity (Webber et al., 2011). Possible mechanisms for this include a conformational change in the LRRK2 dimer induced by the binding of HDAC6 which induces LRRK2 to maintain its active conformation, or alternatively LRRK2 may be deacetylated by HDAC6 which alters its catalytic activity. Whilst no evidence currently exists of any LRRK2 residues undergoing acetylation, this could be investigated through further mass spectrometry PTM analysis.

7 References

Aasly, J.O., Vilariño-Güell, C., Dachsel, J.C., Webber, P.J., West, A.B., Haugarvoll, K., Johansen, K.K., Toft, M., Nutt, J.G., Payami, H., et al. (2010). Novel pathogenic LRRK2 p.Asn1437His substitution in familial Parkinson's disease. Mov. Disord. *25*, 2156–2163.

Ahmad, F.J., Yu, W., McNally, F.J., and Baas, P.W. (1999). An essential role for katanin in severing microtubules in the neuron. J. Cell Biol. *145*, 305–315.

Ahmad-Annuar, A., Ciani, L., Simeonidis, I., Herreros, J., Fredj, N.B., Rosso, S.B., Hall, A., Brickley, S., and Salinas, P.C. (2006). Signaling across the synapse: a role for Wnt and Dishevelled in presynaptic assembly and neurotransmitter release. J. Cell Biol. *174*, 127–139.

Akella, J.S., Wloga, D., Kim, J., Starostina, N.G., Lyons-Abbott, S., Morrissette, N.S., Dougan, S.T., Kipreos, E.T., and Gaertig, J. (2010). MEC-17 is an alpha-tubulin acetyltransferase. Nature *467*, 218–222.

Alegre-Abarrategui, J., Christian, H., Lufino, M.M.P., Mutihac, R., Venda, L.L., Ansorge, O., and Wade-Martins, R. (2009). LRRK2 regulates autophagic activity and localizes to specific membrane microdomains in a novel human genomic reporter cellular model. Hum. Mol. Genet. *18*, 4022–4034.

Alessi, D.R., and Sammler, E. (2018). LRRK2 kinase in Parkinson's disease. Science *360*, 36–37.

Alim, M.A., Hossain, M.S., Arima, K., Takeda, K., Izumiyama, Y., Nakamura, M., Kaji, H., Shinoda, T., Hisanaga, S., and Uéda, K. (2002). Tubulin Seeds α-Synuclein Fibril Formation. J. Biol. Chem. *277*, 2112–2117.

Andres-Mateos, E., Mejias, R., Sasaki, M., Li, X., Lin, B.M., Biskup, S., Zhang, L., Banerjee, R., Thomas, B., Yang, L., et al. (2009). Unexpected Lack of Hypersensitivity in LRRK2 Knock-Out Mice to MPTP (1-Methyl-4-Phenyl-1,2,3,6-Tetrahydropyridine). J. Neurosci. *29*, 15846–15850.

Anheim, M., Elbaz, A., Lesage, S., Durr, A., Condroyer, C., Viallet, F., Pollak, P., Bonaïti, B., Bonaïti-Pellié, C., Brice, A., et al. (2012). Penetrance of Parkinson disease in glucocerebrosidase gene mutation carriers. Neurology *78*, 417–420.

Appel-Cresswell, S., Vilarino-Guell, C., Encarnacion, M., Sherman, H., Yu, I., Shah, B., Weir, D., Thompson, C., Szu-Tu, C., Trinh, J., et al. (2013). Alpha-synuclein p.H50Q, a novel pathogenic mutation for Parkinson's disease. Mov. Disord. *28*, 811–813.

Arduíno, D.M., Esteves, A.R., Cortes, L., Silva, D.F., Patel, B., Grazina, M., Swerdlow, R.H., Oliveira, C.R., and Cardoso, S.M. (2012). Mitochondrial metabolism in Parkinson's disease impairs quality control autophagy by hampering microtubule-dependent traffic. Hum. Mol. Genet. *21*, 4680–4702.

Arnold, B., Cassady, S.J., VanLaar, V.S., and Berman, S.B. (2011). Integrating multiple aspects of mitochondrial dynamics in neurons: Age-related differences and dynamic changes in a chronic rotenone model. Neurobiol. Dis. *41*, 189–200.

Asthana, J., Kapoor, S., Mohan, R., and Panda, D. (2013). Inhibition of HDAC6 Deacetylase Activity Increases Its Binding with Microtubules and Suppresses Microtubule Dynamic Instability in MCF-7 Cells. J. Biol. Chem. *288*, 22516–22526.

Avila, J., Lucas, J.J., Perez, M., and Hernandez, F. (2004). Role of tau protein in both physiological and pathological conditions. Physiol. Rev. *84*, 361–384.

Axe, E.L., Walker, S.A., Manifava, M., Chandra, P., Roderick, H.L., Habermann, A., Griffiths, G., and Ktistakis, N.T. (2008). Autophagosome formation from membrane compartments enriched in phosphatidylinositol 3-phosphate and dynamically connected to the endoplasmic reticulum. J. Cell Biol. *182*, 685–701.

Baird, D.H., Myers, K.A., Mogensen, M., Moss, D., and Baas, P.W. (2004). Distribution of the microtubule-related protein ninein in developing neurons. Neuropharmacology *47*, 677–683.

Bandopadhyay, R., Kingsbury, A.E., Cookson, M.R., Reid, A.R., Evans, I.M., Hope, A.D., Pittman, A.M., Lashley, T., Canet-Aviles, R., Miller, D.W., et al. (2004). The expression of DJ-1 (PARK7) in normal human CNS and idiopathic Parkinson's disease. Brain J. Neurol. *127*, 420–430.

Bandopadhyay, R., Kingsbury, A.E., Muqit, M.M., Harvey, K., Reid, A.R., Kilford, L., Engelender, S., Schlossmacher, M.G., Wood, N.W., Latchman, D.S., et al. (2005). Synphilin-1 and parkin show overlapping expression patterns in human brain and form aggresomes in response to proteasomal inhibition. Neurobiol. Dis. *20*, 401–411.

Bang, Y., Kim, K.-S., Seol, W., and Choi, H.J. (2016). LRRK2 interferes with aggresome formation for autophagic clearance. Mol. Cell. Neurosci. *75*, 71–80.

Barth, S., Glick, D., and Macleod, K.F. (2010). Autophagy: assays and artifacts. J. Pathol. *221*, 117–124.

Bauer, N.G., and Richter-Landsberg, C. (2006). The Dynamic Instability of Microtubules Is Required for Aggresome Formation in Oligodendroglial Cells After Proteolytic Stress. J. Mol. Neurosci. *29*, 153–168.

Beal, M.F. (2005). Mitochondria take center stage in aging and neurodegeneration. Ann. Neurol. *58*, 495–505.

Beausoleil, S.A., Jedrychowski, M., Schwartz, D., Elias, J.E., Villén, J., Li, J., Cohn, M.A., Cantley, L.C., and Gygi, S.P. (2004). Large-scale characterization of HeLa cell nuclear phosphoproteins. Proc. Natl. Acad. Sci. *101*, 12130–12135.

Beavan, M.S., and Schapira, A.H.V. (2013). Glucocerebrosidase mutations and the pathogenesis of Parkinson disease. Ann. Med. *45*, 511–521.

Beecham, G.W., Dickson, D.W., Scott, W.K., Martin, E.R., Schellenberg, G., Nuytemans, K., Larson, E.B., Buxbaum, J.D., Trojanowski, J.Q., Van Deerlin, V.M., et al. (2015). PARK10 is a major locus for sporadic neuropathologically confirmed Parkinson disease. Neurology *84*, 972–980.

Beilina, A., Rudenko, I.N., Kaganovich, A., Civiero, L., Chau, H., Kalia, S.K., Kalia, L.V., Lobbestael, E., Chia, R., Ndukwe, K., et al. (2014). Unbiased screen for interactors of leucine-rich repeat kinase 2 supports a common pathway for sporadic and familial Parkinson disease. Proc. Natl. Acad. Sci. *111*, 2626–2631.

Bellou, V., Belbasis, L., Tzoulaki, I., Evangelou, E., and Ioannidis, J.P.A. (2016). Environmental risk factors and Parkinson's disease: An umbrella review of meta-analyses. Parkinsonism Relat. Disord. *23*, 1–9.

Benamer, H.T.S., and de Silva, R. (2010). LRRK2 G2019S in the North African population: a review. Eur. Neurol. *63*, 321–325.

Bence, N.F., Sampat, R.M., and Kopito, R.R. (2001). Impairment of the ubiquitin-proteasome system by protein aggregation. Science *292*, 1552–1555.

Bennett, E.J., Bence, N.F., Jayakumar, R., and Kopito, R.R. (2005). Global impairment of the ubiquitin-proteasome system by nuclear or cytoplasmic protein aggregates precedes inclusion body formation. Mol. Cell *17*, 351–365.

Benoy, V., Vanden Berghe, P., Jarpe, M., Van Damme, P., Robberecht, W., and Van Den Bosch, L. (2017). Development of Improved HDAC6 Inhibitors as Pharmacological Therapy for Axonal Charcot–Marie–Tooth Disease. Neurotherapeutics *14*, 417–428.

Berger, Z., Smith, K.A., and Lavoie, M.J. (2010). Membrane localization of LRRK2 is associated with increased formation of the highly active lrrk2 dimer and changes in its phosphorylation. Biochemistry (Mosc.) *49*, 5511–5523.

Bertos, N.R., Gilquin, B., Chan, G.K.T., Yen, T.J., Khochbin, S., and Yang, X.-J. (2004). Role of the Tetradecapeptide Repeat Domain of Human Histone Deacetylase 6 in Cytoplasmic Retention. J. Biol. Chem. *279*, 48246–48254.

Berwick, D.C., and Harvey, K. (2012). LRRK2 functions as a Wnt signaling scaffold, bridging cytosolic proteins and membrane-localized LRP6. Hum. Mol. Genet. *21*, 4966–4979.

Betarbet, R., Sherer, T.B., MacKenzie, G., Garcia-Osuna, M., Panov, A.V., and Greenamyre, J.T. (2000). Chronic systemic pesticide exposure reproduces features of Parkinson's disease. Nat. Neurosci. *3*, 1301–1306.

Biosa, A., Trancikova, A., Civiero, L., Glauser, L., Bubacco, L., Greggio, E., and Moore, D.J. (2013). GTPase activity regulates kinase activity and cellular phenotypes of Parkinson's disease-associated LRRK2. Hum. Mol. Genet. *22*, 1140–1156.

Biskup, S., Moore, D.J., Celsi, F., Higashi, S., West, A.B., Andrabi, S.A., Kurkinen, K., Yu, S.-W., Savitt, J.M., Waldvogel, H.J., et al. (2006). Localization of LRRK2 to membranous and vesicular structures in mammalian brain. Ann. Neurol. *60*, 557–569.

Blanca Ramírez, M., Lara Ordóñez, A.J., Fdez, E., Madero-Pérez, J., Gonnelli, A., Drouyer, M., Chartier-Harlin, M.-C., Taymans, J.-M., Bubacco, L., Greggio, E., et al. (2017). GTP binding regulates cellular localization of Parkinsońs disease-associated LRRK2. Hum. Mol. Genet.

Bobrowska, A., Donmez, G., Weiss, A., Guarente, L., and Bates, G. (2012). SIRT2 Ablation Has No Effect on Tubulin Acetylation in Brain, Cholesterol Biosynthesis or the Progression of Huntington's Disease Phenotypes In Vivo. PLOS ONE *7*, e34805.

Boddu, R., Hull, T.D., Bolisetty, S., Hu, X., Moehle, M.S., Daher, J.P.L., Kamal, A.I., Joseph, R., George, J.F., Agarwal, A., et al. (2015). Leucine-rich repeat kinase 2

deficiency is protective in rhabdomyolysis-induced kidney injury. Hum. Mol. Genet. *24*, 4078–4093.

Bodner, R.A., Housman, D.E., and Kazantsev, A.G. (2006). New directions for neurodegenerative disease therapy: using chemical compounds to boost the formation of mutant protein inclusions. Cell Cycle Georget. Tex *5*, 1477–1480.

Bonifati, V. (2014). Genetics of Parkinson's disease – state of the art, 2013. Parkinsonism Relat. Disord. *20, Supplement 1*, S23–S28.

Bonifati, V., Rizzu, P., Baren, M.J. van, Schaap, O., Breedveld, G.J., Krieger, E., Dekker, M.C.J., Squitieri, F., Ibanez, P., Joosse, M., et al. (2003). Mutations in the DJ-1 Gene Associated with Autosomal Recessive Early-Onset Parkinsonism. Science *299*, 256–259.

Bonifati, V., Rohé, C.F., Breedveld, G.J., Fabrizio, E., De Mari, M., Tassorelli, C., Tavella, A., Marconi, R., Nicholl, D.J., Chien, H.F., et al. (2005). Early-onset parkinsonism associated with PINK1 mutations: frequency, genotypes, and phenotypes. Neurology *65*, 87–95.

Bosgraaf, L., and Van Haastert, P.J.M. (2003). Roc, a Ras/GTPase domain in complex proteins. Biochim. Biophys. Acta BBA - Mol. Cell Res. *1643*, 5–10.

Boyault, C., Gilquin, B., Zhang, Y., Rybin, V., Garman, E., Meyer-Klaucke, W., Matthias, P., Müller, C.W., and Khochbin, S. (2006). HDAC6–p97/VCP controlled polyubiquitin chain turnover. EMBO J. *25*, 3357–3366.

Boyault, C., Zhang, Y., Fritah, S., Caron, C., Gilquin, B., Kwon, S.H., Garrido, C., Yao, T.-P., Vourc'h, C., Matthias, P., et al. (2007). HDAC6 controls major cell response pathways to cytotoxic accumulation of protein aggregates. Genes Dev. *21*, 2172–2181.

Braak, H., Ghebremedhin, E., Rüb, U., Bratzke, H., and Del Tredici, K. (2004). Stages in the development of Parkinson's disease-related pathology. Cell Tissue Res. *318*, 121–134.

Brieger, K., Schiavone, S., Miller, F.J., and Krause, K.-H. (2012). Reactive oxygen species: from health to disease. Swiss Med. Wkly. *142*, w13659.

Brion, J.P., and Couck, A.M. (1995). Cortical and brainstem-type Lewy bodies are immunoreactive for the cyclin-dependent kinase 5. Am. J. Pathol. *147*, 1465–1476.

Brush, M.H., Guardiola, A., Connor, J.H., Yao, T.-P., and Shenolikar, S. (2004). Deactylase inhibitors disrupt cellular complexes containing protein phosphatases and deacetylases. J. Biol. Chem. *279*, 7685–7691.

Burke, R.E., and O'Malley, K. (2013). Axon degeneration in Parkinson's disease. Exp. Neurol. *246*, 72–83.

Burré, J., Sharma, M., Tsetsenis, T., Buchman, V., Etherton, M.R., and Südhof, T.C. (2010). Alpha-synuclein promotes SNARE-complex assembly in vivo and in vitro. Science *329*, 1663–1667.

Burré, J., Sharma, M., and Südhof, T.C. (2015). Definition of a Molecular Pathway Mediating α-Synuclein Neurotoxicity. J. Neurosci. *35*, 5221–5232.

Butler, K.V., Kalin, J., Brochier, C., Vistoli, G., Langley, B., and Kozikowski, A.P. (2010). Rational design and simple chemistry yield a superior, neuroprotective HDAC6 inhibitor, tubastatin A. J. Am. Chem. Soc. *132*, 10842–10846.

Cadenas, E., Boveris, A., Ragan, C.I., and Stoppani, A.O.M. (1977). Production of superoxide radicals and hydrogen peroxide by NADH-ubiquinone reductase and ubiquinol-cytochrome c reductase from beef-heart mitochondria. Arch. Biochem. Biophys. *180*, 248–257.

Caesar, M., Zach, S., Carlson, C.B., Brockmann, K., Gasser, T., and Gillardon, F. (2013). Leucine-rich repeat kinase 2 functionally interacts with microtubules and kinase-dependently modulates cell migration. Neurobiol. Dis. *54*, 280–288.

Campêlo, C.L.., Cagni, F.C., de Siqueira Figueredo, D., Oliveira Jr., L.G., Silva-Neto, A.B., Macêdo, P.T., Santos, J.R., Izídio, G.S., Ribeiro, A.M., de Andrade, T.G., et al. (2017). Variants in SNCA Gene Are Associated with Parkinson's Disease Risk and Cognitive Symptoms in a Brazilian Sample. Front. Aging Neurosci. *9*.

Caudle, W.M., Richardson, J.R., Wang, M.Z., Taylor, T.N., Guillot, T.S., McCormack, A.L., Colebrooke, R.E., Di Monte, D.A., Emson, P.C., and Miller, G.W. (2007). Reduced vesicular storage of dopamine causes progressive nigrostriatal neurodegeneration. J. Neurosci. *27*, 8138–8148.

Chang, D., Nalls, M.A., Hallgrímsdóttir, I.B., Hunkapiller, J., Brug, M. van der, Cai, F., Consortium, I.P.D.G., Team, 23andMe Research, Kerchner, G.A., Ayalon, G., et al. (2017). A meta-analysis of genome-wide association studies identifies 17 new Parkinson's disease risk loci. Nat. Genet. *49*, 1511–1516.

Charlesworth, G., Gandhi, S., Bras, J.M., Barker, R.A., Burn, D.J., Chinnery, P.F., Gentleman, S.M., Guerreiro, R., Hardy, J., Holton, J.L., et al. (2012). Tau acts as an independent genetic risk factor in pathologically proven PD. Neurobiol. Aging *33*, 838.e7–838.e11.

Chartier-Harlin, M.-C., Kachergus, J., Roumier, C., Mouroux, V., Douay, X., Lincoln, S., Levecque, C., Larvor, L., Andrieux, J., Hulihan, M., et al. (2004). α-synuclein locus duplication as a cause of familial Parkinson's disease. The Lancet *364*, 1167–1169.

Chartier-Harlin, M.-C., Dachsel, J.C., Vilariño-Güell, C., Lincoln, S.J., Leprêtre, F., Hulihan, M.M., Kachergus, J., Milnerwood, A.J., Tapia, L., Song, M.-S., et al. (2011). Translation initiator EIF4G1 mutations in familial Parkinson disease. Am. J. Hum. Genet. *89*, 398–406.

Chaudhuri, K.R., Healy, D.G., and Schapira, A.H. (2006). Non-motor symptoms of Parkinson's disease: diagnosis and management. Lancet Neurol. *5*, 235–245.

Che, D.L., Chowdary, P.D., and Cui, B. (2016). A close look at axonal transport: cargos slow down when crossing stationary organelles. Neurosci. Lett. *610*, 110–116.

Chen, L., and Feany, M.B. (2005). Alpha-synuclein phosphorylation controls neurotoxicity and inclusion formation in a Drosophila model of Parkinson disease. Nat. Neurosci. *8*, 657–663.

Chen, L., Zhang, S., Liu, Y., Hong, H., Wang, H., Zheng, Y., Zhou, H., Chen, J., Xian, W., He, Y., et al. (2011). LRRK2 R1398H polymorphism is associated with decreased

risk of Parkinson's disease in a Han Chinese population. Parkinsonism Relat. Disord. *17*, 291–292.

Chen, S., Owens, G.C., Makarenkova, H., and Edelman, D.B. (2010). HDAC6 Regulates Mitochondrial Transport in Hippocampal Neurons. PLoS ONE *5*.

Cheng, X.-T., Zhou, B., Lin, M.-Y., Cai, Q., and Sheng, Z.-H. (2015). Axonal autophagosomes use the ride-on service for retrograde transport toward the soma. Autophagy *11*, 1434–1436.

Chia, R., Haddock, S., Beilina, A., Rudenko, I.N., Mamais, A., Kaganovich, A., Li, Y., Kumaran, R., Nalls, M.A., and Cookson, M.R. (2014). Phosphorylation of LRRK2 by casein kinase 1α regulates trans-Golgi clustering via differential interaction with ARHGEF7. Nat. Commun. *5*.

Chinta, S.J., Mallajosyula, J.K., Rane, A., and Andersen, J.K. (2010). Mitochondrial α-synuclein accumulation impairs complex I function in dopaminergic neurons and results in increased mitophagy in vivo. Neurosci. Lett. *486*, 235–239.

Choi, H.G., Zhang, J., Deng, X., Hatcher, J.M., Patricelli, M.P., Zhao, Z., Alessi, D.R., and Gray, N.S. (2012). Brain Penetrant LRRK2 Inhibitor. ACS Med. Chem. Lett. *3*, 658–662.

Chu, Y., Morfini, G.A., Langhamer, L.B., He, Y., Brady, S.T., and Kordower, J.H. (2012). Alterations in axonal transport motor proteins in sporadic and experimental Parkinson's disease. Brain *135*, 2058–2073.

Chung, K.K., Zhang, Y., Lim, K.L., Tanaka, Y., Huang, H., Gao, J., Ross, C.A., Dawson, V.L., and Dawson, T.M. (2001). Parkin ubiquitinates the alpha-synuclein-interacting protein, synphilin-1: implications for Lewy-body formation in Parkinson disease. Nat. Med. *7*, 1144–1150.

Ciani, L., and Salinas, P.C. (2007). c-Jun N-terminal kinase (JNK) cooperates with Gsk3β to regulate Dishevelled-mediated microtubule stability. BMC Cell Biol. *8*, 27.

Clark, I.E., Dodson, M.W., Jiang, C., Cao, J.H., Huh, J.R., Seol, J.H., Yoo, S.J., Hay, B.A., and Guo, M. (2006). Drosophila pink1 is required for mitochondrial function and interacts genetically with parkin. Nature *441*, 1162–1166.

Clark, L.N., Wang, Y., Karlins, E., Saito, L., Mejia-Santana, H., Harris, J., Louis, E.D., Cote, L.J., Andrews, H., Fahn, S., et al. (2006). Frequency of LRRK2 mutations in early- and late-onset Parkinson disease. Neurology *67*, 1786–1791.

Cook, C., and Petrucelli, L. (2009). A Critical Evaluation of the Ubiquitin-Proteasome System in Parkinson's Disease. Biochim. Biophys. Acta *1792*, 664–675.

Cook, C., Gendron, T.F., Scheffel, K., Carlomagno, Y., Dunmore, J., DeTure, M., and Petrucelli, L. (2012). Loss of HDAC6, a novel CHIP substrate, alleviates abnormal tau accumulation. Hum. Mol. Genet. *21*, 2936–2945.

Cookson, M.R. (2016). Cellular functions of LRRK2 implicate vesicular trafficking pathways in Parkinson's disease. Biochem. Soc. Trans. *44*, 1603–1610.

Coombes, C., Yamamoto, A., McClellan, M., Reid, T.A., Plooster, M., Luxton, G.W.G., Alper, J., Howard, J., and Gardner, M.K. (2016). Mechanism of microtubule lumen

entry for the α-tubulin acetyltransferase enzyme αTAT1. Proc. Natl. Acad. Sci. *113*, E7176–E7184.

Cornejo-Olivas, M., Torres, L., Velit-Salazar, M.R., Inca-Martinez, M., Mazzetti, P., Cosentino, C., Micheli, F., Perandones, C., Dieguez, E., Raggio, V., et al. (2017). Variable frequency of LRRK2 variants in the Latin American research consortium on the genetics of Parkinson's disease (LARGE-PD), a case of ancestry. Npj Park. Dis. *3*, 19.

Crews, L., Spencer, B., Desplats, P., Patrick, C., Paulino, A., Rockenstein, E., Hansen, L., Adame, A., Galasko, D., and Masliah, E. (2010). Selective molecular alterations in the autophagy pathway in patients with Lewy body disease and in models of alpha-synucleinopathy. PloS One *5*, e9313.

D'Andrea, M.R., Ilyin, S., and Plata-Salaman, C.R. (2001). Abnormal patterns of microtubule-associated protein-2 (MAP-2) immunolabeling in neuronal nuclei and Lewy bodies in Parkinson's disease substantia nigra brain tissues. Neurosci. Lett. *306*, 137–140.

Daher, J.P.L., Pletnikova, O., Biskup, S., Musso, A., Gellhaar, S., Galter, D., Troncoso, J.C., Lee, M.K., Dawson, T.M., Dawson, V.L., et al. (2012). Neurodegenerative phenotypes in an A53T α-synuclein transgenic mouse model are independent of LRRK2. Hum. Mol. Genet. *21*, 2420–2431.

Daher, J.P.L., Volpicelli-Daley, L.A., Blackburn, J.P., Moehle, M.S., and West, A.B. (2014). Abrogation of α-synuclein–mediated dopaminergic neurodegeneration in LRRK2-deficient rats. Proc. Natl. Acad. Sci. *111*, 9289–9294.

Daher, J.P.L., Abdelmotilib, H.A., Hu, X., Volpicelli-Daley, L.A., Moehle, M.S., Fraser, K.B., Needle, E., Chen, Y., Steyn, S.J., Galatsis, P., et al. (2015). Leucine-rich Repeat Kinase 2 (LRRK2) Pharmacological Inhibition Abates α-Synuclein Gene-induced Neurodegeneration. J. Biol. Chem. *290*, 19433–19444.

Damier, P., Hirsch, E.C., Agid, Y., and Graybiel, A.M. (1999). The substantia nigra of the human brain II: Patterns of loss of dopamine-containing neurons in Parkinson's disease. Brain *122*, 1437–1448.

Daniëls, V., Vancraenenbroeck, R., Law, B.M.H., Greggio, E., Lobbestael, E., Gao, F., De Maeyer, M., Cookson, M.R., Harvey, K., Baekelandt, V., et al. (2011a). Insight into the mode of action of the LRRK2 Y1699C pathogenic mutant. J. Neurochem. *116*, 304–315.

Davis, A.A., Andruska, K.M., Benitez, B.A., Racette, B.A., Perlmutter, J.S., and Cruchaga, C. (2016). Variants in GBA, SNCA, and MAPT Influence Parkinson Disease Risk, Age at Onset, and Progression. Neurobiol. Aging *37*, 209.e1–209.e7.

De Vos, J, K., Chapman, A.L., Tennant, M.E., Manser, C., Tudor, E.L., Lau, K.-F., Brownlees, J., Ackerley, S., Shaw, P.J., et al. (2007). Familial amyotrophic lateral sclerosis-linked SOD1 mutants perturb fast axonal transport to reduce axonal mitochondria content. Hum. Mol. Genet. *16*, 2720–2728.

Deakin, N.O., and Turner, C.E. (2014). Paxillin inhibits HDAC6 to regulate microtubule acetylation, Golgi structure, and polarized migration. J Cell Biol *206*, 395–413.

Deng, H.-X., Shi, Y., Yang, Y., Ahmeti, K.B., Miller, N., Huang, C., Cheng, L., Zhai, H., Deng, S., Nuytemans, K., et al. (2016). Identification of TMEM230 mutations in familial Parkinson's disease. Nat. Genet. *48*, 733–739.

Deng, J., Lewis, P.A., Greggio, E., Sluch, E., Beilina, A., and Cookson, M.R. (2008). Structure of the ROC domain from the Parkinson's disease-associated leucine-rich repeat kinase 2 reveals a dimeric GTPase. Proc. Natl. Acad. Sci. *105*, 1499–1504.

Deng, X., Dzamko, N., Prescott, A., Davies, P., Liu, Q., Yang, Q., Lee, J.-D., Patricelli, M.P., Nomanbhoy, T.K., Alessi, D.R., et al. (2011). Characterization of a selective inhibitor of the Parkinson's disease kinase LRRK2. Nat. Chem. Biol. *7*, 203–205.

Denning, G.M., Ostedgaard, L.S., Cheng, S.H., Smith, A.E., and Welsh, M.J. (1992). Localization of cystic fibrosis transmembrane conductance regulator in chloride secretory epithelia. J. Clin. Invest. *89*, 339–349.

Deribe, Y.L., Wild, P., Chandrashaker, A., Curak, J., Schmidt, M.H.H., Kalaidzidis, Y., Milutinovic, N., Kratchmarova, I., Buerkle, L., Fetchko, M.J., et al. (2009). Regulation of Epidermal Growth Factor Receptor Trafficking by Lysine Deacetylase HDAC6. Sci Signal *2*, ra84–ra84.

Desai, A., and Mitchison, and T.J. (1997). Microtubule Polymerization Dynamics. Annu. Rev. Cell Dev. Biol. *13*, 83–117.

Dice, J.F. (1990). Peptide sequences that target cytosolic proteins for lysosomal proteolysis. Trends Biochem. Sci. *15*, 305–309.

Ding, X., and Goldberg, M.S. (2009). Regulation of LRRK2 Stability by the E3 Ubiquitin Ligase CHIP. PLOS ONE *4*, e5949.

Ding, X., Barodia, S.K., Ma, L., and Goldberg, M.S. (2017). Fbxl18 targets LRRK2 for proteasomal degradation and attenuates cell toxicity. Neurobiol. Dis. *98*, 122–136.

Dodson, M.W., Zhang, T., Jiang, C., Chen, S., and Guo, M. (2012). Roles of the Drosophila LRRK2 homolog in Rab7-dependent lysosomal positioning. Hum. Mol. Genet. *21*, 1350–1363.

Dráberová, E., Viklický, V., and Dráber, P. (2000). Short Communication Exposure of lumenal microtubule sites after mild fixation. Eur. J. Cell Biol. *79*, 982–985.

Du, G., Liu, X., Chen, X., Song, M., Yan, Y., Jiao, R., and Wang, C.-C. (2010). Drosophila histone deacetylase 6 protects dopaminergic neurons against {alpha}-synuclein toxicity by promoting inclusion formation. Mol. Biol. Cell *21*, 2128–2137.

Du, Y., Wang, F., Zou, J., Le, W., Dong, Q., Wang, Z., Shen, F., Yu, L., and Li, Y. (2014). Histone deacetylase 6 regulates cytotoxic α-synuclein accumulation through induction of the heat shock response. Neurobiol. Aging *35*, 2316–2328.

Du, Z.-X., Zhang, H.-Y., Meng, X., Gao, Y.-Y., Zou, R.-L., Liu, B.-Q., Guan, Y., and Wang, H.-Q. (2009). Proteasome inhibitor MG132 induces BAG3 expression through activation of heat shock factor 1. J. Cell. Physiol. *218*, 631–637.

Durrenberger, P.F., Filiou, M.D., Moran, L.B., Michael, G.J., Novoselov, S., Cheetham, M.E., Clark, P., Pearce, R.K.B., and Graeber, M.B. (2009). DnaJB6 is

present in the core of Lewy bodies and is highly up-regulated in parkinsonian astrocytes. J. Neurosci. Res. *87*, 238–245.

Edelstein, A.D., Tsuchida, M.A., Amodaj, N., Pinkard, H., Vale, R.D., and Stuurman, N. (2014). Advanced methods of microscope control using μManager software. J. Biol. Methods *1*, e10.

Edvardson, S., Cinnamon, Y., Ta-Shma, A., Shaag, A., Yim, Y.-I., Zenvirt, S., Jalas, C., Lesage, S., Brice, A., Taraboulos, A., et al. (2012). A Deleterious Mutation in DNAJC6 Encoding the Neuronal-Specific Clathrin-Uncoating Co-Chaperone Auxilin, Is Associated with Juvenile Parkinsonism. PLoS ONE *7*, e36458.

Egelhoff, T.T., Lee, R.J., and Spudich, J.A. (1993). Dictyostelium myosin heavy chain phosphorylation sites regulate myosin filament assembly and localization in vivo. Cell *75*, 363–371.

Engelender, S., Kaminsky, Z., Guo, X., Sharp, A.H., Amaravi, R.K., Kleiderlein, J.J., Margolis, R.L., Troncoso, J.C., Lanahan, A.A., Worley, P.F., et al. (1999). Synphilin-1 associates with alpha-synuclein and promotes the formation of cytosolic inclusions. Nat. Genet. *22*, 110–114.

English, L., Chemali, M., Duron, J., Rondeau, C., Laplante, A., Gingras, D., Alexander, D., Leib, D., Norbury, C., Lippé, R., et al. (2009). Autophagy enhances the presentation of endogenous viral antigens on MHC class I molecules during HSV-1 infection. Nat. Immunol. *10*, 480–487.

Esteves, A.R., G-Fernandes, M., Santos, D., Januário, C., and Cardoso, S.M. (2015). The Upshot of LRRK2 Inhibition to Parkinson's Disease Paradigm. Mol. Neurobiol. *52*, 1804–1820.

Fabunmi, R.P., Wigley, W.C., Thomas, P.J., and DeMartino, G.N. (2000). Activity and regulation of the centrosome-associated proteasome. J. Biol. Chem. *275*, 409–413.

Falsone, S.F., Kungl, A.J., Rek, A., Cappai, R., and Zangger, K. (2009). The Molecular Chaperone Hsp90 Modulates Intermediate Steps of Amyloid Assembly of the Parkinson-related Protein α-Synuclein. J. Biol. Chem. *284*, 31190–31199.

Fauvet, B., Mbefo, M.K., Fares, M.-B., Desobry, C., Michael, S., Ardah, M.T., Tsika, E., Coune, P., Prudent, M., Lion, N., et al. (2012). α-Synuclein in central nervous system and from erythrocytes, mammalian cells, and Escherichia coli exists predominantly as disordered monomer. J. Biol. Chem. *287*, 15345–15364.

Fell, M.J., Mirescu, C., Basu, K., Cheewatrakoolpong, B., DeMong, D.E., Ellis, J.M., Hyde, L.A., Lin, Y., Markgraf, C.G., Mei, H., et al. (2015). MLi-2, a Potent, Selective, and Centrally Active Compound for Exploring the Therapeutic Potential and Safety of LRRK2 Kinase Inhibition. J. Pharmacol. Exp. Ther. *355*, 397–409.

Fergusson, J., Landon, M., Lowe, J., Dawson, S.P., Layfield, R., Hanger, D.P., and Mayer, R.J. (1996). Pathological lesions of Alzheimer's disease and dementia with Lewy bodies brains exhibit immunoreactivity to an ATPase that is a regulatory subunit of the 26S proteasome. Neurosci. Lett. *219*, 167–170.

Fiesel, F.C., Voigt, A., Weber, S.S., Van den Haute, C., Waldenmaier, A., Görner, K., Walter, M., Anderson, M.L., Kern, J.V., Rasse, T.M., et al. (2010). Knockdown of

transactive response DNA-binding protein (TDP-43) downregulates histone deacetylase 6. EMBO J. *29*, 209–221.

Di Fonzo, A., Dekker, M.C.J., Montagna, P., Baruzzi, A., Yonova, E.H., Correia Guedes, L., Szczerbinska, A., Zhao, T., Dubbel-Hulsman, L.O.M., Wouters, C.H., et al. (2009). FBXO7 mutations cause autosomal recessive, early-onset parkinsonian-pyramidal syndrome. Neurology *72*, 240–245.

Forno, L.S. (1996). Neuropathology of Parkinson's disease. J. Neuropathol. Exp. Neurol. *55*, 259–272.

Forno, L.S., Sternberger, L.A., Sternberger, N.H., Strefling, A.M., Swanson, K., and Eng, L.F. (1986). Reaction of Lewy bodies with antibodies to phosphorylated and non-phosphorylated neurofilaments. Neurosci. Lett. *64*, 253–258.

Fortun, J., Dunn, W.A., Joy, S., Li, J., and Notterpek, L. (2003). Emerging role for autophagy in the removal of aggresomes in Schwann cells. J. Neurosci. *23*, 10672–10680.

Freundt, E.C., Maynard, N., Clancy, E.K., Roy, S., Bousset, L., Sourigues, Y., Covert, M., Melki, R., Kirkegaard, K., and Brahic, M. (2012). Neuron-to-neuron transmission of α-synuclein fibrils through axonal transport. Ann. Neurol. *72*, 517–524.

Fujiwara, H., Hasegawa, M., Dohmae, N., Kawashima, A., Masliah, E., Goldberg, M.S., Shen, J., Takio, K., and Iwatsubo, T. (2002). alpha-Synuclein is phosphorylated in synucleinopathy lesions. Nat. Cell Biol. *4*, 160–164.

Fukuda, T., Tanaka, J., Watabe, K., Numoto, R.T., and Minamitani, M. (1993). Immunohistochemistry of neuronal inclusions in the cerebral cortex and brain-stem in Lewy body disease. Acta Pathol. Jpn. *43*, 545–551.

Fuller, W., and Cuthbert, A.W. (2000). Post-translational Disruption of the ΔF508 Cystic Fibrosis Transmembrane Conductance Regulator (CFTR)-Molecular Chaperone Complex with Geldanamycin Stabilizes ΔF508 CFTR in the Rabbit Reticulocyte Lysate. J. Biol. Chem. *275*, 37462–37468.

Funayama, M., Ohe, K., Amo, T., Furuya, N., Yamaguchi, J., Saiki, S., Li, Y., Ogaki, K., Ando, M., Yoshino, H., et al. (2015). CHCHD2 mutations in autosomal dominant late-onset Parkinson's disease: a genome-wide linkage and sequencing study. Lancet Neurol. *14*, 274–282.

Gamerdinger, M., Hajieva, P., Kaya, A.M., Wolfrum, U., Hartl, F.U., and Behl, C. (2009). Protein quality control during aging involves recruitment of the macroautophagy pathway by BAG3. EMBO J. *28*, 889–901.

Gamerdinger, M., Kaya, A.M., Wolfrum, U., Clement, A.M., and Behl, C. (2011). BAG3 mediates chaperone-based aggresome-targeting and selective autophagy of misfolded proteins. EMBO Rep. *12*, 149–156.

Gandhi, S., Muqit, M.M.K., Stanyer, L., Healy, D.G., Abou-Sleiman, P.M., Hargreaves, I., Heales, S., Ganguly, M., Parsons, L., Lees, A.J., et al. (2006). PINK1 protein in normal human brain and Parkinson's disease. Brain J. Neurol. *129*, 1720–1731.

Gao, J., Li, M., Qin, S., Zhang, T., Jiang, S., Hu, Y., Deng, Y., Zhang, C., You, D., Li, H., et al. (2016). Cytosolic PINK1 promotes the targeting of ubiquitinated proteins to the aggresome-autophagy pathway during proteasomal stress. Autophagy *12*, 632–647.

Gao, L., Cueto, M.A., Asselbergs, F., and Atadja, P. (2002). Cloning and functional characterization of HDAC11, a novel member of the human histone deacetylase family. J. Biol. Chem. *277*, 25748–25755.

García-Mata, R., Bebök, Z., Sorscher, E.J., and Sztul, E.S. (1999). Characterization and Dynamics of Aggresome Formation by a Cytosolic Gfp-Chimera✪. J. Cell Biol. *146*, 1239–1254.

Gasper, R., Meyer, S., Gotthardt, K., Sirajuddin, M., and Wittinghofer, A. (2009). It takes two to tango: regulation of G proteins by dimerization. Nat. Rev. Mol. Cell Biol. *10*, 423–429.

Gasser, T., Müller-Myhsok, B., Wszolek, Z.K., Oehlmann, R., Calne, D.B., Bonifati, V., Bereznai, B., Fabrizio, E., Vieregge, P., and Horstmann, R.D. (1998). A susceptibility locus for Parkinson's disease maps to chromosome 2p13. Nat. Genet. *18*, 262–265.

Gautier, C.A., Kitada, T., and Shen, J. (2008). Loss of PINK1 causes mitochondrial functional defects and increased sensitivity to oxidative stress. Proc. Natl. Acad. Sci. *105*, 11364–11369.

Giasson, B.I., Covy, J.P., Bonini, N.M., Hurtig, H.I., Farrer, M.J., Trojanowski, J.Q., and Van Deerlin, V.M. (2006). Biochemical and pathological characterization of Lrrk2. Ann. Neurol. *59*, 315–322.

Giesert, F., Hofmann, A., Bürger, A., Zerle, J., Kloos, K., Hafen, U., Ernst, L., Zhang, J., Vogt-Weisenhorn, D.M., and Wurst, W. (2013). Expression analysis of Lrrk1, Lrrk2 and Lrrk2 splice variants in mice. PloS One *8*, e63778.

Gillardon, F. (2009). Leucine-rich repeat kinase 2 phosphorylates brain tubulin-beta isoforms and modulates microtubule stability – a point of convergence in Parkinsonian neurodegeneration? J. Neurochem. *110*, 1514–1522.

Gilsbach, B.K., and Kortholt, A. (2014). Structural biology of the LRRK2 GTPase and kinase domains: implications for regulation. Front. Mol. Neurosci. *7*, 32.

Gilsbach, B.K., Ho, F.Y., Vetter, I.R., van Haastert, P.J.M., Wittinghofer, A., and Kortholt, A. (2012). Roco kinase structures give insights into the mechanism of Parkinson disease-related leucine-rich-repeat kinase 2 mutations. Proc. Natl. Acad. Sci. *109*, 10322–10327.

Girotto, S., Sturlese, M., Bellanda, M., Tessari, I., Cappellini, R., Bisaglia, M., Bubacco, L., and Mammi, S. (2012). Dopamine-derived quinones affect the structure of the redox sensor DJ-1 through modifications at Cys-106 and Cys-53. J. Biol. Chem. *287*, 18738–18749.

Glick, D., Barth, S., and Macleod, K.F. (2010). Autophagy: cellular and molecular mechanisms. J. Pathol. *221*, 3–12.

Glickman, M.H., and Ciechanover, A. (2002). The ubiquitin-proteasome proteolytic pathway: destruction for the sake of construction. Physiol. Rev. *82*, 373–428.

Gloeckner, C.J., Boldt, K., von Zweydorf, F., Helm, S., Wiesent, L., Sarioglu, H., and Ueffing, M. (2010). Phosphopeptide Analysis Reveals Two Discrete Clusters of Phosphorylation in the N-Terminus and the Roc Domain of the Parkinson-Disease Associated Protein Kinase LRRK2. J. Proteome Res. *9*, 1738–1745.

Godena, V.K., Brookes-Hocking, N., Moller, A., Shaw, G., Oswald, M., Sancho, R.M., Miller, C.C.J., Whitworth, A.J., and De Vos, K.J. (2014). Increasing microtubule acetylation rescues axonal transport and locomotor deficits caused by LRRK2 Roc-COR domain mutations. Nat. Commun. *5*, 5245.

Goker-Alpan, O., Stubblefield, B.K., Giasson, B.I., and Sidransky, E. (2010). Glucocerebrosidase is present in α-synuclein inclusions in Lewy body disorders. Acta Neuropathol. (Berl.) *120*, 641–649.

Golbe, L.I., Lazzarini, A.M., Spychala, J.R., Johnson, W.G., Stenroos, E.S., Mark, M. H., and Sage, J.I. (2001). The tau A0 allele in Parkinson's disease. Mov. Disord. *16*, 442–447.

Gopalai, A.A., Lim, S.-Y., Chua, J.Y., Tey, S., Lim, T.T., Mohamed Ibrahim, N., Tan, A.H., Eow, G.B., Abdul Aziz, Z., Puvanarajah, S.D., et al. (2014). LRRK2 G2385R and R1628P Mutations Are Associated with an Increased Risk of Parkinson’s Disease in the Malaysian Population. BioMed Res. Int. *2014*, e867321.

Gotthardt, K., Weyand, M., Kortholt, A., Van Haastert, P.J.M., and Wittinghofer, A. (2008). Structure of the Roc-COR domain tandem of C. tepidum, a prokaryotic homologue of the human LRRK2 Parkinson kinase. EMBO J. *27*, 2239–2249.

Greco, T.M., Yu, F., Guise, A.J., and Cristea, I.M. (2011). Nuclear Import of Histone Deacetylase 5 by Requisite Nuclear Localization Signal Phosphorylation. Mol. Cell. Proteomics *10*, M110.004317.

Greggio, E., Jain, S., Kingsbury, A., Bandopadhyay, R., Lewis, P., Kaganovich, A., van der Brug, M.P., Beilina, A., Blackinton, J., Thomas, K.J., et al. (2006). Kinase activity is required for the toxic effects of mutant LRRK2/dardarin. Neurobiol. Dis. *23*, 329–341.

Greggio, E., Zambrano, I., Kaganovich, A., Beilina, A., Taymans, J.-M., Daniëls, V., Lewis, P., Jain, S., Ding, J., Syed, A., et al. (2008). The Parkinson Disease-associated Leucine-rich Repeat Kinase 2 (LRRK2) Is a Dimer That Undergoes Intramolecular Autophosphorylation. J. Biol. Chem. *283*, 16906–16914.

Greggio, E., Taymans, J.-M., Zhen, E.Y., Ryder, J., Vancraenenbroeck, R., Beilina, A., Sun, P., Deng, J., Jaffe, H., Baekelandt, V., et al. (2009). The Parkinson's disease kinase LRRK2 autophosphorylates its GTPase domain at multiple sites. Biochem. Biophys. Res. Commun. *389*, 449–454.

Guerreiro, P.S., Huang, Y., Gysbers, A., Cheng, D., Gai, W.P., Outeiro, T.F., and Halliday, G.M. (2013). LRRK2 interactions with α-synuclein in Parkinson's disease brains and in cell models. J. Mol. Med. Berl. Ger. *91*, 513–522.

Habas, R., Kato, Y., and He, X. (2001). Wnt/Frizzled Activation of Rho Regulates Vertebrate Gastrulation and Requires a Novel Formin Homology Protein Daam1. Cell *107*, 843–854.

Häbig, K., Walter, M., Poths, S., Riess, O., and Bonin, M. (2007). RNA interference of LRRK2–microarray expression analysis of a Parkinson's disease key player. Neurogenetics *9*, 83–94.

Haebig, K., Gloeckner, C.J., Miralles, M.G., Gillardon, F., Schulte, C., Riess, O., Ueffing, M., Biskup, S., and Bonin, M. (2010). ARHGEF7 (BETA-PIX) Acts as Guanine Nucleotide Exchange Factor for Leucine-Rich Repeat Kinase 2. PLoS ONE *5*, e13762.

Haggarty, S.J., Koeller, K.M., Wong, J.C., Grozinger, C.M., and Schreiber, S.L. (2003). Domain-selective small-molecule inhibitor of histone deacetylase 6 (HDAC6)-mediated tubulin deacetylation. Proc. Natl. Acad. Sci. *100*, 4389–4394.

Hailey, D.W., Rambold, A.S., Satpute-Krishnan, P., Mitra, K., Sougrat, R., Kim, P.K., and Lippincott-Schwartz, J. (2010). Mitochondria supply membranes for autophagosome biogenesis during starvation. Cell *141*, 656–667.

Hamasaki, M., Furuta, N., Matsuda, A., Nezu, A., Yamamoto, A., Fujita, N., Oomori, H., Noda, T., Haraguchi, T., Hiraoka, Y., et al. (2013). Autophagosomes form at ER-mitochondria contact sites. Nature *495*, 389–393.

Hamza, T.H., Chen, H., Hill-Burns, E.M., Rhodes, S.L., Montimurro, J., Kay, D.M., Tenesa, A., Kusel, V.I., Sheehan, P., Eaaswarkhanth, M., et al. (2011). Genome-Wide Gene-Environment Study Identifies Glutamate Receptor Gene GRIN2A as a Parkinson's Disease Modifier Gene via Interaction with Coffee. PLOS Genet. *7*, e1002237.

Hao, L.-Y., Giasson, B.I., and Bonini, N.M. (2010). DJ-1 is critical for mitochondrial function and rescues PINK1 loss of function. Proc. Natl. Acad. Sci. *107*, 9747–9752.

Hashimoto, M., Takeda, A., Hsu, L.J., Takenouchi, T., and Masliah, E. (1999). Role of cytochrome c as a stimulator of alpha-synuclein aggregation in Lewy body disease. J. Biol. Chem. *274*, 28849–28852.

Hatano, T., Kubo, S.-I., Imai, S., Maeda, M., Ishikawa, K., Mizuno, Y., and Hattori, N. (2007). Leucine-rich repeat kinase 2 associates with lipid rafts. Hum. Mol. Genet. *16*, 678–690.

Hattingen, E., Magerkurth, J., Pilatus, U., Mozer, A., Seifried, C., Steinmetz, H., Zanella, F., and Hilker, R. (2009). Phosphorus and proton magnetic resonance spectroscopy demonstrates mitochondrial dysfunction in early and advanced Parkinson's disease. Brain J. Neurol. *132*, 3285–3297.

Hayashi-Nishino, M., Fujita, N., Noda, T., Yamaguchi, A., Yoshimori, T., and Yamamoto, A. (2009). A subdomain of the endoplasmic reticulum forms a cradle for autophagosome formation. Nat. Cell Biol. *11*, 1433–1437.

Healy, D.G., Falchi, M., O'Sullivan, S.S., Bonifati, V., Durr, A., Bressman, S., Brice, A., Aasly, J., Zabetian, C.P., Goldwurm, S., et al. (2008). Phenotype, genotype, and worldwide genetic penetrance of LRRK2-associated Parkinson's disease: a case-control study. Lancet Neurol. *7*, 583–590.

Heckman, M.G., Elbaz, A., Soto-Ortolaza, A.I., Serie, D.J., Aasly, J.O., Annesi, G., Auburger, G., Bacon, J.A., Boczarska-Jedynak, M., Bozi, M., et al. (2014). The protective effect of LRRK2 p.R1398H on risk of Parkinson's disease is independent of MAPT and SNCA variants. Neurobiol. Aging *35*.

Herzig, M.C., Kolly, C., Persohn, E., Theil, D., Schweizer, T., Hafner, T., Stemmelen, C., Troxler, T.J., Schmid, P., Danner, S., et al. (2011). LRRK2 protein levels are determined by kinase function and are crucial for kidney and lung homeostasis in mice. Hum. Mol. Genet. *20*, 4209–4223.

Hicks, A.A., Pétursson, H., Jónsson, T., Stefánsson, H., Jóhannsdóttir, H.S., Sainz, J., Frigge, M.L., Kong, A., Gulcher, J.R., Stefánsson, K., et al. (2002). A susceptibility gene for late-onset idiopathic Parkinson's disease. Ann. Neurol. *52*, 549–555.

Hideshima, T., Bradner, J.E., Wong, J., Chauhan, D., Richardson, P., Schreiber, S.L., and Anderson, K.C. (2005). Small-molecule inhibition of proteasome and aggresome function induces synergistic antitumor activity in multiple myeloma. Proc. Natl. Acad. Sci. *102*, 8567–8572.

Higashi, S., Moore, D.J., Colebrooke, R.E., Biskup, S., Dawson, V.L., Arai, H., Dawson, T.M., and Emson, P.C. (2007a). Expression and localization of Parkinson's disease-associated leucine-rich repeat kinase 2 in the mouse brain. J. Neurochem. *100*, 368–381.

Higashi, S., Biskup, S., West, A.B., Trinkaus, D., Dawson, V.L., Faull, R.L.M., Waldvogel, H.J., Arai, H., Dawson, T.M., Moore, D.J., et al. (2007b). Localization of Parkinson's disease-associated LRRK2 in normal and pathological human brain. Brain Res. *1155*, 208–219.

Higashi, S., Moore, D.J., Yamamoto, R., Minegishi, M., Sato, K., Togo, T., Katsuse, O., Uchikado, H., Furukawa, Y., Hino, H., et al. (2009). Abnormal localization of leucine-rich repeat kinase 2 to the endosomal-lysosomal compartment in lewy body disease. J. Neuropathol. Exp. Neurol. *68*, 994–1005.

Higashi, S., Moore, D.J., Minegishi, M., Kasanuki, K., Fujishiro, H., Kabuta, T., Togo, T., Katsuse, O., Uchikado, H., Furukawa, Y., et al. (2011). Localization of MAP1-LC3 in vulnerable neurons and Lewy bodies in brains of patients with dementia with Lewy bodies. J. Neuropathol. Exp. Neurol. *70*, 264–280.

Hill-Burns, E.M., Singh, N., Ganguly, P., Hamza, T.H., Montimurro, J., Kay, D.M., Yearout, D., Sheehan, P., Frodey, K., Mclear, J.A., et al. (2013). A genetic basis for the variable effect of smoking/nicotine on Parkinson's disease. Pharmacogenomics J. *13*, 530–537.

Hirokawa, N., and Takemura, R. (2005). Molecular motors and mechanisms of directional transport in neurons. Nat. Rev. Neurosci. *6*, 201–214.

Ho, D.H., Jang, J., Joe, E.-H., Son, I., Seo, H., and Seol, W. (2016). G2385R and I2020T Mutations Increase LRRK2 GTPase Activity. BioMed Res. Int. *2016*, 7917128.

Hook, S.S., Orian, A., Cowley, S.M., and Eisenman, R.N. (2002). Histone deacetylase 6 binds polyubiquitin through its zinc finger (PAZ domain) and copurifies with deubiquitinating enzymes. Proc. Natl. Acad. Sci. *99*, 13425–13430.

Howes, S.C., Alushin, G.M., Shida, T., Nachury, M.V., and Nogales, E. (2014). Effects of tubulin acetylation and tubulin acetyltransferase binding on microtubule structure. Mol. Biol. Cell *25*, 257–266.

Hubbert, C., Guardiola, A., Shao, R., Kawaguchi, Y., Ito, A., Nixon, A., Yoshida, M., Wang, X.-F., and Yao, T.-P. (2002). HDAC6 is a microtubule-associated deacetylase. Nature *417*, 455–458.

Ii, K., Ito, H., Tanaka, K., and Hirano, A. (1997). Immunocytochemical co-localization of the proteasome in ubiquitinated structures in neurodegenerative diseases and the elderly. J. Neuropathol. Exp. Neurol. *56*, 125–131.

Ikenaka, K., Kawai, K., Katsuno, M., Huang, Z., Jiang, Y.-M., Iguchi, Y., Kobayashi, K., Kimata, T., Waza, M., Tanaka, F., et al. (2013). dnc-1/dynactin 1 knockdown disrupts transport of autophagosomes and induces motor neuron degeneration. PloS One *8*, e54511.

Íñigo-Marco, I., Valencia, M., Larrea, L., Bugallo, R., Martínez-Goikoetxea, M., Zuriguel, I., and Arrasate, M. (2017). E46K α-synuclein pathological mutation causes cell-autonomous toxicity without altering protein turnover or aggregation. Proc. Natl. Acad. Sci. *114*, E8274–E8283.

International Parkinson Disease Genomics Consortium, I.P.D.G.C. (2011). Imputation of sequence variants for identification of genetic risks for Parkinson's disease: a meta-analysis of genome-wide association studies. Lancet *377*, 641–649.

Ishizawa, T., Mattila, P., Davies, P., Wang, D., and Dickson, D.W. (2003). Colocalization of tau and alpha-synuclein epitopes in Lewy bodies. J. Neuropathol. Exp. Neurol. *62*, 389–397.

Itakura, E., Kishi-Itakura, C., and Mizushima, N. (2012). The hairpin-type tail-anchored SNARE syntaxin 17 targets to autophagosomes for fusion with endosomes/lysosomes. Cell *151*, 1256–1269.

Ito, G., Okai, T., Fujino, G., Takeda, K., Ichijo, H., Katada, T., and Iwatsubo, T. (2007). GTP Binding Is Essential to the Protein Kinase Activity of LRRK2, a Causative Gene Product for Familial Parkinson's Disease. Biochemistry (Mosc.) *46*, 1380–1388.

Ito, G., Katsemonova, K., Tonelli, F., Lis, P., Baptista, M., Shpiro, N., Duddy, G., Wilson, S., Ho, W.-L., Ho, S.-L., et al. (2016). Phos-tag analysis of Rab10 phosphorylation by LRRK2: a powerful assay for assessing kinase function and inhibitors. Biochem. J.

Iwata, A., Christianson, J.C., Bucci, M., Ellerby, L.M., Nukina, N., Forno, L.S., and Kopito, R.R. (2005a). Increased susceptibility of cytoplasmic over nuclear polyglutamine aggregates to autophagic degradation. Proc. Natl. Acad. Sci. *102*, 13135–13140.

Iwata, A., Riley, B.E., Johnston, J.A., and Kopito, R.R. (2005b). HDAC6 and Microtubules Are Required for Autophagic Degradation of Aggregated Huntingtin. J. Biol. Chem. *280*, 40282–40292.

Iwatsubo, T., Nakano, I., Fukunaga, K., and Miyamoto, E. (1991). Ca2+/calmodulin-dependent protein kinase II immunoreactivity in Lewy bodies. Acta Neuropathol. (Berl.) *82*, 159–163.

Jahreiss, L., Menzies, F.M., and Rubinsztein, D.C. (2008). The itinerary of autophagosomes: from peripheral formation to kiss-and-run fusion with lysosomes. Traffic *9*, 574–587.

Jakes, R., Spillantini, M.G., and Goedert, M. (1994). Identification of two distinct synucleins from human brain. FEBS Lett. *345*, 27–32.

Jaleel, M., Nichols, R.J., Deak, M., Campbell, D.G., Gillardon, F., Knebel, A., and Alessi, D.R. (2007). LRRK2 phosphorylates moesin at threonine-558: characterization of how Parkinson's disease mutants affect kinase activity. Biochem. J. *405*, 307.

Janke, C., and Montagnac, G. (2017). Causes and Consequences of Microtubule Acetylation. Curr. Biol. *27*, R1287–R1292.

Jankovic, J. (2008). Parkinson's disease: clinical features and diagnosis. J. Neurol. Neurosurg. Psychiatry *79*, 368–376.

Jensen, P.H., Islam, K., Kenney, J., Nielsen, M.S., Power, J., and Gai, W.P. (2000). Microtubule-associated protein 1B is a component of cortical Lewy bodies and binds alpha-synuclein filaments. J. Biol. Chem. *275*, 21500–21507.

Jensen, T.J., Loo, M.A., Pind, S., Williams, D.B., Goldberg, A.L., and Riordan, J.R. (1995). Multiple proteolytic systems, including the proteasome, contribute to CFTR processing. Cell *83*, 129–135.

Jin, J., Meredith, G.E., Chen, L., Zhou, Y., Xu, J., Shie, F.-S., Lockhart, P., and Zhang, J. (2005). Quantitative proteomic analysis of mitochondrial proteins: relevance to Lewy body formation and Parkinson's disease. Brain Res. Mol. Brain Res. *134*, 119–138.

Jiwani, S., Wang, Y., Dowd, G.C., Gianfelice, A., Pichestapong, P., Gavicherla, B., Vanbennekom, N., and Ireton, K. (2012). Identification of Components of the Host Type IA Phosphoinositide 3-Kinase Pathway That Promote Internalization of Listeria monocytogenes. Infect. Immun. *80*, 1252–1266.

Johnston, J.A., Ward, C.L., and Kopito, R.R. (1998). Aggresomes: A Cellular Response to Misfolded Proteins. J. Cell Biol. *143*, 1883–1898.

Jongsma, M.L.M., Berlin, I., Wijdeven, R.H.M., Janssen, L., Janssen, G.M.C., Garstka, M.A., Janssen, H., Mensink, M., van Veelen, P.A., Spaapen, R.M., et al. (2016). An ER-Associated Pathway Defines Endosomal Architecture for Controlled Cargo Transport. Cell *166*, 152–166.

Kahle, P.J., Neumann, M., Ozmen, L., Müller, V., Jacobsen, H., Schindzielorz, A., Okochi, M., Leimer, U., Van, D.P., Probst, A., et al. (2000). Subcellular localization of wild-type and Parkinson's disease-associated mutant α-synuclein in human and transgenic mouse brain. J. Neurosci. *20*, 6365–6373.

Kalogeropulou, A.F., Zhao, J., Bolliger, M.F., Memou, A., Narasimha, S., Molitor, T.P., Wilson, W.H., Rideout, H.J., and Nichols, R.J. (2018). P62/SQSTM1 is a novel leucine-rich repeat kinase 2 (LRRK2) substrate that enhances neuronal toxicity. Biochem. J. *475*, 1271–1293.

Katsumata, K., Nishiyama, J., Inoue, T., Mizushima, N., Takeda, J., and Yuzaki, M. (2010). Dynein- and activity-dependent retrograde transport of autophagosomes in neuronal axons. Autophagy *6*, 378–385.

Kaushik, S., and Cuervo, A.M. (2012). Chaperone-mediated autophagy: a unique way to enter the lysosome world. Trends Cell Biol. *22*, 407–417.

Kawaguchi, Y., Kovacs, J.J., McLaurin, A., Vance, J.M., Ito, A., and Yao, T.-P. (2003). The Deacetylase HDAC6 Regulates Aggresome Formation and Cell Viability in Response to Misfolded Protein Stress. Cell *115*, 727–738.

Kawakami, F., Yabata, T., Ohta, E., Maekawa, T., Shimada, N., Suzuki, M., Maruyama, H., Ichikawa, T., and Obata, F. (2012). LRRK2 Phosphorylates Tubulin-Associated Tau but Not the Free Molecule: LRRK2-Mediated Regulation of the Tau-Tubulin Association and Neurite Outgrowth. PLoS ONE *7*.

Kawakami, F., Shimada, N., Ohta, E., Kagiya, G., Kawashima, R., Maekawa, T., Maruyama, H., and Ichikawa, T. (2013). Leucine-rich repeat kinase 2 regulates tau phosphorylation through direct activation of glycogen synthase kinase-3β. FEBS J. *281*, 3–13.

Kawamoto, Y., Akiguchi, I., Nakamura, S., Honjyo, Y., Shibasaki, H., and Budka, H. (2002). 14-3-3 proteins in Lewy bodies in Parkinson disease and diffuse Lewy body disease brains. J. Neuropathol. Exp. Neurol. *61*, 245–253.

Kett, L.R., Boassa, D., Ho, C.C.-Y., Rideout, H.J., Hu, J., Terada, M., Ellisman, M., and Dauer, W.T. (2012). LRRK2 Parkinson disease mutations enhance its microtubule association. Hum. Mol. Genet. *21*, 890–899.

Kettenbach, A.N., Schweppe, D.K., Faherty, B.K., Pechenick, D., Pletnev, A.A., and Gerber, S.A. (2011). Quantitative Phosphoproteomics Identifies Substrates and Functional Modules of Aurora and Polo-Like Kinase Activities in Mitotic Cells. Sci. Signal. *4*, rs5.

Khan, N.L., Jain, S., Lynch, J.M., Pavese, N., Abou-Sleiman, P., Holton, J.L., Healy, D.G., Gilks, W.P., Sweeney, M.G., Ganguly, M., et al. (2005). Mutations in the gene LRRK2 encoding dardarin (PARK8) cause familial Parkinson's disease: clinical, pathological, olfactory and functional imaging and genetic data. Brain J. Neurol. *128*, 2786–2796.

Kim, S.H., Shanware, N.P., Bowler, M.J., and Tibbetts, R.S. (2010). Amyotrophic lateral sclerosis-associated proteins TDP-43 and FUS/TLS function in a common biochemical complex to co-regulate HDAC6 mRNA. J. Biol. Chem. *285*, 34097–34105.

Kimura, S., Noda, T., and Yoshimori, T. (2008). Dynein-dependent movement of autophagosomes mediates efficient encounters with lysosomes. Cell Struct. Funct. *33*, 109–122.

King, S.M. (2000). AAA domains and organization of the dynein motor unit. J. Cell Sci. *113*, 2521–2526.

Kirkin, V., McEwan, D.G., Novak, I., and Dikic, I. (2009). A role for ubiquitin in selective autophagy. Mol. Cell *34*, 259–269.

Kitada, T., Asakawa, S., Hattori, N., Matsumine, H., Yamamura, Y., Minoshima, S., Yokochi, M., Mizuno, Y., and Shimizu, N. (1998). Mutations in the parkin gene cause autosomal recessive juvenile parkinsonism. Nature *392*, 605–608.

Klemm, J.D., Schreiber, S.L., and Crabtree, G.R. (1998). Dimerization as a regulatory mechanism in signal transduction. Annu. Rev. Immunol. *16*, 569–592.

Kokoulina, P., and Rohn, T.T. (2010). Caspase-Cleaved Transactivation Response DNA-Binding Protein 43 in Parkinson's Disease and Dementia with Lewy Bodies. Neurodegener. Dis. *7*, 243–250.

Komatsu, S., Moriya, S., Che, X.-F., Yokoyama, T., Kohno, N., and Miyazawa, K. (2013). Combined treatment with SAHA, bortezomib, and clarithromycin for concomitant targeting of aggresome formation and intracellular proteolytic pathways enhances ER stress-mediated cell death in breast cancer cells. Biochem. Biophys. Res. Commun. *437*, 41–47.

Kopito, R.R. (2000). Aggresomes, inclusion bodies and protein aggregation. Trends Cell Biol. *10*, 524–530.

Kovacs, J.J., Murphy, P.J.M., Gaillard, S., Zhao, X., Wu, J.-T., Nicchitta, C.V., Yoshida, M., Toft, D.O., Pratt, W.B., and Yao, T.-P. (2005). HDAC6 regulates Hsp90 acetylation and chaperone-dependent activation of glucocorticoid receptor. Mol. Cell *18*, 601–607.

Kövari, E., Gold, G., Herrmann, F.R., Canuto, A., Hof, P.R., Bouras, C., and Giannakopoulos, P. (2003). Lewy body densities in the entorhinal and anterior cingulate cortex predict cognitive deficits in Parkinson's disease. Acta Neuropathol. (Berl.) *106*, 83–88.

Krebs, C.E., Karkheiran, S., Powell, J.C., Cao, M., Makarov, V., Darvish, H., Di Paolo, G., Walker, R.H., Shahidi, G.A., Buxbaum, J.D., et al. (2013). The Sac1 domain of SYNJ1 identified mutated in a family with early-onset progressive Parkinsonism with generalized seizures. Hum. Mutat. *34*, 1200–1207.

Krüger, R., Kuhn, W., Müller, T., Woitalla, D., Graeber, M., Kösel, S., Przuntek, H., Epplen, J.T., Schöls, L., and Riess, O. (1998). Ala30Pro mutation in the gene encoding alpha-synuclein in Parkinson's disease. Nat. Genet. *18*, 106–108.

Krüger, R., Sharma, M., Riess, O., Gasser, T., Van Broeckhoven, C., Theuns, J., Aasly, J., Annesi, G., Bentivoglio, A.R., Brice, A., et al. (2011). A large-scale genetic association study to evaluate the contribution of Omi/HtrA2 (PARK13) to Parkinson's disease. Neurobiol. Aging *32*, 548. e9–18.

Kumazawa, R., Tomiyama, H., Li, Y., Imamichi, Y., Funayama, M., Yoshino, H., Yokochi, F., Fukusako, T., Takehisa, Y., Kashihara, K., et al. (2008). Mutation analysis of the PINK1 gene in 391 patients with Parkinson disease. Arch. Neurol. *65*, 802–808.

Kuusisto, E., Parkkinen, L., and Alafuzoff, I. (2003). Morphogenesis of Lewy bodies: dissimilar incorporation of alpha-synuclein, ubiquitin, and p62. J. Neuropathol. Exp. Neurol. *62*, 1241–1253.

Kuzuhara, S., Mori, H., Izumiyama, N., Yoshimura, M., and Ihara, Y. (1988). Lewy bodies are ubiquitinated. A light and electron microscopic immunocytochemical study. Acta Neuropathol. (Berl.) *75*, 345–353.

Kwon, S., Zhang, Y., and Matthias, P. (2007). The deacetylase HDAC6 is a novel critical component of stress granules involved in the stress response. Genes Dev. *21*, 3381–3394.

Lamberts, J.T., Hildebrandt, E.N., and Brundin, P. (2015). Spreading of α-synuclein in the face of axonal transport deficits in Parkinson's disease: A speculative synthesis. Neurobiol. Dis. *77*, 276–283.

Langston, J.W., Ballard, P., Tetrud, J.W., and Irwin, I. (1983). Chronic Parkinsonism in humans due to a product of meperidine-analog synthesis. Science *219*, 979–980.

De Lau, L.M.L., and Breteler, M.M.B. (2006). Epidemiology of Parkinson's disease. Lancet Neurol. *5*, 525–535.

LaVoie, M.J., Ostaszewski, B.L., Weihofen, A., Schlossmacher, M.G., and Selkoe, D.J. (2005). Dopamine covalently modifies and functionally inactivates parkin. Nat. Med. *11*, 1214–1221.

Law, B.M.H., Spain, V.A., Leinster, V.H.L., Chia, R., Beilina, A., Cho, H.J., Taymans, J.-M., Urban, M.K., Sancho, R.M., Ramírez, M.B., et al. (2014). A direct interaction between leucine-rich repeat kinase 2 and specific β-tubulin isoforms regulates tubulin acetylation. J. Biol. Chem. *289*, 895–908.

Lázaro, D.F., Rodrigues, E.F., Langohr, R., Shahpasandzadeh, H., Ribeiro, T., Guerreiro, P., Gerhardt, E., Kröhnert, K., Klucken, J., Pereira, M.D., et al. (2014). Systematic Comparison of the Effects of Alpha-synuclein Mutations on Its Oligomerization and Aggregation. PLOS Genet. *10*, e1004741.

Lee, D.H., and Goldberg, A.L. (1998). Proteasome inhibitors: valuable new tools for cell biologists. Trends Cell Biol. *8*, 397–403.

Lee, C.S., Song, E.H., Park, S.Y., and Han, E.S. (2003). Combined effect of dopamine and MPP+ on membrane permeability in mitochondria and cell viability in PC12 cells. Neurochem. Int. *43*, 147–154.

Lee, J.-H., Mahendran, A., Yao, Y., Ngo, L., Venta-Perez, G., Choy, M.L., Kim, N., Ham, W.-S., Breslow, R., and Marks, P.A. (2013). Development of a histone deacetylase 6 inhibitor and its biological effects. Proc. Natl. Acad. Sci. *110*, 15704–15709.

Lee, J.-Y., Koga, H., Kawaguchi, Y., Tang, W., Wong, E., Gao, Y.-S., Pandey, U.B., Kaushik, S., Tresse, E., Lu, J., et al. (2010a). HDAC6 controls autophagosome maturation essential for ubiquitin-selective quality-control autophagy. EMBO J. *29*, 969–980.

Lee, J.-Y., Nagano, Y., Taylor, J.P., Lim, K.L., and Yao, T.-P. (2010b). Disease-causing mutations in parkin impair mitochondrial ubiquitination, aggregation, and HDAC6-dependent mitophagy. J. Cell Biol. *189*, 671–679.

Lee, S., Sato, Y., and Nixon, R.A. (2011). Lysosomal Proteolysis Inhibition Selectively Disrupts Axonal Transport of Degradative Organelles and Causes an Alzheimer's-Like Axonal Dystrophy. J. Neurosci. *31*, 7817–7830.

Leroy, E., Boyer, R., Auburger, G., Leube, B., Ulm, G., Mezey, E., Harta, G., Brownstein, M.J., Jonnalagada, S., Chernova, T., et al. (1998). The ubiquitin pathway in Parkinson's disease. Nature *395*, 451–452.

Lesage, S., and Brice, A. (2009). Parkinson's disease: from monogenic forms to genetic susceptibility factors. Hum. Mol. Genet. *18*, R48–59.

Lesage, S., and Brice, A. (2012). Role of Mendelian genes in "sporadic" Parkinson's disease. Parkinsonism Relat. Disord. *18, Supplement 1*, S66–S70.

Lesage, S., Janin, S., Lohmann, E., Leutenegger, A.-L., Leclere, L., Viallet, F., Pollak, P., Durif, F., Thobois, S., Layet, V., et al. (2007). LRRK2 exon 41 mutations in sporadic Parkinson disease in Europeans. Arch. Neurol. *64*, 425–430.

Lesage, S., Anheim, M., Condroyer, C., Pollak, P., Durif, F., Dupuits, C., Viallet, F., Lohmann, E., Corvol, J.-C., Honoré, A., et al. (2011). Large-scale screening of the Gaucher's disease-related glucocerebrosidase gene in Europeans with Parkinson's disease. Hum. Mol. Genet. *20*, 202–210.

Lesage, S., Drouet, V., Majounie, E., Deramecourt, V., Jacoupy, M., Nicolas, A., Cormier-Dequaire, F., Hassoun, S.M., Pujol, C., Ciura, S., et al. (2016). Loss of VPS13C Function in Autosomal-Recessive Parkinsonism Causes Mitochondrial Dysfunction and Increases PINK1/Parkin-Dependent Mitophagy. Am. J. Hum. Genet. *98*, 500–513.

Lesage, S., Anheim, M., Letournel, F., Bousset, L., Honoré, A., Rozas, N., Pieri, L., Madiona, K., Dürr, A., Melki, R., et al. (2013). G51D α-synuclein mutation causes a novel Parkinsonian–pyramidal syndrome. Ann. Neurol. *73*, 459–471.

Lewis, P.A. (2009). The function of ROCO proteins in health and disease. Biol. Cell *101*, 183–191.

Lewis, P.A., Greggio, E., Beilina, A., Jain, S., Baker, A., and Cookson, M.R. (2007). The R1441C mutation of LRRK2 disrupts GTP hydrolysis. Biochem. Biophys. Res. Commun. *357*, 668–671.

Li, J.-Q., Tan, L., and Yu, J.-T. (2014). The role of the LRRK2 gene in Parkinsonism. Mol. Neurodegener. *9*, 47.

Li, X., Tan, Y.-C., Poulose, S., Olanow, C.W., Huang, X.-Y., and Yue, Z. (2007). Leucine-rich repeat kinase 2 (LRRK2)/PARK8 possesses GTPase activity that is altered in familial Parkinson's disease R1441C/G mutants. J. Neurochem. *103*, 238–247.

Li, X., Moore, D.J., Xiong, Y., Dawson, T.M., and Dawson, V.L. (2010). Reevaluation of phosphorylation sites in the Parkinson disease-associated leucine-rich repeat kinase 2. J. Biol. Chem. *285*, 29569–29576.

Li, Y., Tomiyama, H., Sato, K., Hatano, Y., Yoshino, H., Atsumi, M., Kitaguchi, M., Sasaki, S., Kawaguchi, S., Miyajima, H., et al. (2005). Clinicogenetic study of PINK1

mutations in autosomal recessive early-onset parkinsonism. Neurology *64*, 1955–1957.

Li, Y., Liu, W., Oo, T.F., Wang, L., Tang, Y., Jackson-Lewis, V., Zhou, C., Geghman, K., Bogdanov, M., Przedborski, S., et al. (2009). Mutant LRRK2R1441G BAC transgenic mice recapitulate cardinal features of Parkinson's disease. Nat. Neurosci. *12*, 826–828.

Li, Y., Shin, D., and Kwon, S.H. (2013). Histone deacetylase 6 plays a role as a distinct regulator of diverse cellular processes. FEBS J. *280*, 775–793.

Lill, C.M. (2016). Genetics of Parkinson's disease. Mol. Cell. Probes *30*, 386–396.

Lim, K.-L. (2007). Ubiquitin-proteasome system dysfunction in Parkinson's disease: current evidence and controversies. Expert Rev. Proteomics *4*, 769–781.

Lin, X., Parisiadou, L., Gu, X.-L., Wang, L., Shim, H., Sun, L., Xie, C., Long, C.-X., Yang, W.-J., Ding, J., et al. (2009). Leucine-Rich Repeat Kinase 2 Regulates the Progression of Neuropathology Induced by Parkinson's-Disease-Related Mutant α-synuclein. Neuron *64*, 807–827.

Lindberg, I., Shorter, J., Wiseman, R.L., Chiti, F., Dickey, C.A., and McLean, P.J. (2015). Chaperones in Neurodegeneration. J. Neurosci. *35*, 13853–13859.

Lindersson, E., Beedholm, R., Højrup, P., Moos, T., Gai, W., Hendil, K.B., and Jensen, P.H. (2004). Proteasomal Inhibition by α-Synuclein Filaments and Oligomers. J. Biol. Chem. *279*, 12924–12934.

Linding, R., Jensen, L.J., Ostheimer, G.J., van Vugt, M.A.T.M., Jørgensen, C., Miron, I.M., Diella, F., Colwill, K., Taylor, L., Elder, K., et al. (2007). Systematic discovery of in vivo phosphorylation networks. Cell *129*, 1415–1426.

Liu, I.-H., Uversky, V.N., Munishkina, L.A., Fink, A.L., Halfter, W., and Cole, G.J. (2005). Agrin binds alpha-synuclein and modulates alpha-synuclein fibrillation. Glycobiology *15*, 1320–1331.

Liu, J., Li, T., Thomas, J.M., Pei, Z., Jiang, H., Engelender, S., Ross, C.A., and Smith, W.W. (2016). Synphilin-1 attenuates mutant LRRK2-induced neurodegeneration in Parkinson's disease models. Hum. Mol. Genet. *25*, 672–680.

Liu, M., Dobson, B., Glicksman, M.A., Yue, Z., and Stein, R.L. (2010). Kinetic mechanistic studies of wild-type leucine-rich repeat kinase 2: characterization of the kinase and GTPase activities. Biochemistry (Mosc.) *49*, 2008–2017.

Liu, S., Sawada, T., Lee, S., Yu, W., Silverio, G., Alapatt, P., Millan, I., Shen, A., Saxton, W., Kanao, T., et al. (2012a). Parkinson's disease-associated kinase PINK1 regulates Miro protein level and axonal transport of mitochondria. PLoS Genet. *8*, e1002537.

Liu, Y., Peng, L., Seto, E., Huang, S., and Qiu, Y. (2012b). Modulation of Histone Deacetylase 6 (HDAC6) Nuclear Import and Tubulin Deacetylase Activity through Acetylation. J. Biol. Chem. *287*, 29168–29174.

Liu, Z., Mobley, J.A., DeLucas, L.J., Kahn, R.A., and West, A.B. (2015). LRRK2 autophosphorylation enhances its GTPase activity. FASEB J. fj.15–277095.

Liu, Z., Bryant, N., Kumaran, R., Beilina, A., Abeliovich, A., Cookson, M.R., and West, A.B. (2018). LRRK2 phosphorylates membrane-bound Rabs and is activated by GTP-bound Rab7L1 to promote recruitment to the trans-Golgi network. Hum. Mol. Genet. *27*, 385–395.

Lücking, C.B., Dürr, A., Bonifati, V., Vaughan, J., De Michele, G., Gasser, T., Harhangi, B.S., Meco, G., Denèfle, P., Wood, N.W., et al. (2000). Association between Early-Onset Parkinson's Disease and Mutations in the Parkin Gene. N. Engl. J. Med. *342*, 1560–1567.

Luzón-Toro, B., Rubio de la Torre, E., Delgado, A., Pérez-Tur, J., and Hilfiker, S. (2007). Mechanistic insight into the dominant mode of the Parkinson's disease-associated G2019S LRRK2 mutation. Hum. Mol. Genet. *16*, 2031–2039.

Ly, N., Elkhatib, N., Bresteau, E., Piétrement, O., Khaled, M., Magiera, M.M., Janke, C., Le Cam, E., Rutenberg, A.D., and Montagnac, G. (2016). αTAT1 controls longitudinal spreading of acetylation marks from open microtubules extremities. Sci. Rep. *6*, 35624.

Maciejewski, P.M., Peterson, F.C., Anderson, P.J., and Brooks, C.L. (1995). Mutation of Serine 90 to Glutamic Acid Mimics Phosphorylation of Bovine Prolactin. J. Biol. Chem. *270*, 27661–27665.

MacLeod, D., Dowman, J., Hammond, R., Leete, T., Inoue, K., and Abeliovich, A. (2006a). The Familial Parkinsonism Gene LRRK2 Regulates Neurite Process Morphology. Neuron *52*, 587–593.

MacLeod, D., Dowman, J., Hammond, R., Leete, T., Inoue, K., and Abeliovich, A. (2006b). The Familial Parkinsonism Gene LRRK2 Regulates Neurite Process Morphology. Neuron *52*, 587–593.

MacLeod, D.A., Rhinn, H., Kuwahara, T., Zolin, A., Di Paolo, G., McCabe, B.D., MacCabe, B.D., Marder, K.S., Honig, L.S., Clark, L.N., et al. (2013). RAB7L1 interacts with LRRK2 to modify intraneuronal protein sorting and Parkinson's disease risk. Neuron *77*, 425–439.

Maday, S., Wallace, K.E., and Holzbaur, E.L.F. (2012). Autophagosomes initiate distally and mature during transport toward the cell soma in primary neurons. J Cell Biol *196*, 407–417.

Madero-Pérez, J., Fdez, E., Fernández, B., Lara Ordóñez, A.J., Blanca Ramírez, M., Gómez-Suaga, P., Waschbüsch, D., Lobbestael, E., Baekelandt, V., Nairn, A.C., et al. (2018). Parkinson disease-associated mutations in LRRK2 cause centrosomal defects via Rab8a phosphorylation. Mol. Neurodegener. *13*, 3.

Maekawa, T., Mori, S., Sasaki, Y., Miyajima, T., Azuma, S., Ohta, E., and Obata, F. (2012). The I2020T Leucine-rich repeat kinase 2 transgenic mouse exhibits impaired locomotive ability accompanied by dopaminergic neuron abnormalities. Mol. Neurodegener. *7*, 15.

Manzoni, C. (2017). The LRRK2–macroautophagy axis and its relevance to Parkinson's disease. Biochem. Soc. Trans. *45*, 155–162.

Manzoni, C., Mamais, A., Dihanich, S., Abeti, R., Soutar, M.P.M., Plun-Favreau, H., Giunti, P., Tooze, S.A., Bandopadhyay, R., and Lewis, P.A. (2013). Inhibition of

LRRK2 kinase activity stimulates macroautophagy. Biochim. Biophys. Acta *1833*, 2900–2910.

Mao, X., Wang, T., Peng, R., Chang, X., Li, N., Gu, Y., Zhao, D., Liao, Q., and Liu, M. (2013). Mutations in GBA and risk of Parkinson's disease: a meta-analysis based on 25 case-control studies. Neurol. Res. *35*, 873–878.

Marsden, C.D. (1994). Problems with long-term levodopa therapy for Parkinson's disease. Clin. Neuropharmacol. *17 Suppl 2*, S32–44.

Marx, F.P., Holzmann, C., Strauss, K.M., Li, L., Eberhardt, O., Gerhardt, E., Cookson, M.R., Hernandez, D., Farrer, M.J., Kachergus, J., et al. (2003). Identification and functional characterization of a novel R621C mutation in the synphilin-1 gene in Parkinson's disease. Hum. Mol. Genet. *12*, 1223–1231.

Marzella, L., Ahlberg, J., and Glaumann, H. (1981). Autophagy, heterophagy, microautophagy and crinophagy as the means for intracellular degradation. Virchows Arch. B Cell Pathol. Incl. Mol. Pathol. *36*, 219–234.

Mata, I.F., Kachergus, J.M., Taylor, J.P., Lincoln, S., Aasly, J., Lynch, T., Hulihan, M.M., Cobb, S.A., Wu, R.-M., Lu, C.-S., et al. (2005). Lrrk2 pathogenic substitutions in Parkinson's disease. Neurogenetics *6*, 171–177.

Mayer, M.P., and Bukau, B. (2005). Hsp70 chaperones: Cellular functions and molecular mechanism. Cell. Mol. Life Sci. *62*, 670–684.

Mazroui, R., Di Marco, S., Kaufman, R.J., and Gallouzi, I.-E. (2007). Inhibition of the ubiquitin-proteasome system induces stress granule formation. Mol. Biol. Cell *18*, 2603–2618.

McCoy, M.K., and Cookson, M.R. (2011). DJ-1 regulation of mitochondrial function and autophagy through oxidative stress. Autophagy *7*, 531–532.

McLean, P.J., Kawamata, H., Shariff, S., Hewett, J., Sharma, N., Ueda, K., Breakefield, X.O., and Hyman, B.T. (2002). TorsinA and heat shock proteins act as molecular chaperones: suppression of alpha-synuclein aggregation. J. Neurochem. *83*, 846–854.

McNaught, K.S.P., Shashidharan, P., Perl, D.P., Jenner, P., and Olanow, C.W. (2002). Aggresome-related biogenesis of Lewy bodies. Eur. J. Neurosci. *16*, 2136–2148.

McNaught, K.S.P., Jackson, T., JnoBaptiste, R., Kapustin, A., and Olanow, C.W. (2006). Proteasomal dysfunction in sporadic Parkinson's disease. Neurology *66*, S37–49.

Miki, Y., Mori, F., Tanji, K., Kakita, A., Takahashi, H., and Wakabayashi, K. (2011). Accumulation of histone deacetylase 6, an aggresome-related protein, is specific to Lewy bodies and glial cytoplasmic inclusions. Neuropathol. *31*, 561–568.

Miklossy, J., Arai, T., Guo, J.-P., Klegeris, A., Yu, S., McGeer, E.G., and McGeer, P.L. (2006). LRRK2 expression in normal and pathologic human brain and in human cell lines. J. Neuropathol. Exp. Neurol. *65*, 953–963.

Millecamps, S., and Julien, J.-P. (2013). Axonal transport deficits and neurodegenerative diseases. Nat. Rev. Neurosci. *14*, 161–176.

Mills, R.D., Mulhern, T.D., Cheng, H.-C., and Culvenor, J.G. (2012). Analysis of LRRK2 accessory repeat domains: prediction of repeat length, number and sites of Parkinson's disease mutations. Biochem. Soc. Trans. *40*, 1086–1089.

Mills, R.D., Mulhern, T.D., Liu, F., Culvenor, J.G., and Cheng, H.-C. (2014). Prediction of the repeat domain structures and impact of parkinsonism-associated variations on structure and function of all functional domains of leucine-rich repeat kinase 2 (LRRK2). Hum. Mutat. *35*, 395–412.

Mir, R., Tonelli, F., Lis, P., Macartney, T., Polinski, N.K., Martinez, T.N., Chou, M.-Y., Howden, A.J.M., König, T., Hotzy, C., et al. (2018). The Parkinson's disease VPS35[D620N] mutation enhances LRRK2 mediated Rab protein phosphorylation in mouse and human. Biochem. J. *11*, 1861-1883.

Mishima, Y., Loredana, S., Homare, E., Diana, C., Neeharika, N., J, Y.A., Elizabeth, O., Karl, S.M., N, Q.S., Shirin, A.-K., et al. (2015). Ricolinostat (ACY-1215) induced inhibition of aggresome formation accelerates carfilzomib-induced multiple myeloma cell death. Br. J. Haematol. *169*, 423–434.

Miyake, Y., Keusch, J.J., Wang, L., Saito, M., Hess, D., Wang, X., Melancon, B.J., Helquist, P., Gut, H., and Matthias, P. (2016). Structural insights into HDAC6 tubulin deacetylation and its selective inhibition. Nat. Chem. Biol. *12*, 748.

Mizuno, Y., Sone, N., and Saitoh, T. (1987). Effects of 1-methyl-4-phenyl-1,2,3,6-tetrahydropyridine and 1-methyl-4-phenylpyridinium ion on activities of the enzymes in the electron transport system in mouse brain. J. Neurochem. *48*, 1787–1793.

Mollapour, M., and Neckers, L. (2012). Post-translational modifications of Hsp90 and their contributions to chaperone regulation. Biochim. Biophys. Acta *1823*, 648–655.

Moller, A., Bauer, C.S., Cohen, R.N., Webster, C.P., De Vos, J.K. (2017). Amyotrophic lateral sclerosis-associated mutant SOD1 inhibits anterograde axonal transport of mitochondria by reducing Miro1 levels. Hum. Mol. Genet. *26*, 4668–4679.

Morfini, G., Pigino, G., Opalach, K., Serulle, Y., Moreira, J.E., Sugimori, M., Llinás, R.R., and Brady, S.T. (2007). 1-Methyl-4-phenylpyridinium affects fast axonal transport by activation of caspase and protein kinase C. Proc. Natl. Acad. Sci. *104*, 2442–2447.

Mori, H., Kondo, T., Yokochi, M., Matsumine, H., Nakagawa-Hattori, Y., Miyake, T., Suda, K., and Mizuno, Y. (1998). Pathologic and biochemical studies of juvenile parkinsonism linked to chromosome 6q. Neurology *51*, 890–892.

Morris, H.R., Janssen, J.C., Bandmann, O., Daniel, S.E., Rossor, M.N., Lees, A.J., and Wood, N.W. (1999). The tau gene A0 polymorphism in progressive supranuclear palsy and related neurodegenerative diseases. J. Neurol. Neurosurg. Psychiatry *66*, 665–667.

Muda, K., Bertinetti, D., Gesellchen, F., Hermann, J.S., Zweydorf, F. von, Geerlof, A., Jacob, A., Ueffing, M., Gloeckner, C.J., and Herberg, F.W. (2014). Parkinson-related LRRK2 mutation R1441C/G/H impairs PKA phosphorylation of LRRK2 and disrupts its interaction with 14-3-3. Proc. Natl. Acad. Sci. *111*, E34–E43.

Müftüoglu, M., Elibol, B., Dalmizrak, O., Ercan, A., Kulaksiz, G., Ogüs, H., Dalkara, T., and Ozer, N. (2004). Mitochondrial complex I and IV activities in leukocytes from patients with parkin mutations. Mov. Disord. *19*, 544–548.

Muqit, M.M.K., Abou-Sleiman, P.M., Saurin, A.T., Harvey, K., Gandhi, S., Deas, E., Eaton, S., Payne Smith, M.D., Venner, K., Matilla, A., et al. (2006). Altered cleavage and localization of PINK1 to aggresomes in the presence of proteasomal stress. J. Neurochem. *98*, 156–169.

Murakami, T., Shoji, M., Imai, Y., Inoue, H., Kawarabayashi, T., Matsubara, E., Harigaya, Y., Sasaki, A., Takahashi, R., and Abe, K. (2004). Pael-R is accumulated in Lewy bodies of Parkinson's disease. Ann. Neurol. *55*, 439–442.

Nagao, M., and Hayashi, H. (2009). Glycogen synthase kinase-3beta is associated with Parkinson's disease. Neurosci. Lett. *449*, 103–107.

Nakamura, S., and Yoshimori, T. (2017). New insights into autophagosome–lysosome fusion. J Cell Sci *130*, 1209–1216.

Nalls, M.A., Pankratz, N., Lill, C.M., Do, C.B., Hernandez, D.G., Saad, M., DeStefano, A.L., Kara, E., Bras, J., Sharma, M., et al. (2014). Large-scale meta-analysis of genome-wide association data identifies six new risk loci for Parkinson's disease. Nat. Genet. *46*, 989–993.

Narendra, D., Walker, J.E., and Youle, R. (2012). Mitochondrial Quality Control Mediated by PINK1 and Parkin: Links to Parkinsonism. Cold Spring Harb. Perspect. Biol. *4*, a011338.

Nawrocki, S.T., Carew, J.S., Pino, M.S., Highshaw, R.A., Andtbacka, R.H.I., Dunner, K., Pal, A., Bornmann, W.G., Chiao, P.J., Huang, P., et al. (2006). Aggresome Disruption: A Novel Strategy to Enhance Bortezomib-Induced Apoptosis in Pancreatic Cancer Cells. Cancer Res. *66*, 3773–3781.

Nguyen, A.P.T., and Moore, D.J. (2017). Understanding the GTPase Activity of LRRK2: Regulation, Function, and Neurotoxicity. Adv. Neurobiol. *14*, 71–88.

Nishiyama, K., Murayama, S., Shimizu, J., Ohya, Y., Kwak, S., Asayama, K., and Kanazawa, I. (1995). Cu/Zn superoxide dismutase-like immunoreactivity is present in Lewy bodies from Parkinson disease: a light and electron microscopic immunocytochemical study. Acta Neuropathol. (Berl.) *89*, 471–474.

North, B.J., Marshall, B.L., Borra, M.T., Denu, J.M., and Verdin, E. (2003). The Human Sir2 Ortholog, SIRT2, Is an NAD+-Dependent Tubulin Deacetylase. Mol. Cell *11*, 437–444.

Nunomura, A., Honda, K., Takeda, A., Hirai, K., Zhu, X., Smith, M.A., and Perry, G. (2006). Oxidative damage to RNA in neurodegenerative diseases. J. Biomed. Biotechnol. *2006*, 82323.

O'Regan, G., deSouza, R.-M., Balestrino, R., and Schapira, A.H. (2017). Glucocerebrosidase Mutations in Parkinson Disease. J. Park. Dis. *7*, 411–422.

Obeso, J.A., Rodríguez-Oroz, M.C., Benitez-Temino, B., Blesa, F.J., Guridi, J., Marin, C., and Rodriguez, M. (2008). Functional organization of the basal ganglia: therapeutic implications for Parkinson's disease. Mov. Disord. *23 Suppl 3*, S548–559.

Odagiri, S., Tanji, K., Mori, F., Kakita, A., Takahashi, H., and Wakabayashi, K. (2012). Autophagic adapter protein NBR1 is localized in Lewy bodies and glial cytoplasmic inclusions and is involved in aggregate formation in α-synucleinopathy. Acta Neuropathol. (Berl.) *124*, 173–186.

Okuda, K., Ito, A., and Uehara, T. (2015). Regulation of Histone Deacetylase 6 Activity via S-Nitrosylation. Biol. Pharm. Bull. *38*, 1434–1437.

Olanow, C.W., Perl, D.P., DeMartino, G.N., and McNaught, K.S.P. (2004). Lewy-body formation is an aggresome-related process: a hypothesis. Lancet Neurol. *3*, 496–503.

Olzmann, J.A., and Chin, L.-S. (2008). Parkin-mediated K63-linked polyubiquitination: a signal for targeting misfolded proteins to the aggresome-autophagy pathway. Autophagy *4*, 85–87.

Olzmann, J.A., Brown, K., Wilkinson, K.D., Rees, H.D., Huai, Q., Ke, H., Levey, A.I., Li, L., and Chin, L.-S. (2004). Familial Parkinson's disease-associated L166P mutation disrupts DJ-1 protein folding and function. J. Biol. Chem. *279*, 8506–8515.

Olzmann, J.A., Li, L., Chudaev, M.V., Chen, J., Perez, F.A., Palmiter, R.D., and Chin, L.-S. (2007). Parkin-mediated K63-linked polyubiquitination targets misfolded DJ-1 to aggresomes via binding to HDAC6. J. Cell Biol. *178*, 1025–1038.

Olzmann, J.A., Li, L., and Chin, L.S. (2008). Aggresome Formation and Neurodegenerative Diseases: Therapeutic Implications. Curr. Med. Chem. *15*, 47–60.

Ouyang, H., Ali, Y.O., Ravichandran, M., Dong, A., Qiu, W., MacKenzie, F., Dhe-Paganon, S., Arrowsmith, C.H., and Zhai, R.G. (2012). Protein Aggregates Are Recruited to Aggresome by Histone Deacetylase 6 via Unanchored Ubiquitin C Termini. J. Biol. Chem. *287*, 2317–2327.

Paisan-Ruiz, C., Bhatia, K.P., Li, A., Hernandez, D., Davis, M., Wood, N.W., Hardy, J., Houlden, H., Singleton, A., and Schneider, S.A. (2009). Characterization of PLA2G6 as a locus for dystonia-parkinsonism. Ann. Neurol. *65*, 19–23.

Paisán-Ruíz, C., Jain, S., Evans, E.W., Gilks, W.P., Simón, J., van der Brug, M., López de Munain, A., Aparicio, S., Gil, A.M., Khan, N., et al. (2004). Cloning of the gene containing mutations that cause PARK8-linked Parkinson's disease. Neuron *44*, 595–600.

Palacino, J.J., Sagi, D., Goldberg, M.S., Krauss, S., Motz, C., Wacker, M., Klose, J., and Shen, J. (2004). Mitochondrial dysfunction and oxidative damage in parkin-deficient mice. J. Biol. Chem. *279*, 18614–18622.

Pals, P., Lincoln, S., Manning, J., Heckman, M., Skipper, L., Hulihan, M., Van den Broeck, M., De Pooter, T., Cras, P., Crook, J., et al. (2004). alpha-Synuclein promoter confers susceptibility to Parkinson's disease. Ann. Neurol. *56*, 591–595.

Pandey, U.B., Nie, Z., Batlevi, Y., McCray, B.A., Ritson, G.P., Nedelsky, N.B., Schwartz, S.L., DiProspero, N.A., Knight, M.A., Schuldiner, O., et al. (2007). HDAC6 rescues neurodegeneration and provides an essential link between autophagy and the UPS. Nature *447*, 859–863.

Pankratz, N., Nichols, W.C., Uniacke, S.K., Halter, C., Rudolph, A., Shults, C., Conneally, P.M., Foroud, T., and Parkinson Study Group (2003a). Significant linkage of Parkinson disease to chromosome 2q36-37. Am. J. Hum. Genet. *72*, 1053–1057.

Pankratz, N., Nichols, W.C., Uniacke, S.K., Halter, C., Murrell, J., Rudolph, A., Shults, C.W., Conneally, P.M., Foroud, T., and Parkinson Study Group (2003b). Genome-wide linkage analysis and evidence of gene-by-gene interactions in a sample of 362 multiplex Parkinson disease families. Hum. Mol. Genet. *12*, 2599–2608.

Parisiadou, L., Xie, C., Cho, H.J., Lin, X., Gu, X.-L., Long, C.-X., Lobbestael, E., Baekelandt, V., Taymans, J.-M., Sun, L., et al. (2009). Phosphorylation of ezrin/radixin/moesin proteins by LRRK2 promotes the rearrangement of actin cytoskeleton in neuronal morphogenesis. J. Neurosci. *29*, 13971–13980.

Parkinson's UK (2018). The incidence and prevalence of Parkinson's in the UK. Retrieved from: http://www.parkinsons.org.uk/sites/default/files/2018-01/CS2960%20Incidence%20and%20prevalence%20report%20branding%20summary%20report.pdf

Piccoli, C., Sardanelli, A., Scrima, R., Ripoli, M., Quarato, G., D'Aprile, A., Bellomo, F., Scacco, S., De Michele, G., Filla, A., et al. (2008). Mitochondrial respiratory dysfunction in familiar parkinsonism associated with PINK1 mutation. Neurochem. Res. *33*, 2565–2574.

Pihlstrøm, L., Rengmark, A., Bjørnarå, K.A., Dizdar, N., Fardell, C., Forsgren, L., Holmberg, B., Larsen, J.P., Linder, J., Nissbrandt, H., et al. (2015). Fine mapping and resequencing of the PARK16 locus in Parkinson's disease. J. Hum. Genet. *60*, 357–362.

Pinho, B.R., Reis, S.D., Guedes-Dias, P., Leitão-Rocha, A., Quintas, C., Valentão, P., Andrade, P.B., Santos, M.M., and Oliveira, J.M.A. (2016). Pharmacological modulation of HDAC1 and HDAC6 in vivo in a zebrafish model: Therapeutic implications for Parkinson's disease. Pharmacol. Res. *103*, 328–339.

Pissadaki, E.K., and Bolam, J.P. (2013). The energy cost of action potential propagation in dopamine neurons: clues to susceptibility in Parkinson's disease. Front. Comput. Neurosci. *7*, 13

Polymeropoulos, M.H., Lavedan, C., Leroy, E., Ide, S.E., Dehejia, A., Dutra, A., Pike, B., Root, H., Rubenstein, J., Boyer, R., et al. (1997). Mutation in the α-Synuclein Gene Identified in Families with Parkinson's Disease. Science *276*, 2045–2047.

Portran, D., Schaedel, L., Xu, Z., Théry, M., and Nachury, M.V. (2017). Tubulin acetylation protects long-lived microtubules against mechanical ageing. Nat. Cell Biol. *19*, 391–398.

Prots, I., Veber, V., Brey, S., Campioni, S., Buder, K., Riek, R., Böhm, K.J., and Winner, B. (2013). α-Synuclein Oligomers Impair Neuronal Microtubule-Kinesin Interplay. J. Biol. Chem. *288*, 21742–21754.

Pu, J., Guardia, C.M., Keren-Kaplan, T., and Bonifacino, J.S. (2016). Mechanisms and functions of lysosome positioning. J Cell Sci *129*, 4329–4339.

Pungaliya, P.P., Bai, Y., Lipinski, K., Anand, V.S., Sen, S., Brown, E.L., Bates, B., Reinhart, P.H., West, A.B., Hirst, W.D., et al. (2010). Identification and

characterization of a leucine-rich repeat kinase 2 (LRRK2) consensus phosphorylation motif. PloS One *5*, e13672.

Purlyte, E., Dhekne, H.S., Sarhan, A.R., Gomez, R., Lis, P., Wightman, M., Martinez, T.N., Tonelli, F., Pfeffer, S.R., and Alessi, D.R. (2018). Rab29 activation of the Parkinson's disease-associated LRRK2 kinase. EMBO J. *37*, 1–18.

Puschmann, A., Englund, E., Ross, O.A., Vilariño-Güell, C., Lincoln, S.J., Kachergus, J.M., Cobb, S.A., Törnqvist, A.-L., Rehncrona, S., Widner, H., et al. (2012). First neuropathological description of a patient with Parkinson's disease and LRRK2 p.N1437H mutation. Parkinsonism Relat. Disord. *18*, 332–338.

Quadri, M., Fang, M., Picillo, M., Olgiati, S., Breedveld, G.J., Graafland, J., Wu, B., Xu, F., Erro, R., Amboni, M., et al. (2013). Mutation in the SYNJ1 gene associated with autosomal recessive, early-onset Parkinsonism. Hum. Mutat. *34*, 1208–1215.

Ramirez, A., Heimbach, A., Gründemann, J., Stiller, B., Hampshire, D., Cid, L.P., Goebel, I., Mubaidin, A.F., Wriekat, A.-L., Roeper, J., et al. (2006). Hereditary parkinsonism with dementia is caused by mutations in ATP13A2, encoding a lysosomal type 5 P-type ATPase. Nat. Genet. *38*, 1184–1191.

Ramonet, D., Daher, J.P.L., Lin, B.M., Stafa, K., Kim, J., Banerjee, R., Westerlund, M., Pletnikova, O., Glauser, L., Yang, L., et al. (2011). Dopaminergic Neuronal Loss, Reduced Neurite Complexity and Autophagic Abnormalities in Transgenic Mice Expressing G2019S Mutant LRRK2. PLoS ONE *6*, e18568.

Rao, R., Fiskus, W., Ganguly, S., Kambhampati, S., and Bhalla, K.N. (2012). HDAC Inhibitors and Chaperone Function. In Advances in Cancer Research, S. Grant, ed. (Academic Press), pp. 239–262.

Ravikumar, B., Duden, R., and Rubinsztein, D.C. (2002). Aggregate-prone proteins with polyglutamine and polyalanine expansions are degraded by autophagy. Hum. Mol. Genet. *11*, 1107–1117.

Ray, S., Bender, S., Kang, S., Lin, R., Glicksman, M.A., and Liu, M. (2014). The Parkinson's disease-linked LRRK2 mutation I2020T stabilizes an active state conformation leading to increased kinase activity. J. Biol. Chem. *289*, 13042–13053.

Reith, A.D., Bamborough, P., Jandu, K., Andreotti, D., Mensah, L., Dossang, P., Choi, H.G., Deng, X., Zhang, J., Alessi, D.R., et al. (2012). GSK2578215A; a potent and highly selective 2-arylmethyloxy-5-substitutent-N-arylbenzamide LRRK2 kinase inhibitor. Bioorg. Med. Chem. Lett. *22*, 5625–5629.

Ritz, B., Rhodes, S.L., Bordelon, Y., and Bronstein, J. (2012). α-Synuclein genetic variants predict faster motor symptom progression in idiopathic Parkinson disease. PloS One *7*, e36199.

Ross, C.A., and Poirier, M.A. (2004). Protein aggregation and neurodegenerative disease. Nat. Med. *10 Suppl*, S10–17.

Ross, O.A., Soto-Ortolaza, A.I., Heckman, M.G., Aasly, J.O., Abahuni, N., Annesi, G., Bacon, J.A., Bardien, S., Bozi, M., Brice, A., et al. (2011). Association of LRRK2 exonic variants with susceptibility to Parkinson's disease: a case–control study. Lancet Neurol. *10*, 898–908.

De Ruijter, A.J.M., van Gennip, A.H., Caron, H.N., Kemp, S., and van Kuilenburg, A.B.P. (2003). Histone deacetylases (HDACs): characterization of the classical HDAC family. Biochem. J. *370*, 737–749.

Ryu, M.Y., Kim, D.W., Arima, K., Mouradian, M.M., Kim, S.U., and Lee, G. (2008). Localization of CKII beta subunits in Lewy bodies of Parkinson's disease. J. Neurol. Sci. *266*, 9–12.

Saha, A.R., Hill, J., Utton, M.A., Asuni, A.A., Ackerley, S., Grierson, A.J., Miller, C.C., Davies, A.M., Buchman, V.L., Anderton, B.H., et al. (2004). Parkinson's disease alpha-synuclein mutations exhibit defective axonal transport in cultured neurons. J. Cell Sci. *117*, 1017–1024.

Saha, S., Ash, P.E.A., Gowda, V., Liu, L., Shirihai, O., and Wolozin, B. (2015). Mutations in LRRK2 potentiate age-related impairment of autophagic flux. Mol. Neurodegener. *10*.

Samaranch, L., Lorenzo-Betancor, O., Arbelo, J.M., Ferrer, I., Lorenzo, E., Irigoyen, J., Pastor, M.A., Marrero, C., Isla, C., Herrera-Henriquez, J., et al. (2010). PINK1-linked parkinsonism is associated with Lewy body pathology. Brain *133*, 1128–1142.

Sánchez-Danés, A., Richaud-Patin, Y., Carballo-Carbajal, I., Jiménez-Delgado, S., Caig, C., Mora, S., Di Guglielmo, C., Ezquerra, M., Patel, B., Giralt, A., et al. (2012). Disease-specific phenotypes in dopamine neurons from human iPS-based models of genetic and sporadic Parkinson's disease. EMBO Mol. Med. *4*, 380–395.

Sancho, R.M., Law, B.M.H., and Harvey, K. (2009). Mutations in the LRRK2 Roc-COR tandem domain link Parkinson's disease to Wnt signalling pathways. Hum. Mol. Genet. *18*, 3955–3968.

Satake, W., Nakabayashi, Y., Mizuta, I., Hirota, Y., Ito, C., Kubo, M., Kawaguchi, T., Tsunoda, T., Watanabe, M., Takeda, A., et al. (2009). Genome-wide association study identifies common variants at four loci as genetic risk factors for Parkinson's disease. Nat. Genet. *41*, 1303–1307.

Sawada, H., Kohno, R., Kihara, T., Izumi, Y., Sakka, N., Ibi, M., Nakanishi, M., Nakamizo, T., Yamakawa, K., Shibasaki, H., et al. (2004). Proteasome mediates dopaminergic neuronal degeneration, and its inhibition causes alpha-synuclein inclusions. J. Biol. Chem. *279*, 10710–10719.

Scarffe, L.A., Stevens, D.A., Dawson, V.L., and Dawson, T.M. (2014). Parkin and PINK1: much more than mitophagy. Trends Neurosci. *37*, 315–324.

Schapansky, J., Nardozzi, J.D., Felizia, F., and LaVoie, M.J. (2014). Membrane recruitment of endogenous LRRK2 precedes its potent regulation of autophagy. Hum. Mol. Genet. *23*, 4201–4214.

Schapira, A.H.V. (2015). Glucocerebrosidase and Parkinson disease: Recent advances. Mol. Cell. Neurosci. *66*, 37–42.

Schapira, A.H., Cooper, J.M., Dexter, D., Clark, J.B., Jenner, P., and Marsden, C.D. (1990). Mitochondrial complex I deficiency in Parkinson's disease. J. Neurochem. *54*, 823–827.

Schindelin, J., Arganda-Carreras, I., Frise, E., Kaynig, V., Longair, M., Pietzsch, T., Preibisch, S., Rueden, C., Saalfeld, S., Schmid, B., et al. (2012). Fiji: an open-source platform for biological-image analysis. Nat. Methods *9*, 676–682.

Schlossmacher, M.G., Frosch, M.P., Gai, W.P., Medina, M., Sharma, N., Forno, L., Ochiishi, T., Shimura, H., Sharon, R., Hattori, N., et al. (2002). Parkin Localizes to the Lewy Bodies of Parkinson Disease and Dementia with Lewy Bodies. Am. J. Pathol. *160*, 1655–1667.

Schmidt, M.L., Murray, J., Lee, V.M., Hill, W.D., Wertkin, A., and Trojanowski, J.Q. (1991). Epitope map of neurofilament protein domains in cortical and peripheral nervous system Lewy bodies. Am. J. Pathol. *139*, 53–65.

Schneider, C., Sepp-Lorenzino, L., Nimmesgern, E., Ouerfelli, O., Danishefsky, S., Rosen, N., and Hartl, F.U. (1996). Pharmacologic shifting of a balance between protein refolding and degradation mediated by Hsp90. Proc. Natl. Acad. Sci. *93*, 14536–14541.

Schopf, F.H., Biebl, M.M., and Buchner, J. (2017). The HSP90 chaperone machinery. Nat. Rev. Mol. Cell Biol. *18*, 345–360.

Schulte, C., and Gasser, T. (2011). Genetic basis of Parkinson's disease: inheritance, penetrance, and expression. Appl. Clin. Genet. *4*, 67–80.

Schwab, A.J., and Ebert, A.D. (2015). Neurite Aggregation and Calcium Dysfunction in iPSC-Derived Sensory Neurons with Parkinson's Disease-Related LRRK2 G2019S Mutation. Stem Cell Rep. *5*, 1039–1052.

Scroggins, B.T., Robzyk, K., Wang, D., Marcu, M.G., Tsutsumi, S., Beebe, K., Cotter, R.J., Felts, S., Toft, D., Karnitz, L., et al. (2007). An Acetylation Site in the Middle Domain of Hsp90 Regulates Chaperone Function. Mol. Cell *25*, 151–159.

Seigneurin-Berny, D., Verdel, A., Curtet, S., Lemercier, C., Garin, J., Rousseaux, S., and Khochbin, S. (2001). Identification of Components of the Murine Histone Deacetylase 6 Complex: Link between Acetylation and Ubiquitination Signaling Pathways. Mol. Cell. Biol. *21*, 8035–8044.

Sen, S., Webber, P.J., and West, A.B. (2009). Dependence of Leucine-rich Repeat Kinase 2 (LRRK2) Kinase Activity on Dimerization. J. Biol. Chem. *284*, 36346–36356.

Seto, E., and Yoshida, M. (2014). Erasers of Histone Acetylation: The Histone Deacetylase Enzymes. Cold Spring Harb. Perspect. Biol. *6*, a018713.

Sharma, S., and Taliyan, R. (2015). Targeting Histone Deacetylases: A Novel Approach in Parkinson's Disease. *Parkinson's Dis., 2015*, pp. 1-11.

Sharma, M., Mueller, J.C., Zimprich, A., Lichtner, P., Hofer, A., Leitner, P., Maass, S., Berg, D., Dürr, A., Bonifati, V., et al. (2006). The sepiapterin reductase gene region reveals association in the PARK3 locus: analysis of familial and sporadic Parkinson's disease in European populations. J. Med. Genet. *43*, 557–562.

Sheng, Z., Zhang, S., Bustos, D., Kleinheinz, T., Le Pichon, C.E., Dominguez, S.L., Solanoy, H.O., Drummond, J., Zhang, X., Ding, X., et al. (2012). Ser1292 autophosphorylation is an indicator of LRRK2 kinase activity and contributes to the cellular effects of PD mutations. Sci. Transl. Med. *4*, 164ra161.

Sherer, T.B., Kim, J.H., Betarbet, R., and Greenamyre, J.T. (2003). Subcutaneous rotenone exposure causes highly selective dopaminergic degeneration and alpha-synuclein aggregation. Exp. Neurol. *179*, 9–16.

Shida, T., Cueva, J.G., Xu, Z., Goodman, M.B., and Nachury, M.V. (2010). The major α-tubulin K40 acetyltransferase αTAT1 promotes rapid ciliogenesis and efficient mechanosensation. Proc. Natl. Acad. Sci. *107*, 21517–21522.

Shin, N., Jeong, H., Kwon, J., Heo, H.Y., Kwon, J.J., Yun, H.J., Kim, C.-H., Han, B.S., Tong, Y., Shen, J., et al. (2008). LRRK2 regulates synaptic vesicle endocytosis. Exp. Cell Res. *314*, 2055–2065.

Shukla, V., Mishra, S.K., and Pant, H.C. (2011). Oxidative Stress in Neurodegeneration. Adv. Pharmacol. Sci. *2011*, 572634.

Sidransky, E., and Lopez, G. (2012). The link between the GBA gene and parkinsonism. Lancet Neurol. *11*, 986–998.

Da Silva, F.L., Coelho Cerqueira, E., de Freitas, M.S., Gonçalves, D.L., Costa, L.T., and Follmer, C. (2013). Vitamins K interact with N-terminus α-synuclein and modulate the protein fibrillization in vitro. Exploring the interaction between quinones and α-synuclein. Neurochem. Int. *62*, 103–112.

Silvestri, L., Caputo, V., Bellacchio, E., Atorino, L., Dallapiccola, B., Valente, E.M., and Casari, G. (2005). Mitochondrial import and enzymatic activity of PINK1 mutants associated to recessive parkinsonism. Hum. Mol. Genet. *14*, 3477–3492.

Simões-Pires, C., Zwick, V., Nurisso, A., Schenker, E., Carrupt, P.-A., and Cuendet, M. (2013). HDAC6 as a target for neurodegenerative diseases: what makes it different from the other HDACs? Mol. Neurodegener. *8*, 7.

Singleton, A.B., Farrer, M., Johnson, J., Singleton, A., Hague, S., Kachergus, J., Hulihan, M., Peuralinna, T., Dutra, A., Nussbaum, R., et al. (2003). α-Synuclein Locus Triplication Causes Parkinson's Disease. Science *302*, 841–841.

Skoge, R.H., and Ziegler, M. (2016). SIRT2 inactivation reveals a subset of hyperacetylated perinuclear microtubules inaccessible to HDAC6. J. Cell Sci. *129*, 2972–2982.

Smith, W.W., Liu, Z., Liang, Y., Masuda, N., Swing, D.A., Jenkins, N.A., Copeland, N.G., Troncoso, J.C., Pletnikov, M., Dawson, T.M., et al. (2010). Synphilin-1 attenuates neuronal degeneration in the A53T α-synuclein transgenic mouse model. Hum. Mol. Genet. *19*, 2087–2098.

Snyder, H., Mensah, K., Theisler, C., Lee, J., Matouschek, A., and Wolozin, B. (2003). Aggregated and monomeric alpha-synuclein bind to the S6' proteasomal protein and inhibit proteasomal function. J. Biol. Chem. *278*, 11753–11759.

Song, Y., Kirkpatrick, L.L., Schilling, A.B., Helseth, D.L., Chabot, N., Keillor, J.W., Johnson, G.V.W., and Brady, S.T. (2013). Transglutaminase and Polyamination of Tubulin: Posttranslational Modification for Stabilizing Axonal Microtubules. Neuron *78*, 109–123.

Spillantini, M.G., Schmidt, M.L., Lee, V.M., Trojanowski, J.Q., Jakes, R., and Goedert, M. (1997). Alpha-synuclein in Lewy bodies. Nature *388*, 839–840.

Steger, M., Tonelli, F., Ito, G., Davies, P., Trost, M., Vetter, M., Wachter, S., Lorentzen, E., Duddy, G., Wilson, S., et al. (2016). Phosphoproteomics reveals that Parkinson's disease kinase LRRK2 regulates a subset of Rab GTPases. eLife *5*.

Steger, M., Diez, F., Dhekne, H.S., Lis, P., Nirujogi, R.S., Karayel, O., Tonelli, F., Martinez, T.N., Lorentzen, E., Pfeffer, S.R., et al. (2017). Systematic proteomic analysis of LRRK2-mediated Rab GTPase phosphorylation establishes a connection to ciliogenesis. eLife *6*.

Stirnimann, C.U., Petsalaki, E., Russell, R.B., and Müller, C.W. (2010). WD40 proteins propel cellular networks. Trends Biochem. Sci. *35*, 565–574.

Strauss, K.M., Martins, L.M., Plun-Favreau, H., Marx, F.P., Kautzmann, S., Berg, D., Gasser, T., Wszolek, Z., Müller, T., Bornemann, A., et al. (2005). Loss of function mutations in the gene encoding Omi/HtrA2 in Parkinson's disease. Hum. Mol. Genet. *14*, 2099–2111.

Su, B., Liu, H., Wang, X., Chen, S.G., Siedlak, S.L., Kondo, E., Choi, R., Takeda, A., Castellani, R.J., Perry, G., et al. (2009). Ectopic localization of FOXO3a protein in Lewy bodies in Lewy body dementia and Parkinson's disease. Mol. Neurodegener. *4*, 32.

Su, M., Shi, J.-J., Yang, Y.-P., Li, J., Zhang, Y.-L., Chen, J., Hu, L.-F., and Liu, C.-F. (2011). HDAC6 regulates aggresome-autophagy degradation pathway of α-synuclein in response to MPP+-induced stress. J. Neurochem. *117*, 112–120.

Surmeier, D.J., Guzman, J.N., and Sanchez-Padilla, J. (2010). Calcium, cellular aging, and selective neuronal vulnerability in Parkinson's disease. Cell Calcium *47*, 175–182.

Taes, I., Timmers, M., Hersmus, N., Bento-Abreu, A., Van Den Bosch, L., Van Damme, P., Auwerx, J., and Robberecht, W. (2013). Hdac6 deletion delays disease progression in the SOD1G93A mouse model of ALS. Hum. Mol. Genet. *22*, 1783–1790.

Takai, Y., Sasaki, T., and Matozaki, T. (2001). Small GTP-binding proteins. Physiol. Rev. *81*, 153–208.

Takayama, S., and Reed, J.C. (2001). Molecular chaperone targeting and regulation by BAG family proteins. Nat. Cell Biol. *3*, E237–241.

Tan, E.-K. (2006). Identification of a common genetic risk variant (LRRK2 Gly2385Arg) in Parkinson's disease. Ann. Acad. Med. Singapore *35*, 840–842.

Tan, E.K., Shen, H., Tan, L.C.S., Farrer, M., Yew, K., Chua, E., Jamora, R.D., Puvan, K., Puong, K.Y., Zhao, Y., et al. (2005). The G2019S LRRK2 mutation is uncommon in an Asian cohort of Parkinson's disease patients. Neurosci. Lett. *384*, 327–329.

Tan, E.-K., Peng, R., Teo, Y.-Y., Tan, L.C., Angeles, D., Ho, P., Chen, M.-L., Lin, C.-H., Mao, X.-Y., Chang, X.-L., et al. (2010). Multiple LRRK2 variants modulate risk of Parkinson disease: a Chinese multicenter study. Hum. Mutat. *31*, 561–568.

Tan, J.M.M., Wong, E.S.P., Kirkpatrick, D.S., Pletnikova, O., Ko, H.S., Tay, S.-P., Ho, M.W.L., Troncoso, J., Gygi, S.P., Lee, M.K., et al. (2008). Lysine 63-linked

ubiquitination promotes the formation and autophagic clearance of protein inclusions associated with neurodegenerative diseases. Hum. Mol. Genet. *17*, 431–439.

Tanaka, M., Kim, Y.M., Lee, G., Junn, E., Iwatsubo, T., and Mouradian, M.M. (2004). Aggresomes formed by alpha-synuclein and synphilin-1 are cytoprotective. J. Biol. Chem. *279*, 4625–4631.

Tanji, K., Tanaka, T., Mori, F., Kito, K., Takahashi, H., Wakabayashi, K., and Kamitani, T. (2006). NUB1 suppresses the formation of Lewy body-like inclusions by proteasomal degradation of synphilin-1. Am. J. Pathol. *169*, 553–565.

Tanji, K., Mori, F., Kakita, A., Takahashi, H., and Wakabayashi, K. (2011). Alteration of autophagosomal proteins (LC3, GABARAP and GATE-16) in Lewy body disease. Neurobiol. Dis. *43*, 690–697.

Taylor, J.P., Tanaka, F., Robitschek, J., Sandoval, C.M., Taye, A., Markovic-Plese, S., and Fischbeck, K.H. (2003). Aggresomes protect cells by enhancing the degradation of toxic polyglutamine-containing protein. Hum. Mol. Genet. *12*, 749–757.

Taymans, J.-M., and Greggio, E. (2016). LRRK2 Kinase Inhibition as a Therapeutic Strategy for Parkinson's Disease, Where Do We Stand? Curr. Neuropharmacol. *14*, 214–225.

Taymans, J.-M., Vancraenenbroeck, R., Ollikainen, P., Beilina, A., Lobbestael, E., De Maeyer, M., Baekelandt, V., and Cookson, M.R. (2011). LRRK2 Kinase Activity Is Dependent on LRRK2 GTP Binding Capacity but Independent of LRRK2 GTP Binding. PLoS ONE *6*, e23207.

Thaler, A., Ash, E., Gan-Or, Z., Orr-Urtreger, A., and Giladi, N. (2009). The LRRK2 G2019S mutation as the cause of Parkinson's disease in Ashkenazi Jews. J. Neural Transm. *116*, 1473–1482.

Tofaris, G.K., Razzaq, A., Ghetti, B., Lilley, K.S., and Spillantini, M.G. (2003). Ubiquitination of alpha-synuclein in Lewy bodies is a pathological event not associated with impairment of proteasome function. J. Biol. Chem. *278*, 44405–44411.

Tompkins, M.M., and Hill, W.D. (1997). Contribution of somal Lewy bodies to neuronal death. Brain Res. *775*, 24–29.

Tong, Y., Pisani, A., Martella, G., Karouani, M., Yamaguchi, H., Pothos, E.N., and Shen, J. (2009). R1441C mutation in LRRK2 impairs dopaminergic neurotransmission in mice. Proc. Natl. Acad. Sci. *106*, 14622–14627.

Tong, Y., Yamaguchi, H., Giaime, E., Boyle, S., Kopan, R., Kelleher, R.J., and Shen, J. (2010). Loss of leucine-rich repeat kinase 2 causes impairment of protein degradation pathways, accumulation of alpha-synuclein, and apoptotic cell death in aged mice. Proc. Natl. Acad. Sci. *107*, 9879–9884.

Tong, Y., Giaime, E., Yamaguchi, H., Ichimura, T., Liu, Y., Si, H., Cai, H., Bonventre, J.V., and Shen, J. (2012). Loss of leucine-rich repeat kinase 2 causes age-dependent bi-phasic alterations of the autophagy pathway. Mol. Neurodegener. *7*, 2.

Tran, A.D.-A., Marmo, T.P., Salam, A.A., Che, S., Finkelstein, E., Kabarriti, R., Xenias, H.S., Mazitschek, R., Hubbert, C., Kawaguchi, Y., et al. (2007). HDAC6 deacetylation of tubulin modulates dynamics of cellular adhesions. J. Cell Sci. *120*, 1469–1479.

Trojanowski, J.Q., and Lee, V.M. (1998). Aggregation of neurofilament and alpha-synuclein proteins in Lewy bodies: implications for the pathogenesis of Parkinson disease and Lewy body dementia. Arch. Neurol. *55*, 151–152.

Tsika, E., Kannan, M., Foo, C.S.-Y., Dikeman, D., Glauser, L., Gellhaar, S., Galter, D., Knott, G.W., Dawson, T.M., Dawson, V.L., et al. (2014). Conditional expression of Parkinson's disease-related R1441C LRRK2 in midbrain dopaminergic neurons of mice causes nuclear abnormalities without neurodegeneration. Neurobiol. Dis. *71*, 345–358.

Tumbarello, D.A., Waxse, B.J., Arden, S.D., Bright, N.A., Kendrick-Jones, J., and Buss, F. (2012). Autophagy-receptors link myosin VI to autophagosomes to mediate Tom1-dependent autophagosome maturation and fusion with the lysosome. Nat. Cell Biol. *14*, 1024–1035.

Ubl, A., Berg, D., Holzmann, C., Krüger, R., Berger, K., Arzberger, T., Bornemann, A., and Riess, O. (2002). 14-3-3 protein is a component of Lewy bodies in Parkinson's disease-mutation analysis and association studies of 14-3-3 eta. Brain Res. Mol. Brain Res. *108*, 33–39.

Uhlén, M., Fagerberg, L., Hallström, B.M., Lindskog, C., Oksvold, P., Mardinoglu, A., Sivertsson, Å., Kampf, C., Sjöstedt, E., Asplund, A., et al. (2015). Proteomics. Tissue-based map of the human proteome. Science *347*, 1260419.

Vale, R.D. (2003). The molecular motor toolbox for intracellular transport. Cell *112*, 467–480.

Valente, E.M., Abou-Sleiman, P.M., Caputo, V., Muqit, M.M.K., Harvey, K., Gispert, S., Ali, Z., Del Turco, D., Bentivoglio, A.R., Healy, D.G., et al. (2004). Hereditary early-onset Parkinson's disease caused by mutations in PINK1. Science *304*, 1158–1160.

Valenzuela-Fernández, A., Cabrero, J.R., Serrador, J.M., and Sánchez-Madrid, F. (2008). HDAC6: a key regulator of cytoskeleton, cell migration and cell-cell interactions. Trends Cell Biol. *18*, 291–297.

Vaquero, A., Scher, M.B., Lee, D.H., Sutton, A., Cheng, H.-L., Alt, F.W., Serrano, L., Sternglanz, R., and Reinberg, D. (2006). SirT2 is a histone deacetylase with preference for histone H4 Lys 16 during mitosis. Genes Dev. *20*, 1256–1261.

Vaughan, K.T., and Vallee, R.B. (1995). Cytoplasmic dynein binds dynactin through a direct interaction between the intermediate chains and p150Glued. J. Cell Biol. *131*, 1507–1516.

Verdel, A., Curtet, S., Brocard, M.-P., Rousseaux, S., Lemercier, C., Yoshida, M., and Khochbin, S. (2000). Active maintenance of mHDA2/mHDAC6 histone-deacetylase in the cytoplasm. Curr. Biol. *10*, 747–749.

Vilariño-Güell, C., Rajput, A., Milnerwood, A.J., Shah, B., Szu-Tu, C., Trinh, J., Yu, I., Encarnacion, M., Munsie, L.N., Tapia, L., et al. (2014). DNAJC13 mutations in Parkinson disease. Hum. Mol. Genet. *23*, 1794–1801.

Volpicelli-Daley, L.A., Luk, K.C., Patel, T.P., Tanik, S.A., Riddle, D.M., Stieber, A., Meaney, D.F., Trojanowski, J.Q., and Lee, V.M.-Y. (2011). Exogenous α-Synuclein Fibrils Induce Lewy Body Pathology Leading to Synaptic Dysfunction and Neuron Death. Neuron *72*, 57–71.

De Vos, K.J., Grierson, A.J., Ackerley, S., and Miller, C.C.J. (2008). Role of axonal transport in neurodegenerative diseases. Annu. Rev. Neurosci. *31*, 151–173.

Wakabayashi, K., Engelender, S., Yoshimoto, M., Tsuji, S., Ross, C.A., and Takahashi, H. (2000). Synphilin-1 is present in Lewy bodies in Parkinson's disease. Ann. Neurol. *47*, 521–523.

Wakabayashi, K., Tanji, K., Mori, F., and Takahashi, H. (2007). The Lewy body in Parkinson's disease: molecules implicated in the formation and degradation of alpha-synuclein aggregates. Neuropathol. *27*, 494–506.

Wakabayashi, K., Tanji, K., Odagiri, S., Miki, Y., Mori, F., and Takahashi, H. (2013). The Lewy Body in Parkinson's Disease and Related Neurodegenerative Disorders. Mol. Neurobiol. *47*, 495–508.

Wallingford, J.B., and Habas, R. (2005). The developmental biology of Dishevelled: an enigmatic protein governing cell fate and cell polarity. Dev. *132*, 4421–4436.

Wang, L., Xie, C., Greggio, E., Parisiadou, L., Shim, H., Sun, L., Chandran, J., Lin, X., Lai, C., Yang, W.-J., et al. (2008). The chaperone activity of heat shock protein 90 is critical for maintaining the stability of leucine-rich repeat kinase 2. J. Neurosci. *28*, 3384–3391.

Wang, L., Cheng, L., Lu, Z.-J., Sun, X.-Y., Li, J.-Y., and Peng, R. (2016). Association of three candidate genetic variants in RAB7L1/NUCKS1, MCCC1 and STK39 with sporadic Parkinson's disease in Han Chinese. J. Neural Transm. *123*, 425–430.

Wang, X., Venable, J., LaPointe, P., Hutt, D.M., Koulov, A.V., Coppinger, J., Gurkan, C., Kellner, W., Matteson, J., Plutner, H., et al. (2006). Hsp90 Cochaperone Aha1 Downregulation Rescues Misfolding of CFTR in Cystic Fibrosis. Cell *127*, 803–815.

Wang, X., Winter, D., Ashrafi, G., Schlehe, J., Wong, Y.L., Selkoe, D., Rice, S., Steen, J., LaVoie, M.J., and Schwarz, T.L. (2011). PINK1 and Parkin target Miro for phosphorylation and degradation to arrest mitochondrial motility. Cell *147*, 893–906.

Wang, X.-X., Wan, R.-Z., and Liu, Z.-P. (2018). Recent advances in the discovery of potent and selective HDAC6 inhibitors. Eur. J. Med. Chem. *143*, 1406–1418.

Ward, C.L., and Kopito, R.R. (1994). Intracellular turnover of cystic fibrosis transmembrane conductance regulator. Inefficient processing and rapid degradation of wild-type and mutant proteins. J. Biol. Chem. *269*, 25710–25718.

Watabe, M., and Nakaki, T. (2011). Protein kinase CK2 regulates the formation and clearance of aggresomes in response to stress. J Cell Sci *124*, 1519–1532.

Waxman, E.A., Covy, J.P., Bukh, I., Li, X., Dawson, T.M., and Giasson, B.I. (2009). Leucine-Rich Repeat Kinase 2 Expression Leads to Aggresome Formation That Is Not Associated With α-Synuclein Inclusions. J. Neuropathol. Exp. Neurol. *68*, 785–796.

Webber, P.J., Smith, A.D., Sen, S., Renfrow, M.B., Mobley, J.A., and West, A.B. (2011). Autophosphorylation in the Leucine-Rich Repeat Kinase 2 (LRRK2) GTPase Domain Modifies Kinase and GTP-Binding Activities. J. Mol. Biol. *412*, 94–110.

West, A.B. (2017). Achieving neuroprotection with LRRK2 kinase inhibitors in Parkinson disease. Exp. Neurol. *298*, 236–245.

West, A.B., Moore, D.J., Biskup, S., Bugayenko, A., Smith, W.W., Ross, C.A., Dawson, V.L., and Dawson, T.M. (2005). Parkinson's disease-associated mutations in leucine-rich repeat kinase 2 augment kinase activity. Proc. Natl. Acad. Sci. *102*, 16842–16847.

West, A.B., Moore, D.J., Choi, C., Andrabi, S.A., Li, X., Dikeman, D., Biskup, S., Zhang, Z., Lim, K.-L., Dawson, V.L., et al. (2007). Parkinson's disease-associated mutations in LRRK2 link enhanced GTP-binding and kinase activities to neuronal toxicity. Hum. Mol. Genet. *16*, 223–232.

West, A.B., Cowell, R.M., Daher, J.P.L., Moehle, M.S., Hinkle, K.M., Melrose, H.L., Standaert, D.G., and Volpicelli-Daley, L.A. (2014). Differential LRRK2 expression in the cortex, striatum, and substantia nigra in transgenic and nontransgenic rodents. J. Comp. Neurol. *522*, 2465–2480.

Wigley, W.C., Fabunmi, R.P., Lee, M.G., Marino, C.R., Muallem, S., DeMartino, G.N., and Thomas, P.J. (1999). Dynamic association of proteasomal machinery with the centrosome. J. Cell Biol. *145*, 481–490.

Williams, K.A., Zhang, M., Xiang, S., Hu, C., Wu, J.-Y., Zhang, S., Ryan, M., Cox, A.D., Der, C.J., Fang, B., et al. (2013). Extracellular Signal-regulated Kinase (ERK) Phosphorylates Histone Deacetylase 6 (HDAC6) at Serine 1035 to Stimulate Cell Migration. J. Biol. Chem. *288*, 33156–33170.

Winklhofer, K.F., and Haass, C. (2010). Mitochondrial dysfunction in Parkinson's disease. Biochim. Biophys. Acta BBA - Mol. Basis Dis. *1802*, 29–44.

Winner, B., Jappelli, R., Maji, S.K., Desplats, P.A., Boyer, L., Aigner, S., Hetzer, C., Loher, T., Vilar, M., Campioni, S., et al. (2011a). In vivo demonstration that α-synuclein oligomers are toxic. Proc. Natl. Acad. Sci. *108*, 4194–4199.

Winner, B., Melrose, H.L., Zhao, C., Hinkle, K.M., Yue, M., Kent, C., Braithwaite, A.T., Ogholikhan, S., Aigner, R., Winkler, J., et al. (2011b). Adult neurogenesis and neurite outgrowth are impaired in LRRK2 G2019S mice. Neurobiol. Dis. *41*, 706–716.

Wooten, M.W., Hu, X., Babu, J.R., Seibenhener, M.L., Geetha, T., Paine, M.G., and Wooten, M.C. (2006). Signaling, Polyubiquitination, Trafficking, and Inclusions: Sequestosome 1/p62's Role in Neurodegenerative Disease. J. Biomed. Biotechnol. *2006*.

Xiong, Y., Coombes, C.E., Kilaru, A., Li, X., Gitler, A.D., Bowers, W.J., Dawson, V.L., Dawson, T.M., and Moore, D.J. (2010). GTPase activity plays a key role in the pathobiology of LRRK2. PLoS Genet. *6*, e1000902.

Xiong, Y., Yuan, C., Chen, R., Dawson, T.M., and Dawson, V.L. (2012). ArfGAP1 is a GTPase activating protein for LRRK2: reciprocal regulation of ArfGAP1 by LRRK2. J. Neurosci. *32*, 3877–3886.

Xu, Z., Graham, K., Foote, M., Liang, F., Rizkallah, R., Hurt, M., Wang, Y., Wu, Y., and Zhou, Y. (2013). 14-3-3 protein targets misfolded chaperone-associated proteins to aggresomes. J. Cell Sci. *126*, 4173–4186.

Xu, Z., Schaedel, L., Portran, D., Aguilar, A., Gaillard, J., Marinkovich, M.P., Théry, M., and Nachury, M.V. (2017). Microtubules acquire resistance from mechanical breakage through intralumenal acetylation. Science *356*, 328–332.

Yamamoto, A., Cremona, M.L., and Rothman, J.E. (2006). Autophagy-mediated clearance of huntingtin aggregates triggered by the insulin-signaling pathway. J. Cell Biol. *172*, 719–731.

Yan, J., Seibenhener, M.L., Calderilla-Barbosa, L., Diaz-Meco, M.-T., Moscat, J., Jiang, J., Wooten, M.W., and Wooten, M.C. (2013). SQSTM1/p62 Interacts with HDAC6 and Regulates Deacetylase Activity. PLOS ONE *8*, e76016.

Yan, Y., Tian, J., Mo, X., Zhao, G., Yin, X., Pu, J., and Zhang, B. (2011). Genetic Variants in the RAB7L1 and SLC41A1 Genes of the PARK16 Locus in Chinese Parkinson's Disease Patients. Int. J. Neurosci. *121*, 632–636.

D' Ydewalle, C., Krishnan, J., Chiheb, D.M., Van Damme, P., Irobi, J., Kozikowski, A.P., Vanden Berghe, P., Timmerman, V., Robberecht, W., and Van Den Bosch, L. (2011). HDAC6 inhibitors reverse axonal loss in a mouse model of mutant HSPB1-induced Charcot-Marie-Tooth disease. Nat. Med. *17*, 968–974.

D' Ydewalle, C., Bogaert, E., and Van Den Bosch, L. (2012). HDAC6 at the Intersection of Neuroprotection and Neurodegeneration. Traffic *13*, 771–779.

Ylä-Anttila, P., Vihinen, H., Jokitalo, E., and Eskelinen, E.-L. (2009). 3D tomography reveals connections between the phagophore and endoplasmic reticulum. Autophagy *5*, 1180–1185.

Yorimitsu, T., and Klionsky, D.J. (2005). Autophagy: molecular machinery for self-eating. Cell Death Differ. *12 Suppl 2*, 1542–1552.

Yu, W., and Baas, P.W. (1994). Changes in microtubule number and length during axon differentiation. J. Neurosci. *14*, 2818–2829.

Yu, M., Arshad, M., Wang, W., Zhao, D., Xu, L., and Zhou, L. (2018). LRRK2 mediated Rab8a phosphorylation promotes lipid storage. Lipids Health Dis. *17*, 34

Zaffagnini, G., and Martens, S. (2016). Mechanisms of Selective Autophagy. J. Mol. Biol. *428*, 1714–1724.

Zarranz, J.J., Alegre, J., Gómez-Esteban, J.C., Lezcano, E., Ros, R., Ampuero, I., Vidal, L., Hoenicka, J., Rodriguez, O., Atarés, B., et al. (2004). The new mutation, E46K, of α-synuclein causes parkinson and Lewy body dementia. Ann. Neurol. *55*, 164–173.

Zhang, P., Wang, Q., Jiao, F., Yan, J., Chen, L., He, F., Zhang, Q., and Tian, B. (2016). Association of LRRK2 R1628P variant with Parkinson's disease in Ethnic Han-Chinese and subgroup population. Sci. Rep. *6*, 35171.

Zhang, X., Yuan, Z., Zhang, Y., Yong, S., Salas-Burgos, A., Koomen, J., Olashaw, N., Parsons, J.T., Yang, X.-J., Dent, S.R., et al. (2007). HDAC6 modulates cell motility by altering the acetylation level of cortactin. Mol. Cell *27*, 197–213.

Zhang, Y., Li, N., Caron, C., Matthias, G., Hess, D., Khochbin, S., and Matthias, P. (2003). HDAC-6 interacts with and deacetylates tubulin and microtubules in vivo. EMBO J. *22*, 1168–1179.

Zhang, Y., Gilquin, B., Khochbin, S., and Matthias, P. (2006). Two catalytic domains are required for protein deacetylation. J. Biol. Chem. *281*, 2401–2404.

Zhang, Y., Kwon, S., Yamaguchi, T., Cubizolles, F., Rousseaux, S., Kneissel, M., Cao, C., Li, N., Cheng, H.-L., Chua, K., et al. (2008). Mice lacking histone deacetylase 6 have hyperacetylated tubulin but are viable and develop normally. Mol. Cell. Biol. *28*, 1688–1701.

Zhao, R., and Houry, W.A. (2005). Hsp90: a chaperone for protein folding and gene regulation. Biochem. Cell Biol. *83*, 703–710.

Zhao, Z., Xu, H., and Gong, W. (2010). Histone deacetylase 6 (HDAC6) is an independent deacetylase for alpha-tubulin. Protein Pept. Lett. *17*, 555–558.

Zhen, Y., and Stenmark, H. (2015). Cellular functions of Rab GTPases at a glance. J Cell Sci *128*, 3171–3176.

Zheng, Y., Liu, Y., Wu, Q., Hong, H., Zhou, H., Chen, J., Wang, H., Xian, W., Li, J., Liu, Z., et al. (2011). Confirmation of LRRK2 S1647T variant as a risk factor for Parkinson's disease in southern China. Eur. J. Neurol. *18*, 538–540.

Zhou, L.-L., Zhang, X., Bao, Q.-Q., Liu, R.-P., Gong, M.-Y., Mao, G.-Y., Zou, M., and Zhu, J.-H. (2014). Association analysis of PARK16-18 variants and Parkinson's disease in a Chinese population. J. Clin. Neurosci. *21*, 1029–1032.

Zhu, X., Babar, A., Siedlak, S.L., Yang, Q., Ito, G., Iwatsubo, T., Smith, M.A., Perry, G., and Chen, S.G. (2006). LRRK2 in Parkinson's disease and dementia with Lewy bodies. Mol. Neurodegener. *1*, 17-25.

Zilberman, Y., Ballestrem, C., Carramusa, L., Mazitschek, R., Khochbin, S., and Bershadsky, A. (2009). Regulation of microtubule dynamics by inhibition of the tubulin deacetylase HDAC6. J. Cell Sci. *122*, 3531–3541.

Zimprich, A., Benet-Pagès, A., Struhal, W., Graf, E., Eck, S.H., Offman, M.N., Haubenberger, D., Spielberger, S., Schulte, E.C., Lichtner, P., et al. (2011). A mutation in VPS35, encoding a subunit of the retromer complex, causes late-onset Parkinson disease. Am. J. Hum. Genet. *89*, 168–175.

Zondler, L., Kostka, M., Garidel, P., Heinzelmann, U., Hengerer, B., Mayer, B., Weishaupt, J.H., Gillardon, F., and Danzer, K.M. (2017). Proteasome impairment by α-synuclein. PLOS ONE *12*, e0184040.

Zou, H., Wu, Y., Navre, M., and Sang, B.-C. (2006). Characterization of the two catalytic domains in histone deacetylase 6. Biochem. Biophys. Res. Commun. *341*, 45–50.